IONIC LIQUIDS AND DEEP EUTECTIC SOLVENTS AS ELECTROLYTES FOR ENERGY EFFICIENT ELECTRICAL DOUBLE LAYER CAPACITOR

Submitted in Partial Fulfilment of the Requirements

for the Degree of

DOCTOR OF PHILOSOPHY

By

Upasana Mahanta

DEPARTMENT OF CHEMICAL ENGINEERING

INDIAN INSTITUTE OF TECHNOLOGY GUWAHATI

February 2021

भारतीय प्रौद्योगिकी संस्थान गुवाहाटी
रासायनिक अभियांत्रिकी विभाग
गुवाहाटी ७८१ ०३९, असम, भारत

INDIAN INSTITUTE OF TECHNOLOGY GUWAHATI
Department of Chemical Engineering
Guwahati 781039, Assam, India

CERTIFICATE

This is to certify that the work contained in the thesis entitled "***Ionic Liquids and Deep Eutectic Solvents as Electrolytes for Energy Efficient Electrical Double Layer Capacitor***" is the result of investigations carried out by **Upasana Mahanta**, under our supervision and is submitted to the Indian Institute of Technology Guwahati, Guwahati-781039, Assam, India for the award of degree of Doctor of Philosophy. This work has not been submitted elsewhere for a degree.

Date:

Dr. R. Prasanna Venkatesh	Prof. Tamal Banerjee
Associate Professor	Professor
Department of Chemical Engineering	Department of Chemical Engineering

भारतीय प्रौद्योगिकी संस्थान गुवाहाटी
रासायनिक अभियांत्रिकी विभाग
गुवाहाटी ७८१ ०३९, असम, भारत

INDIAN INSTITUTE OF TECHNOLOGY GUWAHATI
Department of Chemical Engineering
Guwahati 781039, Assam, India

DECLARATION

I hereby declare that the matter embodied in this thesis is the result of investigations carried out by me in the Department of Chemical Engineering, Indian Institute of Technology Guwahati, Assam, India under the supervision of **Prof. Tamal Banerjee** and **Dr. R. Prasanna Venkatesh** Department of Chemical Engineering and is submitted to the Indian Institute of Technology Guwahati, Guwahati-781039, Assam, India for the award of degree of Doctor of Philosophy. This work has not been submitted elsewhere for any degree or diploma of any institute or university to the best of my knowledge and belief.

In keeping with the general practice of reporting scientific observations, due acknowledgements have been made wherever the work of other investigators are referred, and copyright licenses have been taken from respective publishers.

IIT Guwahati — **Upasana Mahanta**

February 2021 — Roll No: 166107001

Dedicated
To
My Parents

ACKNOWLEDGEMENT

The journey throughout the PhD tenure has been a pleasant learning process for me. These wonderful years of the thesis work would not exist without the guidance, encouragement, care and support of certain people. Hence, I would like to take this opportunity and thank everyone who contributed to this thesis work either directly or indirectly.

First and foremost, I express my sincere gratitude to my supervisors **Prof. Tamal Banerjee** and **Dr. Prasanna Venkatesh Rajaraman** for their guidance and support throughout the due course of research work. I am indebted to Prof. Tamal Banerjee for providing me the opportunity to work in a very engrossing area of research. His constant motivation for exploring new ideas encouraged me to build the researcher in me. He taught me the art of technical writing and presentation. He provided a very healthy research environment which helped me to overcome the gloomy phases of PhD tenure. I am grateful to Dr. Prasanna Venkatesh Rajaraman for helping me to learn electrochemical theories. The worthwhile discussions with him accelerated my learning process. His constructive guidance and suggestions immensely helped me to develop experimental research skills. Most importantly, I am thankful to both my supervisors for giving me the freedom to work. I highly acknowledge them for their valuable time and mentorship. It was really an honor to work under their supervision.

I would like to convey my sincere gratitude to my Doctoral Committee members, **Prof. Chandan Das** and **Dr. Prabu Vairakannu,** Department of Chemical Engineering and **Dr. Uday Narayan Maiti,** Department of Physics, for proving valuable time, constructive assessments and suggestions during the research period. Their valuable criticisms enriched the thesis.

My heartiest thanks to **RESPOND** program of **Indian Space Research Organization (ISRO)** for providing the financial assistance to carry out this research work. I am thankful to the mentors form Vikram Sarabhai Space Centre (VSSC), **Dr. S.A. Illangovan**, Advanced Power Systems and **S. Sujatha**, Chemical Systems Division.

I am grateful to **Prof. Mihir Kumar Purkait** for allowing me to access the facility of ionic conductivity measurements in his laboratory. I would like to thank **Prof. Animes Kumar Golder** for helping me with the preparation of glassy carbon electrode.

I am thankful to **Prof. Pallab Ghosh** for teaching me skills of research methodology and technical writing during the course work in the first semester of PhD. I would like to extend my gratitude to **Prof. Bishnupada Mandal** and **Prof. Anugrah Singh,** former and present Heads of the Department of Chemical Engineering for their valuable administrative support. Furthermore, I would like to acknowledge the other faculty and staff members of Department of Chemical Engineering for their assistance.

I would like to express my gratitude to **Analytical Laboratory,** Department of Chemical Engineering and **Central Instrument Facility**, IIT Guwahati for providing characterization facilities.

I am indebted to my fellow researcher and husband **Mr. Pyarimohan Dehury** for his technical support, constant motivation and criticism from the very beginning of this research work. Especially his inspiration to deal with tough situations always boosts my spirit. I am thankful to **Ms. Sambita Choudhury** (M.Tech, IITG) and **Mr. Ashraykumar Karodiya** (B.Tech, Ahmedabad University) for their contribution.

I would like to specially mention the names of my seniors from the department, **Dr. Basudhrity Banejee, Dr. Prince Kumar Baranwal and Dr. Rahul Saha**. Dr. Basudhrity Banerjee has always been an elder sister to me who shared her experiences to deal with the

PhD life. Dr. Prince Kumar Baranwal taught me the basics of electrochemical techniques and was there to share my success or failure of research. It has been an immense pleasure for me to share laboratory with them. Further, Dr. Rahul Saha taught me the operation of Rheometer. I am thankful to my friend, **Ms. Preetisagar Talukdar** for being there for me whenever needed. I would like to duly acknowledge **Mr. Dhirendra Kumar Mishra** for the humorous conversations which have always been stress relievers and caused a cheerful environment to work in the laboratory. The scientific group discussions with Mr. Pyarimohan, Mr. Dhirendra and Dr. Basudhirty helped me to address the problems faced in the thesis work.

My heartiest gratitude to **Dr. Anirban Bhowal** (Department of Electronics and Electrical Engineering, IITG) for being a close friend to share the professional problems. I would like to covey my thanks to **Mr. Anirban Sikdar** (Department of Physics, IITG) for helping me to understand the concept of galvanostatic charge-discharge process.

My heartful thanks to the fellow lab members, **Dr. Mood Mohan**, **Dr. Anand Bharti**, **Mr. Janardan Singh**, **Mr. Nikhil Kumar**, **Mr. Nabendu Paul**, **Mr. Harish Kumar Bhupathi** and **Mr. Arindam Dutta** for providing a co-operative research environment. I also convey my profound thanks to fellow researchers from the department, **Dr. Murchana Changmai, Ms. Barnali Bhui, Mr. Piyal Mondal**, **Mr. Siddharth Thakur, Ms. Sushma Chakraborty, Mr. Pranjal Pratim Das** and **Mr. Anirban Chowdhury** for their assistance.

Above all, my beholden gratitude to my parents, **Mrs. Mina Mahanta** and **Mr. Chakrapani Mahanta** and younger brother, **Mr. Devabrat Mahanta** for their never-ending love, care and support without which this thesis would not have been completed. A special thanks to my father who always encourages both his children to be equally qualified

and attain the highest academic degree. I am also thankful to other family members for their wholehearted support and motivation.

Upasana Mahanta

February 2021

SYNOPSIS

Electrical double layer capacitor (EDLC) is the advanced version of capacitor, possessing better energy storage than conventional dielectric capacitor. The power deliverable capability of EDLC is also better than batteries and fuel cells. Hence, research on EDLC has become an interesting topic in the field of applied electrochemistry as well as energy conversion and storage. The performance of an EDLC depends on the properties of both electrolyte and working electrode materials. Therefore, research on these two basic constituents of EDLC are equally important. The improved energy storage of an EDLC can be achieved with wider electrochemical stable potential of the electrolyte and further delivery of that energy can be accelerated by reducing the internal resistance of system. These are the two key factors for choosing suitable electrolyte for an EDLC.

The present work explores ionic liquids (ILs) and two novel deep eutectic solvents (DESs) as electrolytes for exfoliated carbon based EDLC. A set of ILs based on ethyl, propyl and butyl substituted 1-alkyl-3-methylimidazolium [AMIM] cations with bis(trifluoromethylsulfonyl)imide (Tf_2N) and tetrafluroborate (BF_4) anions are chosen for electrochemical study. This work also incorporates mixture of ILs as electrolytes for EDLC. Further two more ILs namely 1-butyl-4-methylpyridinium tetraflouroborate ([BMpy][BF_4]) and Triethylsulfonium bis(trifluoromethylsulfonyl)imide (TESu][Tf_2N]) are also added in this study. ILs are investigated in neat form as well as solution in organic solvents namely acetonitrile (AN), propylene carbonate (PC) and butyronitrile (BN). Moreover, 1-butyl-3-methyl imidazolium methanesulphonate ([BMIM][$MeSO_3$]) is chosen as hydrogen bond acceptor (HBA) for DESs. In this regard N-methylacetamide (NMAc) and ethylene glycol (EG) are taken as the corresponding hydrogen bond donors (HBDs).

Electrochemical characterization methods such as cyclic voltammetry (CV), galvanostatic charge-discharge (GCD) and electrochemical impedance spectroscopy (EIS) are employed to evaluate the performance parameters for the IL electrolyte-electrode combinations. Moreover, transport properties namely ionic conductivity and viscosity measurements are executed for the favourable IL based electrolytes using both experimental tools and molecular dynamic (MD) simulation. MD studies enlighten the diffusive nature of ions with or without the presence of organic solvent. Further, Conductor like Screening Model-Segment Activity Coefficient (COSMO-SAC) thermodynamic model is used to study the solid-liquid phase equilibria where eutectic point of DES is evaluated. NMR study confirms the physical interaction between HBA and HBD of the DESs. Water content measurement and thermal stability of the novel DESs are also carried out. The physicochemical properties e.g. density, viscosity and ionic conductivity of the DESs are further determined. Afterwards, linear scan voltammetry (LSV) is performed to obtain the stable potential window of the DESs. Lastly, electrochemical performance is appraised using CV and GCD techniques.

The IL with co-solvent systems result in lower equivalent series resistance (ESR) and higher specific capacitance than pure ILs. On the contrary pure ILs exhibit the widest operating potential window (OPW) and the same decreases with the addition of organic solvent. [PMIM][Tf_2N] with 57 weight percentage of AN delivers the best result regarding OPW (3 V), specific capacitance (121.95 F g^{-1}), ESR (7.28 Ω), energy storage (152.44 Wh kg^{-1}) and specific power (10.10 kW kg^{-1}). The electrochemical performance of IL varies with variation in co-solvent concentration. AN and PC show opposite effects when mixed with [BMPy][BF_4]. It is noted that co-solvent improvises the rate determining parameters

of EDLC up to a certain composition. The ILs, [EMIM][Tf_2N] and [TESu][Tf_2N] impart similar results irrespective of the difference in type of cationic core.

Transport properties of pure ILs and their solutions support the electrochemical findings. The ionic conductivity value reaches the maximum at the composition corresponding to maximum specific capacitance. MD simulation provides the molecular level understanding regarding ion diffusion. It shows how co-solvent enhances the mean square displacement of ions and hence affects ionic conductivity and viscosity. The simulation successfully validates the experimental observations.

COSMO-SAC predicts the molar ratio to be 1:3.5 and 1:2 for [BMIM][$MeSO_3$]:EG and [BMIM][$MeSO_3$]: NMAc respectively. The computed melting points of the formulated DESs are found to be 70 – 100 ºC lower than that of HBA. The viscosity of the newly developed DESs (~15 cp) are significantly lower than neat room temperature IL electrolytes and their ionic conductivity is found to be comparable to ILs. TGA study reveals no mass loss up to ~90 ºC favouring high temperature application of EDLC. LSV provides electrochemical stability up to 3.8 V against glassy carbon electrode. [BMIM][$MeSO_3$]: EG and [BMIM][$MeSO_3$]: NMAc result in OPW of 2 and 3 V respectively with porous exfoliated carbon electrode. Moderate values of specific capacitance (55-67 Fg^{-1}) and power (0.56-1.3 $kWkg^{-1}$) are observed due to higher internal resistance. However, [BMIM][$MeSO_3$]: NMAc results in noteworthy high specific energy (~ 84 Wh kg^{-1}) due to its wider OPW.

An overall summary of the thesis is presented in Figure A.

Key Words: Ionic Liquids, Deep Eutectic Solvents, EDLC, Specific Capacitance, OPW, ESR

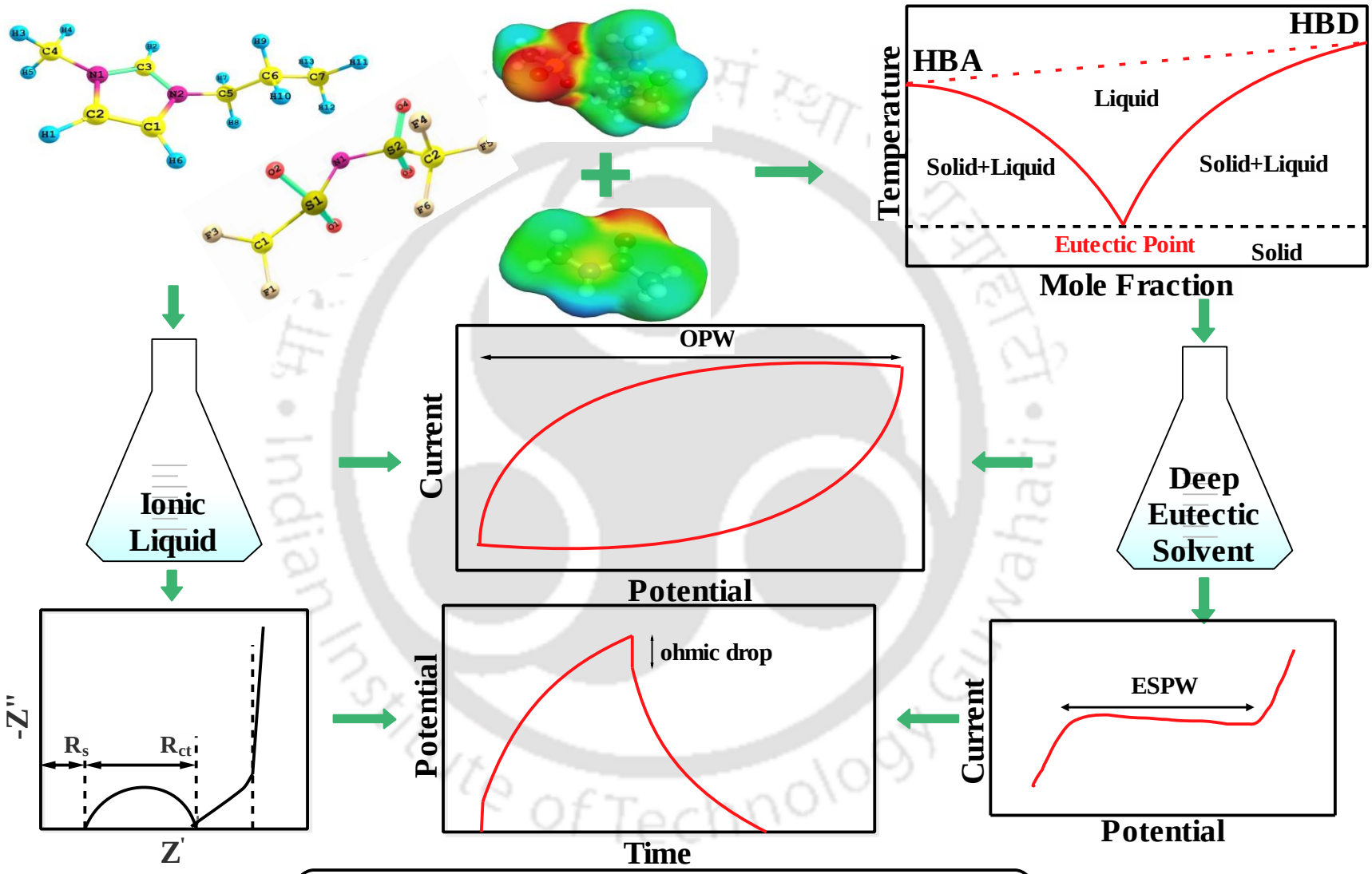

Figure A: Graphical Representation of Thesis Work

CONTENTS

LIST OF FIGURES

LIST OF TABLES

NOMENCLATURE

Abbreviations

AN	Acetonitrile
BN	Butyronitrile
bp	Boiling Point
COSMO-SAC	Conductor like Screening Model-Segment Activity Coefficient
CV	Cyclic Voltammetry
DES	Deep Eutectic Solvent
DFT	Density Functional Theory
EC	Electrochemical Capacitor
EDLC	Electrical Double Layer Capacitor
ESR	Equivalent Series Resistance
ESPW	Electrochemical Stable Potential Window
EIS	Electrochemical Impedance Spectroscopy
FRA	Frequency Response Analysis
GCD	Galvanostatic Charge-discharge
GAFF	Generalized Amber Force Field
HBA	Hydrogen Bond Acceptor
HBD	Hydrogen Bond Donor
IL	Ionic Liquid
KFT	Karl Fischer Titration
LSV	Linear Scan Voltammetry
MD	Molecular Dynamics

MSD	Mean Square Displacement
mp	Melting Point
NMR	Nuclear Magnetic Resonance
NOESY	Nuclear Overhauser Effect Spectroscopy
OPW	Operating Potential Window
OCP	Open Circuit Potential
PC	Propylene Carobonate
RTIL	Room Temperature Ionic Liquid
TGA	Thermogravimetric Analysis
SC	Supercapacitor
SLE	Solid-liquid Equilibrium
WE	Working Electrode

English Symbols

A	Ampere
Ag	Silver
C	Capacitance
C_{sp}	Specific Capacitance
D	Self-diffusion Coefficient
E	Energy
F	Farad
f	Frequency
I	Current
kWh	Kilowatt-hour
m	Weight of Working Electrode

M	Molar
P	Power
R_s	Solution Resistance
R_{ct}	Charge Transfer Resistance
T	Temperature
V	Volt
Wh	Watt-hour
Z'	Real Part of Impedance
Z''	Imaginary Part of Impedance

Greek/Roman Symbols

ρ	Density
σ	Ionic Conductivity
η	Viscosity
Ω	Ohm

Ionic Liquids

[EMIM][Tf_2N]	1-ethyl-3-methylimidazolium bis(trifluoromethylsulfonyl)imide
[PMIM][Tf_2N]	1-propyl-3-methylimidazolium bis(trifluoromethylsulfonyl)imide
[BMIM][Tf_2N]	1-butyl-3-methylimidazolium bis(trifluoromethylsulfonyl)imide
[AMIM][Tf_2N]	1-alkyl-3-methylimidazolium bis(trifluoromethylsulfonyl)imide
[EMIM][BF_4]	1-ethyl-3-methylimidazolium tetrafluroborate
[BMIM][BF_4]	1-butyl-3-methylimidazolium tetrafluroborate
[AMIM][BF_4]	1-alkyl-3-methylimidazolium tetrafluroborate
[BMpy][BF_4]	1-butyl-4-methylpyridinium tetraflouroborate

[TESu][Tf_2N] Triethylsulfonium bis(trifluoromethylsulfonyl)imide

Deep Eutectic Solvents

[BMIM][$MeSO_3$]:EG 1-butyl-3-methyl imidazolium methanesulphonate: ethylene glycol

[BMIM][$MeSO_3$]:NMAc 1-butyl-3-methyl imidazolium methanesulphonate: N-methylacetamide (NMAc)

CHAPTER 1

Introduction

1.1 Fundamentals, Properties and Applications of Supercapacitors

The class of hybrid capacitors, called supercapacitors (SCs), have attracted attention from both academia and industry due to their high power density resulted from very fast charge-discharge mechanism and longer life cycle [1]. The supercapacitors are also named as ultracapacitors or electrochemical capacitors (ECs) [2]. The prefix super implies the higher specific capacitance than the conventional dielectric capacitors. The growth of SCs commenced in the 50s of 20^{th} century where General Electric and Standard Oil of Ohio conducted the first experiments in US [2]. The capacitance obtained with these first series of SCs was limited to 1 F. During the period of advancements in electrochemical devices, energy and power densities are being considered as the two most important parameters and the relation between these two properties is expressed as Rangone Plot. SCs can deliver more power density than other electrochemical devices e.g. batteries, fuel cells; and higher energy density than classical capacitors (Figure 1.1).

SCs or ECs primarily include two types of capacitors based on the charging mechanism namely pseudocapacitors and electrical double layer capacitors (EDLCs). Pseudocapacitors refer the type of SCs where significant amount of electrochemical response is contributed by the pseudocapacitance. As the name suggests pseudocapacitance is not the real capacitance arising from double layer charging. Pseudocapacitor stores energy by involvement of redox reactions similar to batteries. On the other hand, EDLCs are distinct from batteries and pseudocapacitors as the surface materials do not undergo electrochemical reactions. EDLCs are becoming an interesting and important area of research because of its potential to deliver higher power than the conventional batteries. EDLCs use electrostatic interaction to accumulate energy in Helmholtz double layer on the electrode/electrolyte interface. Double-layer capacitance arises from potential-dependence

of the surface energy stored electrostatically at the interface of the porous and electrically conductive electrodes. Another type of SCs is also available in literature namely Li- ion hybrid supercapacitor [2,3]. However, EDLCs occupy the majority of the commercially available ECs' market due to their technical advancements [1].The use of carbon electrodes in EDLCs also leads to easy waste disposal [4].

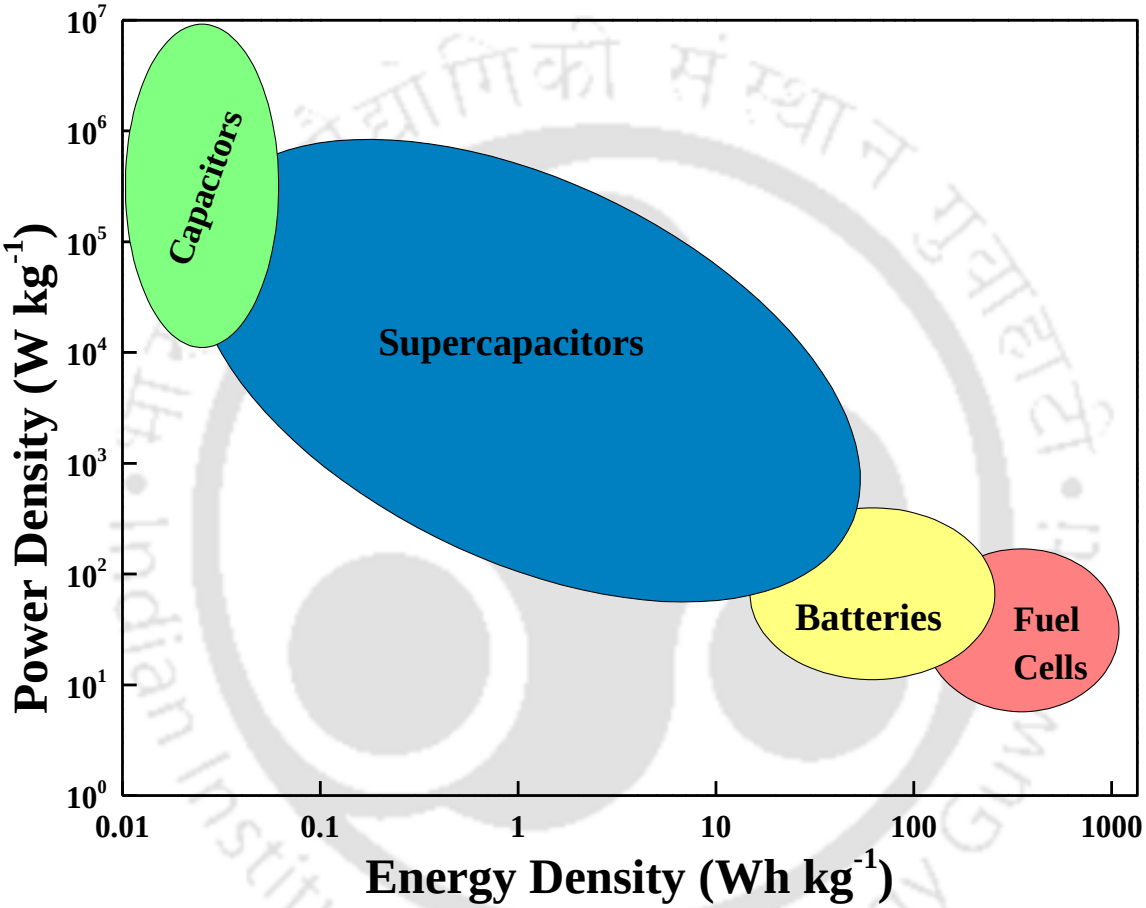

Figure 1.1: Ragone Plot

ECs or EDLCs can replace batteries and fuel cells in wide variety of applications, which demand large amount of energy in a very short span of time. The applications of ECs include portable electronics, fuel cell vehicles like passenger cars, trains and trolleybuses, electric or hybrid electric vehicles (HEVs), aircrafts and smart grids [1,2]. HEVs use ECs to restart the engine once the car stops and hence lead-acid batteries are replaced. Literature suggests that there are nearly 600 thousands HEVs which utilize ECs for engine stop-start

process [2]. Moreover, in energy harvesting system e.g. solar cells and wind turbines, ECs or EDLCs can assist batteries [2]. Recent advances have drawn the attention of space scientists also to use EDLC in space technology. Storage of electrical energy on satellites is a crucial factor. During solar eclipse, solar panels stop generating electricity and a spacecraft needs to rely on stored energy which can be fulfilled by EDLCs since they have the ability to deliver very high bursts of electricity for a few seconds [5].

1.2 Motivation for the Study

Limited sources of fossil fuels and simultaneous increase in population of mankind motivate the scientists and engineers to carry forward the research on alternative energy resources. Additionally, greenhouse gases, air and water pollution from fossil fuels initiate the exploration of sustainable and clean energy storage technologies. Renewable energy resources e.g. solar and wind are highly weather dependent, while biomass energy may lead to deforestation without proper maintenance. Further, the world cannot be totally dependent on renewable energy sources in near future. The energy from renewable energy resources needs to be stored properly and used in future as per requirements. Hence, energy storage is a crucial issue for non-conventional energy resources. Batteries are used in hydropower plants to store the generated energy [2]. Moreover, fuel cells and SCs are also considered as potential energy storage devices [1] for several applications as discussed in previous section.

As mentioned earlier, SCs or EDLCs can deliver energy at a faster rate than other electrochemical device despite their lower their energy density. The energy of EDLCs (E) is related to the capacitance (C) stored and operating potential window (OPW, V) as per equation 1.1 [6]. Moreover, specific power also depends on OPW and is determined using

equation 1.2, where ESR defines equivalent series resistance and *m* is the mass of the active electrode.

$$E = \frac{1}{2}CV^2 \qquad [1.1]$$

$$P = \frac{V^2}{ESR \times m} \qquad [1.2]$$

Hence, this study incorporates the suitable electrolytes for EDLCs to enhance their energy accumulation and discharge. Despite their cost ionic liquids (ILs) were reported as potential electrolytes for EDLCs due to their wider electrochemical stability [6,7] and longer cycle life. However, ILs with imidazolium and pyrrolidium cations were studied the most. In addition to imidazolium based ILs, our study also includes pyridinium and sulfonium cation based ILs to interpret the effects of different cations. Deep eutectic solvents (DESs) have emerged as alternative solvents to ILs in variety of applications [8], yet their study as electrolytes for energy storage is limited. Therefore, DESs are considered as the second choice as electrolytes for this work.

1.3 A Brief Layout of the Dissertation

The dissertation includes screening of electrolytes based on literature survey with respect to their favourable properties e.g. OPW, ionic conductivity and viscosity. A series of ILs comprising three different cationic cores and two types of anion are characterized as electrolytes for graphene based EDLC. Pure ILs as well as their mixtures with organic solvents namely acetonitrile (AN), butyronitrile (BN) and propylene carbonate (PC) are investigated in a three-electrode configuration. Additionally, molecular dynamics (MD) study was also performed to have an insight of diffusive nature of cation and anion. Thereafter the study is directed towards DESs preparation and their application as electrolyte. Conductor like Screening Model-Segment Activity Coefficient (COSMO-

SAC) model is used to predict the eutectic composition of DESs. The brief layout of this thesis work can be found below (Figure 1.2). The detailed work will be discussed in the subsequent chapters.

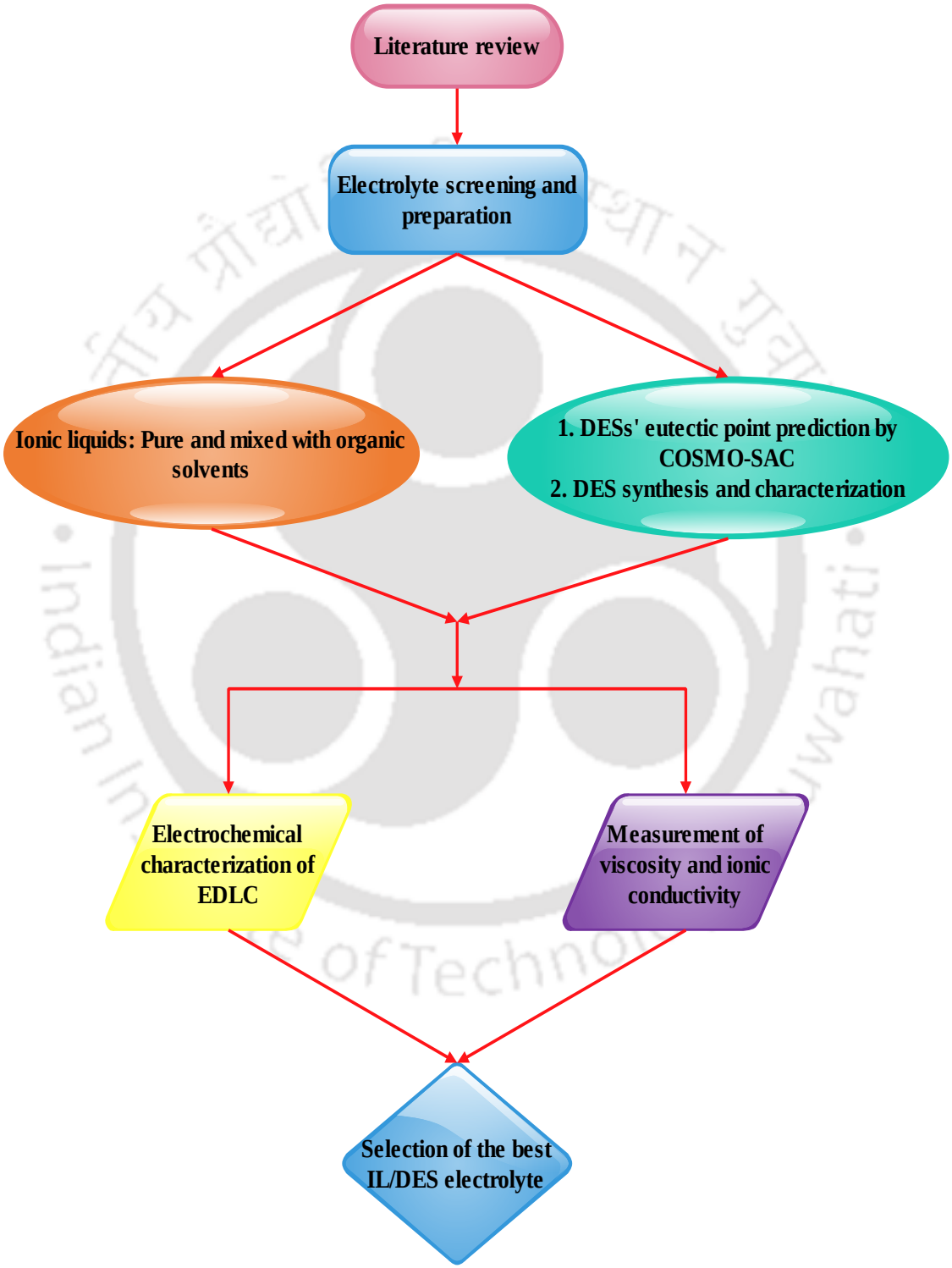

Figure 1.2: A brief layout of the thesis work

CHAPTER 2

Literature Review and Objectives of the Thesis

2.1 Introduction

Figure 2.1 indicates how EDLCs' performance depends on various parameters [1,9] associated with both electrolyte and electrode material. Ionic conductivity and viscosity of the electrolyte are associated with the bulk diffusion of ions and responsible for the ESR of the cell. Electrochemical stability of the electrolyte determines the operating potential window (OPW) of the device and affects energy and power densities. Further, ionic strength of the electrolyte, ion diffusion through the pores, pore diameter and surface area of the electrode material are responsible for the electrode capacitance. Absence of any chemical reaction between electrolyte and electrode indicates better cycle life of the EDLC. Moreover, reactions during charge-discharge process can release heat, which may raise safety issues. Thermal stability of the EDLC determines the operating temperature of the EDLC.

Electrolyte plays a crucial role in determining EDLCs' performance. The electrolytes for ECs can be classified in several categories e.g. liquid electrolytes, solid-state electrolytes, quasi-solid state electrolytes and redox active electrolytes [1]. Redox active electrolytes will not be discussed in this chapter since they are associated with pseudocapacitors. Liquid electrolytes further can be classified into two distinct categories namely aqueous and non-aqueous electrolytes. The non-aqueous electrolytes include organic and ILs electrolytes as suggested by literature [1]. The scope of this study covers only two non-aqueous electrolytes, those are: 1) room temperature ILs (RTILs) and 2) DESs. As already mentioned DESs are yet a new concept in the field of EDLCs. This chapter includes a detailed literature survey on each type of electrolyte used for ECs and their desirable properties.

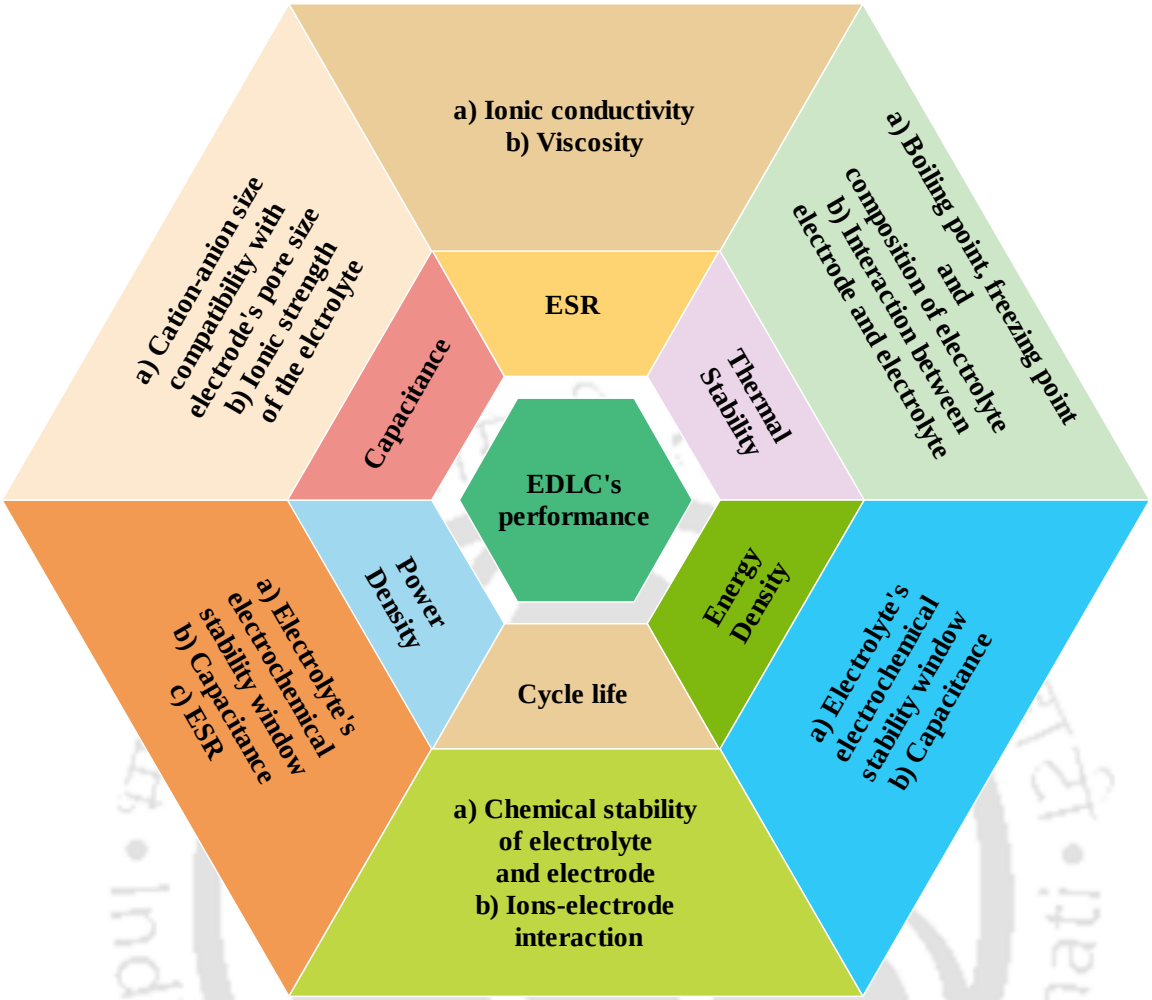

Figure 2.1: Factors affecting EDLCs' performance

2.2 Electrolytes used for EDLCs

2.2.1 Aqueous Electrolytes

Aqueous electrolytes have been already used extensively in electrochemistry and specifically for ECs due to their easy handling and lesser cost compared to organic and IL electrolytes. In 2014, nearly 84.14% of the published literature on ECs reported aqueous electrolytes [1]. The higher ionic conductivity of aqueous electrolytes makes them advantageous over organic and IL electrolytes. This results in lower ESR and enhances the power density. However, most of the aqueous electrolytes suffers from narrower OPW due

to early decomposition of water, which limits the energy density and hence they are not preferable for commercial EDLCs [1].

Aqueous electrolytes mainly consist of different inorganic salt at various concentrations in water. The choice of cations and anions depend on their sizes in both bare and hydrated forms [1], which decides ion diffusion . Additionally, electrochemical stability is affected by the choice of the electrolyte. Aqueous electrolytes are further segregated as acid, alkaline and neutral electrolyte. H_2SO_4 at different molar concentration in water is the common choice of acid electrolyte due to its higher ionic conductivity. Further KOH and Na_2SO_4 are the preferred electrolytes when alkaline and neutral electrolytes are discussed.

The double layer behaviour of 2 M KCl solution was investigated against amorphous MnO_2 by Lee *et al.,* where 200 F g^{-1} specific capacitance was reported with 1.2 V of OPW [10]. Chandrasekaran *et al.,* studied aqueous $Mg(NO_3)_2$ as electrolyte for activated carbon based EDLC [11]. The maximum specific capacitance was reported to be 124.1 F g^{-1} with OPW of 0.8 V and corresponding energy density was found to be 8.5 kWh kg^{-1} for 1 M aqueous solution of $Mg(NO_3)_2$. Further, hierarchically porous carbon based EDLC was tested with four different aqueous electrolytes namely $(NH_4)_2SO_4$, Na_2SO_4, H_2SO_4 and KOH by Zhang *et al.,* [12]. The analysis reported 6 M KOH solution to be the best performing electrolyte with the highest specific capacitance of 61.5 F g^{-1} and the lowest ESR of 2.83 Ω. Moreover, the same electrolyte delivered the most stable cyclic behaviour up to 1.2 V of OPW. Following this work, Barzegar *et al.,* have reported aqueous solutions of KOH, LiCl and Na_2SO_4 for activated carbon based EDLCs [13]. Similar to Zhang *et al.,* this study also stated 6 M KOH to be the most advantageous electrolyte with 129 F g^{-1} specific capacitance, 0.66 Ω ESR and 0.8 V OPW. 1 M KCl showed 1.6 V of OPW with porous

silicon carbide electrode material in a study reported by Kim *et al.*, [14].The observed specific capacitance and energy density were 82.9 F g^{-1} and 29.47 Wh kg^{-1} respectively.

H_2SO_4 in water was investigated simultaneously by various researchers during 2013-2014. Zhang *et al.*, used 1 M H_2SO_4 acid electrolyte to test the performance of hierarchical porous carbon electrode and observed a combination of double layer and pseudo capacitive behaviour [15]. They have reported extra high capacitance of 428.1 F g^{-1}, even though corresponding OPW was limited to only 0.8 V. Capacitive behaviour of liquefied wood fiber containing carbon electrode was examined using 1 M H_2SO_4 electrolyte by Jin *et al.*,[16]. The authors observed 1 V of OPW with specific capacitance of 280 F g^{-1}. Further, the same electrolyte was tested for graphene quantum dots based electrode by Chen *et al.*, where a purely double layer behaviour was observed for an OPW of 0.8 V with a specific capacitance value of 268 F g^{-1} [17]. Hybrid graphene electrode's performance was evaluated using 1 M aqueous H_2SO_4 by Liu *et al.*, where an ultra-high capacitance of 1045.51 F g^{-1} was measured due to faradic reactions with an OPW of 1 V [18]. In a similar study by Jana *et al.*, chemically derived graphene was investigated and pseudocapacitance (375 F g^{-1}) dominating behaviour was observed [19].

Chen *et al.*, studied heteroatom doped carbon nanofiber based EDLC using 2 M aqueous solution of H_2SO_4 and found maximum power density of 186.03 kWh kg^{-1} for 1 V of OPW [20]. Previously same electrolyte was tested by Mun *et al.*, to rate hierarchically structured partially graphitized carbon electrode [21]. However, pseudo capacitive (maximum 120 F g^{-1}) behaviour was observed by the authors and OPW was also limited to 1 V only.

Aqueous solution of KOH and Na_2SO_4 were also studied by Wang *et al.*, to evaluate the double layer nature of flower like porous carbon electrode [22]. They have reported double layer capacitance (294 F g^{-1}) with 1 V OPW for 6 M KOH using three-electrode set up.

Further two-electrode configuration was employed for 1 M Na_2SO_4 where corresponding power and energy densities are 317.5 W kg^{-1} and 15.9 Wh kg^{-1} respectively with 1.8 V OPW. Antifreezing aqueous electrolytes were prepared by dissolving $NaClO_4$ in pure water as well as in binary solvents e.g. methanol-water, ethanol-water, glycerol water and ethylene glycol-water at room temperature [23]. Nearly 1.2 V of OPW was reported for all the electrolytes and $NaClO_4$ in methanol-water was sustained up to -40 °C. The highest specific capacitance was limited to nearly 21 F g^{-1}.

The main drawback observed from the literature in case of aqueous electrolytes is their lower OPW. This results in lower energy storage despite higher specific capacitance. Surprisingly, a recent study reported by Tomiyasu *et al.*, showed that saturated aqueous solution of sodium perchlorate could be stable up to 3.2 V for graphite based capacitor [24]. However, such cases are very rare to locate with aqueous electrolytes. Hence, here the necessity to study organic electrolytes appears.

2.2.2 Organic Electrolytes

Organic electrolytes are the common choice for commercial EDLCs due to their wider OPW (2.5-2.8 V) than aqueous electrolytes [1], which can result into the enhancement of both energy and power densities. However, lower ionic conductivity of organic electrolytes cause reduction in specific capacitance. The fabrication cost of organic electrolyte based EDLCs is more as compared to aqueous one. Tetraethylammonium tetrafluroborate [$TEABF_4$] is the most common organic salt used for EDLCs. Similar to aqueous electrolytes, ion size, ion-solvent interaction, ionic conductivity and viscosity of the solution are the key factors while choosing organic electrolyte for EDLCs or ECs.

Tetraethylammonim (TEA^+) and tetrabutylammonium (TBA^+) salts of hexafluorophosphate (PF_6), tetrafluroborate (BF_4) and perchlorate (ClO_4^-) were solvated

with ethylene carbonate and the effects of anion size on ionic conductivity, viscosity and electrochemical stable potential window (ESPW) were observed by Morita *et al.,* [25]. Lai *et al.,* did a comparative study of electrolytes using 1 M $TEABF_4$ and 1.6 M Tetraethylammonium difluoro(oxalato)borate (TEAODFB) in PC with activated carbon electrode [26]. The authors suggested 1.6 M TEAODFB as better electrolyte than 1 M $TEABF_4$ in terms of ionic conductivity, ESR and capacitance. $TEABF_4$ in adiponitrile (ADN) was experimented as electrolyte for EDLC by Brandt *et al.,* [27]. Even though the ionic conductivity of this novel electrolyte was lesser, the OPW achieved was wider (3.5 V) than standard 1 M $TEABF_4$ in AN.

$TEABF_4$ in AN remains as the most popular choice of electrolyte during the past 10-15 years [1,9] . This is primarily used to evaluate the efficiency of newly developed electrode material for EDLCs. $TEABF_4$ as 1 M solution in AN was studied through carbon aerogel electrode containing EDLC whereby 2.5 V OPW was reported with 9.1 F g^{-1} at 1 A g^{-1} [28]. The same electrolyte was again used by Yang *et al.,* for pore size controlled carbon aerogels where 2.5 V of OPW was observed [29]. However, reported specific capacitance was limited to 20 F g^{-1}. Density functional theory (DFT) study was also performed by Jiang *et al.,* to observe the electrode pore size dependence of EDLCs' capacitance using $TEABF_4$+AN electrolyte [30]. 1 M $TEABF_4$ in methoxypropionitrile and ethylene carbobnate (EC) mixture was formulated by Perricone *et al.,* [31] and EDLC performance was further compared with 1 M $TEABF_4$ in AN and PC. However, the capacitance and resistance performances are not better than 1 M $TEABF_4$ in AN.

$LiPF_6$ at 1 M concentration in EC [32] and PC [33] were also investigated as electrolytes for EDLCs with human hair derived carbon and graphene based electrode respectively. An OPW of 3 V with 126 F g^{-1} was obtained using 1 M $LiPF_6$ with human hair derived carbon

electrode [32]. An ultra-high specific capacitance of 424 F g^{-1} was achieved for nano-porous Co_3O_4 and graphene composite electrode [33]. $TEABF_4$ in PC was examined by Jung *et al.,* for GO-CNT based EDLC, where 3 V of OPW was reported with maximum capacitance of 35 F g^{-1} [34]. Later Zhou *et al.,* used the same electrolyte for fluorine rich carbon electrode whereby double layer behaviour of 168 F g^{-1} with 2.5 V was concluded [35]. $LiClO_4$ salt as in 0.5 M solution PC was tested as supporting electrolyte with polyaniline as the primary electrolyte for graphite EDLC by Zhang *et al.,* [36]. The study revealed consistency up to 30000 cycles with 300 F g^{-1} and 1 V. Further, 1 M solution of $LiClO_4$ salt in PC resulted in pseudo capacitive behaviour with MoO_3 nanosheet and SWCNT composite electrode [37]. Francke *et al.,* tried to replace AN and PC with 1,1,1,3,3,3-Hexafluoropropan-2-ol for different TEA^+ salts [38]. This novel solvent possesses non-flammability in contrast to AN and PC. However, ionic conductivity of the electrolyte solutions in 1,1,1,3,3,3-Hexafluoropropan-2-ol is lower than that in the other two solvents. The observed electrochemical stability was similar for all the three solvents. Literature suggested some other studies using 1 M $TEABF_4$ in AN and PC to rate the performance of novel electrode materials [14,39–41]. The reason behind this preference given to 1 M $TEABF_4$ is its better ionic conductivity and reasonable electrochemical stability. Nitrogen containing carbon nanospheres based electrode was characterized by 1 M $LiPF_6$ in EC electrolyte by Li *et al.,* ,whether reported OPW was limited to 2 V [42].

The basic advantage of organic electrolytes over aqueous is their wider electrochemical stability. The reviewed literature suggests the same even though they observed a lower specific capacitance. Moreover, capacitance is more dependent on electrode morphology rather than type of electrolyte. Despite wider OPW than aqueous electrolytes, the research on alternatives to organic electrolytes commenced to avoid the safety issues related to their

lower thermal stability. Lower ionic conductivity than aqueous electrolytes [1] is another flaw in organic electrolytes.

2.2.3 Ionic Liquid Electrolytes

ILs are basically composed of ions: an organic cation and either organic or inorganic anion, having melting point lower than 100 °C [1]. The flexibility in cation-anion combinations results in a wide variety of ILs. Majority of ILs possess melting point below room temperature and hence they are termed as room temperature ILs (RTILs). ILs are well known for their non-flammability, low volatility, thermal and chemical stability and hence they cover wide range of applications. Moreover, reasonable ionic conductivity and higher ESPW are the two more attractive properties of ILs or RTILs for their use in electrochemical storage device [43]. Reported literature thoroughly reviewed the scope of ILs as energy storage material for EDLCs [7,44]. However, the main disadvantage with pure ILs is their higher viscosity than organic electrolytes at room temperature, which leads to higher ESR. In this regard again the secondary approach with respect to IL and organic solvent mixture electrolyte was developed [6].

ILs, containing imidazolium and pyrrolidinium cations were studied extensively. The most essential properties for EDLCs' electrolyte, e.g. ESPW, ionic conductivity, viscosity and thermal conductivity, are affected by size and type of cations and anions [44]. The literature suggested the following order of cations with respect to reduction stability: piperidinium>pyrrolidinium>ammonium>imidazolium>pyridinium. Commonly used anions are BF_4, PF_6 and bis(trifluoromethylsulfonyl)imide (Tf_2N). Due to the smaller cation size, 1-ethyl-3-methylimidazolium (EMIM) gained the highest attention from the researchers worldwide. The next choice of imidazolium cation is 1-butyl-3-methylimidazolium (BMIM), which offers a higher resistance because of its size. Generally

imidazolium cations offer better ionic conductivity, while pyrrolidinium offers wider ESPW [1]. Wider potential window results in higher energy storage following equation 1.1. On the other hand, higher ionic conductivity and lesser viscosity reduce the ESR by enabling faster charge-discharge and hence facilitates the faster delivery of the stored energy. Therefore, the different properties of the cationic core affect the performance of the EDLC differently. Further, type of anion also influences the electrochemical stability of the ILs [45]. It should be noted that as per standard protocol, the reduction potential corresponds to cathodic limit. On the contrary oxidation potential is determined by the anodic limit. However, literature suggests that the cationic core can undergo oxidation ahead of the anion [45].

Pure [EMIM][Tf_2N] and [EMIM][BF_4] have been the preferred choice of researchers when novel electrode materials for ECs were investigated with IL electrolytes. This is primarily due to its smaller size of the cationic core [6,7]. Polypyrole derived activated carbon electrode material was tested against [EMIM][BF_4] by Wei *et al.*, in 2011. The OPW was found to be 2.3-3 V [46]. The highest specific capacitance reported was 300 Fg^{-1}. Sun *et al.*, investigated the same IL for mesoporous carbon spheres based EDLC which resulted in a specific capacitance of 147 Fg^{-1} [47]. Further Zhou *et al.*, also studied [EMIM][BF_4] for porous carbon sheets containing EDLC. This resulted in an OPW of 3 V along with specific capacitance 147 Fg^{-1} [48]. Moreover, AN diluted [EMIM][BF_4] was also examined by Hantel *et al.*, to measure the capacitance of intercalation like carbon materials. Here the highest specific capacitance of 180 Fg^{-1} was found [49].

[EMIM] cation with different anions have been tested in 2014 by Shi *et al.*, for graphene based EDLC [50]. Among different ion pairs, [EMIM][DCA] gave the best value of specific capacitance (95 Fg^{-1}) due to the lowest viscosity, molecular weight and size among

all the other ILs followed by [EMIM][BF_4] and [EMIM][Tf_2N]. However, the corresponding OPW was quite low (2.3 V), whereas [EMIM][BF_4] and [EMIM][Tf_2N] delivered OPW ~ 4 and 3.5 V respectively. Again, [EMIM][BF_4] was reported to be less viscous than [EMIM][Tf_2N]. This study revealed the effects of anion on the electrochemical behaviour of the EDLC. Further [EMIM][Tf_2N] was examined by Tran *et al.,* where 80 Wh kg^{-1} energy density was reported for binder free EDLC [51]. Aken *et al.,* formulated mixture of [EMIM][BF_4] and [EMIM][Tf_2N] at different weight ratios for onion like carbon based EDLC and compared electrochemical stability to that of neat ILs [52]. Further, specific capacitance, ESR and cyclic stability were also reported.

EMIM cation with bis(fluorosulfonyl)imide anion was also investigated for activated carbon based EDLCs by Handa *et al.,* [53]. The results obtained with this neat IL were comparable to that of 1.96 M triethylmethylammonium tetrafluoroborate dissolved in PC. The authors reported higher ionic conductivity of this IL than [EMIM][Tf_2N]. An OPW of 3.5 V and corresponding specific capacitance of 174 F g^{-1} were obtained for graphene-derived carbon EDLC with [EMIM][Tf_2N] in AN [54].

[BMIM][BF_4] mixed with AN was found to have OPW of 3.5 V when tested for activated carbon based EDLC [55]. [BMIM][Tf_2N] was used by Qiao *et al.,* with different varieties of Si-nanowire based electrodes and the observed OPW was limited to 1.7 V only [56]. Moreover, different specific capacitance values were also reported for different electrodes. Earlier BMIM cation with PF_6 and BF_4 anions were investigated for ECs by Balducci *et al.,* and obtained results were compared to 1 M $TEABF_4$ in PC [57]. Among all three, [BMIM][PF_6] provided the best cathodic and anodic stability limits. N-butyl-n-methylpyrrolidinium bis(trifluoromethane sulfonyl) imide ([PYR_{14}][TF_2N]) IL was studied as organic solvent diluted electrolyte for EDLC by Ruiz *et al.,*[58]. The authors reported

that IL+BN mixture provided the highest specific capacitance (125 Fg^{-1}) and widest range of operating temperature (-20 to 80 ºC). The IL+solvent electrolytes showed ESPW of 4-6 V. The same IL was further used to evaluate the performance of cellulose nanofibrils modified activated carbon electrode by Li *et al.*,[59]. This particular combination of electrolyte and electrode resulted in OPW of 3 V and the observed specific capacitance was limited to nearly 85 F g^{-1}. A series of imidazolium and ammonium cations comprising of alkyl, vinyl, allyl and 1-butenyl groups with Tf_2N and BF_4 anions were examined as EDLC's electrolyte by Orita *et al.*,[60]. The authors reported that substitution of allyl group induces viscosity reduction. The study basically compared the specific capacitance, viscosity and ionic conductivity among several ILs and organic solvent diluted ILs.

Triethylammonium bis(tetrafluoromethylsulfonyl)amide neat IL and solution in AN was explored by Timperman *et al.*, as an electrolyte for activated carbon based EDLC [61]. The favourable ESPW against Pt electrode and OPW were found to be 4 and 2.5 V respectively. The same group of authors also reported a variable temperature study on AN diluted tributylphosphonium tetrafluoroborate IL as electrolyte for EDLC [62]. The OPW was limited to 1.5 V and the authors commented that the specific capacitance was comparable to aqueous electrolytes. Three different types of sulfonium cations with Tf_2N anion along with $[PYR_{14}][Tf_2N]$ were investigated by Rennie *et al.*,[63]. The authors suggested that diethylmethyl sulfonium Tf_2N can perform better than $[PYR_{14}][Tf_2N]$ in terms of power and energy density at room temperature despite its lower OPW (2.7 V). A study by Mousavi *et al.*, covered several ionic liquids with structurally diverse anions (BF_4, trifluoromethanesulfonate and Tf_2N) and cations (imidazolium, ammonium, pyridinium, piperidinium,pyrrolidinium) [64].The study analysed the effects of anion and cation on ESPW of neat ILs with respect to glassy carbon electrode and specific capacitance for a

mesoporous carbon model electrode. Further pyridinium based room temperature protic ILs were examined with metal oxide based electrode containing EC [65]. The authors confirmed the presence of pseudocapacitive behaviour. The specific capacitance was reported to be 40-50 F g^{-1}.

Ong *et al.*, employed molecular dynamics (MD) simulations and density functional theory (DFT) calculations to investigate the cathodic and anodic stable potential limits of six RTILs formed from a combination of two common cations, BMIM and N,N-propylmethylpyrrolidinium and three anions PF_6, BF_4 and Tf_2N [66]. This study suggested that pyrrolidinium based ILs possessed lower cathodic stability than BMIM. Further it has been observed that anodic stability of the anions behaved differently for different cation.

2.2.4 Deep Eutectic Solvent Electrolytes

DESs constitute another class of newly emerging solvents, which is earning a lot of attention from the scientific and industrial community for their attractive physicochemical properties. A DES is an eutectic mixture of a hydrogen bond acceptor (HBA) and a hydrogen bond donor (HBD) which are associated through hydrogen bond interactions, when those are mixed in a specific molar ratio [67]. The newly formed phase is characterized by a freezing point, which is lower than the fusion or melting temperatures of both the constituent materials. This difference in the temperatures is defined as the depression in freezing point of a DES. Although DESs share many characteristics with conventional ILs (non-reactive with water, non-volatile, biodegradable) [68], they cannot be labelled as ionic liquids because they are not entirely comprised of ions . Further deep eutectic solvents can be prepared from non-ionic species as well [67]. Most of the of the studies on DESs were primarily focused on quaternary ammonium and imidazolium salts as the hydrogen bond acceptor (HBA) with a hydrated metal salt or a suitable hydrogen

bond donor (HBD) such as amides, alcohols, glycols and carboxylic acids [68]. Choline chloride (ChCl) was the most commonly used HBA as suggested by literature [68]. Table 2.1 represents the conventional types of DESs as suggested by Smith *et al.,* [68].

Table 2.1: Classification of DESs

Types of DES	General Notation	
Type I	$Cat^+X^- zMCl_x$	M= Zn, Sn, Fe, Al, Ga and In
Type II	$Cat^+X^- zMCl_x.yH_2O$	M= Cr, Co, Cu, Ni and Fe
Type III	$Cat^+X^- zRZ$	Z= $CONH_2$, COOH and OH
Type IV	$MCl_x + RZ$	M= Al, Zn and Z= $CONH_2$, OH

The use of deep eutectic solvents as electrolytes in EDLCs or supercapacitors have not been explored in depth until very recent years. Ju *et al.,* reported ChCl based DESs having glycerol, malonic acid and urea as HBDs for EDLC [69].The OPW observed in this study was limited to 2 V. Electrochemical characterization of DES having sodium nitrate and N-methyl acetamide (NMAc) for carbon based supercapacitor application was done by Zaidi *et al.,* [70]. Reasonable results were obtained at 80 °C with a two-electrode configuration at an operating voltage up to 2.0 V. The cell remained stable after 1000 charge-discharge cycles. However, presence of psuedocapacitance (~ 302 Fg^{-1}) was also reported. Further, the combination of ChCl and glycerol was again studied against platinum, gold and glassy carbon as working electrodes [71]. The electrochemical stability was found to be nearly 1 V only. Zaidi *et al.,* further investigated DESs based on NMAc and lithium salts of PF_6, Tf_2N and NO_3 [72]. Previously, the combination of $LiTf_2N$ and NMAc was also studied by Boisset *el al.,*[73]. The authors characterized the DES as electrolyte for activated carbon based EDLC as well as for Li ion batteries with $LiFePO_4$ electrode. A protic IL, sulfonium bis(trifluoromethylsulfonyl)imide was tested as HBA with two HBDs namely formamide

and trifluoroamide to apply as electrolytes for EDLCs [74]. The DESs were characterized at different potential window and corresponding specific capacitance were measured. A DES consisting of $LiTf_2N$ salt and formamide as HBA and HBD respectively; was prepared and used as electrolyte for activated carbon based EDLC by Phadke *et al.*, [75]. The authors measured energy density close to 30 Wh kg^{-1} at 2.4 V of OPW with this system.

2.2.5 Solid or Quasi Solid-State Electrolytes

The solid-state electrolytes have gained great interest in the recent past since it is liquid-leakage proof and has the advantage of easy packaging and fabrication. Moreover, solid state electrolytes can act as the ion transport media and electrode separators simultaneously [1]. Majority of the work on solid or quasi solid-state electrolytes covers polymer-based electrolytes. However, inorganic materials e.g. ceramic based solid electrolytes are the least explored. Polymer based electrolytes are further classified as solid polymer electrolyte (SPE), gel polymer electrolyte (GPE) and polyelectrolyte. SPE is totally solvent free and formed by combining a polymer and a salt. GPE is also termed as quasi solid-state electrolytes. It is composed of a polymer and a conducting media dissolved in a solvent. Polyelectrolytes are made of charged polymer chains. Due to the presence of a liquid phase GPE, it possesses the highest ionic conductivity among all the three types. Hence GPE acts as the dominant electrolyte in the field of solid-state electrolytes.

GPE consisting of polyvinylpyrrolidone (PVP) and PVP–polyvinylacetate (PVP–PVAc) as base polymers and $TEABF_4$ as the electrolyte salt were reported by Matsuda *et al.*,[76].The ionic conductivity at 25 °C was measured to be 10^{-3} S cm^{-1} and calculated discharge capacitance was 38 F g^{-1} for activated carbon based electrodes. Further, in the recent past several studies were conducted with GPE. Pandey *et al.*, experimented IL based GPEs containing [EMIM][Tf_2N] incorporated with ploy(ethyleneoxide) based Mg^{2+} and Li^{+} ion

conducting polymers [77]. The ionic conductivity of the electrolytes at ambient temperature was measured to be ~10^{-4} S cm^{-1}. The ESPW and OPW of the electrolytes were 4 and 2 V against stainless steel and MWCNT electrodes respectively. The EDLC cells with Mg and Li-based polymer electrolytes delivered capacitance of 2.6-3 and 1.7-2.1 F g^{-1} respectively. A combination of [BMIM][Tf_2N] IL and poly(methyl methacrylate) was investigated for graphene based EDLC whereby OPW of 3 V was observed [78]. A novel boron cross-linked graphene oxide/polyvinyl alcohol nanocomposite gel with KOH solution was chosen as GPE in activated carbon based EDLC [79]. The electrolyte showed potential window of nearly 1 V with specific capacitance up to 140 F g^{-1}.

Syahindah *et al.,* performed EDLC studies using GPE based on poly(vinyl pyrrolidone)/poly(vinylidenefluoride-co-hexafluoropropylene) containing 1-butyl-2,3-dimethylimidazolium BF_4 IL [80]. The electrolyte resulted in ionic conductivity of 2.92 × 10^{-3} S cm^{-1} and the widest OPW of 2 V. High performance GPE having $LiClO_4$ gel and poly(arylene ether ketone)/poly (ethylene glycol) grafted poly(arylene ether ketone) polymer composite was studied by Ruiqi *et al.*,[81].The authors claimed that the microporous polymer electrolyte had ionic conductivity as high as 8×10^{-3} S cm^{-1} and delivered specific capacitance of 118.63 F g^{-1} with activated carbon electrode. They also synthesized solvent free SPE based on [EMIM][Tf_2N] and poly(ethylene oxide)-copoly(propylene oxide) . The study revealed 3 V OPW with porous carbon electrode and power density of 12.3 kW kg^{-1} [82]. Succinonitrile and [BMIM][BF_4] were combined with copolymer poly(vinylidene fluoride-co-hexafluoropropylene) to form thermostable GPE by Pandey *et al.*, [83]. The authors suggested ESPW ~ 5.5 V even though OPW was limited to only 2.5 V when applied for activated carbon EDLC. The GPE-activated carbon system resulted in nearly 176 F g^{-1}. Around 80% of the initial capacitance was observed after 10000

cycles. SPE based on fumed silica nanoparticles, hydroxylethyl cellulose, EMIM trifluoromethanesulfonate (IL) and Mg trifluoromethanesulfonate was prepared by Chong *et al.,* to characterize its electrolytic behaviour for activated carbon based EDLC [84]. This study suggested that use of silica nanoparticles brought enhancement on specific capacitance (25 F g^{-1}). However, observed OPW was limited to 2 V. In the same year, a novel GPE composed of polyurethane-poly(acrylic acid) and 1 M KOH was used in order to apply them as electrolytes by Wang *et al.*,[85]. The ionic conductivity was observed to be 10^{-2} S cm^{-1}. The potential window was found to be 1 V due to the use of aqueous KOH when tested against acid treated carbon paper electrode. Recently, the scope of a poly(vinyl alcohol) based SPE having sodium trifluoromethanesulfonate salt and [BMIM][Br] was explored by Farah *et al.*,[86]. The electrochemical studies resulted in OPW of 1 V and specific capacitance of 16.32 F g^{-1} for carbon coated aluminium electrode.

2.3 Other Applications of Ionic Liquids and Deep Eutectic Solvents

ILs or RTILs are considered as effective solvents for numerous chemical engineering applications. In this regard, DESs have also emerged as substitutes to ILs in past two decades. The lower cost and ease of preparation accelerate the research on DESs. This section includes a brief literature survey on some applications of ILs and DESs other than electrolytes for ECs to interpret their ability to serve as potential solvents for different scientific and industrial practices.

2.3.1 Ionic Liquids

Reported literatures suggest several applications of ILs for the development of science and technology. However, only a few of recent literature will be discussed here. Yue *et al.*, reviewed different types of task-specific ILs to be used as catalysts or solvents in organic reactions [87].This study discussed ILs of different categories studied previously e.g.

acidic, basic, chiral and OH- group containing ILs. The use of [BMIM][Cl] IL as a medium for electrodeposition of gold-platinum alloy nanoparticles on glassy carbon electrode was reported by Safavi *et al.*, [88]. Liu *et al.*, investigated the thermal performance of [HMIM]BF_4] as graphene added heat transfer fluid for solar energy collectors [89]. EMIM ethylsulfate IL was used as solvent for extraction of toluene from a mixture of cycloalkanes for room temperature liquid-liquid extraction [90]. A review study by Ventura *et al.*, extensively discussed the effectiveness of ILs as extraction and separation media for bioactive compounds e.g. fats, proteins, amino acids, vitamins, essential oils, pharmaceuticals and drugs [91]. Recently a study on separation of hydrocarbon gases were conducted by Makino *et al.*, using imidazolium and phosphonium based RTILs [92]. BMIM cation with three different anions were considered as liquid membrane for phenol removal [93]. This work covered both experimental and optimization research. Further BMIM thiocyanate IL supported by metal-organic framework was explored for CO_2 capture by Gupta *et al.*,[94]. A recent review study done by Hijo *et al.*, explained thoroughly the applications of ILs or RTILs in food and bioproduct [95]. Watanabe *et al.*, analysed the use of ILs as electrolytes for energy storage devices e.g. Li/Na, Li-S, Li-O_2 and fuel cells [44]. ILs were used successfully to remove unwanted compounds e.g. sulphur and nitrogen containing compounds, aromatics, naphthenic acids and asphaltenes from refinery feedstock as suggested by Palou and Luque [96]. A series of ILs consisted of imidazolium, pyridinium, ammonium and phosphonium cations were investigated as chemicals for enhanced oil recovery process by Dahbag *et al.*, [97]. Allyl based IL facilitated thermal dehydrogenation of ethylene diaminebisborane was reported by Banerjee *et al.*, in 2016 [98]. A combination of experimental and simulation studies were performed by Dehury *et al.*, for extraction of butanol from aqueous phase [99]. Further,

solid-liquid equilibrium studies were carried out by evaluating the solvation efficiency of several ILs for cellulosic materials [100]. This study by Mohan *et al.*, includes both quantum chemical and experimental studies. A recent development by Le *et al.*, published in May 2020 illustrated the IL-protein complex interactions for better understanding of IL catalysed biological processes [101].

2.3.2 Deep Eutectic Solvents

DESs are considered as emerging solvents with comparable physicochemical properties to ILs. The review by Tome *et al.*, published in 2018 clearly depicted how ChCl based DESs have dominated the research on DESs from the beginning of 21st century [102]. The authors discussed the applications of DES mainly in the fields of polymer science, metal processing and nanomaterials. Previously Gracia *et al.*, compared the physicochemical properties of several reported DESs based on ChCl, ammonium and phosphonium salts and also analysed their use for gas separation primarily for absorption of CO_2 and SO_2 [103]. A work by Malaquis *et al.*, reported electrodeposition of Cu-In alloy using ChCl:Urea (1:2) DES for photovoltaic applications [104]. ChCl based DESs with urea and glycerol as HBDs were investigated as surfactants for enhanced oil recovery by Hadj-Kali *et al.*,[105]. A series of DESs having $ZnCl_2$ as HBA were prepared and characterized for electrolytic use by Bagh *et al.*,[106]. Further ChCl: p-chlorophenol at 1:2 molar ratio was prepared and used as extractive solvent by Farajzadeh *et al.*, for separation of polycyclic aromatic hydrocarbons from aqueous phase [107].

A phosphonium based DES was explored as the catalyst for esterification reaction of oleic acid with glycerol by Williamson *et al.*,[108]. DES was considered for gold nanoparticles synthesis to be used in enzymatic biosensor by Krishnan *et al.*, [109]. A review study by Morales *et al.*, highlighted the free radical polymerisation and the use of DES as functional

materials in different applications. The authors primarily evaluated the literature based on ChCl consisting DESs [110]. Moreover, ChCl based DES was also employed to functionalize graphene derivative as flame reductant [111]. Nevertheless, DESs without quaternary ammonium salts were also suggested for solvent extraction operation [112] and heat transfer fluids [113,114]. For ammonia absorption, a DES prepared with [BMIM][$MeSO_3$] and urea was also a viable option [115].

2.4 Knowledge Gap in the Literature

As per the discussion in section 2.2, it can be well understood that IL based electrolytes are the preferred sustainable choices for the researchers. In this regard, primarily cations like imidazolium and pyrrolidinium remained as the core application. However scant literature is observed with cations e.g. pyridinium, sulfonium, phosphonium and ammonium with respect to the applications of these ILs. Therefore, this thesis work involves pyridinium and sulfonium group containing ILs with BF_4 and Tf_2N anions respectively along with other frequently used imidazolium ILs. Additionally, one unfamiliar imidazolium IL namely 1-propyl-3-methylimidazolium Tf_2N is also investigated as EDLC's electrolyte. The choice of three different cationic cores and two anions is made to encapsulate the effects of IL's molecular structure (alkyl chain) on the performance of the EDLC.

The recent developments on DESs encourage us to explore their scope in the domain of EDLCs. Moreover, till date only a handful of DES electrolytes were reported which further builds interest on electrolytic behaviour of DES. The feasible association between several HBAs and HBDs gives the advantage of preparation of a DES according to their application. Hence, considering the requirement of favourable ionic conductivity of the DES, IL is used as HBA in this work. Further, the limitation with majority of the studied DESs is their high viscosity [8,67,110,116]. Here the disadvantage of using them as

electrolytes comes into the picture. Hence, this study aims at preparation of low viscous DESs for EDLC application.

2.5 Objectives of the Thesis Work

The thesis work is based on mainly four basic objectives as mentioned below.

1. Electrochemical Characterization of IL-based Electrolytes

The primary requirements for being an effective electrolyte for EDLCs are wider OPW, better charge storage capacity, higher power densities and longer cycle life. Hence, electrochemical characterization of pure ILs as well as their mixtures in co-solvents was performed and subsequently OPW, specific capacitance (*C*), ESR, specific power and energy were evaluated.

2. Measurement of Transport Properties of IL-based Electrolytes

Based on the electrochemical performance of ILs, some of the favourable electrolytes were further used to measure ionic conductivity and viscosity. Evaluation of these two transport properties predicted the effects of dilution of ILs with different solvent concentration. Moreover, molecular dynamics (MD) simulation tool was also adopted to provide microscopic insights through the diffusional behaviour of ions.

3. Preparation of DESs

For novel DESs, the preparation procedure needs to be done iteratively to determine the appropriate HBA: HBD ratio and corresponding freezing point so as to satisfy the definition of eutectic mixture. In order to eliminate experimental iterative process, Conductor like Screening Model-Segment Activity Coefficient (COSMO-SAC) thermodynamic model was chosen for determination of eutectic points of the DESs. Further DESs were prepared following standard experimental procedure according to the molar ratio obtained from computation.

4. Physical and Electrochemical Characterization of DESs

Initially ^{1}H and 2-D NMR analysis were executed for the DESs. Thereafter physical properties of the DESs e.g. density, viscosity and ionic conductivity were measured. Further thermogravimetric analysis (TGA) of the DESs was carried out. Finally, electrochemical performance was investigated using CV and GCD techniques.

CHAPTER 3

Materials and Methods

3.1 Materials

3.1.1 Electrolytes

ILs, namely 1-ethyl-3-methylimidazolium bis(trifluoromethylsulfonyl)imide ([EMIM][Tf_2N]), 1-propyl-3-methylimidazolium bis(trifluoromethylsulfonyl)imide ([PMIM][Tf_2N]), 1-butyl-3-methylimidazolium bis(trifluoromethylsulfonyl)imide ([BMIM][Tf_2N]), 1-ethyl-3-methylimidazolium tetrafluroborate ([EMIM][BF_4]), 1-butyl-3-methylimidazolium tetrafluroborate ([BMIM][BF_4]), 1-butyl-4-methylpyridinium tetraflouroborate ([BMpy][BF_4]) and Triethylsulfonium bis(trifluoromethylsulfonyl)imide ([TESu][Tf_2N]) were considered for our work. Primarily acetonitrile (AN), propylene carbonate (PC) and butyronitrile (BN) were used as co-solvents.

Table 3.1: List of chemicals

Chemical Name	Purity Grade	Supplier
[EMIM][Tf_2N]	≥ 98% (HPLC)	Sigma-Aldrich
[PMIM][Tf_2N]	≥ 98% (H-NMR)	Sigma-Aldrich
[BMIM][Tf_2N]	≥ 98%	Sigma-Aldrich
[EMIM][BF_4]	≥ 98% (HPLC)	Sigma-Aldrich
[BMIM][BF_4]	≥ 98% (BFSA)	Sigma-Aldrich
[BMPy][BF_4]	>97% (T)	Sigma-Aldrich
[TESu][Tf_2N]	>95% (qNMR)	Sigma-Aldrich
AN (bp: 81-82°C, mp: -45 °C)	99.8%	Sigma-Aldrich
PC (bp: 240 °C, mp: -55 °C)	99.7%	Sigma-Aldrich
BN (bp: 115 °C, mp: -112 °C)	99%	Sigma-Aldrich
[BMIM][MeSO3]	95%	Sigma-Aldrich
NMAc	99%	Sigma-Aldrich
EG	Extra pure AR	SRL Pvt. Ltd

1-butyl-3-methyl imidazolium methanesulphonate ([BMIM][$MeSO_3$]) was chosen as HBA for IL-based DESs. In this regard N-methylacetamide (NMAc) and ethylene glycol (EG)

were taken as the corresponding HBDs. Table 3.1 reports the chemical purities and the corresponding supplier. All the ILs and HBDs were vacuum dried at 70-100 °C for 10-12 hrs to remove volatile impurities. The Table below (Table 3.2) represents the molecular structure of the studied electrolytes.

Table 3.2: Molecular structures of cations, anions, HBA and HBDs

Ionic Liquids	
Cations	**Anions**
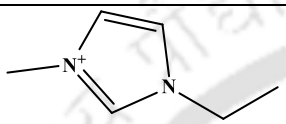 1-Ethyl-3-methylimidazolium	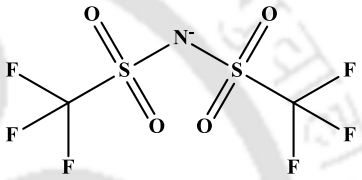 bis(trifluoromethylsulfonyl)imide
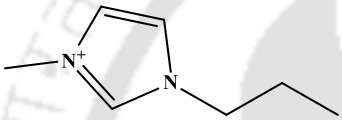 1-Propyl-3-methylimidazolium	
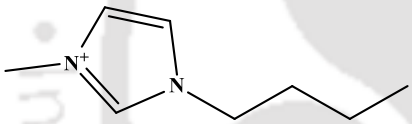 1-Butyl-3-methylimidazolium	
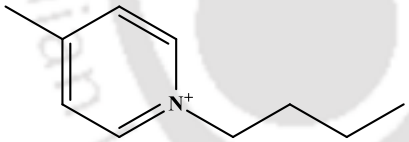 1-Butyl-4-methylpyridinium	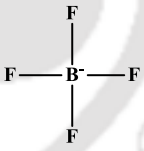 Tetrafluoroborate
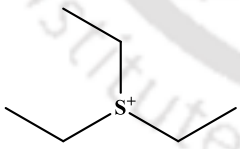 Triethylsulfonium	

Deep Eutectic Solvents	
Hydrogen Bond Acceptor (HBA)	**Hydrogen Bond Donors (HBDs)**
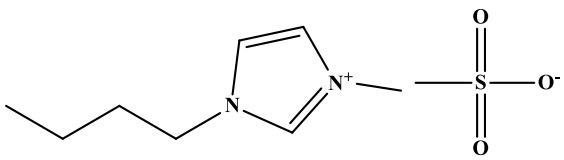 1-Butyl-3-methylimidazolium-methanesulphonate	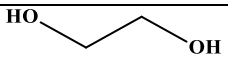 Ethylene Glycol
	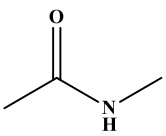 N-Methylacetamide

Initially 1-alkyl-3-methylimidazolium (AMIM) Tf_2N ILs with organic solvent AN were taken for analytical studies. The amount of IL in the solvent was considered in terms of molar concentration, which were 2, 1 and 0.5 mol dm^{-3}. These three molar concentrations were nearly equivalent to 25, 57 and 75 weight percentage (wt. %) of AN in the electrolyte solution. However, for other ILs due to the difference in molecular weight, the same molar concentrations do not result the corresponding wt. %. Hence, to maintain the consistency of the study, for other ILs the same wt. % of organic solvents were maintained. Table 3.3 show the solvent wt. % and corresponding abbreviations used for the IL electrolytes.

Table 3.3: Composition of IL+ co-solvent electrolytes and corresponding abbreviations

wt. % of organic solvent	Abbreviation
25	IL+AN/PC/BN_I
57	IL+ AN/PC/BN _II
75	IL+ AN/PC/BN _III

3.1.2 Electrodes

All the electrochemical experiments were performed using the three-electrode method. This particular set up requires three different electrodes which are working electrode (WE), reference electrode (RE) and counter electrode (CE). Two different WEs: a) exfoliated carbon electrodes (reduced graphene oxide, RGO) for capacitive measurements and b) glassy carbon electrode to evaluate the ESPW of novel DESs were employed. The porous exfoliated carbon sheet electrodes comprising of butyl rubber binder were supplied by Vikram Sarabhai Space Center, Thiruvanthapuram. BET surface area of the electrodes was found to be 635 m^2/g in presence of binder with average pore size of 2.6 nm as measured by Quantachrome (Autosorb-IQ MP) surface area and pore size analysis. Glassy carbon electrode was prepared by uniform heating of glassy carbon powder and paraffin wax (5:3 wt/wt ratio) at 60 ºC followed by moulding in a rectangular shape and inserting a Cu wire

at the middle of the mould [117]. Subsequently the mould was cooled to room temperature. Glassy carbon powder (spherical, 2-12 µm, 99.5% trace metals basis) and paraffin wax (99%) were purchased from Sigma Aldrich and Loba Chemie Pvt. Ltd respectively. Further, the choice of RE depends on the composition of electrolytes. The standard RE namely a) Ag/Ag^{+},0.1 M $AgNO_3$ in AN+IL solution and b) Ag/AgCl, 0.1 M tetrabutylammonium chloride in AN+ IL were adopted for IL based electrolytes as per literature [118]. The IL, used as electrolyte, was also employed to prepare the solution for RE's glass compartment. However, ILs namely [EMIM][Tf_2N] and [EMIM][BF_4] went through some chemical changes when mixed with $AgNO_3$ and tetrabutylammonium chloride salts. Therefore, Ag wire [119] was used for these two ILs. Again, there is no such standard RE for DES. Hence Ag wire was employed as pseudo RE for DES electrolytes [70] . For all the systems, spiral platinum (Pt) electrode was used as CE. Ag and Pt electrodes were collected from CH instruments Inc. (Austin. USA). The salts extra pure $AgNO_3$ and tetrabutylammonium chloride (> 97%) were supplied by Sisco Research Laboratories Pvt. Ltd and Sigma-Aldrich respectively.

3.2 Evaluation of Eutectic Composition and Preparation of DESs

3.2.1 Eutectic Temperature and HBA: HBD Molar Ratio

Preparation of DESs involves heating and continuous stirring of a definite ratio of HBA: HBD at 100 ºC until a clear liquid is formed [8]. Subsequent cooling of the prepared DES is done to determine the freezing point. For new DESs, the preparation procedure needs to be done iteratively to determine the appropriate HBA: HBD ratio and corresponding freezing point to satisfy the definition of eutectic mixture. However, this process seems to be not economical regarding the use of chemicals. Literature suggests a handful of computational approach for eutectic point calculation of DES using Conductor like

Screening Model-Segment Activity Coefficient (COSMO-SAC) [120] and Perturbed-Chain Statistical Associating Fluid Theory(PC-SAFT) [121–123] models. Further, PC-SAFT thermodynamic model was successfully applied for vapour pressure calculation of DESs [124]. COSMO-SAC model was used also applied successfully to predict activity coefficient of solid ethylene diaminebisborane in ILs [98].

This work incorporates prediction of eutectic temperature and corresponding composition of HBA and HBD using COSMO-SAC approach. Literature reports agreement between experimental findings and predicted data from COSMO-SAC [114,125]. COSMO-SAC is a variant of Conductor like Screening Model for real solvent (COSMO-RS) [126] and can be used to predict activity coefficient along with other thermodynamic properties. It considers the molecule as a segmented surface and computes the chemical potential of each segment using statistical mechanical framework. The chemical potential is further used to compute the segmental activity coefficients. The summation of all the segmental activity coefficients results in the activity coefficient of the molecule. More details of this model was discussed explicitly in reported literature [127]. To evaluate the eutectic point of DES, the concept of mutual solubility was applied. Initially activity coefficients of HBA and HBD as a function of temperature were calculated using COSMO-SAC. Further, the eutectic composition and temperature were calculated employing the solid-liquid equilibrium (SLE) theory (equation 3.1) as per standard chemical engineering thermodynamics [128]. The basic requirements to apply COSMO-SAC are the freezing point or melting point (T_m) and heat of fusion (ΔH_{fus}) data of each components, which are reported in Table 3.4.

$$\ln(\gamma_{solute} x_{solute}) = \frac{-\Delta H_{fus}}{RT_m}\left(\frac{1}{T} - \frac{1}{T_m}\right) \qquad [3.1]$$

where, γ_{solute} and x_{solute} are the activity coefficient and mole fraction of the solute respectively.

Table 3.4: Melting point and heat of fusion data for COSMO-SAC calculations

Name of the compound	T_m (K)	ΔH_{fus} (kJ/mol)
[BMIM][$MeSO_3$][129]	347.65	12.86
EG [130]	260.80	11.62
NMAc [131]	303.72	10.11

Prior to COSMO-SAC calculations, molecular structures were first drawn using Gauss View 5.0 [132] software followed by geometry optimization in Gaussian 09 [133] using density functional theory (DFT) B3LYP [134] along with 6-311G* basis set. Thereafter the COSMO files were obtained from Gaussian 09 by the BVP86/TZVP/DFT level of theory. Standard global adjustable parameters such as surface area of the segment (=6.32 $Å^2$), misfit energy interaction constant (=8419 kcal $Å^4$ mol^{-1} e^{-2}), cut off for hydrogen-bonding interaction (= 0.0084 e $Å^{-2}$) and hydrogen-bonding interaction constant (= 75,006 kcal $Å^4$ mol^{-1} e^{-2}) were adopted to compute activity coefficient [114] using COSMO-SAC. The computation procedure basically involves three steps. Initially the activity coefficient was taken to be unity and ideal case mole fractions of the solute were calculated as a function of temperature using equation 3.1. This step is first done considering HBA as the solute and HBD as the solvent. Further the procedure is repeated by inverting the components since mutual solubility data is required for SLE predictions. The mole fractions obtained from step 1 were employed to compute the non-ideal liquid phase activity coefficient by invoking the COSMO-SAC model. This step was also repeated twice as previous step. With the activity coefficients obtained in step 2, mole fractions of HBA and HBD were computed corresponding to the SLE equation unless both the sides of SLE data plots satisfy each other. The desired mole ratio for HBA: HDB was found to be 1:3.5 and 1:2 for

[BMIM][$MeSO_3$]:EG and [BMIM][$MeSO_3$]:NMAc respectively. The detailed discussion and SLE plots are provided in Chapter 6.

3.2.2 Preparation of Deep Eutectic Solvents

Initially the constituent compounds of DES were inserted in a flat bottom flask following the HBA:HBD ratio obtained from COSMO-SAC calculations (Figure 3.1). A reflux condenser was fitted to the flask to prevent any solvent loss due to vaporization. The HBA-HBD mixture was subjected to heating at ~70 °C (343.15 K) with continuous stirring for 12-24 hours so that a homogenous solution is obtained [67]. Further, the liquid obtained is allowed to cool down for 12-24 hours. However, no crystal formation or solidification was observed at room temperature.

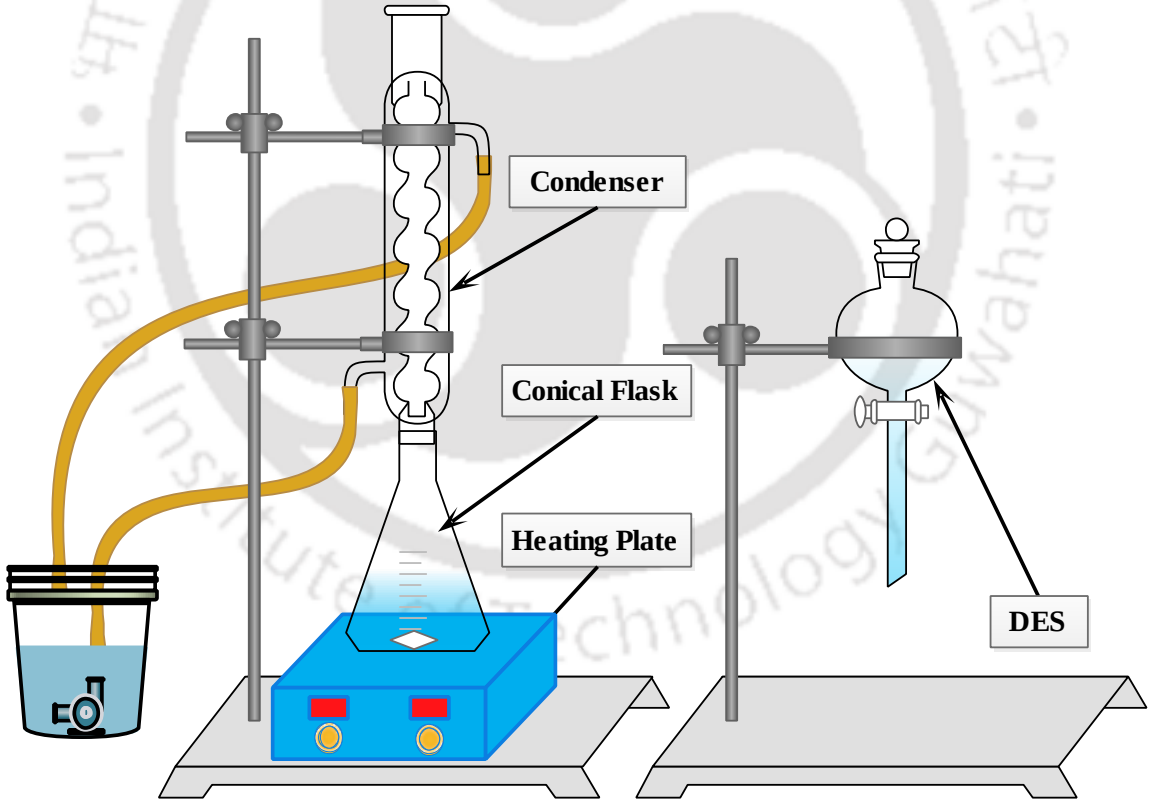

Figure 3.1: Preparation of DES

3.3 Physical Characterization of Deep Eutectic Solvents

3.3.1 Water Content Measurement

The presence of water affects the electrochemical stability of the electrolytes. Hence, determination of the moisture content for the laboratory prepared DESs was essential. The water content was analysed by Karl Fischer Titration (KFT) method using Metrohm 787 KF Titrino. KFT is a reagent-based titration in which the reagent reacts with water to convert water into a non-conductive chemical whereby dry methanol is used as the base solvent. Karl Fischer reagent (526 KFR) was collected from Thermo Fisher Scientific India Pvt. Ltd for this study.

3.3.2 Nuclear Magnetic Resonance (NMR) Spectroscopy

NMR spectroscopy primarily reveals the detailed and quantitative information on the molecular structure, functional groups, topology and dynamics of molecules in solution and the solid state [135]. The sample is initially placed within the high-power magnetic field and exposed to the radio wave, which gets further processed so as to extract the information about the composition of atomic groups within the molecule. In this work, NMR (Bruker ASCEND) was operated at 600 MHz at 295 K. ^{1}H NMR was performed to evaluate the chemical stability of HBA and HBD after the formation of DESs. The Nuclear Overhauser Effect Spectroscopy (NOESY) technique [136] was executed for eight scans to investigate spatial arrangement of protons. NOESY is one of the 2-D NMR techniques which elucidates H-H interactions. It uses the dipolar interaction of spins (the nuclear Overhauser effect, nOe) for correlation of protons.

3.3.3 Thermogravimetric Analysis (TGA)

TGA is a basic technique to observe mass loss of a compound with increase in temperature. It gives the information about change in composition, thermal stability and chemical

reaction's kinetic parameters of the sample[137]. A derivative of TGA data can be used for interpreting the point where mass loss is more apparent. Here, TGA (TG209 F1, Libra, NETZSCH, Germany) was performed to analyse the thermal stability profiles for DESs at a heating rate of 10 ºC per minute for the temperature range of 30-400 ºC. Aluminium crucible was used for holding the sample under nitrogen environment.

3.4 Physicochemical Properties of Electrolytes

3.4.1 Density

Density (ρ) measurement was done for favourable IL-based electrolytes and the novel DESs prepared in this work. Anton Paar density meter (DMA 4500 M) was used to measure density within the temperature range of 10-60 °C. The density meter works on the principle of oscillating U-tube method. The sample is injected into a U-shaped borosilicate glass tube which vibrates at corresponding characteristic frequency. The characteristic frequency basically changes with the density of the sample. Hence, characteristic frequency is recorded as input and density is the measured output of the instrument. The accuracy of the measurement is ±0.00001 g cm^{-3}.

3.4.2 Ionic Conductivity

Ionic conductivity (σ) is the most important physical property of an electrolytes regarding capacitive and resistive behaviour of the EDLC. The measurement of ionic conductivity was completed using Microprocessor based digital ionic conductivity meter (VSI 302, VSI Electronic Private Ltd.) at 25 ºC. It uses an electrode to measure the ionic conductivity. The probe of the electrode is dipped inside the sample. The instrument then displays the result after a few seconds. The displayed result is allowed to have a stable value before it is noted.

3.4.3 Viscosity

Viscosity (η) is another diffusional property of an electrolyte which can affect the capacitive performance of EDLCs. Viscosity study was done using Anton Paar Phsica MCR301 Rheometer following cone plate (CP25-2/S) method. The rheometer measures the viscosity of a liquid or gel which is kept on a stationary plate by imposing shear stress on it through a rotating plate. Nearly, 0.5-1 mL of sample was used for viscosity measurement. The instrument allows us to perform several experiments e.g. viscosity vs. temperature, shear stress vs shear strain profiles, constant shear stress or strain method. The instrument also provides the facility of parallel plate (PP) for rheological studies.

3.5 Electrochemical Characterization

3.5.1 Types of Electrochemical Experimental Set-up

Generally electrochemical experiments can be set-up to run two-electrode, three-electrode or four-electrode measurements [138]. A brief introduction about each of these three is reported below.

a. Two-Electrode: Two electrode experiment is the simplest one. In a two-electrode set-up the current-carrying electrodes are also used for voltage measurement. Working (W) and Working Sense (WS) are connected to a (working) electrode and Reference (R) and Counter (C) are connected to a second electrode. Two-electrode set-ups are mostly used in two configurations. One is where measurement of the whole cell voltage is significant, such as electrochemical-energy devices. The other configuration is where the counter-electrode potential can be expected not to drift over the course of the experiment. This is generally in systems which exhibit very low currents or relatively short time scales, and which also have a well-poised counter, e.g., a micro working electrode and a much larger silver counter electrode.

b. Three-Electrode*:* In three electrode mode, the reference lead is separated from the Counter and connected to a third electrode. This electrode is most often positioned so that it is measuring a point very close to the working electrode. Three-electrode setups have a distinct experimental advantage over two-electrode setups as they measure only one half of the cell. That is, the potential changes of the working electrode are measured independent of changes that may occur at the counter electrode which allows for a specific reaction to be studied with more accuracy. For this reason, 3-electrode mode is the most common set-up used in electrochemical experimentation.

c. Four-Electrode: In four-electrode mode the Working Sense lead is decoupled from the working electrode and other two are reference and counter electrode. In 4-electrode mode, the potentials for any electrochemical reactions that are occurring at the working (and counter) electrode(s) are not being measured. Here the effect of an applied current on the solution itself or some barrier in that solution is measured. This is not a common practice in electrochemistry.

3.5.2 Electrochemical Experiments

To characterize several electrolytes studied in this work, three-electrode electrochemical cell set-up was employed due to the convenience of its use. The pictorial view of the experimental set-up can be found below (Figure 3.2). The electrochemical experiments were performed using a potentiostat (PARSTAT-3000A) in a three-electrode assembly as discussed above. All the measurements were done at standard room temperature (25 °C). Nearly 12 ml of electrolyte solution was taken for 0.77 cm^2 (0.0214 g) of carbon electrode. The cell assembly was placed inside a Faraday shield to prevent external perturbations. The cell was connected to the potentiostat as shown in the following figure. The

characterizations were executed using *VersaStudio* software associated with the potentiostat. All the experiments were repeated twice to check the reproducibility.

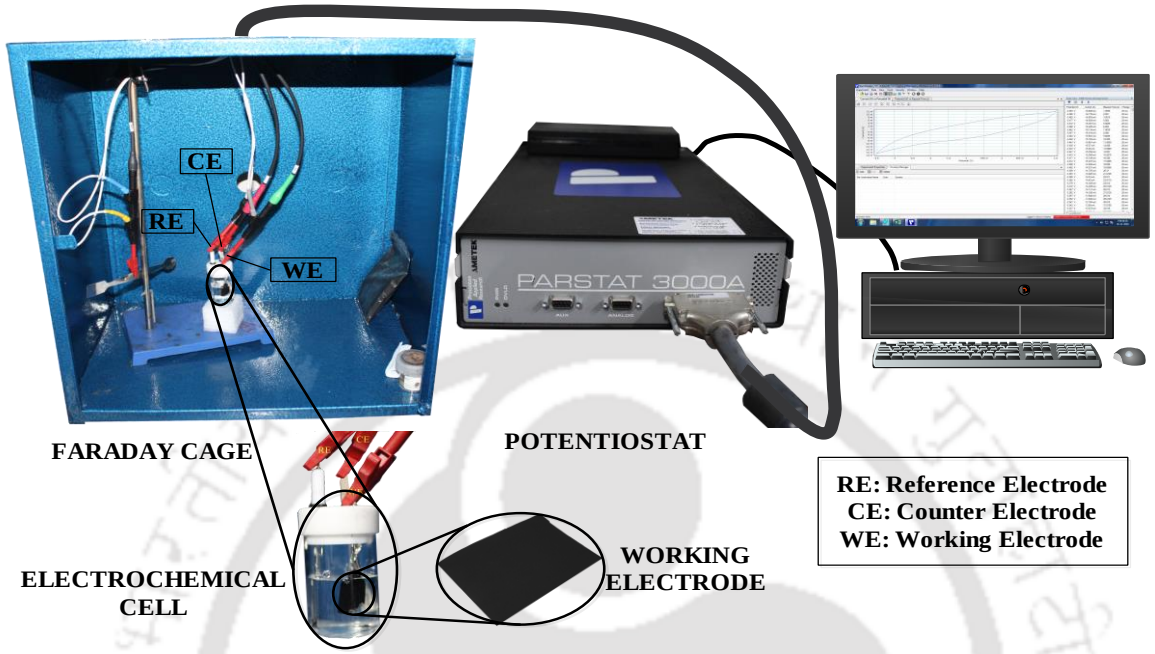

Figure 3.2: The electrochemical experimental set-up

At the beginning of electrochemical measurements open circuit potential (OCP) was calculated to check the stability of the system. OCP of the WE was measured with respect to the corresponding RE for a certain time period, until the potential became stable.

3.5.2.1 Cyclic Voltammetry (CV)

CV is a powerful and widely used characterization method for electrochemistry. As name suggests it represents the forward and reverse current vs potential profiles of an electrochemical cell. CV is a direct current (DC) electrochemical technique, which collects the change in current while a potential scan is applied to the working electrode at a particular scan rate in both forward and reverse directions. CV scans can be performed single or multiple times. For the processes involving faradic reactions, cyclic voltammograms indicate oxidation and reduction of the redox species. CV profile with oxidation and reduction peaks are the characteristics of pseudocapacitor [7]. However, for

EDLC, pure physical adsorption-desorption is represented by uniform variation in current as a function of potential. EDLC's CV plot tends to be more rectangular in shape with increase in the capacitance [7]. Figure 3.3 depicts an ideal cyclic voltammogram for EDLCs.

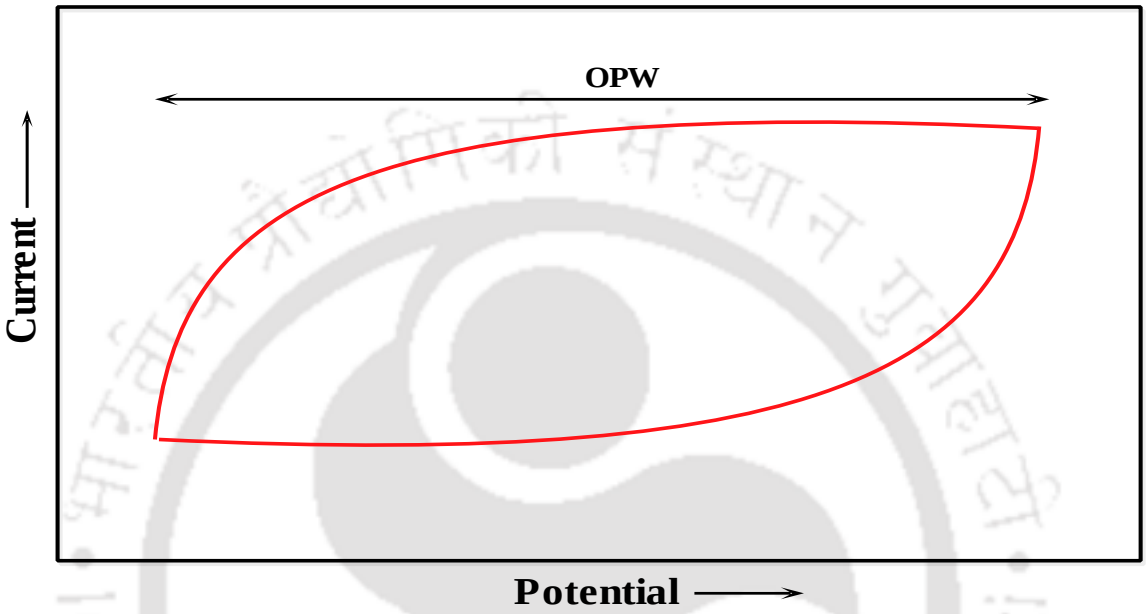

Figure 3.3: Schematic of ideal cyclic voltammogram for EDLC

In the current work, CV experiments were performed for a set of scan rates (3-20 mV/s). The area covered by the CV plot gives the total charge storage (Q). Hence capacitance from CV can be found from the following expression [14].

$$C = \frac{1}{2v(V_c - V_a)} \int_{V_a}^{V_c} I(V)dV \qquad [3.2]$$

where C is the capacitance, v is the scan rate, $V_c - V_a$ represents OPW and $I(V)$ is the current.

3.5.2.2 Galvanostatic Charge-discharge (GCD)

GCD is a valuable characterization technique for EDLCs. Here current is kept fixed and potential is varied. In GCD, the system gets charged and then discharged at a fixed specific

current within the potential limits obtained from CV. The results from GCD include capacitance, resistance and cycle life of the EDLC. At the beginning of the discharging curve a steep potntial drop can be found which is termed as ohmic drop or IR drop (Figure 3.4). This IR drop attributes from the system's internal resistance. The equations [83] for calculation of ESR and specific capacitance (C_{sp}) from GCD can be found below.

$$ESR = \frac{\Delta V}{\Delta I} \qquad [3.3]$$

$$C_{sp} = \frac{I}{m.dV/dt} \qquad [3.4]$$

where I is the applied current, dV/dt represents the slope of discharge curve excluding the IR drop or ohmic drop, m is the mass of the electrode, ΔV depicts the potential drop at the beginning of discharge and ΔI is the change in current while shifting from charging to discharging.

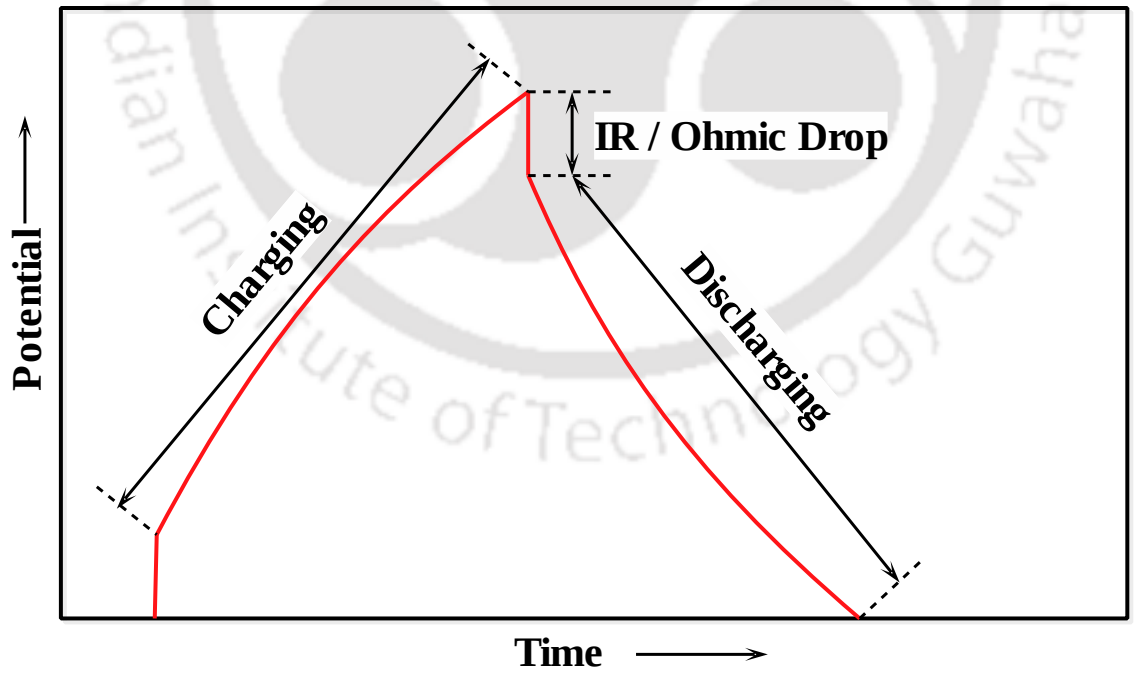

Figure 3.4: Schematic of GCD plot for an EDLC

3.5.2.3 Electrochemical Impedance Spectroscopy (EIS)

EIS has been considered a reliable tool for characterizing electrochemical energy storage devices e.g. ECs, batteries and fuel cells [139]. Unlike other electrochemical techniques EIS is extraordinarily sensitive. Literature reported different DC or AC methods for EIS measurements [140]. However, among such methods frequency response analyser (FRA) has become a more prominent technique to measure impedance [141]. FRA provides a low amplitude (5-15 mV) sinusoidal perturbation to the working electrode whereby corresponding AC current measurement is then performed. The output provides the impedance (Z) of electrochemical cell as a function of frequency. Z combines both the real (Z') and imaginary (Z'') parts. - Z'' vs Z' plot is named as Nyquist plot and it provides different types of resistive and capacitive behaviour of the system. A typical Nyquist plot and corresponding electrical equivalent circuit is represented by Figure 3.5 [142]. The first part represents the insertion of the curve on the x-axis, which depicts the solution resistance (R_s) and the semicircle whose diameter gives the charge transfer resistance (R_{ct}). The second part depicts a straight line with slope of 45° representing Warburg impedance (Z_w) [143]. However, due to the usual smaller value of Z_w, ESR can be considered as a combined effect of of R_s and R_{ct} [144]. The authors stated that electrochemical capacitor starts with the 45° impedance line. Further, the concluding part gives a nearly vertical tail at lower frequencies representing purely capacitive behaviour. In this study EIS was performed within the frequency range from 100 kHz to 10 mHz by applying a sinusoidal signal of 10 mV RMS at OCP. The specific capacitance (C_{sp}) from EIS data can be evaluated from equation 3.5 [14].

$$C_{sp} = \frac{-1}{2m\pi f Z''(f)} \qquad [3.5]$$

where f denotes frequency employed for AC current in EIS and $Z''(f)$ stands for imaginary part of the impedance and *m* is the mass of the WE.

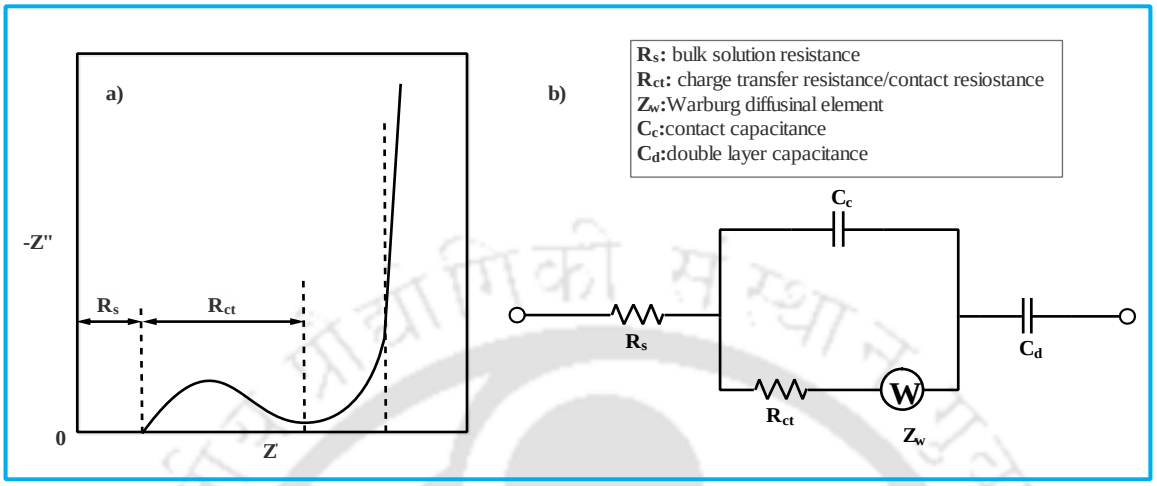

Figure 3.5: a) Schematic of a typical Nyquist Plot and b) equivalent electrical circuit for EDLC

3.5.2.4 Linear Scan Voltammetry (LSV)

LSV technique evaluates the ESPW without considering the capacitive performance. Hence often this technique is executed with non-reactive electrodes e.g. platinum, gold or glassy carbon electrodes [7,80,83] to investigate newly developed electrolytes. In this method change in current is observed in between an applied potential limit. No reverse current and cyclic measurements happen unlike CV. It is also termed as linear sweep voltammetry. To determine the ESPW of the novel DESs, LSV was performed against glassy carbon electrode in this thesis. The schematic representation of an LSV plot is given in Figure 3.6.

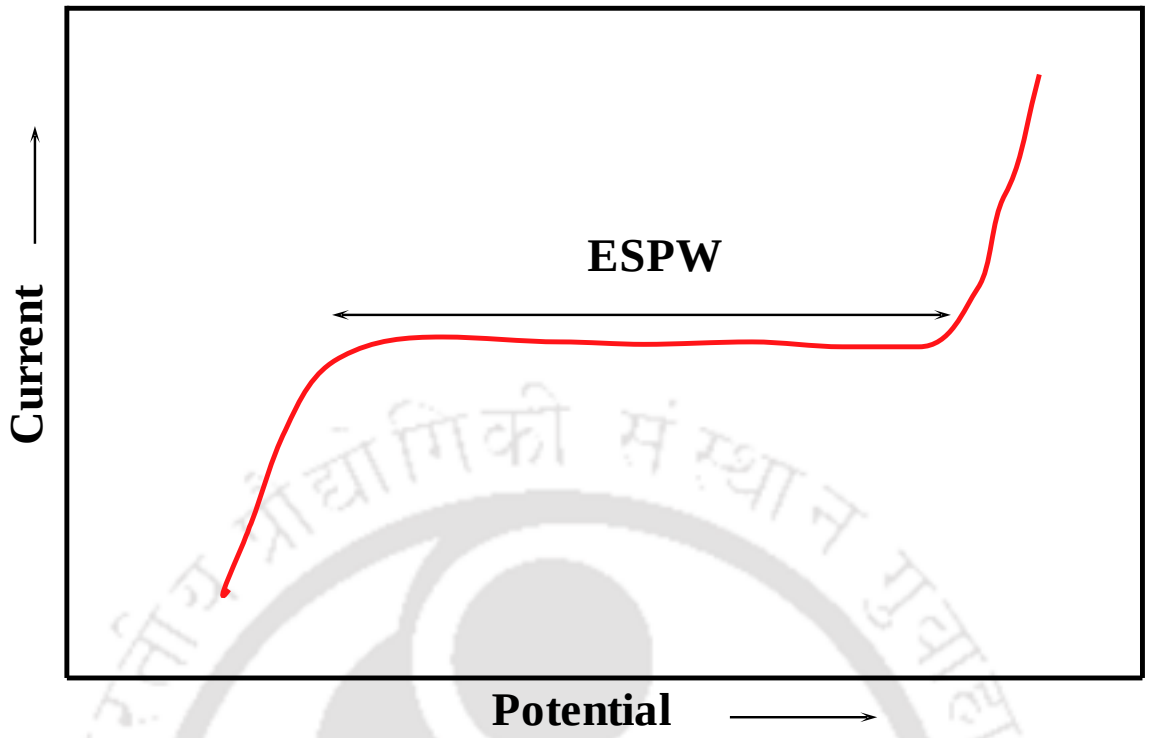

Figure 3.6: Schematic of LSV indicating ESPW

3.6 Molecular Dynamics (MD) Simulation Details

MD simulation tool was adopted for validating the transport properties obtained experimentally. MD simulation predicts physical properties as per standard protocol [145,146]. MD provides better insights regarding self-diffusion coefficient of ions and how it affects ionic conductivity and viscosity. The method to execute MD studies is divided into several parts which should be followed stepwise as discussed below.

3.6.1 Structure Drawing and Geometry Optimization

Prior to MD study the molecular structures were build using Gauss View 5 [132] visualization package. Thereafter the optimized geometry for the molecules were obtained using Gaussian 09 [133] employing the hybrid B3LYP/6-31G* [134] theory. Simultaneously frequency calculation was done by choosing the job type *Opt+Freq*. The electrostatic charges of each atom were calculated using the CHELPG method available in

Gaussian 09. The final output file from optimization was used to generate the protein data bank (PDB) file.

3.6.2 Simulation Methodology

The *.pdb* files of electrolyte obtained from quantum chemical calculations were then taken for preparation of the simulation box. 100 molecules were randomly packed in a cubic configuration (30×30×30 $Å^3$) using Packmol package [147]. Required force field parameters were generated according to Generalized Amber Force Field (GAFF) [148] functional form with the help of ANTECHAMBER [149] module of AMBER 12 [150]. The functional form of the GAFF includes the bonded interactions i.e. the contribution of bond stretching, angular bending, torsional interactions, whereas van der Waals contribution and columbic interaction contribute to the non-bonded interaction. The functional form is given by equation 3.6. The partial charges obtained from Gaussian were then fitted with restricted electrostatic potential module of AMBER 12. The reliability of force field parameters was validated by comparing simulated density and experimental densities of all the system.

$$V_{total} = \sum_{bonds} k_r \left(r - r_{eq}\right)^2 + \sum_{angles} k_\theta \left(\theta - \theta_{eq}\right)^2 + \sum_{dihedrals} \frac{V_n}{2}\left[1 + \cos\left(n\phi - \lambda\right)\right] + \sum_{i=j}^{N-1}\sum_{i<j}^{N}\left[4\varepsilon_{ij}\left\{\left(\frac{\sigma_{ij}}{r_{ij}}\right)^{12} - \left(\frac{\sigma_{ij}}{r_{ij}}\right)^{6}\right\} + \frac{q_i q_j}{4\varepsilon_0 \pi r_{ij}}\right] \quad [3.6]$$

The equation includes the force constants: k_r, k_θ and V_n, the equilibrium structural parameters: r_{eq} and θ_{eq}, multiplicity n and phase angle λ for torsional angle parameters. ε_{ij} is the Lennard-Jones well depth and σ_{ij} is the distance between the atoms i and j where the energy of the two atoms become zero. The partial atomic charges q_i and q_j contribute to the electrostatic interactions.

To predict the transport properties of ILs realistically, force fields must consider the dynamic electronic polarization effects. In this regard, reduction of partial charges has become an alternative approach to the use of polarizable force fields, which experiences higher computational cost [146]. Literature suggests that reducing the charges by a factor of about 0.7 for ions in general can take care of the electronic polarization effect [151]. For [BMIM][Cl], scaling factor of 0.73 has been already used [151]. In our study, the more accurate scaling factor was found to be 0.72 for pure ILs after comparing the self-diffusion coefficient and ionic conductivity with available literature. For mixture of ILs with organic solvent, a scaling factor of 0.85 has been adopted from literature [146] where similar charge reduction was done for IL+ethanol mixture. This particular choice of scaling factor eventually came up as the effective one when comparison of transport properties was made with experimental findings. For simulation of IL solutions, a scaling factor was used only for ionic species and not for organic solvent [146].

MD simulations were performed using NAMD version 2.9 [152]. The system was brought to its experimental density through a 2 ns equilibration run in NPT ensemble. Thereafter the equilibrated configuration was taken for a production run of 50 ns in NVT ensemble at 298.15 K. Langevin thermostat [153] with damping coefficient of 1 /ps and Nose-Hoover Langevin barostat [154] with a period of 100 fs and decay of 50 fs were applied to monitor temperature and pressure throughout the simulation. Pressure imposed for simulation was 1.01325 bar. The Verlet algorithm was implemented with a time step of 2 fs [155] to integrate Newton's equation of motion. A 12 Å cut off distance was employed for short-range L-J potential. In a similar manner, long-range electrostatic interactions were taken care using *Particle Mesh Ewald* Approximation [156].

3.6.3 Determination of Ionic Conductivity and Viscosity

Ionic conductivity being a transport property is associated with self-diffusion coefficients of the respective ions. In this regard, self-diffusion coefficient or self-diffusivity (*D*) was estimated for the ion pairs using Einstein relation [157] as given below.

$$D = \frac{1}{6}\lim_{t\to\infty}\frac{d}{dt}\left\langle \sum_{i=1}^{N}\left[\vec{r}_i(t) - \vec{r}_i(0)\right]^2 \right\rangle \qquad [3.7]$$

where the term inside the angular bracket stands for mean square displacement (MSD) of the molecules, the angular bracket represents ensemble average and the factor 1/6 is attributed to the three-dimensionality of the system. MSD data were obtained from the last 10 ns production run of MD simulation. Further ionic conductivity (σ) was computed with the help of Nernst- Einstein relation [146] as follows:

$$\sigma = \frac{q^2(n^+D^+ + n^-D^-)}{Vk_BT} \qquad [3.8]$$

where q is the electron charge, D^+ and D^- are the self-diffusion coefficients ($cm^2\ s^{-1}$) and n^+ and n^- gives the number of cations and anions, V is the system volume ($Å^3$), k_B is the Boltzmann constant and T is the temperature (K).

Viscosity (η) calculations for equilibrium MD was performed using Green-Kubo relation [158].

$$\eta = \frac{V}{k_BT}\int_0^{\alpha}\langle\sum P_{xy}(t).P_{xy}(0)\rangle dt \qquad [3.9]$$

Here, P_{xy} depicts the *xy* component of the pressure tensor, V is the system volume, k_B is the Boltzmann constant and T is the temperature. The angular bracket indicates the average over all the time origins and the summation considers all the three off diagonal elements of pressure tensor i.e. P_{xy}, P_{yz} and P_{zx}.

CHAPTER 4

Electrochemical Performance of Ionic Liquids

4.1 Results and Discussion on [AMIM][Tf_2N] Ionic Liquids

Three-electrode electrochemical cell set-up was employed to characterize the electrolytes as described in Figure 3.2. Pt wire, Ag/Ag^+ or Ag and exfoliated carbon were incorporated as CE, RE and WE respectively as reported in section 3.1.2. 10-12 ml of electrolyte solutions are used for every experiment to characterize 0.0214 g active mass of WE. The reproducibility of results was ensured by repeating the experiments. To begin with [AMIM][Tf_2N] ILs were considered for electrochemical studies.

4.1.1 Analysis from Cyclic Voltammetry

Figures 4.1-4.3 represents the cyclic voltammogram at scan rates of 5, 10 and 20 mV/s for [EMIM][Tf_2N], [PMIM][Tf_2N] and [BMIM][Tf_2N] respectively at different solvent concentrations. Nearly rectangular shape of the CV plots is observed at the lower scan rates. The symmetry against the zero line of y-axis bring the studied systems closer to ideal double layer capacitive behaviour of EDLC [14]. Moreover, absence of any peak in CV curves denies the possibility of any redox reaction, which eventually proves a pure double layer behaviour. Figure 4.1a depicts the lowest current and the widest OPW for pure [EMIM][Tf_2N].

Addition of organic solvent dilutes the IL and reduces the diffusion resistances which enhances current generation. Nonetheless this is achieved at the expense of OPW (Figure 4.1b-d). The study on other two neat ILs was not performed considering the resistive nature of pure [EMIM][Tf_2N]. For all the three ILs, IL+AN_II systems show the highest charge transfer. Moreover, [PMIM][Tf_2N]+AN_II (Figure 4.2b) gives the highest current among all the electrolytes irrespective of scan rate which corresponds to the higher ionic strength of this IL solution.

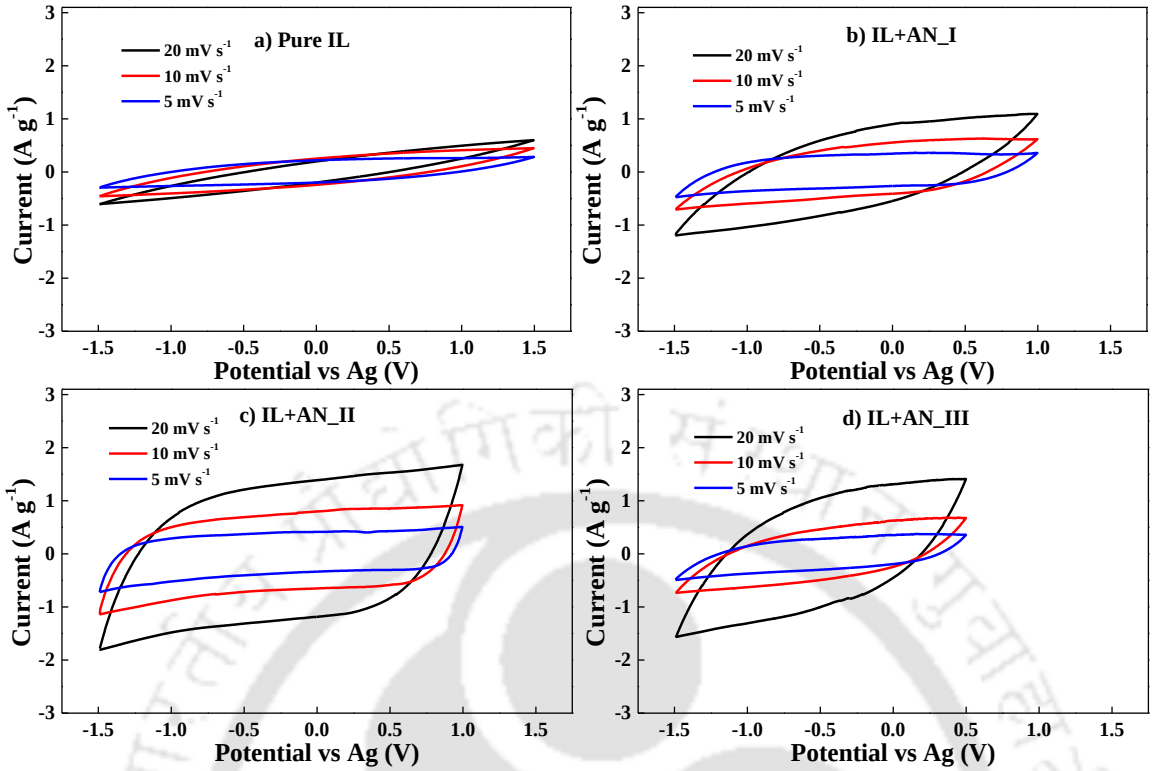

Figure 4.1: CV of [EMIM][Tf_2N] a) Pure RTIL b) IL+AN_I c) IL+AN_II and d) IL+AN_III

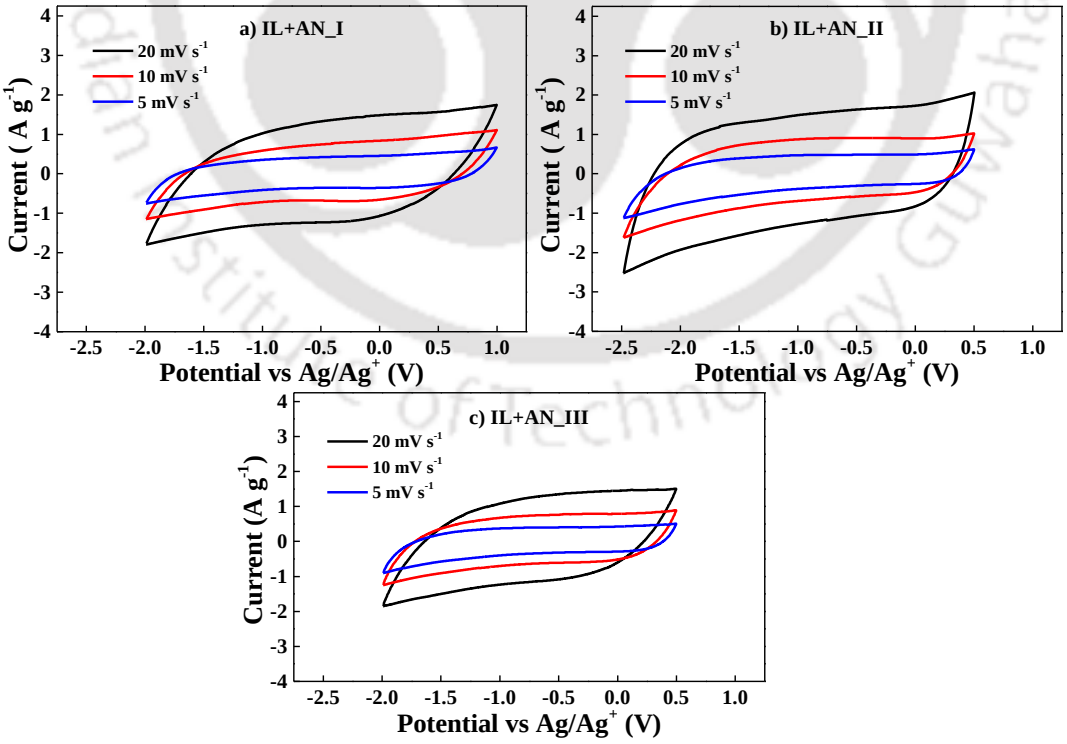

Figure 4.2: CV of [PMIM][Tf_2N] a) IL+AN_I b) IL+AN_II and c) IL+AN_III

The measured electrochemical stability is wider for [PMIM][Tf_2N] and [BMIM][Tf_2N] as compared to [EMIM][Tf_2N]. The presence of impurities in ILs can lower the OPW [119]. The OPW achieved for the electrolytes used in our work is comparable with literature [7,52] and still higher than aqueous electrolytes as cited in Chapter 2. Previous work also suggested that electrochemical stability window is dependent on type of working electrode [46,50,52,119]. A decrease in electrochemical window by 0.5 V because of reduction in the anodic potential limit is observed while the concentration goes down from IL+AN_II to IL+AN_III. This indicates the co-solvent effect on narrowing the OPW. Similar pattern was observed by Scalia *et al.*, [159] upon increase of the co-solvent PC wt. % for N-butyl-N-methylpyrrolidinium 4,5-dicyano-2-(trifluoromethyl) imidazole. Although OPW remains same for IL+AN_I and IL+AN_II solutions, higher specific current is observed for former (Figure 4.4).

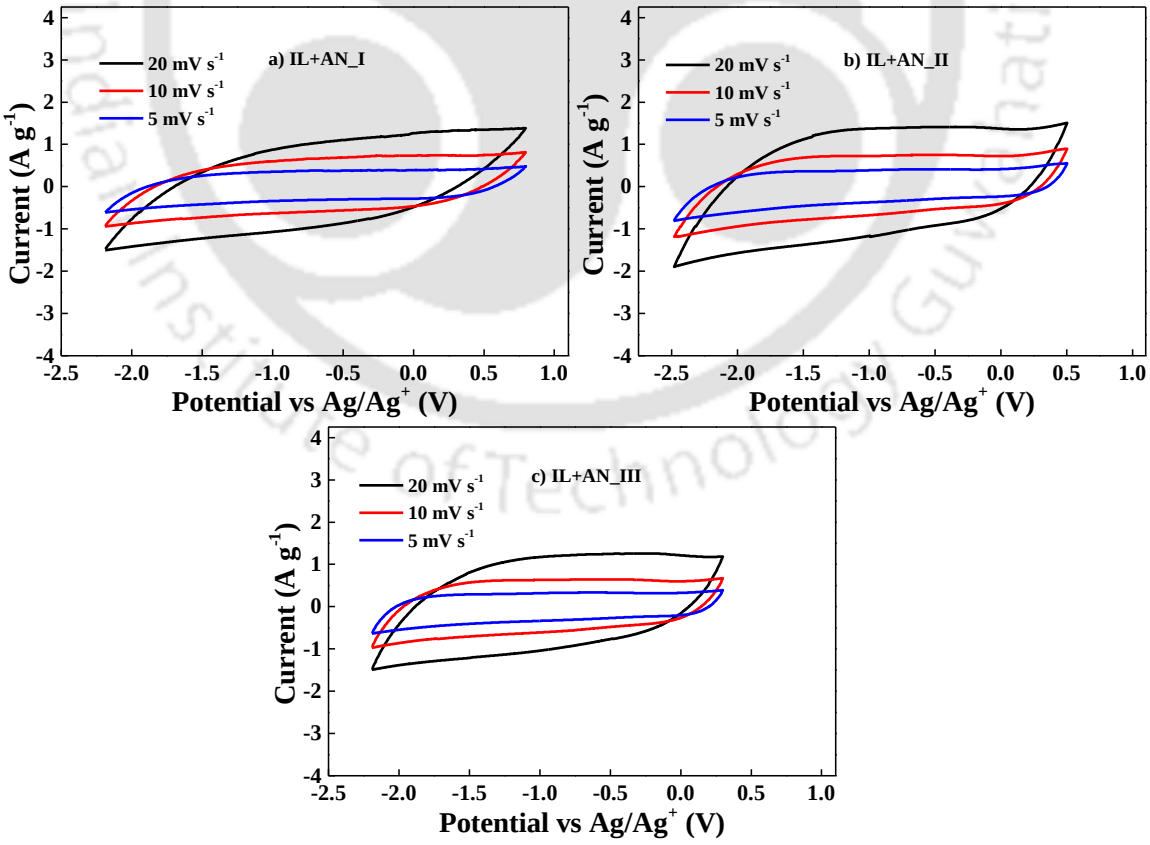

Figure 4.3: CV of [BMIM][Tf_2N] a) IL+AN_I b) IL+AN_II and c) IL+AN_III

Apart from electrochemical stability analysis, CV data was also used for calculation of specific capacitance using equation 3.2. Specific capacitance as a function of scan rate applied for CV measurement can be found in Figure 4.4. For all the three ILs, the highest specific capacitance is observed for IL+AN_II systems, which correlates the highest specific current generated from cyclic voltammogram. However, addition of more solvent (IL+AN_III) decreases the current (Figures 4.1-4.3) and specific capacitance owing to lower concentration of ionic species. Further pure [EMIM][Tf_2N] results in the minimum capacitance which indicates greater ESR. The specific capacitance increases with decrease in CV scan rate due to delay in reverse adsorption of ions on the electrode/electrolyte interface, which is also known as "Electrolyte Starvation Effect" [160]. Working electrode having high rate performance can nullify this effect.

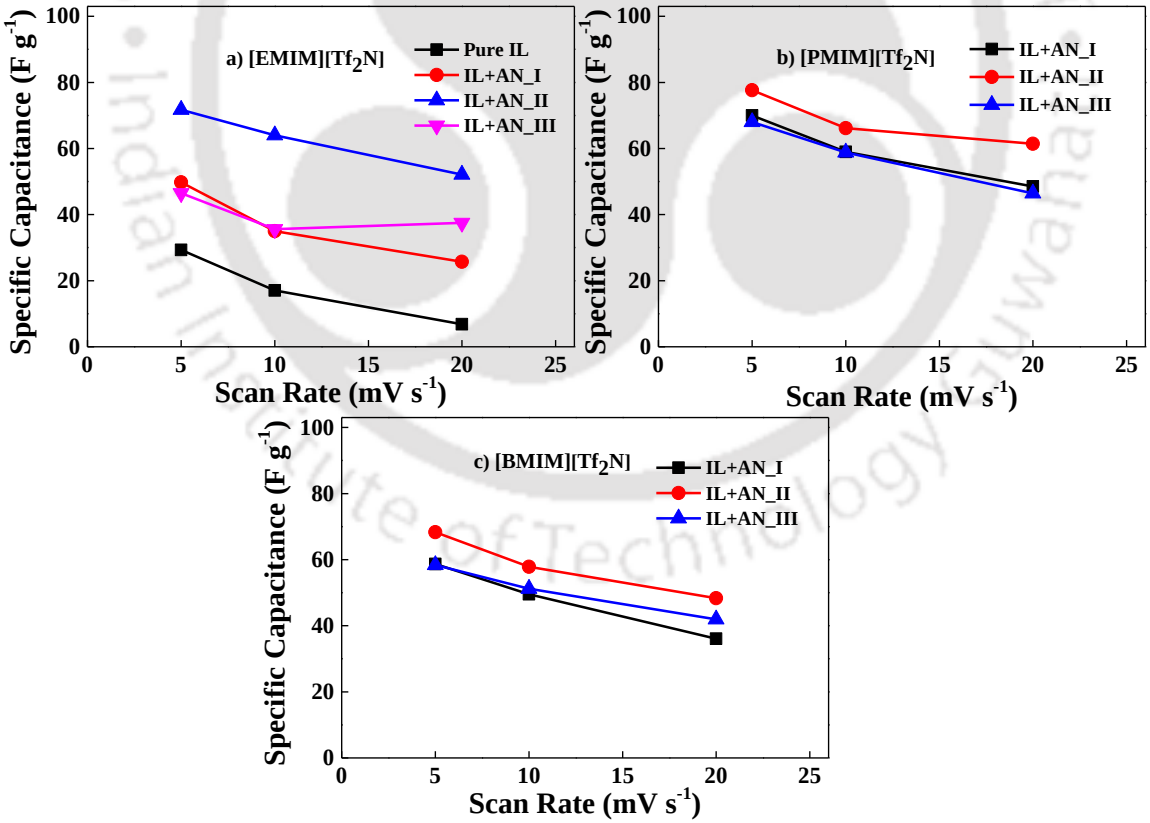

Figure 4.4: Capacitance obtained from CV for [AMIM][Tf_2N] ILs

Even though the specific capacitance for all the [AMIM][Tf_2N] ILs are comparable for IL+AN_II systems, [PMIM][Tf_2N] and [BMIM][Tf_2N] possess wider OPW. Hence these two IL with same wt. % as in IL+AN_II were further investigated with PC and BN co-solvents. Figure 4.5 reports the CV plots for [PMIM][Tf_2N] and [BMIM][Tf_2N] respectively. The plots clearly indicate lower specific current than the same with AN despite having equal OPW. It is seen that PC offers more resistance when results with BN and PC are compared. Hence the order of current generation rate with different co-solvents is found to be AN>BN>PC. [BMIM][Tf_2N] delivers a higher capacitive performance (Figure 4.6) when diluted with BN unlike AN. This indicates that the similar trend in capacitive behaviour may not be observed for an IL electrolyte solvated with different organic solvent. Both the ILs in PC result in equivalent specific capacitance.

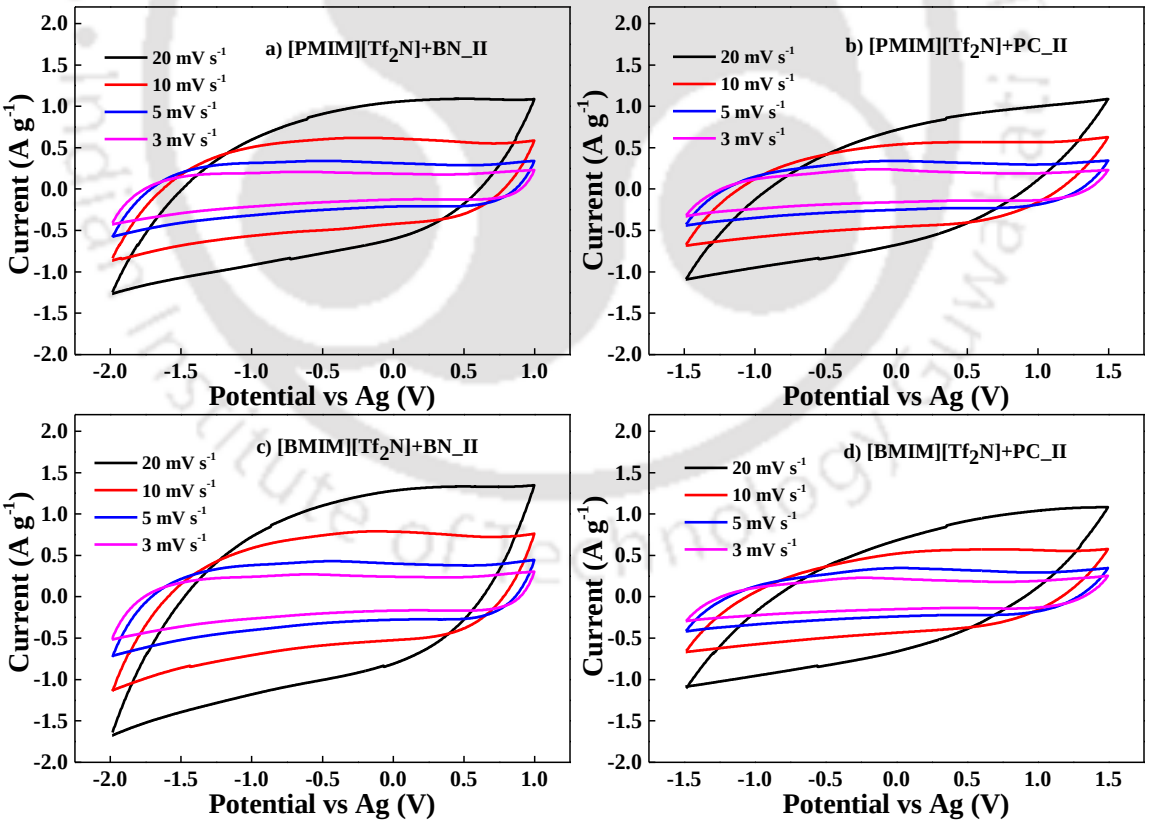

Figure 4.5: CV for BN and PC diluted [AMIM][Tf_2N] ILs

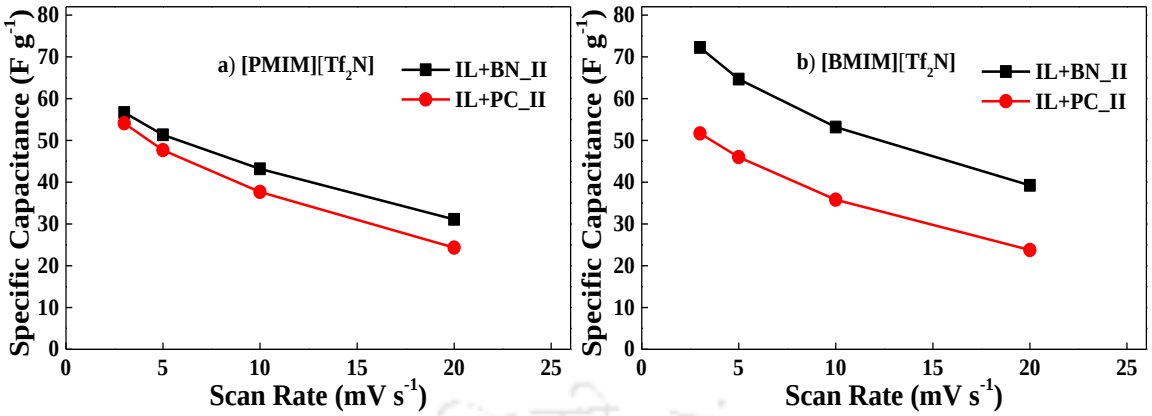

Figure 4.6: Capacitance obtained from CV for [AMIM][Tf_2N] solvated in BN and PC

4.1.2 Galvanostatic Charge-discharge Measurements

The OPW obtained from CV is successfully reproduced by GCD. The charge-discharge profiles of [AMIM][Tf_2N] ILs at various specific current (0.3-1 A g^{-1}) can be found in figures 4.7-4.10. The IR drop is directly proportional to *I* and for any electrolyte, IR drop lowers when specific current decreases. Again, the minimum IR drop for the AN diluted ILs is observed for IL+AN_II, which confirms the highest specific current and capacitance from CV. Pure [EMIM][Tf_2N] shows IR drop of almost 2V (Figure 4.7) which is a high value, even though OPW is limited to 3 V. Further with dilution, IR drop starts decreasing up to IL+AN_II. Further, IL+AN_III encounters enhancement in the IR drop.

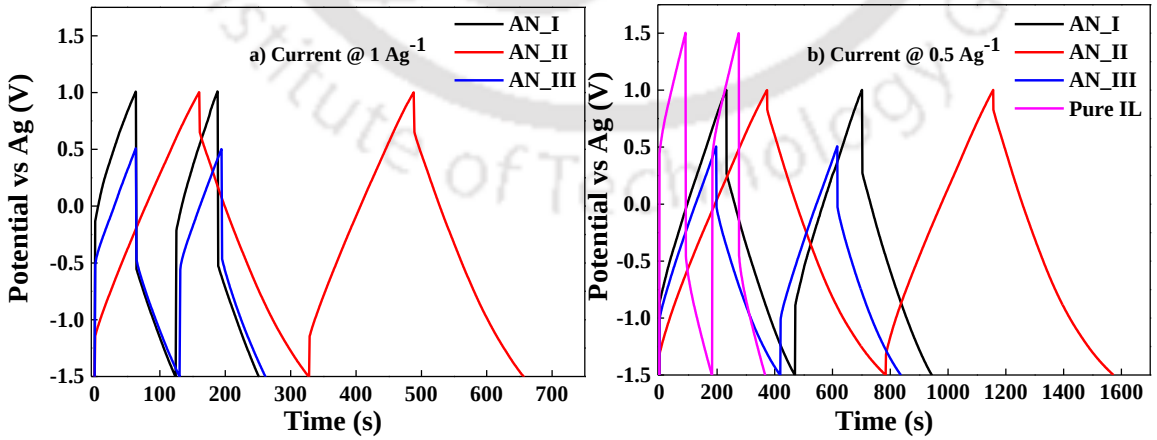

Figure 4.7: GCD of [EMIM][Tf_2N] at specific current a)1 A g^{-1} and b) 0.5 A g^{-1}

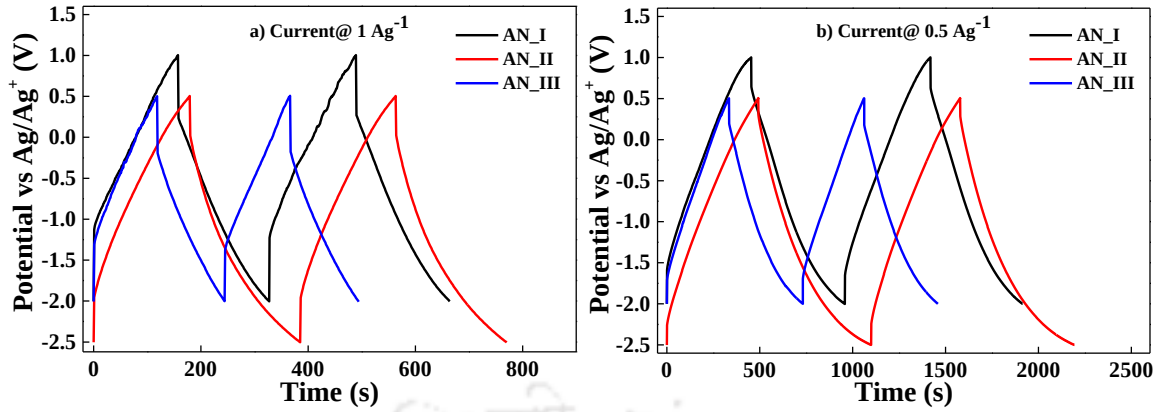

Figure 4.8: GCD of [PMIM][Tf_2N] at specific current a) 1 A g^{-1} and b) 0.5 A g^{-1}

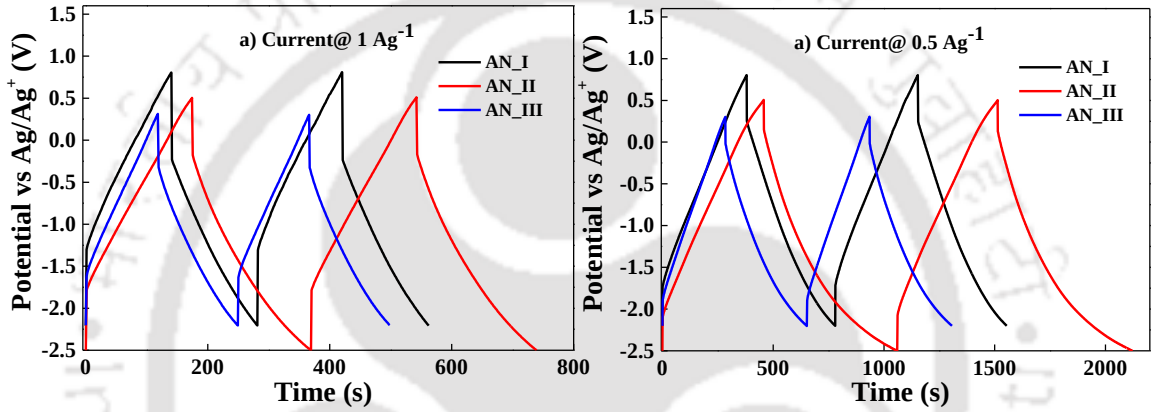

Figure 4.9: GCD of [BMIM][Tf_2N] at specific current a) 1 A g^{-1} and b) 0.5 A g^{-1}

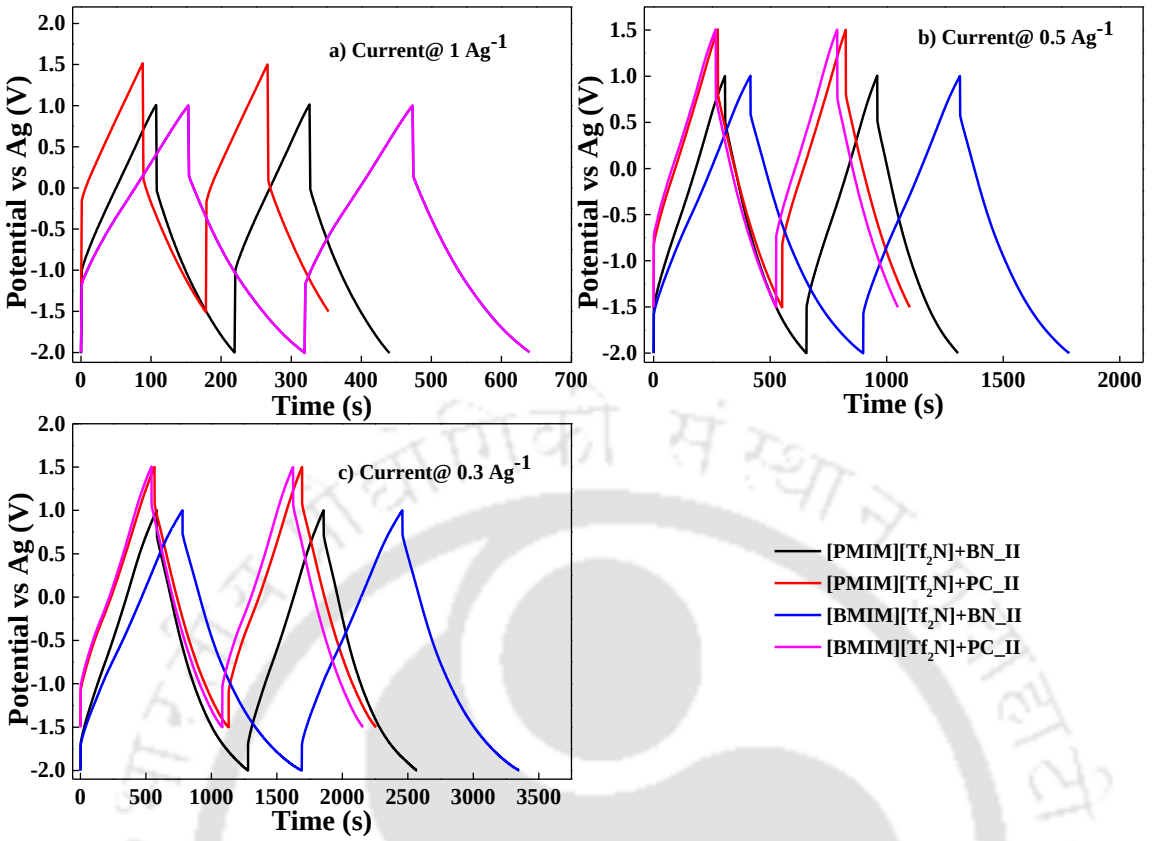

Figure 4.10: GCD plots of [AMIM][Tf_2N] at specific current a) 1 A g^{-1}, b) 0.5 A g^{-1} and c) 0.3 A g^{-1}

The ESR is calculated from equation 3.3 and reported in Figure 4.11, which reflects the role of organic solvent in improving the capacitive nature of the cell. For [EMIM][Tf_2N], maximum ESR is obtained for pure IL which further reduces on dilution. ESR does not vary with scan rate for any electrolyte solution. Hence as discussed above, IR drop changes with change in the applied current while the resistance remains almost constant. Figure 4.10 elucidates higher IR drop for [BMIM][Tf_2N] and [PMIM][Tf_2N] when they are in solution of BN and PC unlike AN at the same specific current (0.5 and 1 A g^{-1}). This increase in IR drop attributes from the greater ESR with BN and PC (Figure 4.11b and c). Overall [EMIM][Tf_2N]+AN_II and [PMIM][Tf_2N]+AN_II have the lowest ESR (~ 7 Ω) among all the systems.

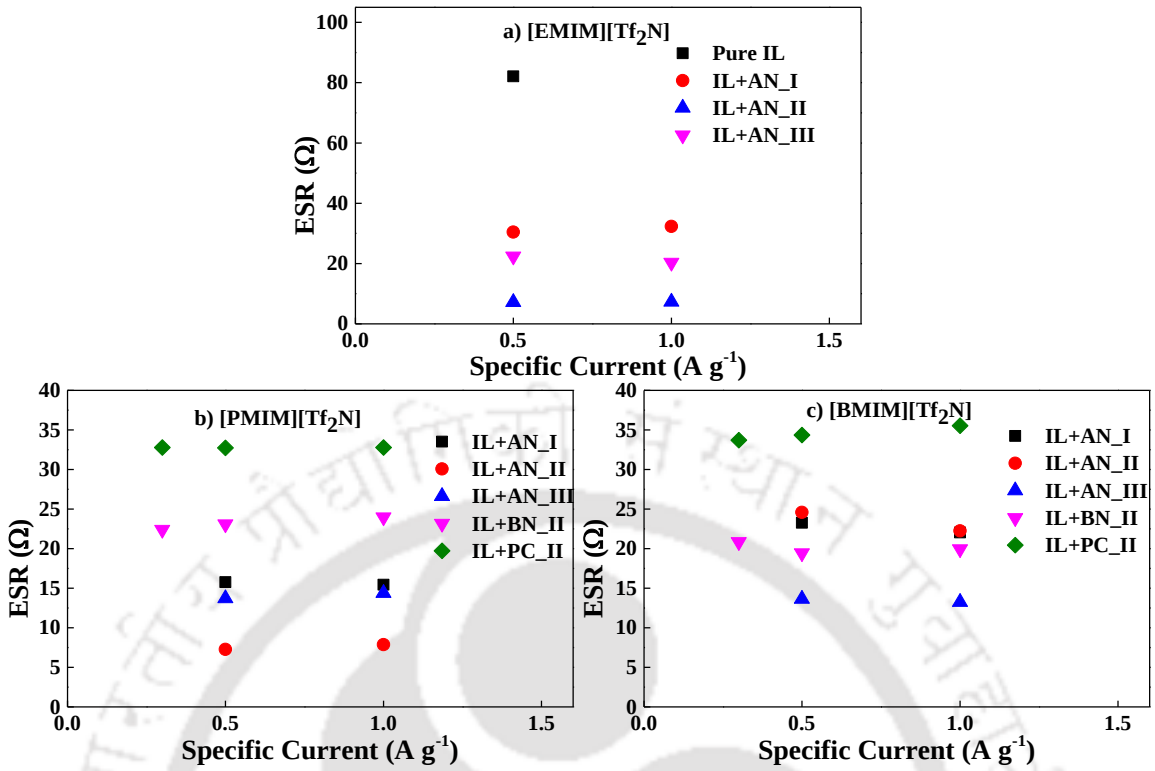

Figure 4.11: ESR of [AMIM][Tf_2N] ILs from GCD a) [EMIM][Tf_2N], b) [PMIM][Tf_2N] and c) [BMIM][Tf_2N]

The capacitive behaviour of the [AMIM][Tf_2N] ILs, evaluated from GCD data, can be found in Figure 4.12. It is well known that capacitance in inversely proportional to resistance. Hence IL+AN_II systems results in the highest specific capacitance for each type of [AMIM][Tf_2N] IL. Overall, the least capacitance (46.29 F g^{-1}) is for pure [EMIM][Tf_2N] and the highest is for [PMIM][Tf_2N]+AN_II (121.95 F g^{-1}) and [BMIM][Tf_2N]+AN_II (125.00 F g^{-1}) at 0.5 A g^{-1}. Moreover, specific current dependency of the charge storage behaviour is also observed. Analogous observation was also made in previously reported study [48]. It may be expected that due to its smaller cation size, [EMIM][Tf_2N] should have the best charge storage. However, here the observed specific capacitance is higher for [PMIM][Tf_2N]/[BMIM][Tf_2N]+AN_II. Literature suggests that [EMIM][Tf_2N] possesses the highest ionic strength in AN when IL content is 10 mole %

[161]. For [EMIM][Tf_2N]+AN_II solution, the IL content is 6 mole %. Hence, the specific capacitance may not be the maximum.

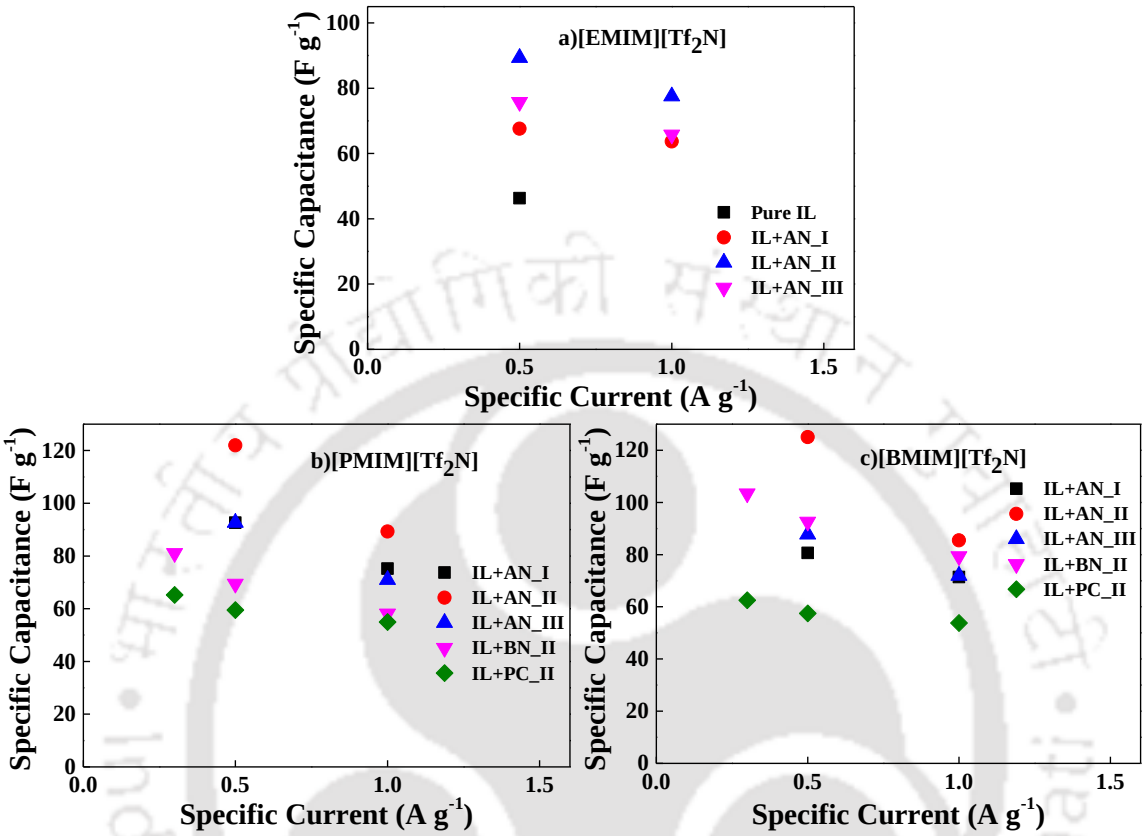

Figure 4.12: Specific capacitance of [AMIM][Tf_2N] ILs from GCD a) [EMIM][Tf_2N], b) [PMIM][Tf_2N] and c) [BMIM][Tf_2N]

[PMIM][Tf_2N]+BN_II (Figure 4.12b) possesses lower capacitance when compared to [BMIM][Tf_2N] +BN_II (Figure 4.12c). For both the ILs, PC offers the least capacitance due to the maximum ESR as discussed above (Figure 4.11). The analysis from Figures 4.12b and 4.12c reveals that the co-solvents follow the order of AN>BN>PC when capacitive behaviour is considered. The same is also observed for rate of current generation from CV.

4.1.3 Electrochemical Impedance Spectroscopy

The characterization technique was implemented for the IL+co-solvent solutions which resulted in better performance. Hence, all three [AMIM][Tf_2N]+AN_II electrolytes were

considered for EIS measurements. The Nyquist plot and corresponding frequency dependant capacitance as calculated using equation 3.4 can be found in Figure 4.13. As discussed in section 3.5, different parts of Nyquist plot represent the resistive and capacitive nature of the electrode-electrolyte system. The solution resistance (R_s) is the minimum for [PMIM][Tf_2N]+AN_II system whereas other two electrolytes offers nearly equal value of R_s. However, charge transfer resistance (R_{ct}), defined by the diameter of the semicircle, is almost similar for [EMIM][Tf_2N] and [PMIM][Tf_2N]. Charge transfer resistance can be divided into two parts: the electronic and ionic resistances [143]. The electronic part attributes from the intrinsic electronic conductivity of WE constituent particles, the electronic contact between particles and contact between active layer and current collector. The ionic resistance part specifies the electrolyte ionic resistance inside the pores of the electrode, which depends on ionic conductivity of electrolyte, porous texture and thickness of the active layer. The second part i.e. Warburg impedance (Z_w) is more lucid for [BMIM][Tf_2N] which interprets that more diffusional limitation is encountered by the ions inside the pores than the other two ILs. Nevertheless, the resistances incurring the capacitive behaviour is solely dependent on the lower frequencies (equation 3.5). Figure 4.13b depicts how the specific capacitance evolves as frequency decreases. From EIS predicted data it can be concluded that all the three systems show close match in their capacitive nature.

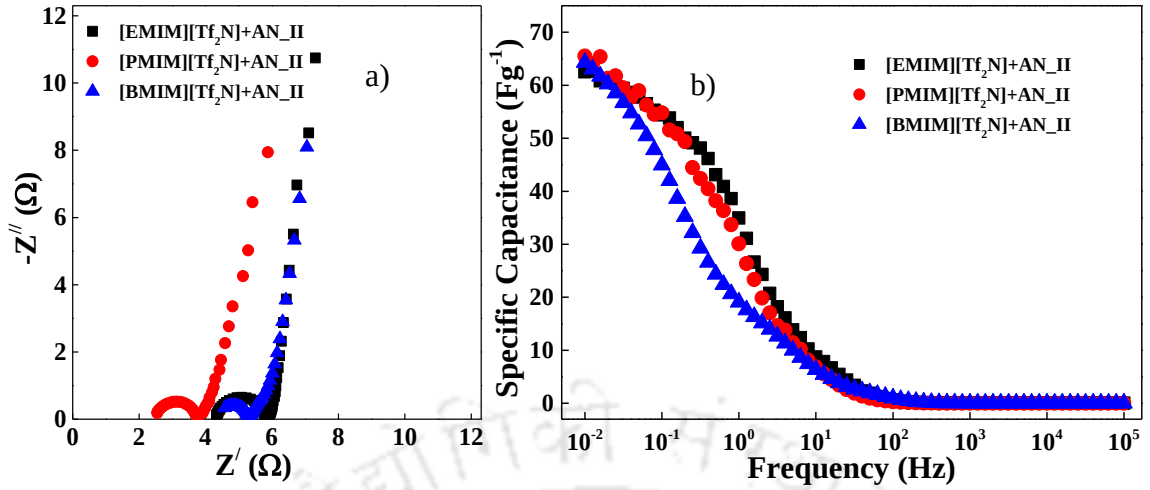

Figure 4.13: a) Nyquist plot at 0 V vs OCP and b) frequency dependant specific capacitance for AN solvated [AMIM][Tf_2N] electrolyte solutions

EIS confirms the analysis from CV and GCD regarding the effectiveness of different co-solvents. Nyquist plots (Figures 4.14a and c) indicate resistive nature of PC based solutions. Due to the higher internal resistance, the specific capacitance values for PC based electrolytes show some fluctuations. The higher charge storage of [BMIM][Tf_2N]+BN_II can also be recognized from Nyquist plot similar to CV and GCD data. Hence R_s and R_{ct} values for this particular system are lower than other three solutions even though those are higher than [AMIM][Tf_2N] +AN_II electrolytes.

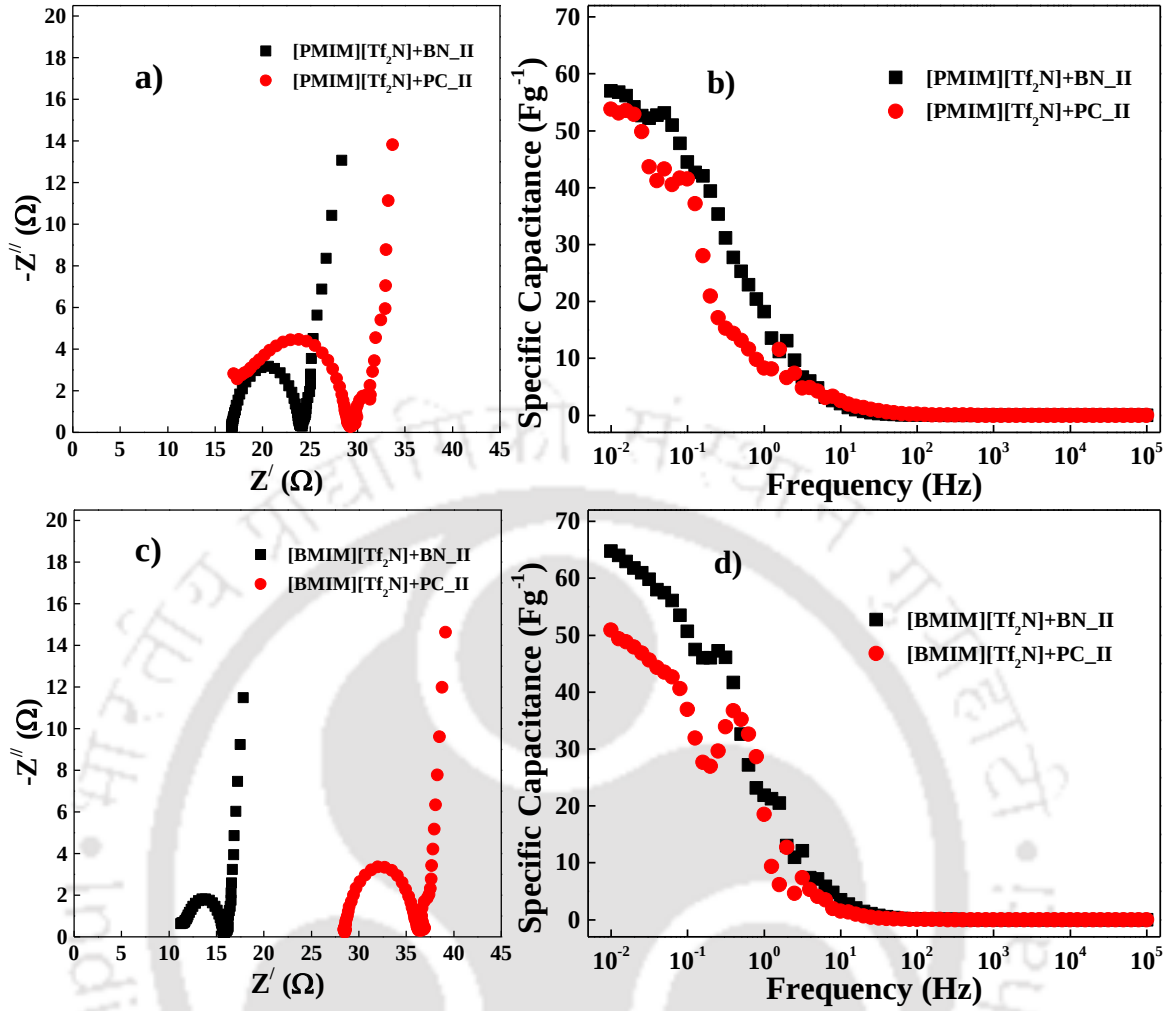

Figure 4.14: a), c) Nyquist plot at 0 V vs OCP and b), d) frequency dependant specific capacitance for [PMIM][Tf_2N] and [BMIM][Tf_2N] electrolyte solutions in BN and PC

4.1.4 Summary of Section 4.1

Pure [EMIM][Tf_2N] offers the highest ESR even though it results in the widest OPW compared to its solutions. The OPW of the three ILs gradually constricts with increase in co-solvent concentration as confirmed by both CV and GCD. As compared to BN and PC, AN contributes to better charge storage and lesser ESR at room temperature. Alkyl chain length shows noteworthy effects on electrochemical performance, particularly OPW and ESR, when EMIM cation is compared to PMIM and BIMIM.

4.2 Results and Discussion on [AMIM][BF_4] Ionic Liquids

Following [AMIM][Tf_2N] ILs, [AMIM][BF_4] ILs containing ethyl and butyl groups were also studied. The new addition here is the investigation of mixture of ILs. Equimolar ratio of [EMIM][BF_4] and [BMIM][BF_4] diluted with AN was considered for electrochemical characterization.

4.2.1 Analysis from Cyclic Voltammetry

CV diagrams clearly depicts ideal double layer capacitive nature of [AMIM][BF_4] ILs (Figures 4.15-4.17). When the ILs are compared without solvent, it is observed that [EMIM][BF_4] generates higher current than [BMIM][BF_4]. This is due to lower viscosity of the former (26 cp at 298.15 K* and 28 cp at 303.15 K [162]) than the later (80.05 cp at 298.15 K* and 81.4 cp at 303.15 K [163]). The highest current is measured for IL+AN_II systems similar to [AMIM][Tf_2N] ILs. The gradual shrinking of potential window is observed from pure IL to IL+AN_III. [BMIM][BF_4] reports to have wider electrochemical stability. This is likely due to longer alkyl chain length of BMIM cation [119] that extends the potential limit.

*Please refer to APPENDIX B: Table B1

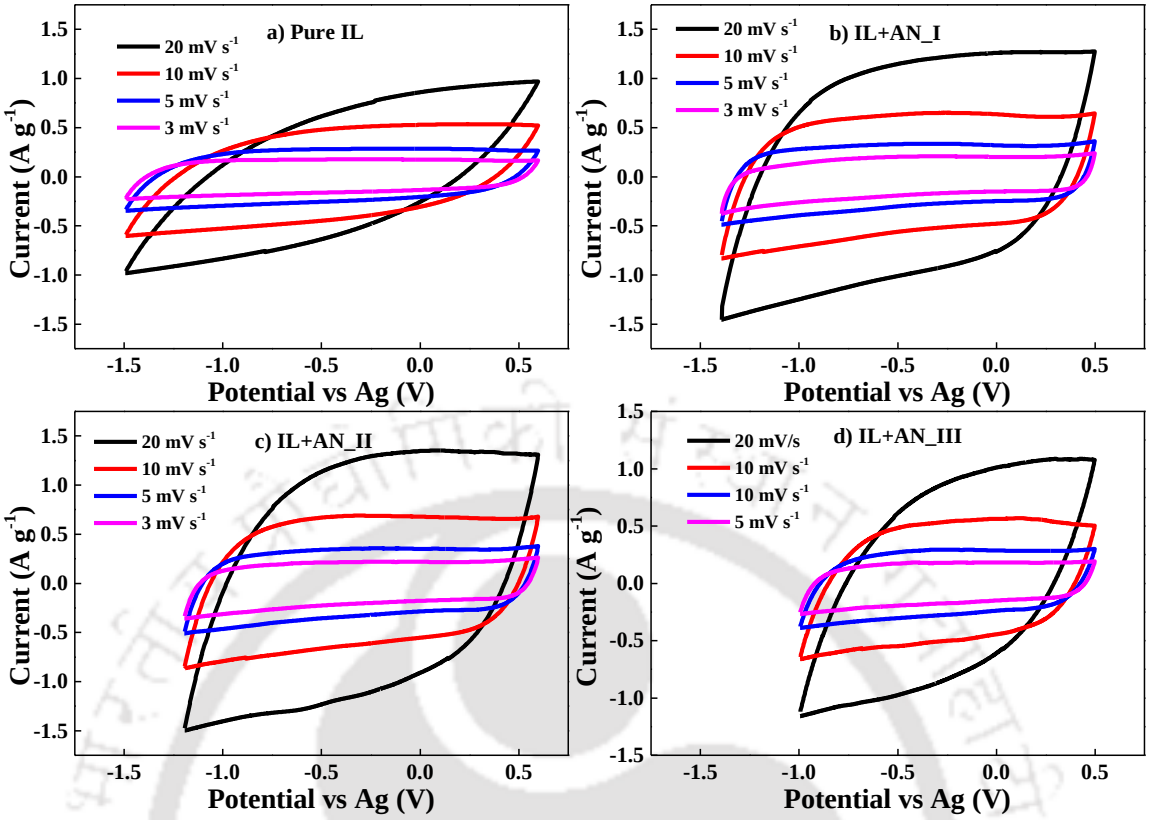

Figure 4.15: CV of [EMIM][BF_4] a) Pure IL, b) IL+AN_I c) IL+AN_II and d) IL+AN_III

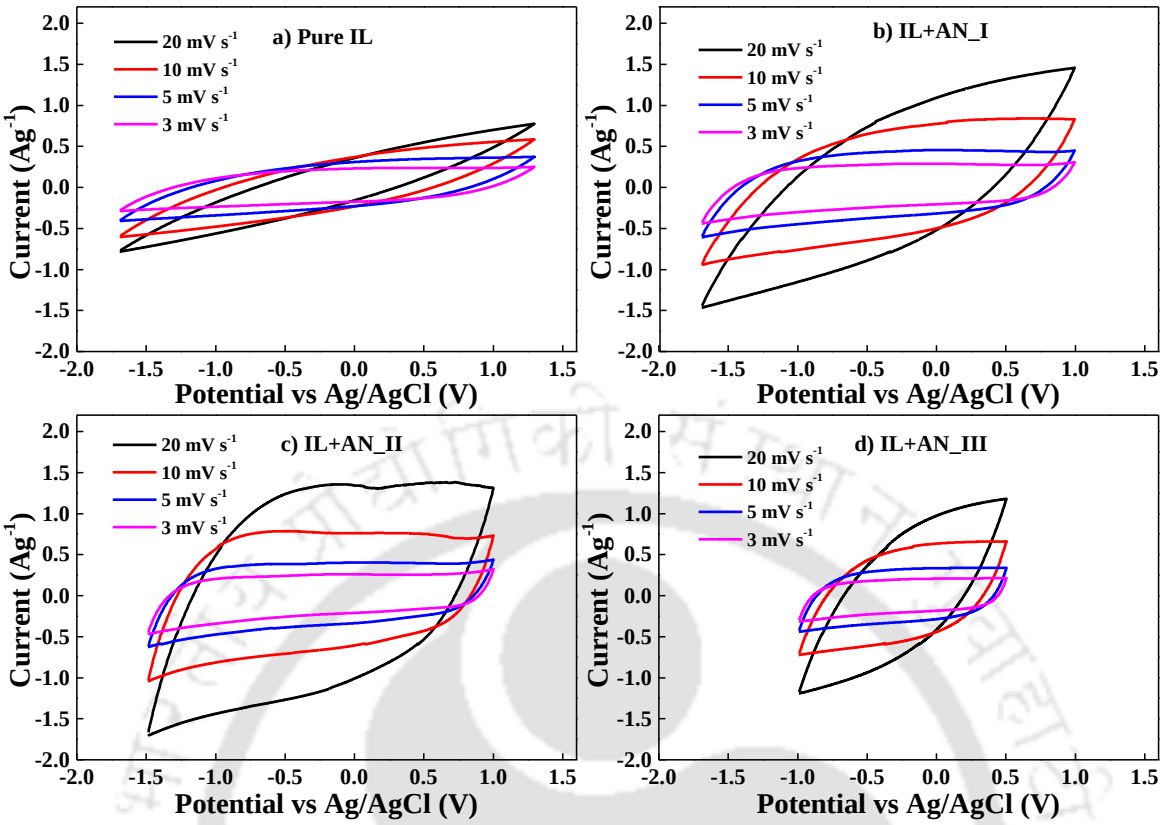

Figure 4.16: CV of [BMIM][BF_4] a) Pure IL, b) IL+AN_I c) IL+AN_II and d) IL+AN_III

The CV analysis reveals that IL+AN_I and IL+AN_II systems are most effective electrolytes. Hence for these, two concentrations were considered for investigation of mixed ILs. The OPW (2.3 V) for equimolar mixture of the two [AMIM][BF_4] ILs lies in between the electrochemical stability of the individual ILs (Figure 4.17). Both anodic and cathodic potential limits widen slightly for the mixture as compared to [EMIM][BF_4]. With increase in solvent concentration, rectangular shape of CV plot is more distinct which indicates improvement in capacitive behaviour. Although similar electrochemical stability is achieved for both concentrations of IL mixture, a little tendency of appearance of peaks can be figured out at both ends of CV plot of IL+AN_II (Figure 4.17b) which is absent in IL+AN_I solution (Figure 4.17a). This is attributed from higher co-solvent concentration that affects the electrochemical stability of ILs. Mixture of two ILs having same cation and

different anions were previously studied by Aken *et. al*, [52] and enhancement of OPW was obtained. In our study, cations are different which leads to additional cation-cation interaction and that results in lower specific capacitance (Figure 4.18). Reported study evidenced the formation of hydrogen bonds between cations leading to the formation of cation-cation clusters and reduction of the like-charge repulsion in ionic liquids [164]. This can result in additional resistance to cation diffusion in the study of mixed ILs, which prohibits the electrochemical dissociation of cations and hence improves OPW when compared to pure [EMIM][BF_4]. A mixture of [EMIM][Tf_2N] and 1-Propyl-3-methylpyrrolidinium Tf_2N was studied and a wide OPW of 3.5 V was achieved [165]. However, this study did not report the performance of individual ILs with same working electrode.

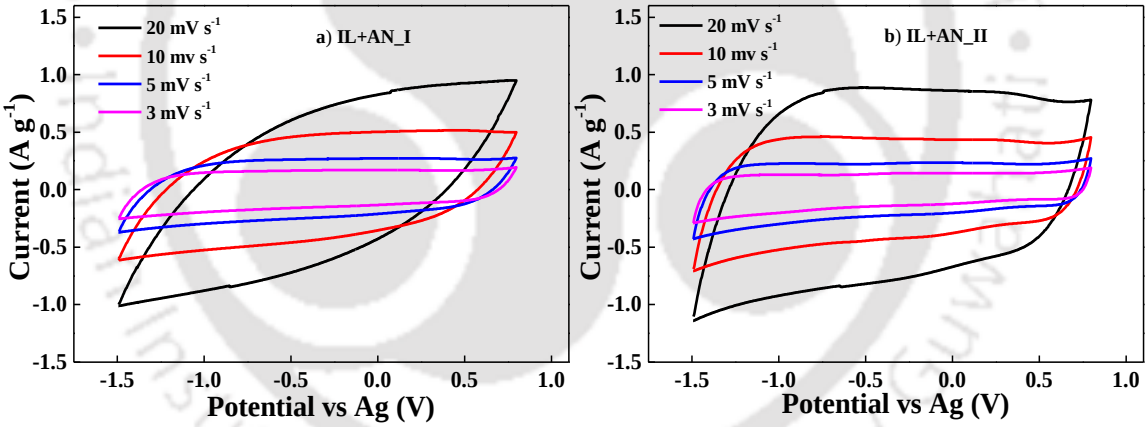

Figure 4.17: CV of [EMIM][BF_4] + [BMIM] [BF_4] a) IL+AN_I and b) IL+AN_II

The specific capacitance of [EMIM][BF_4] (Figure 4.18a) is more than [BMIM][BF_4] (Figure 4.18b) when pure ILs are compared. However, after dilution, charge storage is higher for the later one. “Electrolyte Starvation Effect” is also present with these ILs like [AMIM][Tf_2N] ILs since it is related to WE. As discussed above due to the cation-cation interaction, specific capacitance for the mixed ILs is the lowest (Figure 4.18c). Hence,

addition of [BMIM][BF_4] improves the electrochemical stability of [EMIM][BF_4]+AN solution nevertheless reducing the capacitance.

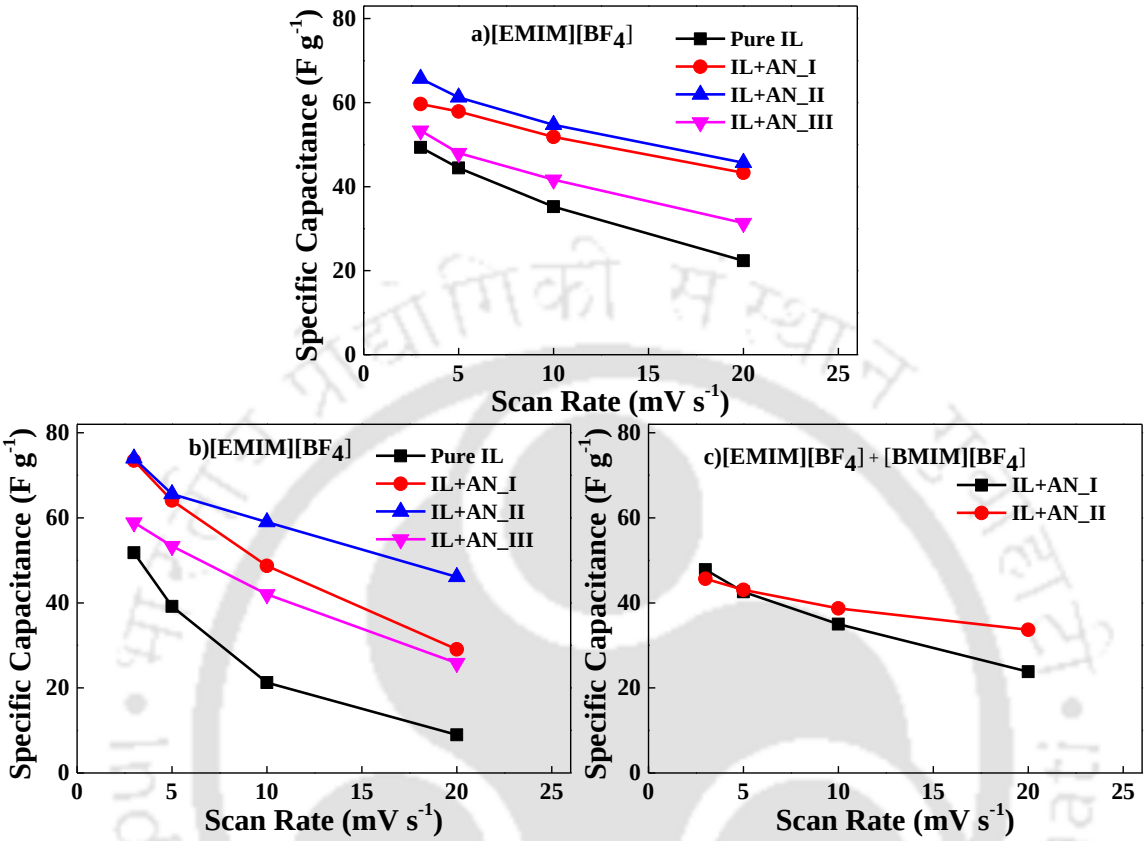

Figure 4.18: Specific capacitance of [AMIM][BF_4] from CV a) IL+AN_I and b) IL+AN_II

4.2.2 Galvanostatic Charge-discharge Measurements

The OPW obtained from CV were further confirmed from GCD for all the [AMIM][BF_4] based electrolytes (Figures 4.19-4.21). Here, the observed electrochemical stability window is narrower than [AMIM][Tf_2N] ILs. Hence, the effect of anion on OPW is notable. Moreover, [EMIM][BF_4] incurs significant loss in OPW upon dilution by co-solvent. The nature of charge-discharge profiles for [AMIM][BF_4] ILs are similar to that of [AMIM][Tf_2N] ILs. The highest IR drop is noted for pure ILs. Further it decreases with co-solvent addition and the least is for IL+AN_II. The least IR drop for all the electrolyte solutions are recorded at 0.3 A g^{-1}.

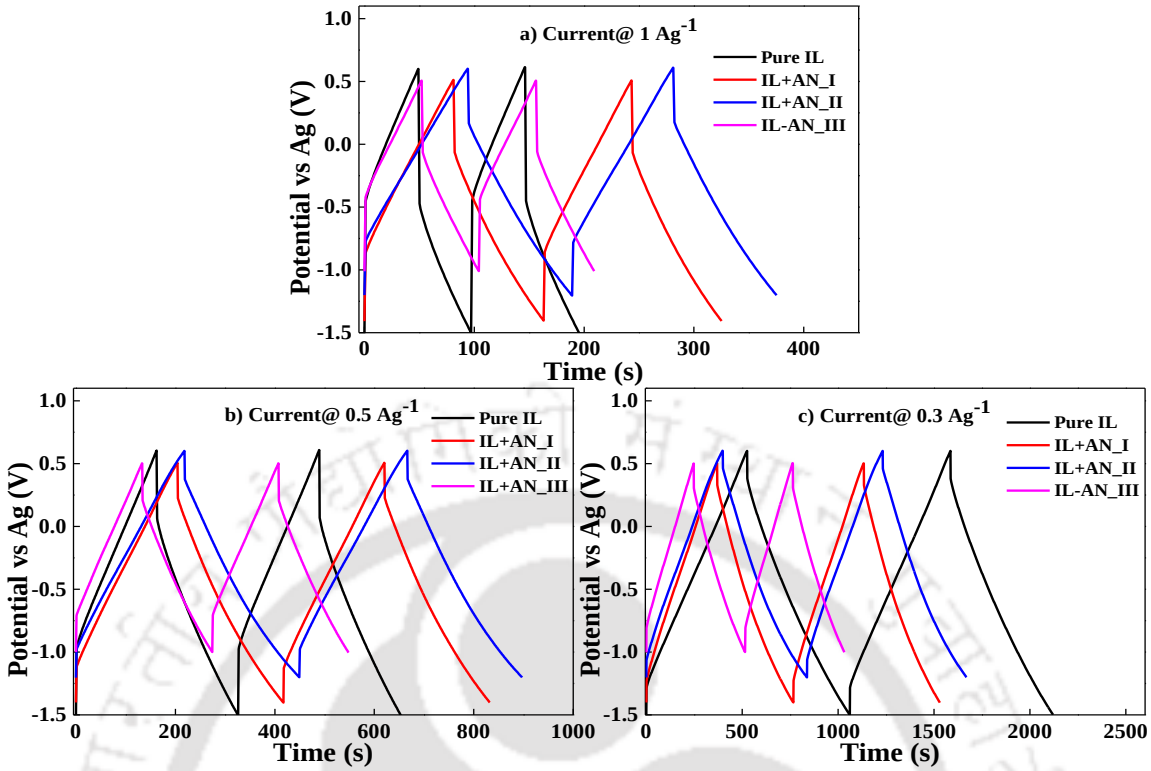

Figure 4.19: GCD of [EMIM][BF_4] at specific current a)1 Ag^{-1}, b)0.5 Ag^{-1} and c)0.3 Ag^{-1}

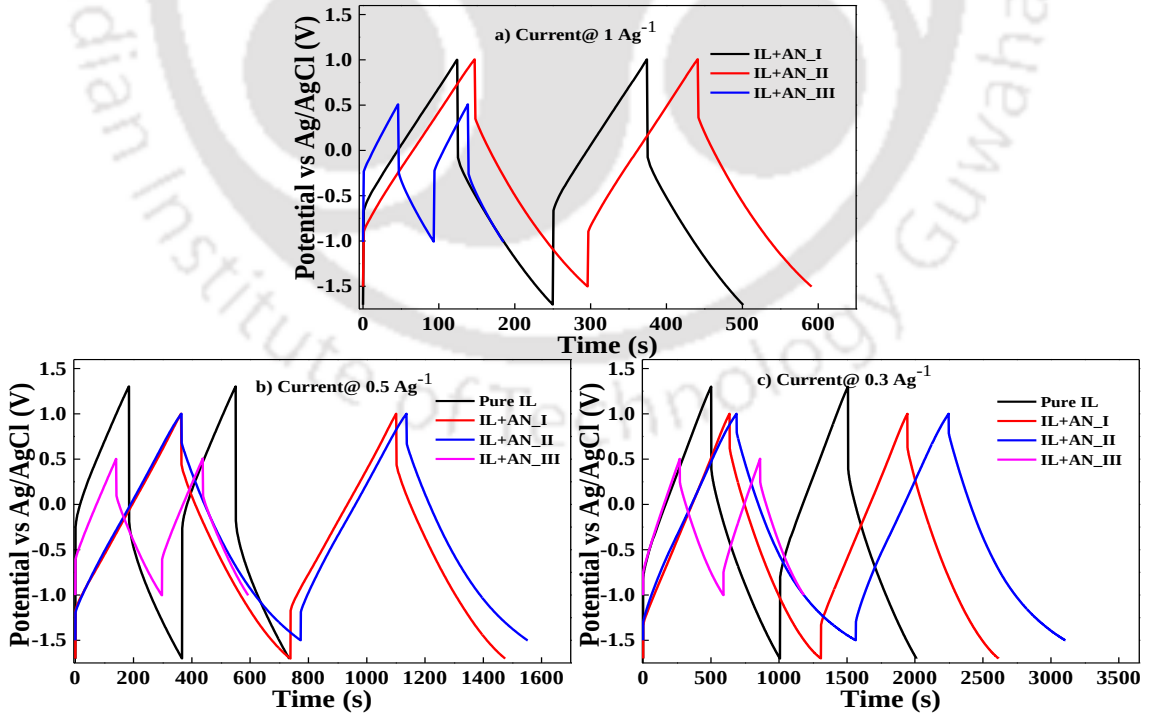

Figure 4.20: GCD of [BMIM][BF_4] at specific current a)1 Ag^{-1}, b)0.5 Ag^{-1} and c)0.3 Ag^{-1}

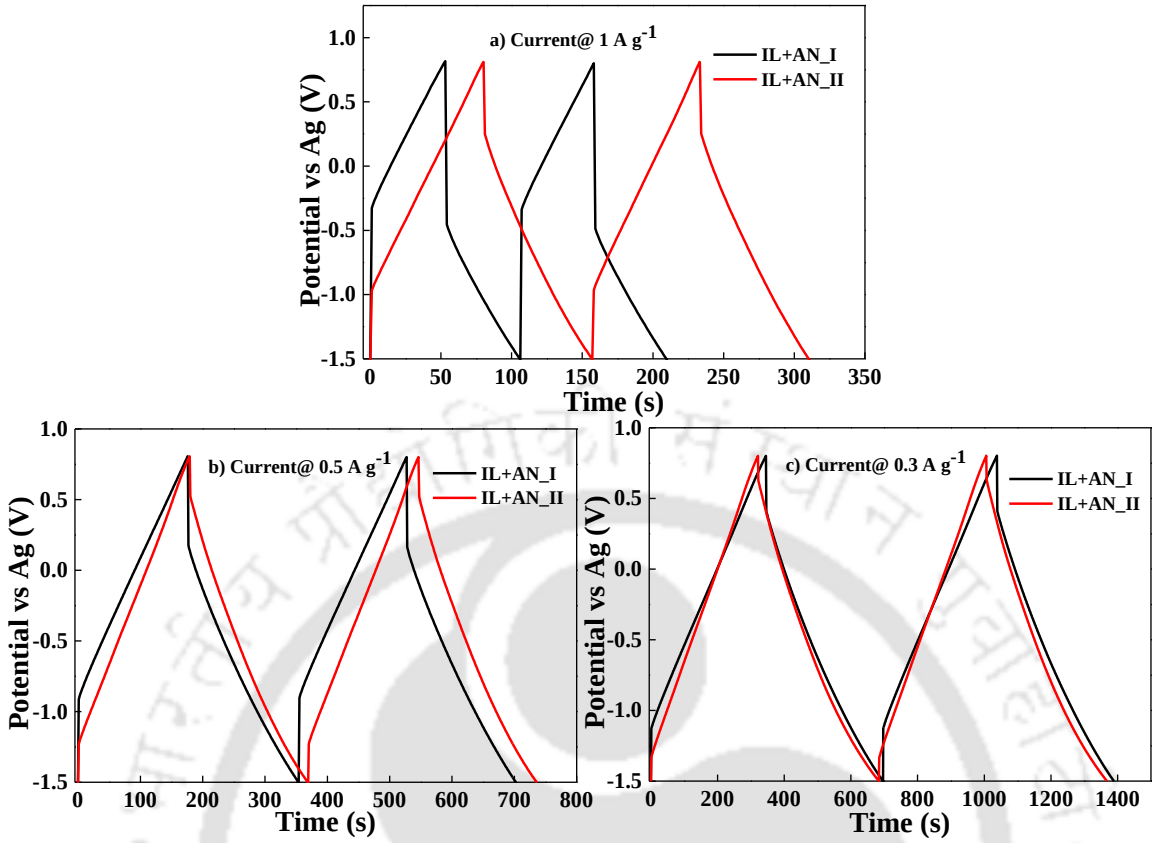

Figure 4.21: GCD of equimolar mixture of [EMIM][BF_4] and [BMIM][BF_4] at specific current a)1 A g^{-1}, b) 0.5 A g^{-1} and c) 0.3 A g^{-1}

Moreover, calculation of capacitance and ESR from GCD data were also done following equations 3.3 and 3.4 respectively. The ESR for the electrolyte solutions (Figure 4.22) does not vary with current density except for pure [EMIM][BF_4] (Figure 4.22a). Here, ESR reduces significantly at 0.3 A g^{-1} unlike [EMIM][BF_4]+co-solvent electrolytes. At lower specific current, the electrolyte-electrode system gets sufficient time for charging and hence more charge can be stored. Additionally, since pure ILs has the highest concentration of ionic species, it can deliver more charge when discharge takes place at lower specific current. As a result, ESR minimizes and specific capacitance (Figure 4.23) maximizes thereby contradicting the findings from CV. Moreover, since the effect of dilution on OPW in case of [EMIM][BF_4] is significant, use of this IL without co-solvent will be preferable for low current applications to retain higher energy density.

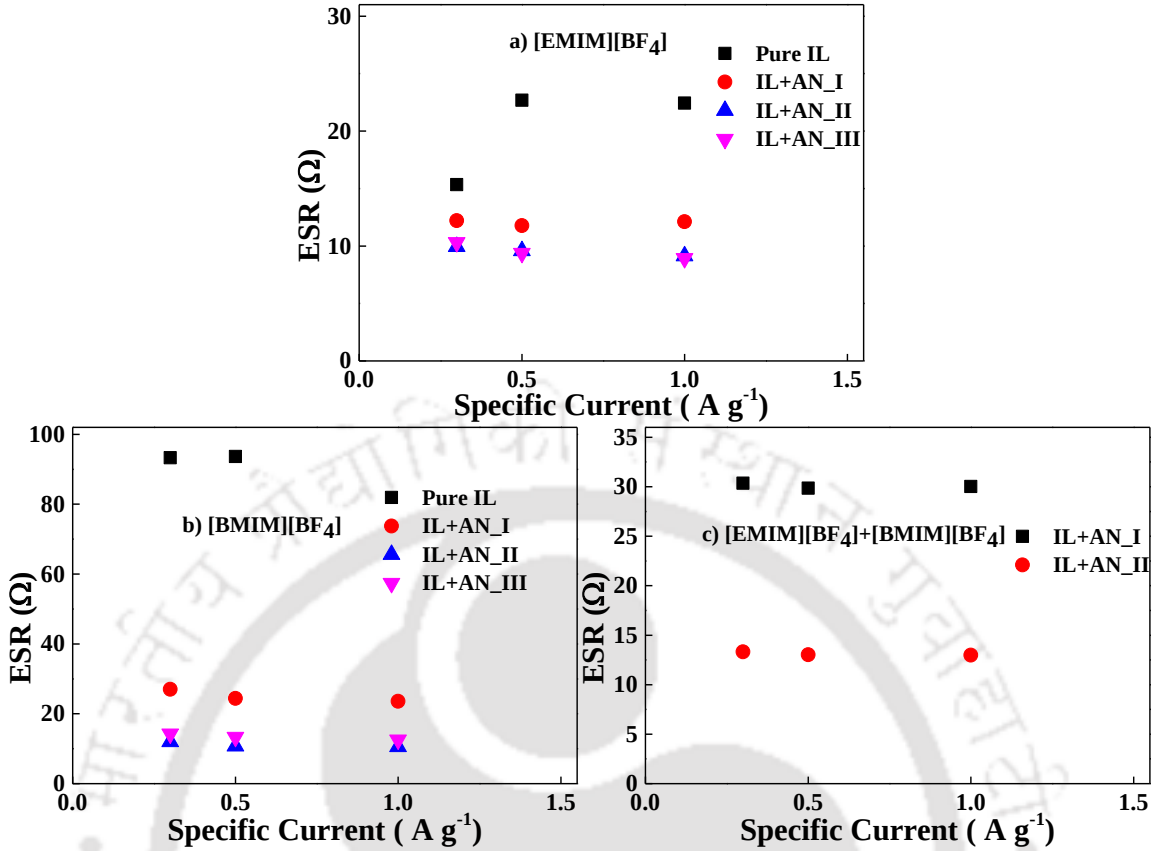

Figure 4.22: ESR of [AMIM][BF_4] ILs from GCD a) [EMIM][BF_4] b) [BMIM][BF_4] and c) equimolar mixture of [EMIM][BF_4] and [BMIM][BF_4]

The capacitive trend of [BMIM][BF_4] matches the already discussed three [AMIM][Tf_2N] ILs. The ESR for pure [BMIM][BF_4] is much higher (Figure 4.23b) and not favourable for longer durability of the EDLC. Here, the specific capacitance passes through the maxima at IL+AN_II. Following the data obtained from CV, both IL mixtures store nearly equal charge (Figure 4.23c) even though ESR for IL+AN_I is higher (Figure 4.22c). Two different dominating factors for charge storage may be possible here. In IL+AN_I, ion concentration is more and hence higher specific capacitance. Furthermore, ion diffusion is faster for IL+AN_II due to its greater solvent concentration resulting higher charge storage. In this regard, IL+AN_II is a more favourable electrolyte with a lower ESR when IL mixture is opted.

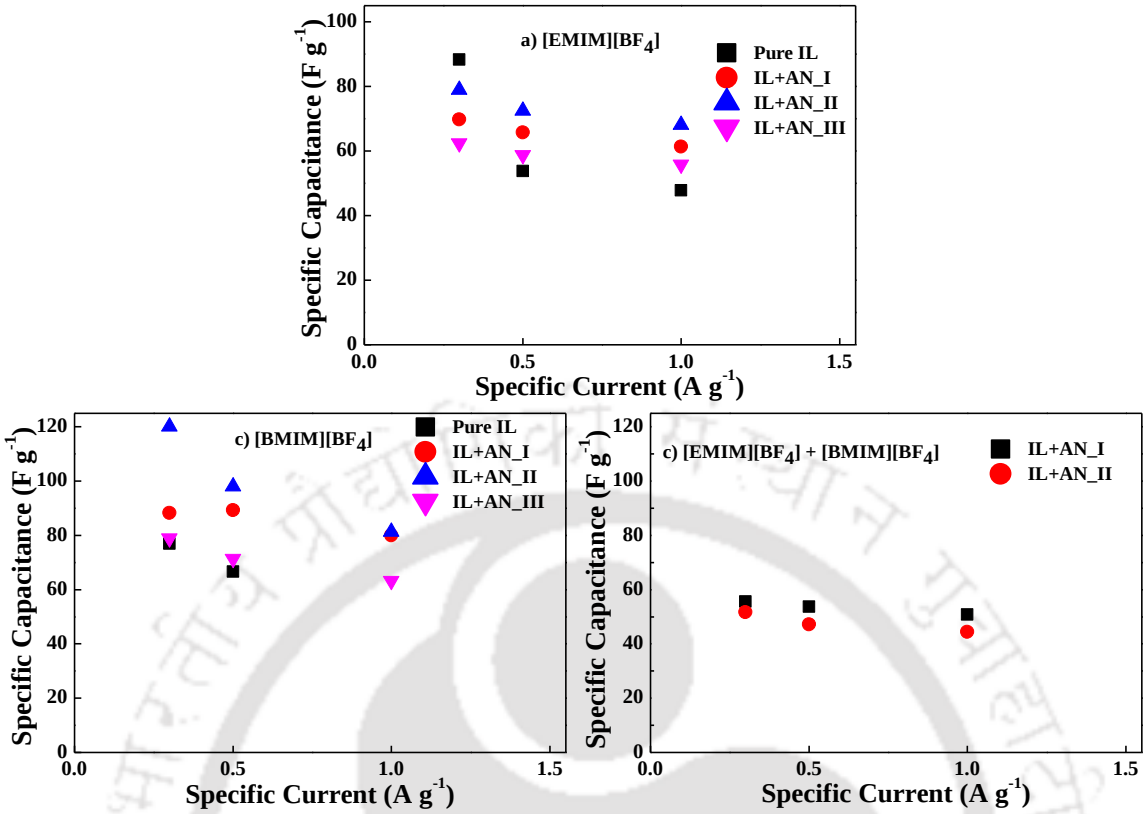

Figure 4.23: Specific capacitance of [AMIM][BF_4] ILs from GCD a) [EMIM][BF_4] b) [BMIM][BF_4] and c) equimolar mixture of [EMIM][BF_4] and [BMIM][BF_4]

4.2.3 Electrochemical Impedance Spectroscopy

The systems with the minimum ESR (IL+AN_II) were further considered for EIS evaluation. Figure 4.24 reflects the types of resistances associated with ion diffusion. The impedance data obtained was further iterated using *ZSimpWin* software by fitting electrical equivalent circuit (Figure 3.5) to compute the ESR or internal resistance as discussed in Chapter 3. Table 4.1 compares the internal resistance obtained from GCD and EIS. Both the techniques work on different principles and EIS is highly sensitive to external electric field. Hence variation in ESR values cannot be denied. ESR obtained from GCD and EIS closely matches each other when [EMIM][BF_4] +AN_II is considered. However, for the other two systems noteworthy deviation is recorded. Additionally, both the methods confirm the lowest ESR for [EMIM][BF_4]. Again, GCD predicts the highest ESR for

mixture of ILs whereas EIS indicates the same for [BMIM][BF_4] due to greater contribution from R_{ct}. Due to bigger size of the BMIM cations, it suffers more ionic resistance inside the pores of the electrode. The shorter capacitive tail can be observed when [AMIM][BF_4] ILs are compared with their mixture which reflects the lower value of $Z^{//}$ at a particular frequency and hence better specific capacitance is reported for the individual ILs.

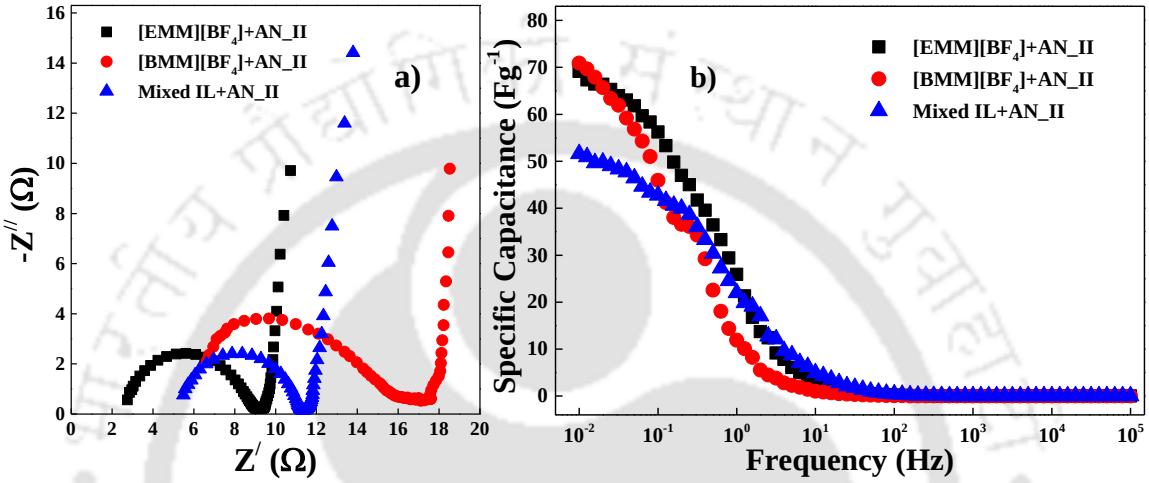

Figure 4.24: a) Nyquist plot at 0 V vs OCP and b) frequency dependant specific capacitance for AN solvated [AMIM][BF_4] electrolyte solutions

Table 4.1: Comparison of ESR obtained from electrochemical cell equivalent circuit modelling and GCD

System	R_s (Ω)	R_{ct} (Ω)	ESR from EIS (Ω)	ESR from GCD at 0.5 A g^{-1} (Ω)
[EMIM][BF_4] +AN_II	2.85	5.70	8.87	9.53
[BMIM][BF_4] +AN_II	6.88	9.02	15.9	10.73
[EMIM][BF_4] +[BMIM][BF_4] +AN_II	5.54	5.22	10.76	13.03

4.2.4 Summary of Section 4.2

The highest ESR is obtained for ILs without solvents despite their widest OPW. The OPW of [AMIM][BF_4] gradually decreases with increase in co-solvent concentration similar to [AMIM][Tf_2N] in the previous section. The OPW obtained for mixed ILs lies in between the same obtained for the constituents at same solvent concentration. The effects of alkyl chain length on electrochemical performance is significant. Double layer charging behaviour is confirmed from electrochemical characterization. EIS data modelling reveals the contribution of solution and charge transfer resistances on total ESR of the system.

4.3 Results and Discussion on [BMPy][BF_4] Ionic Liquid

This section includes the solvation effects on electrochemical stability, ESR and specific capacitance of [BMPy][BF_4]. Due to highly viscous nature (APPENDIX B: Table B1) of the IL, electrochemical studies were not conducted for pure IL. Two solvents namely AN and PC were added to the IL at same composition and further characterization was done.

4.3.1 Solvation Effects Predicted by Cyclic Voltammetry

The OPW of RGO based EDLC was determined using CV by measuring the cathodic and anodic stability limits of different mixtures of [BMPy][BF_4] in AN (Figure 4.25) and PC (Figure 4.26).

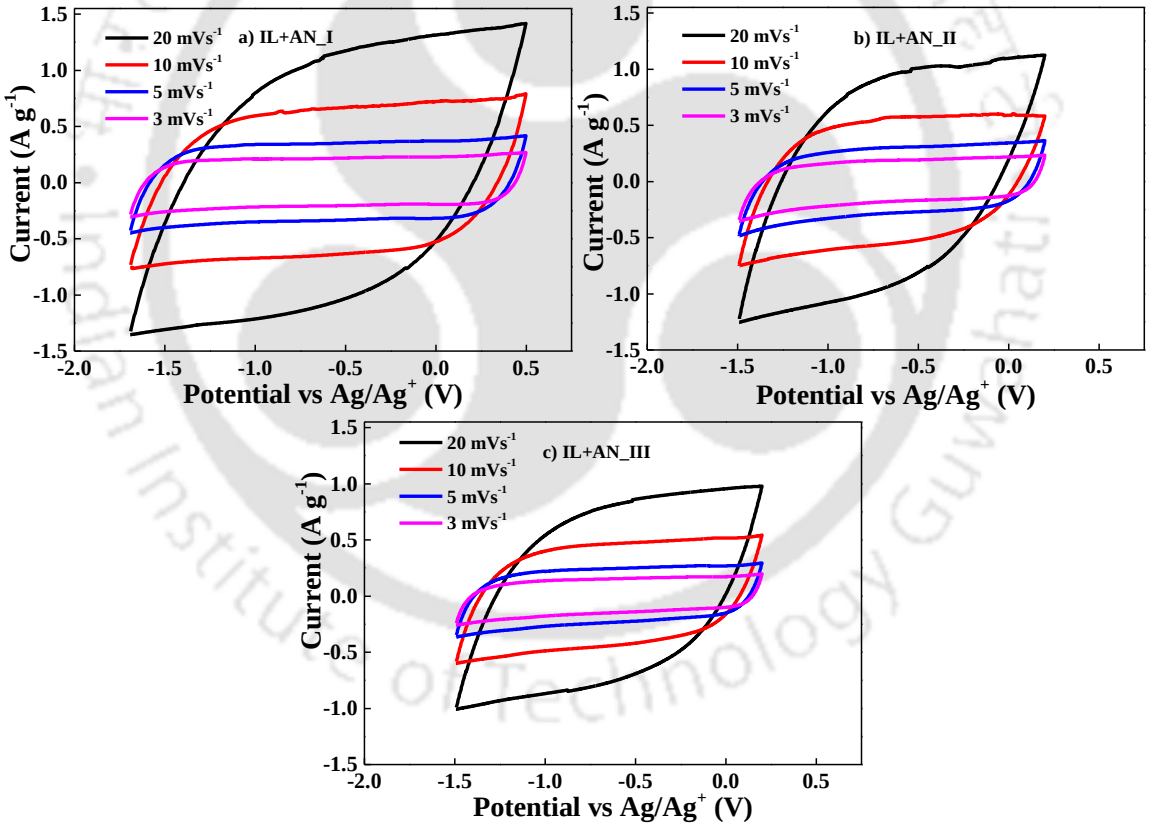

Figure 4.25: CV plots of [BMPy][BF_4] in AN a) IL+AN_I, b) IL+AN_II and c) IL+AN_III

For AN-based of electrolytes, widest OPW (2.2 V) is obtained for 25% AN in IL i.e. IL+AN_I, whereas for other two compositions the measured electrochemical stability is

limited to only 1.7 V. However, OPW of 2.2 V is obtained with all concentrations of PC. The higher concentration of PC does not shrink the OPW of the electrolyte solution unlike AN. The results from imidazolium ILs also confirm that increased wt. % of AN narrows down the OPW. All the CV plots reflect the ideal double layer capacitive behaviour. Further, application of a potential difference of 2.2 V to IL+AN_II electrolyte solution leads to the tendency of appearance of peaks at both the ends indicating evolution of gas [75] when compared to PC_II solution (Figure 4.27). Studies on TEABF4 salt as a solution of equal concentration in AN and PC also showed that TEABF4/PC system had OPW wider by 0.5 V than $TEABF_4$/AN [166]. Moreover, wider temperature range of PC than AN as mentioned in Table 3.1 leads to better thermal stability of PC based electrolytes.

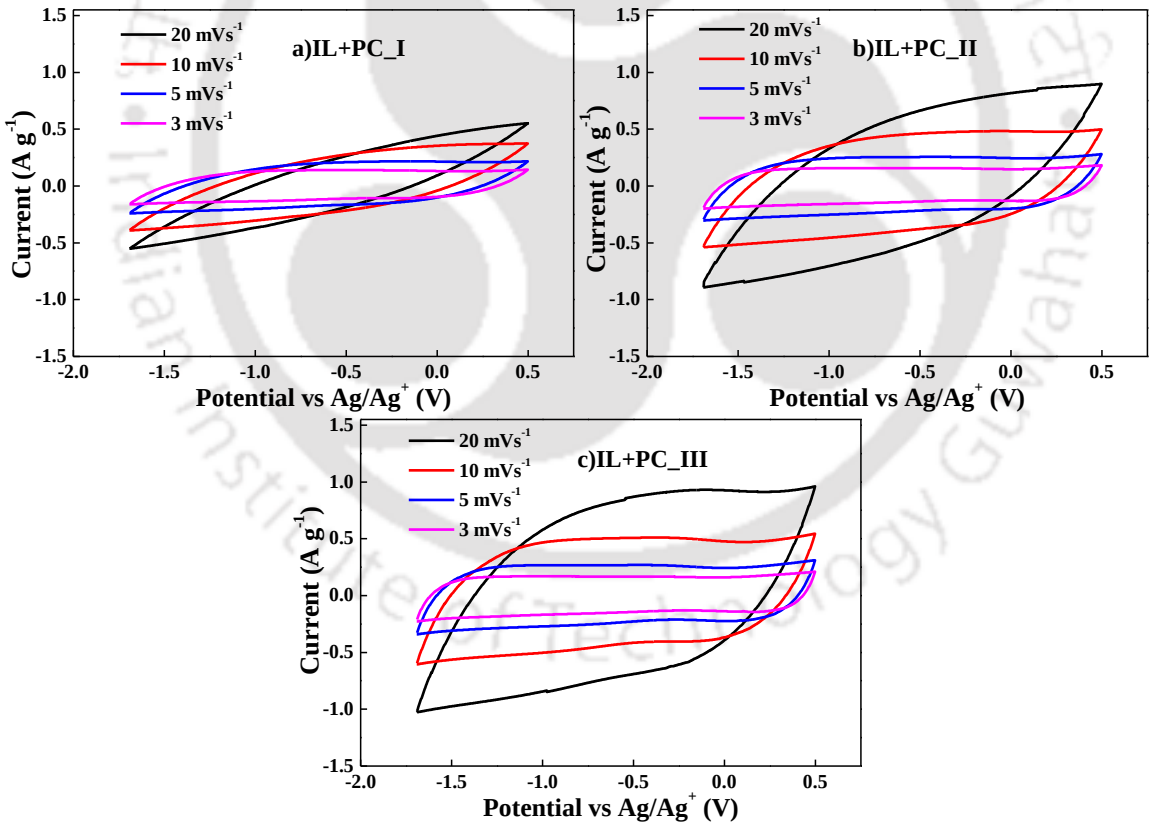

Figure 4.26: CV plots of [BMPy][BF_4] in PC a) IL+PC_I, b) IL+PC_II and c) IL+PC_III

For IL electrolytes, conventionally the cathodic limit is set by the reduction potential of cation and the anodic limit is bounded by the oxidation potential of anion. However,

reported literature states that this convention may not be true always and anodic stability can be limited by oxidation of cation [167,168]. The observed OPW is narrower than [BMIM][BF_4] due to the lower anodic limit. This predicts that pyridinium cation has probably went through oxidation earlier than BF_4 anion, since wider electrochemical stability of BF_4 was reported from computational studies [169]. Electrochemical stability of 1.2 V was obtained by Ruiz *et. al.*, for 2-methoxypyridinium trifluroacetate and MnO_2 based electrode [170] which suggests lower electrochemical stability of pyridinium based cation. Apart from type of the electrolytes, electrochemical stability also depends on the impurity of the electrolyte solution ,trace of water present and type of electrode material [45].

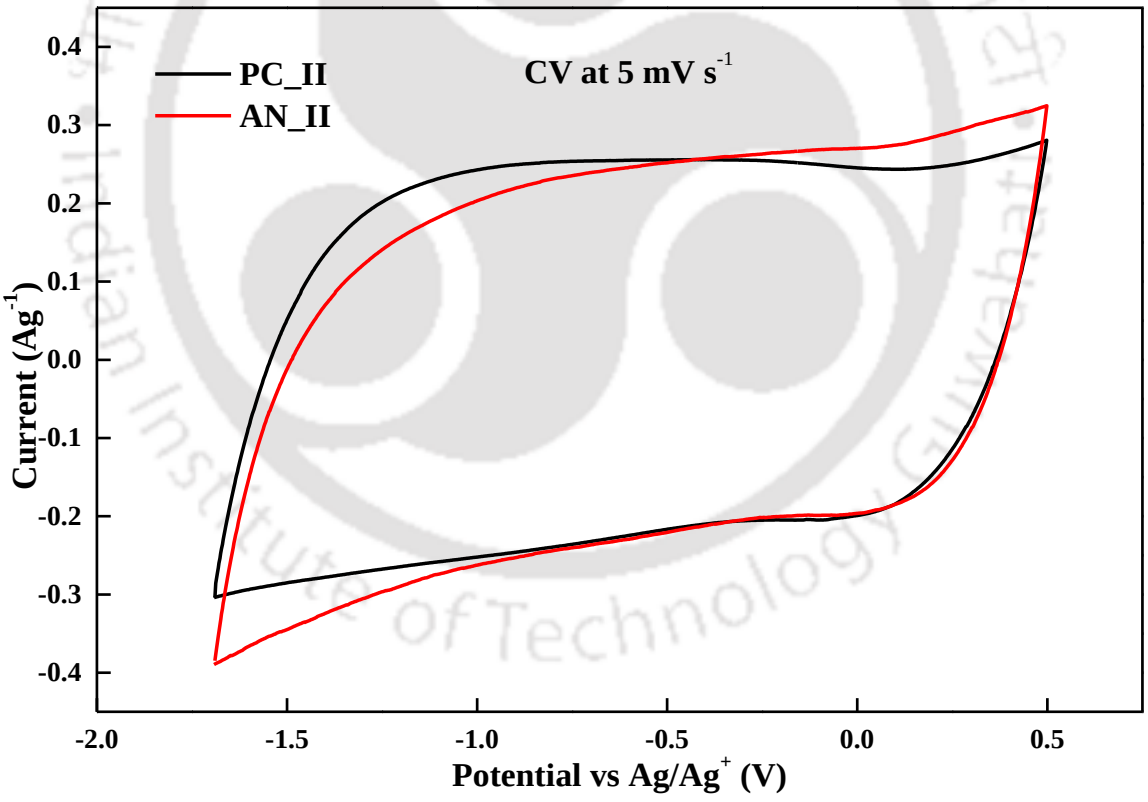

Figure 4.27: Comparison of electrochemical stability of AN and PC based IL solutions

The dilution effect on specific capacitance for [BMPy][BF_4] is reported in Figure 4.28. The two co-solvents i.e. AN and PC act differently on specific capacitance. AN-based IL

solutions possess better capacitive performance irrespective of scan rate. IL+AN_I results in the highest specific capacitance whereas the lowest is observed for IL+PC_I. Even though specific capacitance is superior for IL+PC_III solution when all three PC based solutions are compared, it is lesser than IL+AN_I by ~20 F g^{-1}. "Electrolyte Starvation Effect" is also prominent for pyridinium based IL which leads to the scan rate affected capacitive behaviour. CV analysis for [BMPy][BF_4] reveals that IL+AN_I electrolyte solution is more beneficial than the others when both OPW and specific capacitance are considered.

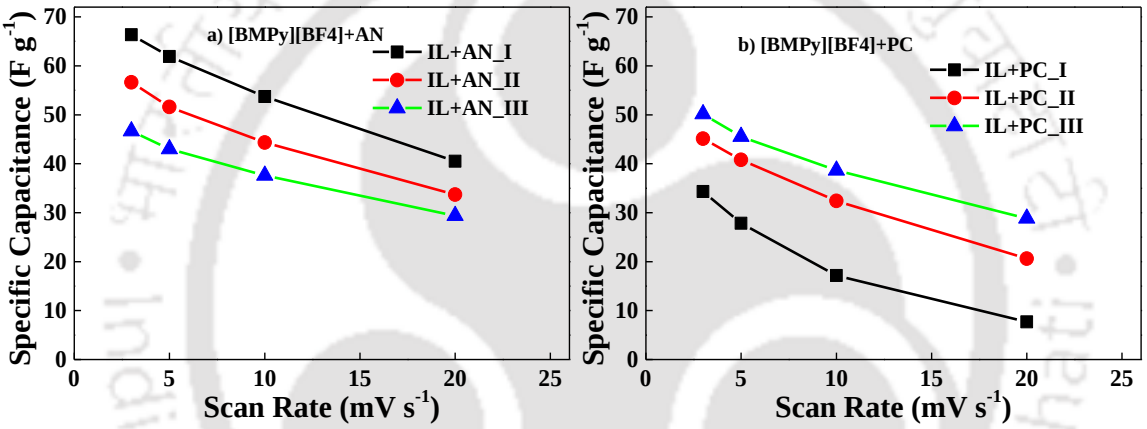

Figure 4.28: Specific capacitance as a function of CV scan rate for [BMPy][BF_4] in a) AN and b) PC

4.3.2 Insights from Galvanostatic Charge-discharge

GCD profiles elucidate higher IR drop for PC based electrolyte solutions (Figure 4.29). This indicates lower ionic conductivity of those solutions. However, all the figures reproduce the OPW and double layer capacitive nature as discussed in the previous section. IL+PC_I solution is highly viscous (APPENDIX B: Table B1) and hence at a higher current of 1 A g^{-1}, GCD could not be executed (Figure 4.29d). Even at 0.5 A g^{-1}, IR drop is very high (Figure 4.29e). On the contrary, for IL+AN solutions, no such difficulties were encountered while performing GCD experiments. This elucidates better dissociation of the

electrolyte in AN. AN can facilitate breaking of ion-pair interaction of the IL in a more effective manner than PC. Hence, solution resistance or resistance to ion transport in the solution can be reduced easily for AN solvated IL. Overall, the ohmic loss of potential is minimum for IL+AN_I system (Figure 4.29a). The results from ESR and specific capacitance measurements provide a comprehensive idea about solvation effects on electrochemical performance of [BMPy][BF_4]. The internal resistance values for IL+AN solution (Figure 4.30a) as predicted by GCD reside in the range of 10-20 Ω unlike PC based electrolytes (Figure 4.30b). IL+ AN_I and IL+AN_II depict nearly equivalent ESR and specific capacitance (Figures 4.30a and 4.31a) from GCD. However, owing to better OPW of IL+AN_I, it is more favourable for better energy storage.

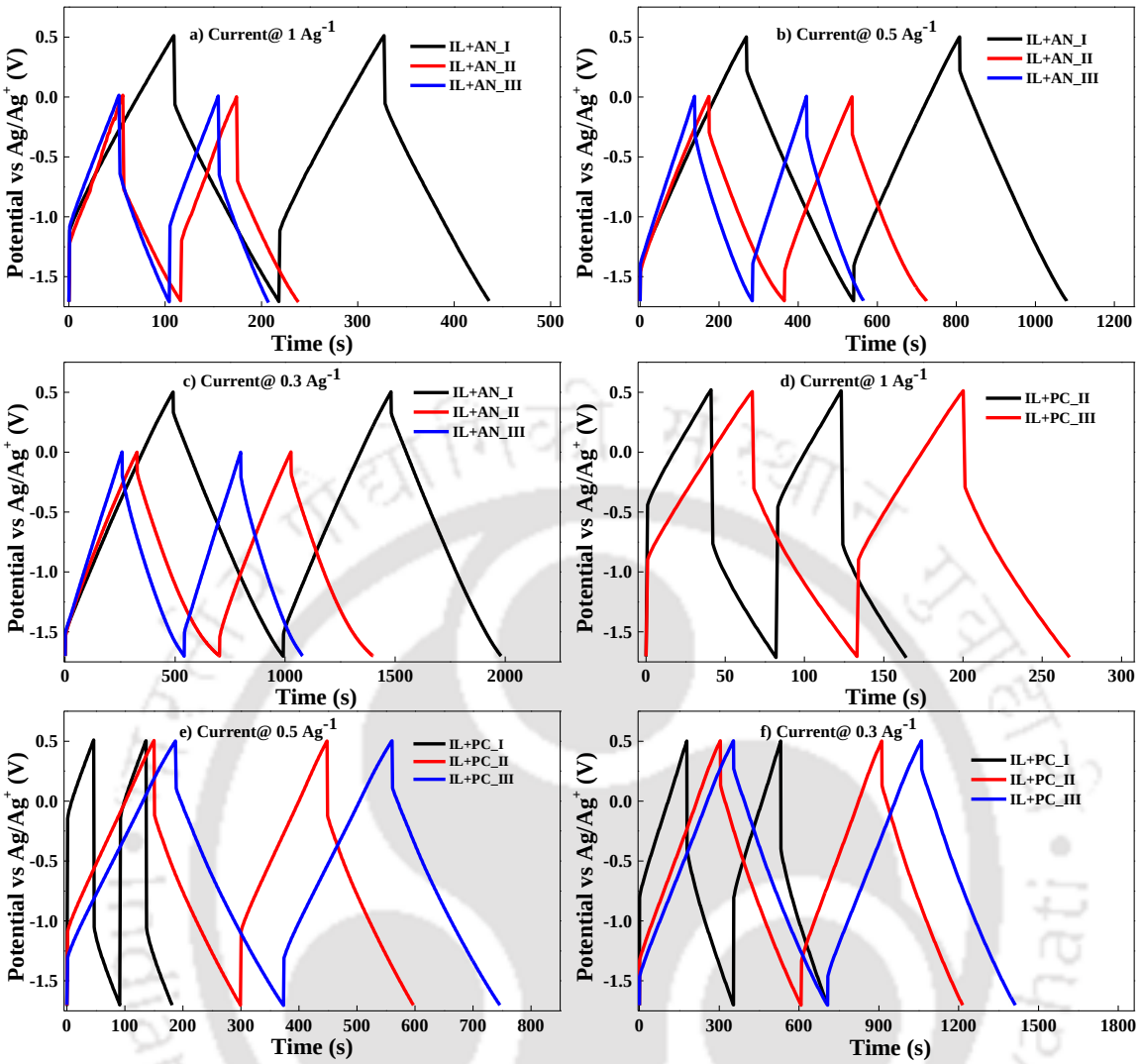

Figure 4.29: GCD profiles for [BMPy][BF_4] solvated by AN and PC

IL+PC_I reports the highest ESR (Figure 4.30b) and hence the lowest specific capacitance (Figure 4.31b). Further the reverse is observed for IL+PC_III solution and its ESR closely matches AN based electrolyte. This can be directly related to the viscosity trend (APPENDIX B, Table B1) for the PC based electrolytes. Lower the viscosity, better is the specific capacitance. Nonetheless, the same convention is not applicable to AN. Despite of having higher viscosity of IL+AN_I than other two solutions, it possesses more ionic strength and hence better charge storage. In this regard it can be confirmed that AN has inherent ability to break the strong ionic interaction more easily even at a lower concentration (25 wt. %). Further with addition of more AN, specific capacitance decreases

regardless of viscosity reduction. Therefore, for room temperature and higher temperature applications, IL+AN_I and IL+PC_III are recommended to be respective electrolytes.

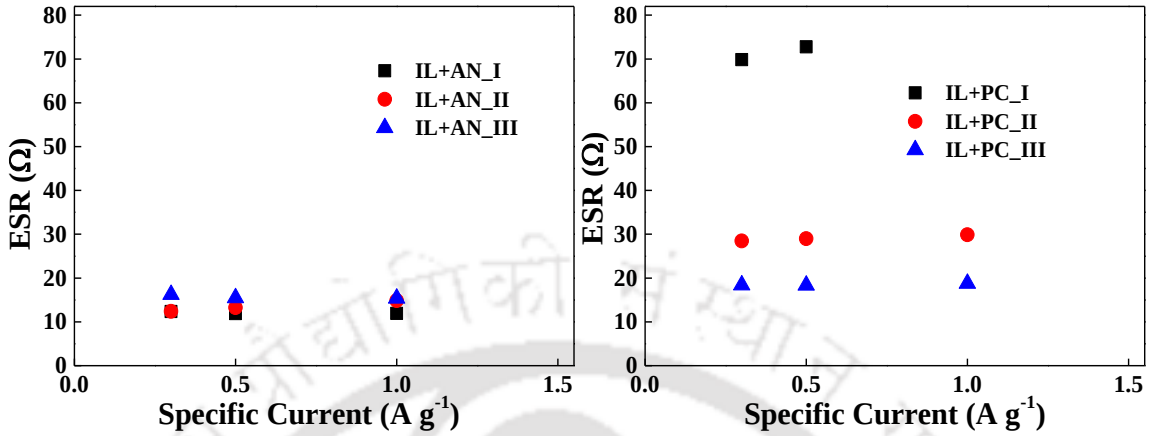

Figure 4.30: Comparison of ESR between AN and PC based [BMPy][BF_4] solutions

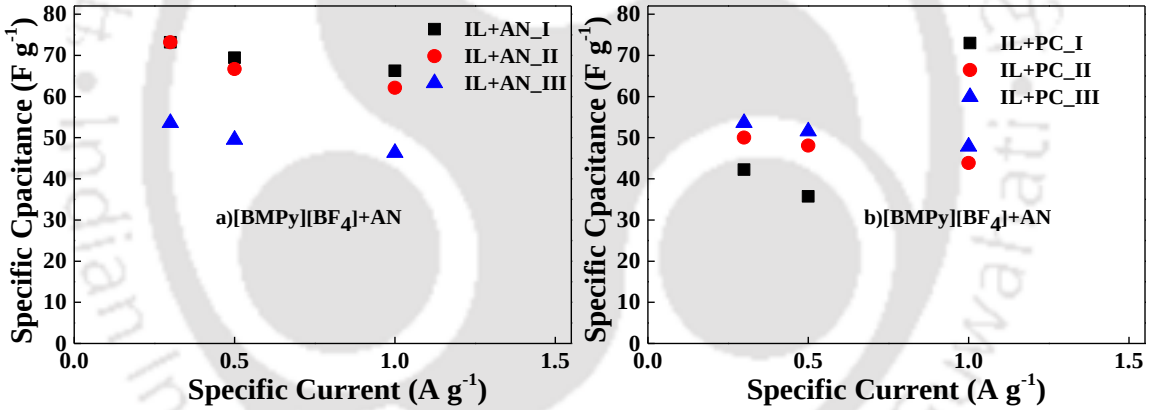

Figure 4.31: Specific capacitance for AN and PC based [BMPy][BF_4] solutions

4.3.3 Impedance Analysis

Following the recommendation from CV and GCD analysis, IL+AN_I and IL+PC_III were further characterised with FRA. The impedance analysis clearly reveals higher R_s and R_{ct} for [BMPy][BF_4] (Figure 4.32) than imidazolium ILs. The more resistive nature of IL+PC_III can be confirmed from its higher R_s value (~23 Ω). Moreover, Z_w as represented by the 45° line is more prominent for PC_III than AN_I indicating lager pore diffusional

resistances. EIS also shows lower specific capacitance for IL+PC_III. The vertical tail for AN_I is shorter than PC_III resulting in improved specific capacitance.

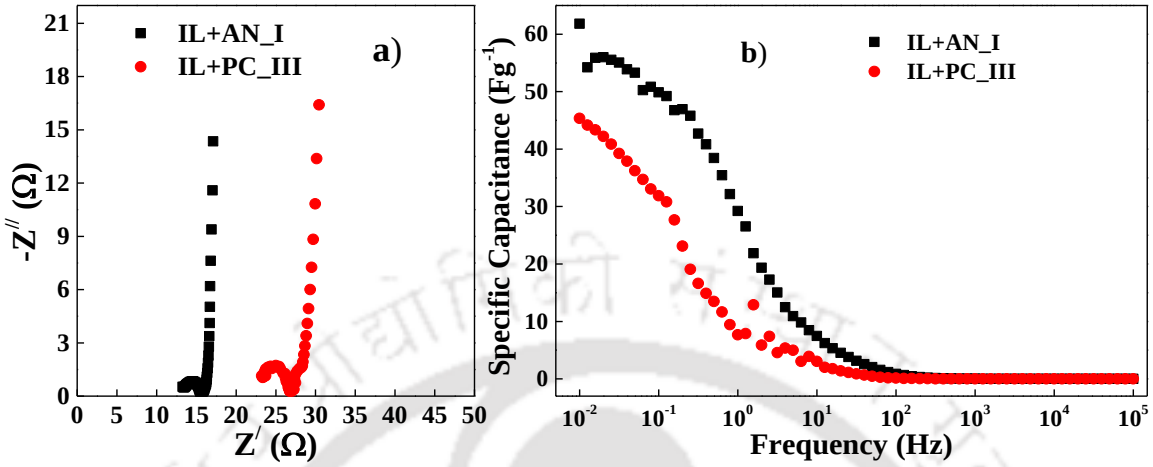

Figure 4.32: a) Nyquist plots and b) frequency dependant capacitance for [BMPy][BF_4] based electrolyte solutions

4.3.4 Summary of Section 4.3

[BMPy][BF_4] IL resulted in narrower OPW than already discussed imidazolium ILs. Both the solvents behaved differently in regards of electrochemical characterization. With the increase in AN wt % in the IL electrolyte, both OPW and specific capacitance decreases with a slight increase in ESR. On the contrary, addition of more amount of PC did not affect the OPW and confirmed large reduction in ESR hence, enhancement in specific capacitance was obtained. Impedance studies for AN_I and PC_III revealed good capacitive nature of these electrolyte systems.

4.4 Results and Discussion on [TESu][Tf_2N] Ionic Liquid

This section covers the electrochemical performance of pure [TESu][Tf_2N] as well as its solutions in PC. All three electrochemical techniques were performed following the previously reported ILs.

4.4.1 Analysis from Cyclic Voltammetry

The OPW for [TESu][Tf_2N] (Figure 4.33) with addition of co-solvent starts to constrict in a similar pattern to the ILs of other categories. Pure [TESu][Tf_2N] provides the OPW of 3 V which is equal to [EMIM][Tf_2N]. Further there is a decrease of 0.4 V for its solutions in PC. Even though current increases with addition of PC, it is not comparable to imidazolium ILs + co-solvents. Ion mobility does not increase much with dilution by PC. Specific capacitance from CV data also agrees to the above statement (Figure 4.34). Addition of co-solvent cannot enhance the specific capacitance significantly. The highest specific capacitance was observed for IL+PC_II system even though the difference is ~10 F g^{-1} when compared to pure IL. Pure IL and IL+PC_III electrolytes possess equivalent capacitive performance. From CV also, similar current generation can be noted (Figures 4.33a and d). The IL when tested for activated carbon based EDLC delivered ~ 20 F g^{-1} at 5 mV s^{-1} with OPW of 2.8 V [63]. Hence it is understood explicitly that the capacitance behaviour of [TESu][Tf_2N] in PC is not very impressive although it has reasonable electrochemical stability.

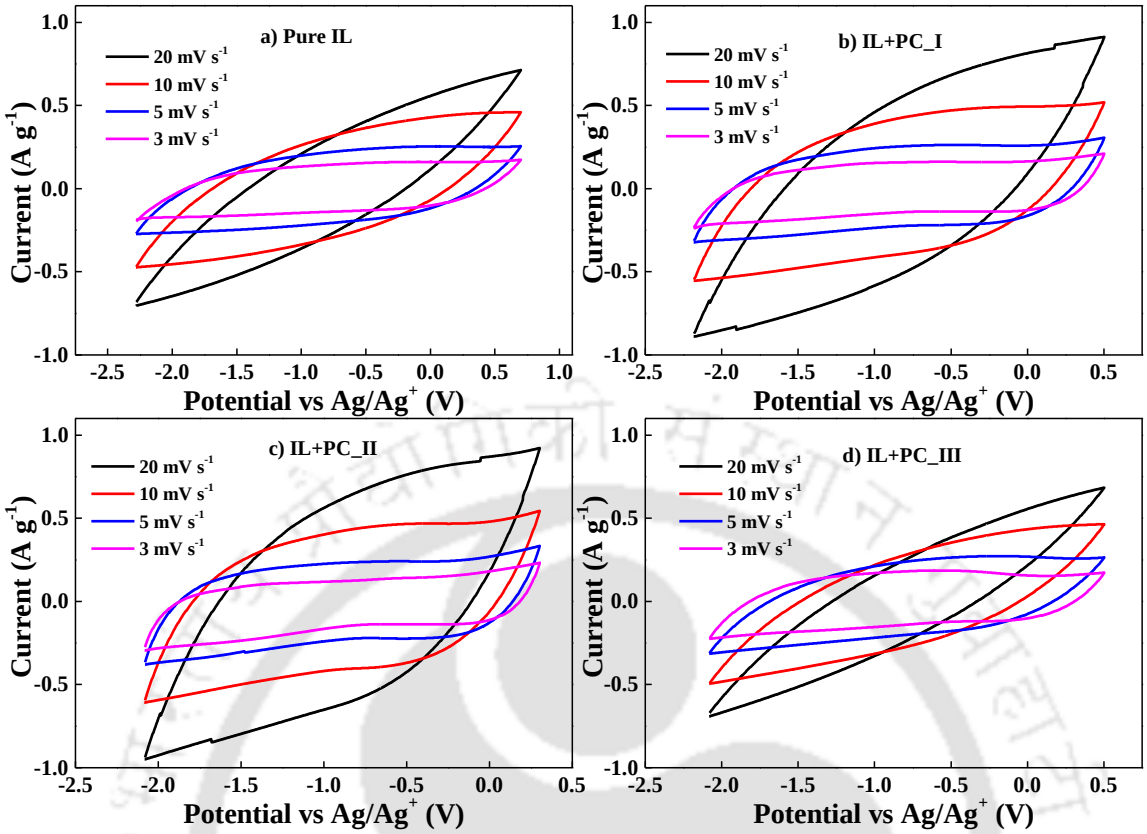

Figure 4.33: Cyclic voltammogram for [TESu][Tf_2N] based electrolytes

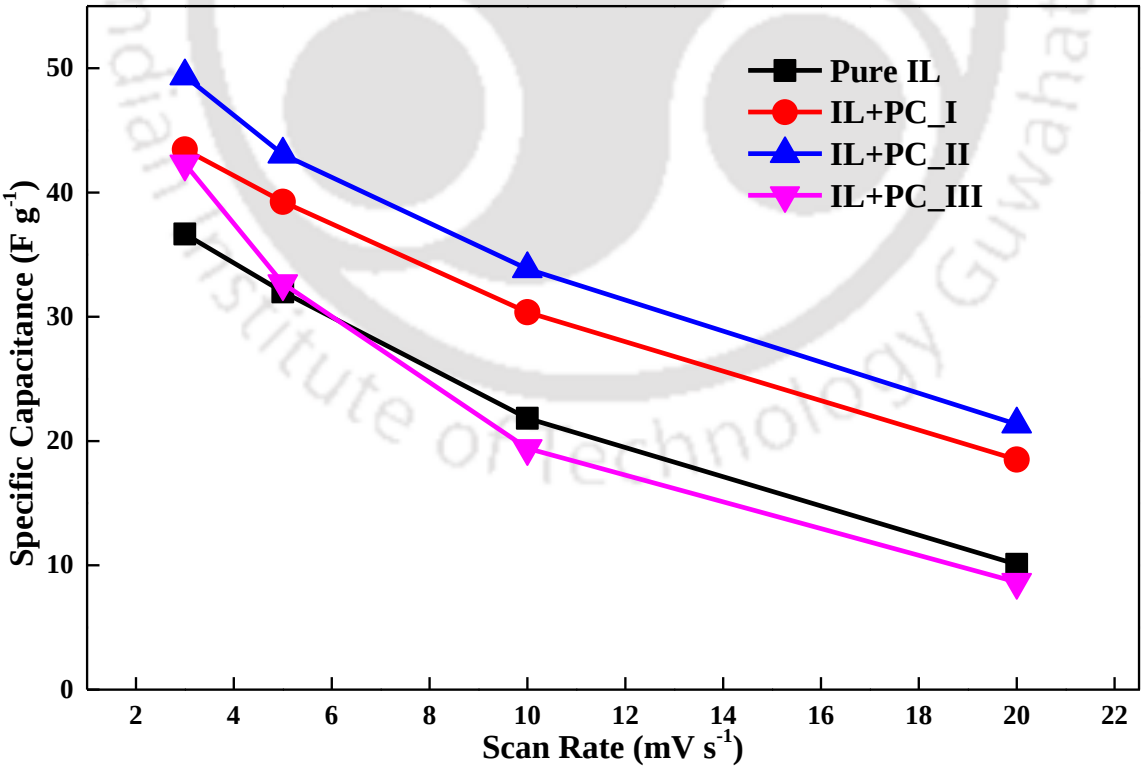

Figure 4.34: Specific capacitance evaluated from CV for [TESu][Tf_2N] based electrolytes

4.4.2 Insights from Galvanostatic Charge-discharge

The analysis from GCD results imparts how change in wt. % of co-solvent affect the OPW and IR drop of the IL (Figure 4.35). The ion dissociation is the least for pure IL as it delivers the highest ohmic drop. With the addition of PC, the system's ESR (Figure 4.36a) and specific capacitance (Figure 4.36b) are more affected compared to electrochemical stability. Pure IL possess very high ESR (90-100 Ω) resulting from its higher viscosity (33.9 cp at 298.15 K) [171]. The reciprocal relationship between ESR and capacitance can be observed similar to other ILs. Overall, IL+PC_II solution can be proposed to be the favourable electrolyte with the highest charge storage (58.8 F g^{-1}), lowest ESR (29.76 Ω) and reasonable OPW (2.6 V). Hence it was further considered for EIS measurements.

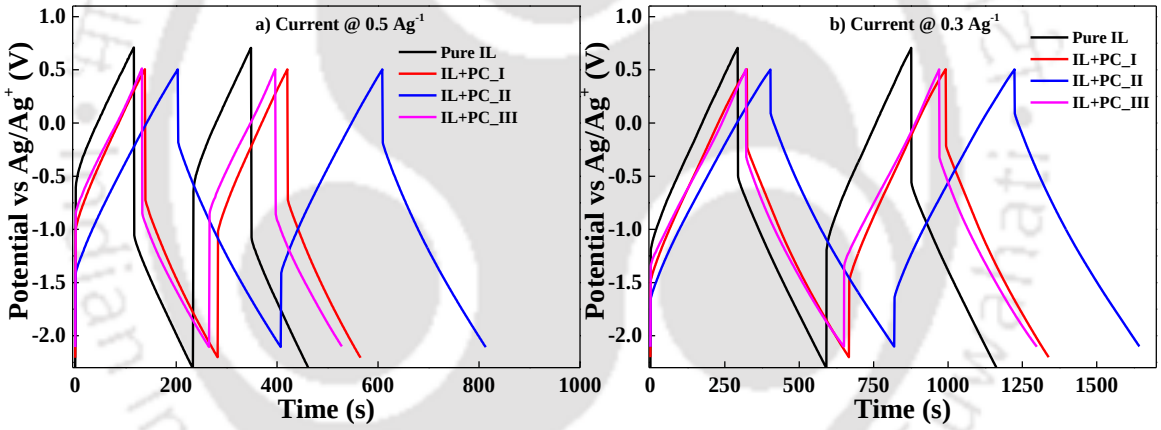

Figure 4.35: GCD plots for [TESu][Tf_2N] electrolytes at a) 0.5 A g^{-1} and b) 0.3 A g^{-1}

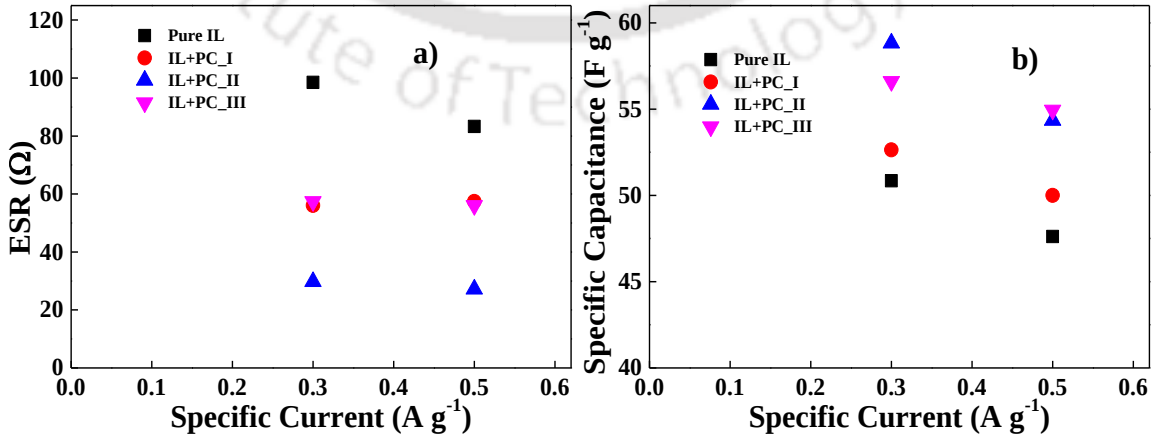

Figure 4.36: a) ESR and b) specific capacitance for [TESu][Tf_2N] based electrolytes

4.4.3 Electrochemical Impedance Measurements

The Nyquist plot (Figure 4.37a) provides a clear indication of higher R_s than AN-based electrolytes as discussed earlier in this chapter. However, the R_{ct} is much lower compared to R_s. Hence it can be noted that the diffusional limitation encountered by ions plays a crucial role in determining specific capacitance (Figure 4.37b) for this electrolyte solution. The longer vertical tail depicts the increased imaginary part of the impedance which is inversely proportional to the specific capacitance according to equation 3.5. The highest specific capacitance obtained from FRA is nearly 45 F g^{-1}.

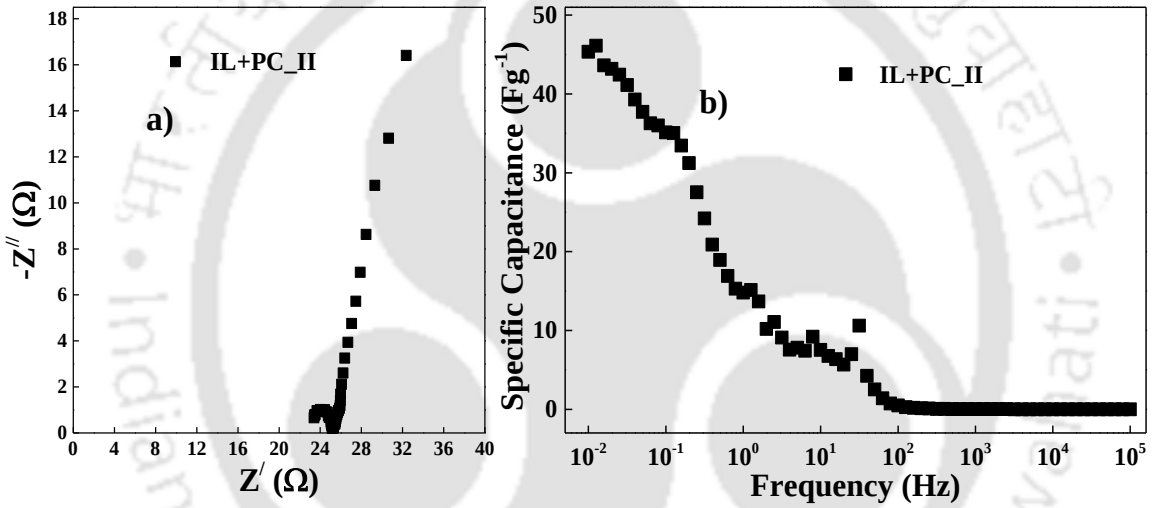

Figure 4.37: a) Nyquist plot and b) specific capacitance for [TESu][Tf_2N]+PC_II

4.4.4 Summary of Section 4.4

[TESu][Tf_2N] shows equivalent performance to [EMIM][Tf_2N] when pure ILs are compared. This indicates similar electrochemical behaviour of sulfonium and imidazolium cations. Use of organic solvent PC enhances electrochemical performance of [TESu][Tf_2N] by lowering the ESR. However, the results are not comparable to imidazolium ILs in organic solvents. The observations for this unconventional ILs follow the similar trend to imidazolium ILs with respect to OPW and ESR.

4.5 Comparative Performance Evaluation of Ionic Liquid Electrolytes

The results obtained so far from the electrochemical characterization of IL based electrolytes provides the information how different anions and cations affect the performance of EDLC. Table 4.2 suggests the basic parameters to assess electrolytes' effectiveness. The ESR and specific capacitance are measured from GCD data at 0.5 A g^{-1} for each system. Further these two parameters are employed to calculate specific energy and power following equations 1.1 and 1.2. When ILs without organic solvents are considered, it is observed that [EMIM][BF_4] delivered the least internal resistance (22.69 Ω) and hence the highest power density (2.05 kW kg^{-1}) despite having lower energy storage due to narrower OPW. Pure [EMIM][Tf_2N] and [TESu][Tf_2N] resulted in nearly equivalent characteristics. Therefore, the effect of cationic core is not distinguishable for these two ILs. Moreover, pure [BMIM][BF_4] shows the highest value of ESR (93.67 Ω) among all the electrolytes studied in this work due to its higher viscosity as reported in section 4.2. AN is found to be the most effective co-solvent for better charge storage and power delivery. [EMIM][Tf_2N]+AN_II and [PMIM][Tf_2N]+AN_II exhibit the lowest ESR (~ 7 Ω) and thereby the highest power density (~9-10 kW kg^{-1}). Further [PMIM][Tf_2N]+AN_II and [BMIM][Tf_2N]+AN_II remain electrochemically stable up to 3 V, which is the widest OPW recorded during the characterization of the IL based electrolytes. Therefore, energy storage (~ 152-156 Wh kg^{-1}) is the highest for both.

Mixture of [AMIM][BF_4] ILs improves the energy storage of the cell when compared to [EMIM][BF_4]. [BMPy][BF_4]+AN solutions deliver reasonable power but a narrower OPW limits the energy storage. Despite possessing equal OPW, [BMPy][BF_4]+AN_I shows better energy and power rating than [BMPy][BF_4]+PC_III. This happens due to the lower ESR and higher capacitance of the former.

Table 4.2: OPW, ESR, specific capacitance, energy and power of ILs

Electrolyte		OPW (V)	ESR (Ω)	Capacitance (F g^{-1}) @ 0.5 Ag^{-1}	Energy (Wh kg^{-1}) @ 0.5 Ag^{-1}	Power (kW kg^{-1}) @ 0.5 Ag^{-1}
[EMIM][Tf_2N]	Pure IL	3	82.09	46.29	57.87	1.16
	IL+AN_I	2.5	30.05	67.56	58.65	2.16
	IL+AN_II	2.5	7.18	89.28	77.50	9.18
	IL+AN_III	2	22.44	75.75	42.09	1.87
[PMIM][Tf_2N]	IL+AN_I	3	15.77	92.59	115.74	6.02
	IL+AN_II	3	7.28	121.95	152.44	10.10
	IL+AN_III	2.5	13.69	92.59	80.38	4.81
	IL+BN_II	3	23.11	69.44	86.81	4.55
	IL+PC_II	3	32.74	59.52	74.4	3.21
[BMIM][Tf_2N]	IL+AN_I	3	23.26	80.64	100.81	4.08
	IL+AN_II	3	24.58	125.00	156.25	5.98
	IL+AN_III	2.5	13.64	87.72	76.15	4.83
	IL+BN_II	3	19.45	92.59	115.74	5.41
	IL+PC_II	3	34.34	57.47	71.84	3.06
[EMIM][BF_4]	Pure IL	2.1	22.69	53.76	32.93	2.05
	IL+AN_I	1.9	11.77	65.78	32.98	3.24
	IL+AN_II	1.8	9.58	72.46	32.61	3.57
	IL+AN_III	1	9.57	58.82	18.38	1.86
[BMIM][BF_4]	Pure IL	3	93.67	66.67	96.15	1.53
	IL+AN_I	2.7	24.41	89.28	90.4	3.25
	IL+AN_II	2.5	10.73	98.04	85.10	4.61
	IL+AN_III	1.5	13.34	71.42	22.32	1.33
[EMIM][BF_4]+ [BMIM][BF_4]	IL+AN_I	2.3	29.84	53.76	52.48	2.08
	IL+AN_II	2.3	13.03	47.17	34.65	4.74

Table 4.2 continues

Electrolyte		OPW (V)	ESR (Ω)	Capacitance (F g^{-1}) @ 0.5 Ag^{-1}	Energy (Wh kg^{-1}) @ 0.5 Ag^{-1}	Power (kW kg^{-1}) @ 0.5 Ag^{-1}
[BMPy][BF_4]	IL+AN_I	2.2	11.86	69.44	46.68	4.31
	IL+AN_II	1.7	13.22	66.67	26.76	2.31
	IL+AN_III	1.7	15.45	52.63	21.13	2.19
	IL+PC_I	2.2	72.75	35.71	24.00	0.78
	IL+PC_II	2.2	28.99	48.08	32.32	1.95
	IL+PC_III	2.2	18.35	51.54	34.65	3.08
[TESu][Tf_2N]	Pure IL	3	83.29	47.62	59.52	1.26
	IL+PC_I	2.7	57.42	50	50.63	1.48
	IL+PC_II	2.6	27.16	54.35	51.03	2.91
	IL+PC_III	2.6	63.7	54.94	51.58	1.24

For [TESu][Tf_2N] based electrolytes, delivered power becomes maximum (2.91 kW kg^{-1}) for IL+PC_II. For rest, it is limited up to 1.5 kW kg^{-1}. Altogether, calculated energy and power data at different specific currents are reported in Table A1 of APPENDIX A. No significant difference in energy performance is observed with change in current except for a few systems.

Overall, imidazolium based ILs have evolved as better electrolytes for EDLC than pyridinium IL. Additionally, they have better thermal stability [172]. [AMIM][Tf_2N] and [AMIM][BF_4] retain thermal stability up to 400-450 °C. Literature suggests that sulfonium based ILs are found to have less thermal stability than imidazolium [173]. ILs with AN are

advisable to use at room temperature only to avoid evaporation loss (BP 82 °C). However, both BN and PC have wider liquid range (Table 3.1) which facilitates their use as co-solvent at higher temperature also. However, it should be noted that at higher temperature, viscosity of ILs get reduced significantly [162,163] which eases their use in neat form.

The electrochemical performance of [PMIM][Tf_2N] +AN_II and [BMIM][Tf_2N]+AN_II is similar at either of the current densities and significantly better than other studied systems. Therefore, life cyclic study was conducted for only these two systems. The retention of original capacitance observed after 1000 cycles at original OPW (3 V) of GCD at 1 A g^{-1} was 75% and 70% for solutions [PMIM][Tf_2N] and [BMIM][Tf_2N] respectively.

CHAPTER 5

Transport Properties of Ionic Liquids

The analysis from previous chapter reveals that [AMIM][Tf_2N]+AN_II solutions perform more effectively with respect to OPW, specific capacitance, ESR, energy storage and power density. Therefore, ionic conductivity and viscosity of these solutions were evaluated as per discussion in section 3.4. To have a comprehensive assessment regarding the effects of AN on-transport properties and how they influence capacitive performance of the electrolyte, experimental measurements were also executed for pure ILs along with the other two solutions in AN. Simultaneously, atomistic MD simulations was carried out for pure ILs and IL+AN_II solutions to obtain molecular level insights.

5.1 Experimental Measurements

The experimental findings for ionic conductivity of [AMIM][Tf_2N] ILs are provided in Figure 5.1a. Ionic conductivity data passes through a maximum at IL+AN_II, which follows the trend of specific capacitance and specific current as shown in previous chapter (Section 4.1). Similar trend was also suggested in the literature for [EMIM][Tf_2N] [161]. The electrolyte solution (IL+AN_II) with the highest ionic strength has the lowest ESR (Table 4.1). As expected [EMIM][Tf_2N]+AN_II does not possess the maximum ionic strength unlike pure [EMIM][Tf_2N], thereby agrees to the statement that co-solvent concentration for maximum ionic strength varies with type of IL. This has been already discussed in Chapter 4.

Viscosity decreases with increase in solvent concentration (Figure 5.1b). The difference in viscosity is the highest between IL in pure state and IL+AN_I. The increase in solvent concentration further (AN_II) improves viscosity, which eventually attributes to the highest ionic conductivity. The lowering of IL concentration again (AN_III) reduces viscosity, although ionic conductivity also decreases due to insufficient ion concentration. Nevertheless, the difference in viscosity is insignificant between IL+AN_II and

IL+AN_III. Analysis from MD simulation further enlighten how AN enhances the diffusive nature of the ions and facilitates the transport properties.

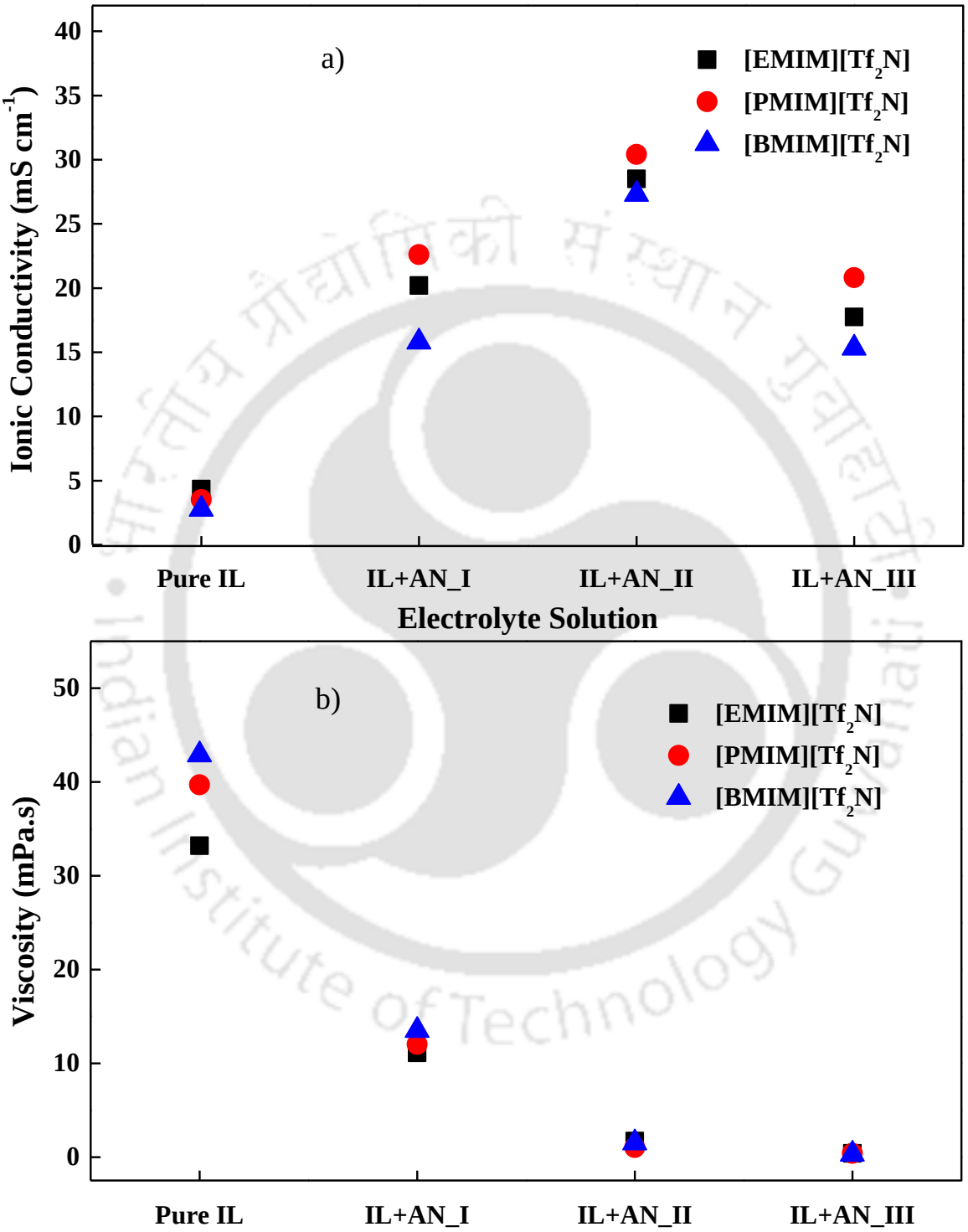

Figure 5.1: a) Ionic conductivity and b) viscosity of [AMIM][Tf_2N] electrolytes at 298.15 K

5.2 Results from Computation

The optimized geometries of the molecules obtained from Gaussian 09 appear in Figure 5.2. The corresponding partial charges are included in APPENDIX C (Table C1). To validate the accuracy of the force field parameters used in MD simulation, density (ρ) of the simulated IL systems was computed after equilibration for 2 ns and compared with experimental density (Table 5.1). It can be noted that density from simulation matches the experimental one, thereby proving the reliability of force field parameters.

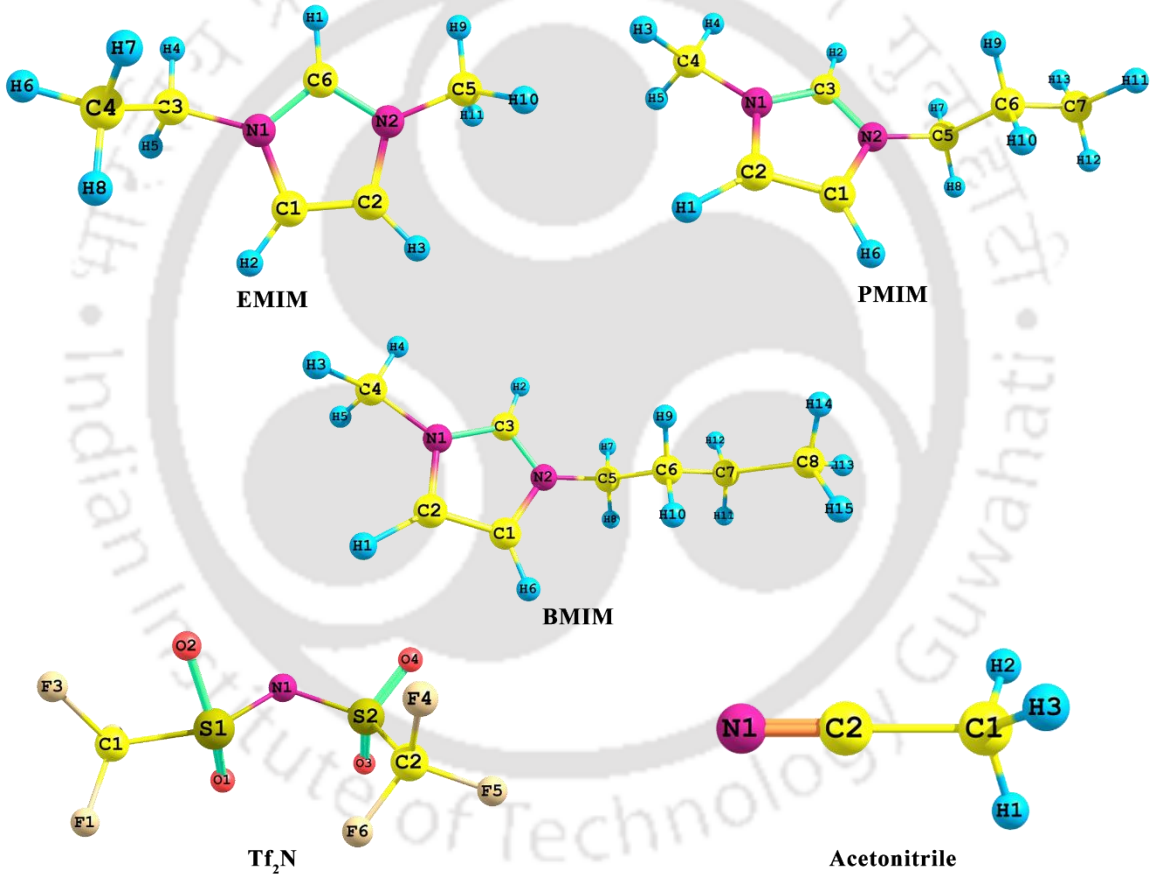

Figure 5.2: Molecular structures used for MD simulation

Table 5.1: Density of pure ILs and solutions in AN at T=298.15 K

	ρ [a] (kg m^{-3})	ρ [b] (kg m^{-3})	ρ [c] (kg m^{-3})
[EMIM][Tf_2N]	1.55	1.55	1.52 [174]
[EMIM][Tf_2N]+AN_II	0.99	0.95	-
[PMIM][Tf_2N]	1.46	1.47	1.47 [175]
[PMIM][Tf_2N]+AN_II	0.97	0.97	-
[BMIM][Tf_2N]	1.43	1.44	1.43 [176]
[BMIM][Tf_2N]+AN_II	0.96	0.97	-

[a] MD simulation from this work, [b] Experiment from this work and [c] Experiment from literature

Following density, ionic conductivity (σ) was calculated as explained in section 3.6 using equation 3.8. 10 ns long trajectory from MD simulations was considered to compute MSD and hence σ. The corresponding D and σ values are reported in Table 5.2. The increasing MSD (Figure 5.3) for IL+AN_II clearly indicates the enhancement of D and σ over pure ILs. AN breaks the large ion pair clusters by weakening the ionic interaction which helps in obtaining higher σ. The smaller size of the cation EMIM resulting from shorter alkyl chain facilitates a higher diffusivity D than PMIM and BMIM (Table 5.2). Overall, MD provides better insights on effect of alkyl chain length on diffusivity and agrees to the trend reported earlier [177]. The use of a particular scaling factor takes care of the effect of charge transfer and polarizability [151]. Ionic conductivity values predicted from MD simulation shows a close match with experimental findings.

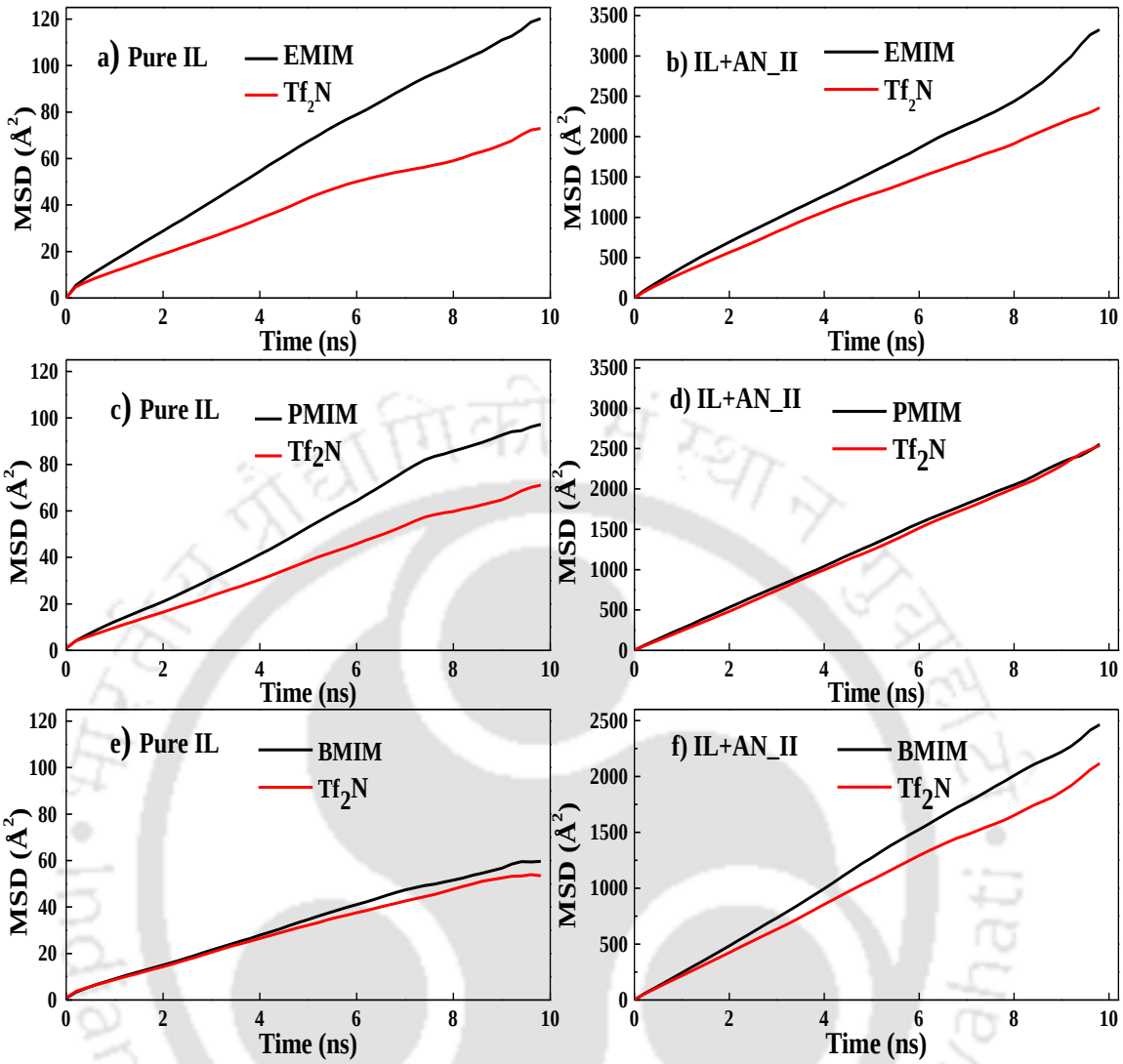

Figure 5.3: Mean square displacement (MSD) plots a) [EMIM][Tf_2N], b) [EMIM][Tf_2N]+AN_II, c) [PMIM][Tf_2N] d) [PMIM][Tf_2N]+AN_II , e) [BMIM][Tf_2N] and f) [BMIM][Tf_2N]+AN_II

Table 5.2: Self-diffusion coefficients and ionic conductivity of pure ILs and solution in AN at T=298.15 K

	D ($.10^{-7}$ cm^2 s^{-1})		σ [a] (mS cm^{-1})	σ [b] (mS cm^{-1})	σ [c] (mS cm^{-1})
	D^+	D^-			
[EMIM][Tf_2N]	2.17	1.13	4.91	4.33	6.67 [174]
[EMIM][Tf_2N]+AN_II	50.63	40.55	30.31	28.50	32 [161]
[PMIM][Tf_2N]	1.80	0.78	3.48	3.51	-
[PMIM][Tf_2N]+AN_II	46.14	34.47	30.99	30.40	-
[BMIM][Tf_2N]	1.24	0.92	2.44	2.76	3.80 [176]
[BMIM][Tf_2N]+AN_II	31.89	34.79	24.67	27.30	-

[a] MD simulation from this work, [b] Experiment from this work and [c] Experiment from literature

The dynamic viscosity of pure ILs and IL+AN_II solutions were also measured using equation 3.9 and reported in Table 5.3. As expected, significant viscosity reduction of ILs has been obtained with addition of co-solvent. Addition of less viscous AN mobilises the ions of IL by lowering intermolecular friction. Experimentally measured viscosity of pure [EMIM][Tf_2N] obtained from simulation data agrees reasonably well with literature [174]. However, the same for [BMIM][Tf_2N] and [PMIM][Tf_2N] is slightly lower than literature [175,176]. Additionally, experimental viscosities for pure ILs obtained in this study show a fair match with that obtained from simulation (deviation ~1.5-7.7%) except [EMIM][Tf_2N] where the deviation is ~11%. On the contrary, viscosities observed for mixtures of ILs and organic solvent show significant deviation from when experimental

and MD results are compared. However, results from both the studies follows a decreasing trend with the addition of co-solvent.

Table 5.3: Viscosity of pure ILs and their solutions in AN at *T*=298.15 K

	η^a **(mPa.s)**	η^b **(mPa.s)**	η^c **(mPa.s)**
[EMIM][Tf_2N]	37.76	33.2	33.9 [174]
[EMIM][Tf_2N]+ACN	2.04	1.70	-
[PMIM][Tf_2N]	43.04	39.70	43.70 [175]
[PMIM][Tf_2N]+ACN	2.98	1.00	-
[BMIM][Tf_2N]	43.57	42.90	48 [176]
[BMIM][Tf_2N]+ACN	3.12	1.50	-

[a] MD simulation from this work, [b] Experiment from this work and [c] Experiment from literature

CHAPTER 6

Results and Discussion on Deep Eutectic Solvents

The motivation to study DESs arises from the disadvantage of high viscosity of ILs. The requirement of organic solvents for ILs leads to the loss of OPW and brings chemical and thermal limitations as discussed in Chapter 4. While choosing suitable DESs for EDLC application, factors like higher ionic strength and lower viscosity were considered carefully. To have comparable ionic strength to ILs, a high melting IL namely [BMIM][$MeSO_3$] was considered as HBA together with N-methylacetamide (NMAc) and ethylene glycol (EG) as HBDs as mentioned in section 3.1. The DESs used in this work belong to Type III as defined in Table 2.1.

6.1 Insights from COSMO-SAC Calculations

The input files for SLE calculations can be found in Figure 6.1a. The red, yellow, blue and green colours of COSMO cavities represent electronegative, partially electronegative, electropositive and partially electropositive zones respectively. Furthermore, higher electronegative and electropositive portions can be signified by the brown and dark blue colours. Hence, the compounds selected for this work have both hydrogen bond acceptor and donor sites. This can be well understood from the probability distribution of surface screening charges (sigma profiles) obtained from COSMO-SAC calculation. As it can be seen in Figure 6.1b, the compounds have a considerable number of hydrogen bond donors and acceptors based on their hydrogen bond cut off (±0.0084 e $Å^{-2}$) indicating they are soluble within itself as well as in the solution. This implies that both EG and NMAC are miscible in the IL. The area under the curve for [BMIM][$MeSO_3$] in hydrogen bond donor region is lower than EG and NMAc. This corresponds to a lesser tendency of [BMIM][$MeSO_3$] for donating hydrogen bond. EG shows the highest probability for initiating hydrogen bond. Moreover, all the three compounds possess nearly equivalent

distribution in hydrogen bond acceptor region even though most of the surface charges belong to the non-polar region.

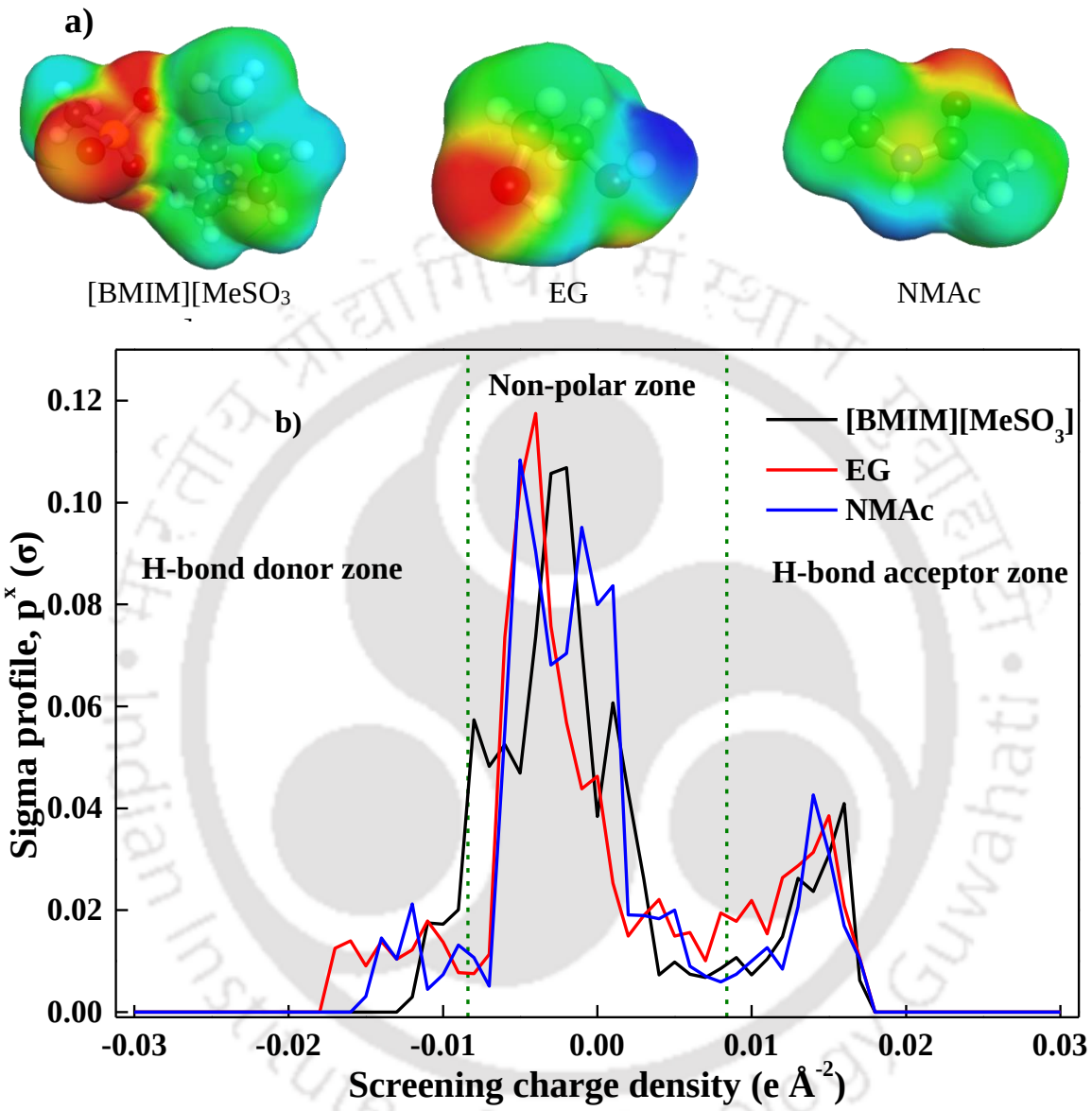

Figure 6.1: a) COSMO files generated using Gaussian 09 package and b) distribution of surface screening charge obtained from COSMO-SAC calculations

The solubility data (Section 3.2) obtained from COSMO-SAC calculations are plotted in Figure 6.2 as a function of temperature. T_A and T_B indicate the melting points of HBA and HBD respectively. Both the DESs possess significant depression in melting point compared to corresponding HBA and HBD. The ideal eutectic point corresponds to the activity

coefficient equals to unity. Real condition eutectic temperature is slightly lower than that of ideal state. The molar ratios of HBA: HBD are calculated to be 1:3.5 and 1:2 for [BMIM][$MeSO_3$]:EG and [BMIM][$MeSO_3$]:NMAc having corresponding eutectic temperatures 247.7 K (~ -25 ºC) and 274.25 K (~1 ºC) respectively. [BMIM][$MeSO_3$]: EG offers comparable melting points to room temperature ILs. The important outcome of this study is the formation of low melting solvents with [BMIM][$MeSO_3$], which has a higher melting temperature of nearly 75ºC and this facilitates investigation of these two IL based DESs as electrolyte for EDLC application. Although COSMO-SAC calculations predict the eutectic composition and temperature, yet slight variation in experimentally computed eutectic point can be expected since reproducibility of exact experimental environment by modelling cannot be assured.

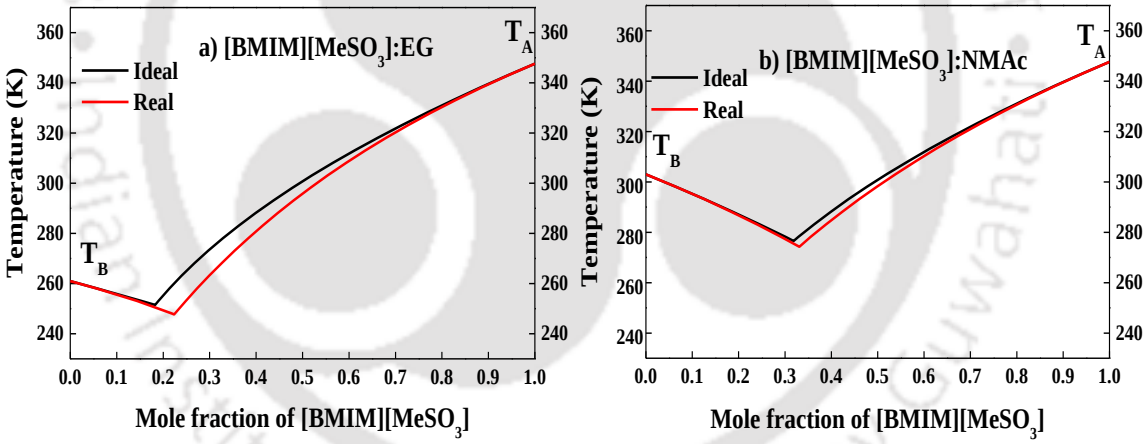

Figure 6.2: SLE data from COSMO-SAC calculations

6.2 Measurement of Water Content

The water content of the prepared DESs was analysed by Karl Fischer Titration (KFT) method as discussed in section 3.3. The analysis was repeated for three times and average wt. % of water was considered. The calculated wt. % of water for [BMIM][$MeSO_3$]:EG and [BMIM][$MeSO_3$]:NMAc are 1.62 and 0.29 respectively. Hence, [BMIM][$MeSO_3$]:NMAc results in better hydrophobicity.

6.3 NMR Analysis

The chemical shift for NMR spectroscopy is referred to $CDCl_3$ external standard. ^1H study indicates slight shifting of peaks for DES from individual spectra of HBA and HBD (Figures 6.3 and 6.4). This can be expected due to formation of hydrogen bonds. However, no new peak appears for both the DESs confirming absence of any chemical reaction. NOESY analysis reveals H-H interactions between HBA and HBD indicated by the contours above and below the diagonal, which are also termed as crossing peaks (Figures 6.5 and 6.6). The diagonal represents the interaction between same molecules [136]. [BMIM][$MeSO_3$] shows only one interaction (3.62, 9.07, 0.02) with EG (Figure 6.5a), while three interactions [(3.96, 2.65, 0), (1.88, 0.86, 0), (1.81, 1.29, 0)] with NMAc (Figure 6.6a) for a total of eight NOESY scans. Higher number of interactions can be expected by increasing number of scans [136]. Closely located hydrogen atoms i.e. H-H interactions (Figures 6.5b and 6.6b) corresponds to the probable hydrogen bonding between the hydrogen, which is bonded to the HBD, and the acceptor electronegative atom near to the other hydrogen atom.

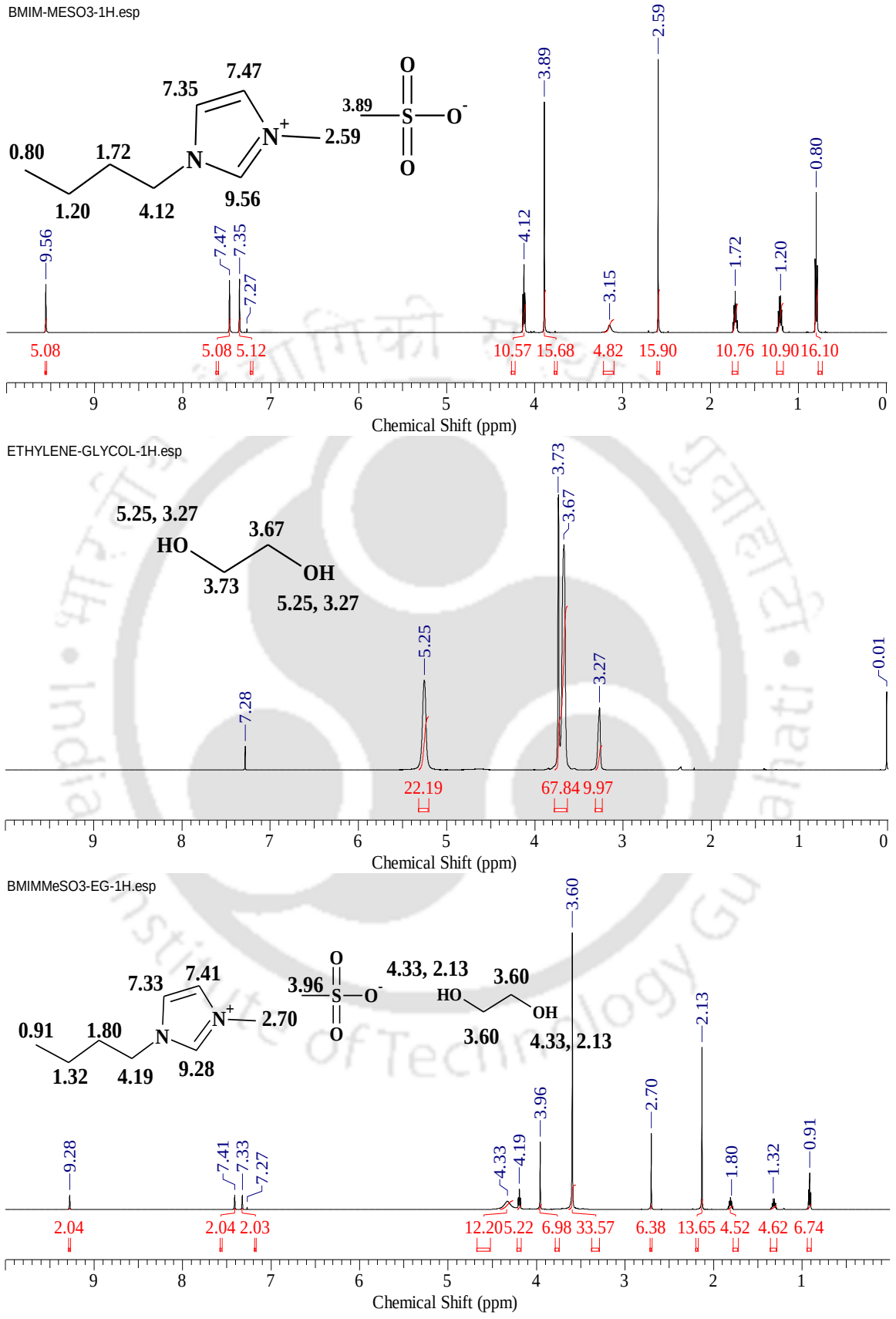

Figure 6.3: ^{1}H NMR spectra for [BMIM][$MeSO_3$], EG and [BMIM][$MeSO_3$]: EG

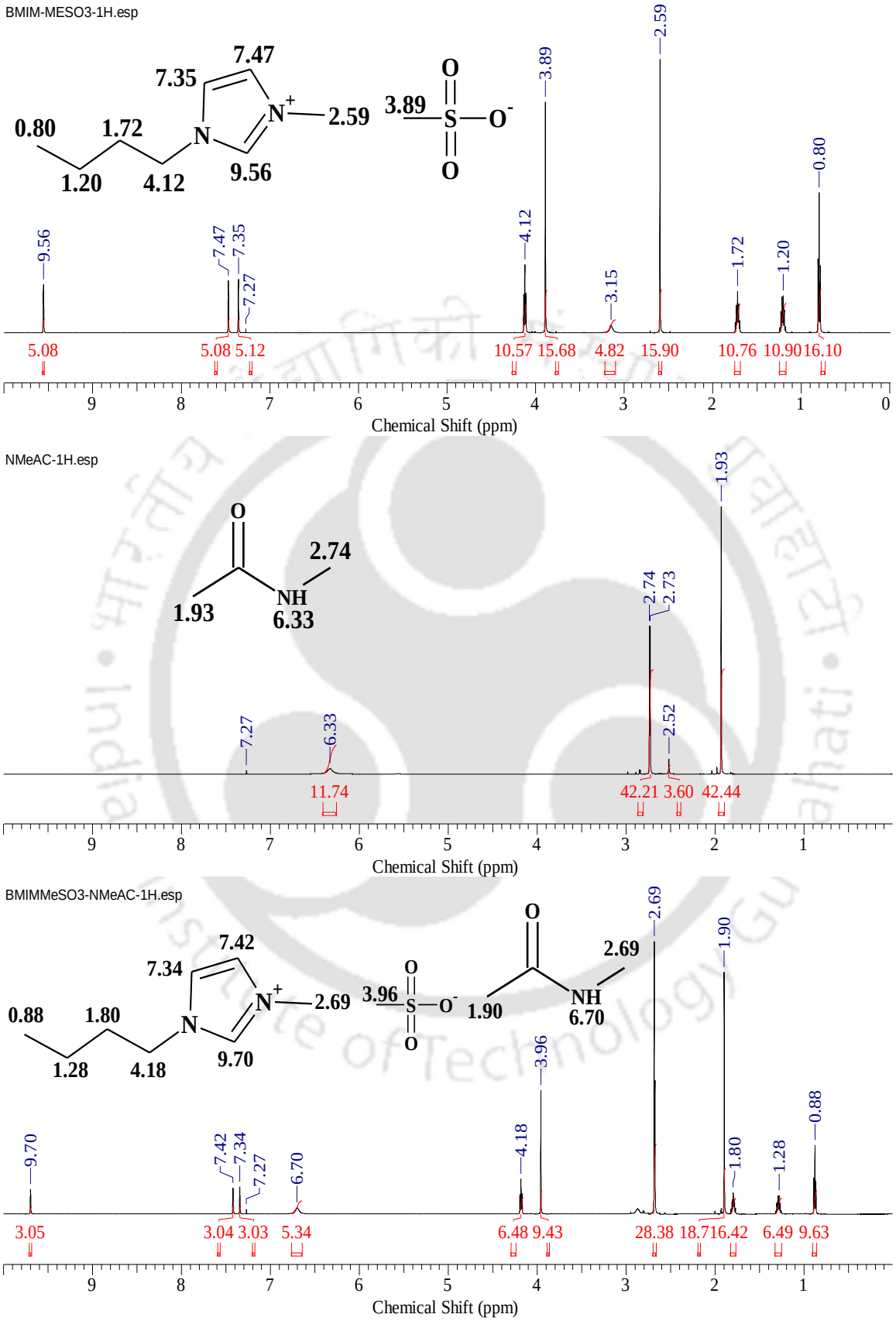

Figure 6.4: ^{1}H NMR spectra for [BMIM][$MeSO_3$], NMAc and [BMIM][$MeSO_3$]: NMAc

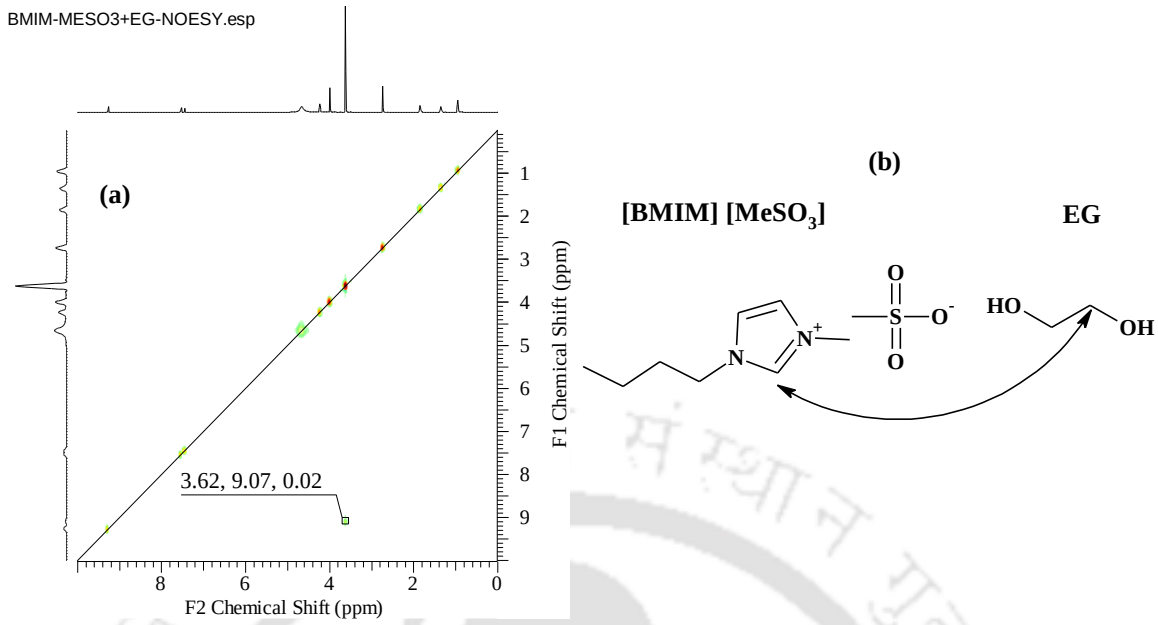

Figure 6.5: a) NOESY spectra of [BMIM][$MeSO_3$]:EG at 295 K and b) H-H interactions

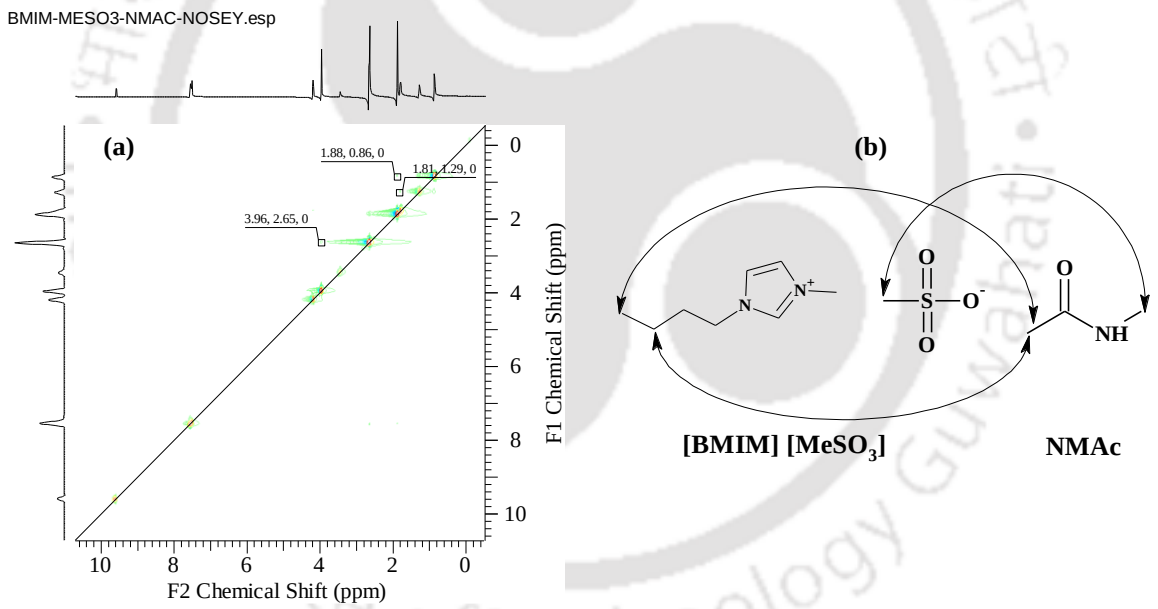

Figure 6.6: a) NOESY spectra of [BMIM][$MeSO_3$]: NMAc at 295 K and b) H-H interactions

6.4 Thermal Stability Analysis

The thermogravimetric analysis was performed for temperature of 30-400 ºC (303.15-673.15 K) for both the DESs under nitrogen atmosphere with a heating rate of 10 ºC per minute. TGA data (Figure 6.7a) indicates insignificant mass loss up to 360 K (87ºC), which

elucidates the maximum operational temperature limit for the EDLC. Only the water present in the DESs is released in this region. Particularly, the onset degradation temperature (T_{onset}) for the DESs, which is also onset degradation temperature of HBDs, can be considered as ~ 363 K (~90 ºC), after which the DESs encountered appreciable mass loss.

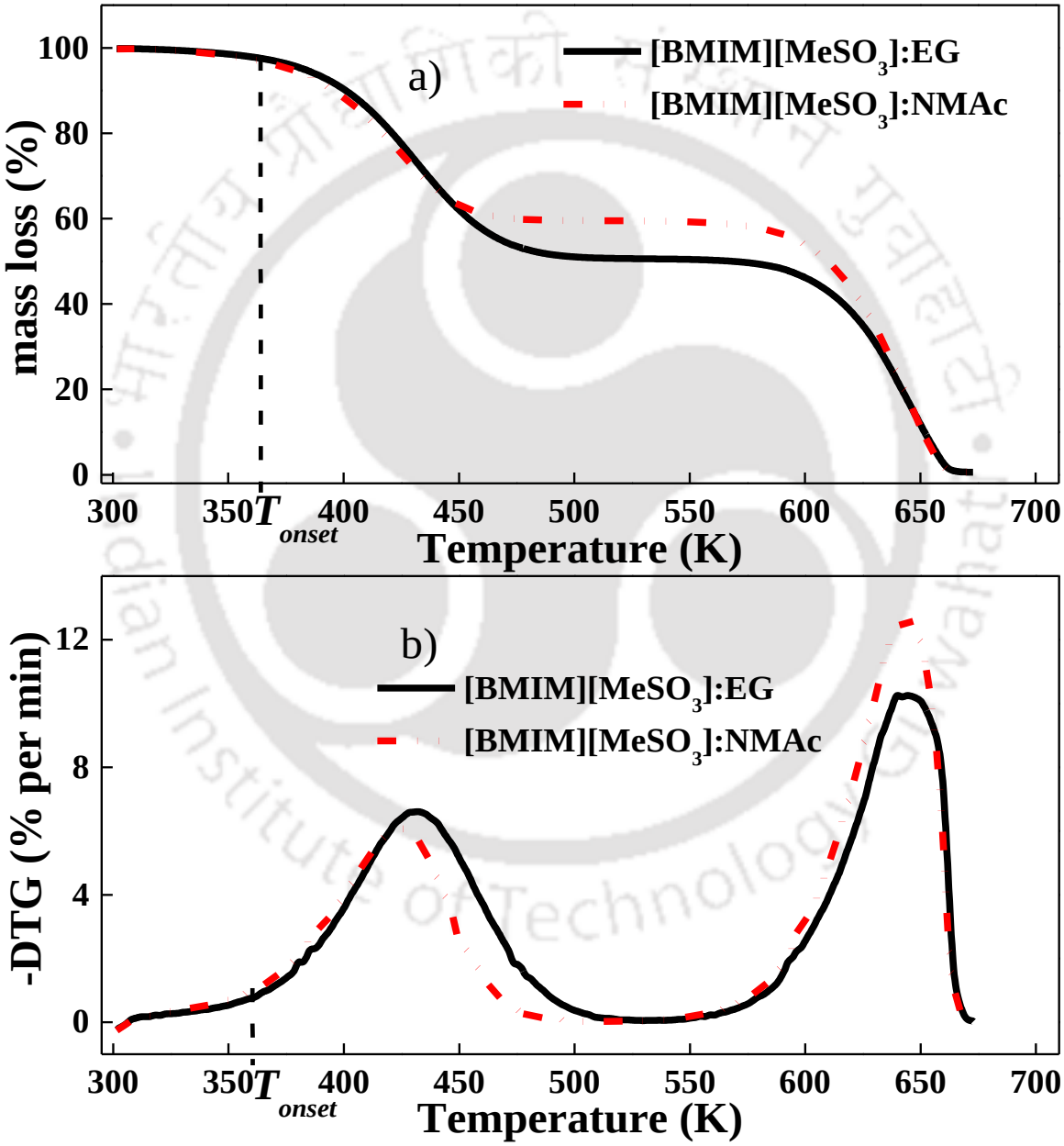

Figure 6.7: a) % mass loss vs temperature and b) derivative of % mass loss vs temperature

Since DES is composed of two non-reacting compounds, two distinct mass degradation slopes appear in the TGA plot. From DTG plot (Figure 6.7b), the second maximum mass loss temperature appears to be nearly 640 K, which confirms decomposition of the HBA at that temperature. The onset temperature for decomposition of HBA is almost 600 K. The first peaks of DTG plot appear at different temperatures corresponding to the maximum mass loss of HBDs. NMAc (425 K) decomposes slightly earlier than EG (432 K).

6.5 Physical Properties

As explained in section 3.4, density of the prepared solvents was measured and plotted as a function of temperature (Figure 6.8). Decrease in density with increase in temperature can be observed for both the solvents. The density of [BMIM][$MeSO_3$]:EG (1:3.5) is more than that of [BMIM][$MeSO_3$]:NMAc (1:2) due to the difference in molar ratio of the DESs and the higher density of EG as compared to NMAc.

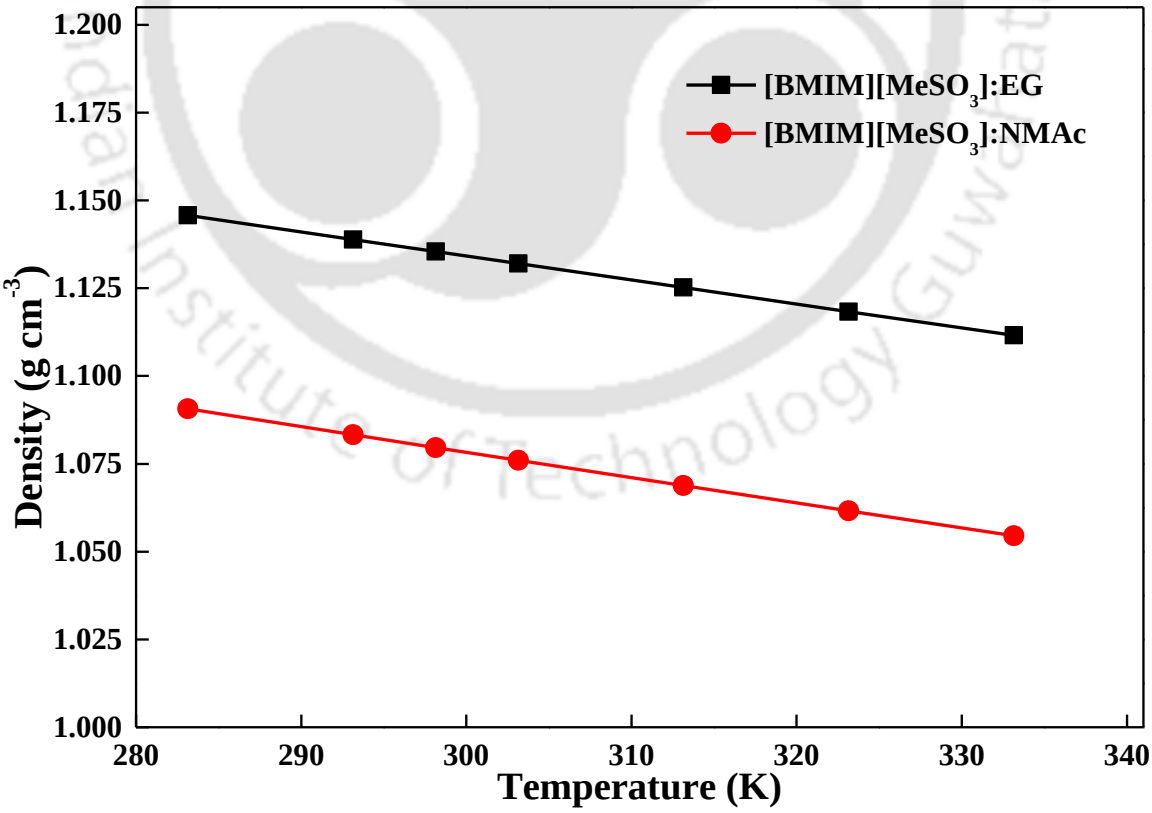

Figure 6.8: Density as a function of temperature

The densities of the mixture are slightly higher than those of the pure HBDs (EG: 1. 11 g cm^{-3} at 298.15 K and 1.1 g cm^{-3} at 323.15 K [178]; NMAc: 0.93 g cm^{-3} at 323.15 K [179]). This can be well described from the hole theory of liquids [67,180], which suggests that HBDs composed of holes and upon addition of the HBA, the radius of the hole decreases and more compact structure is achieved resulting in increase in density of the mixture.

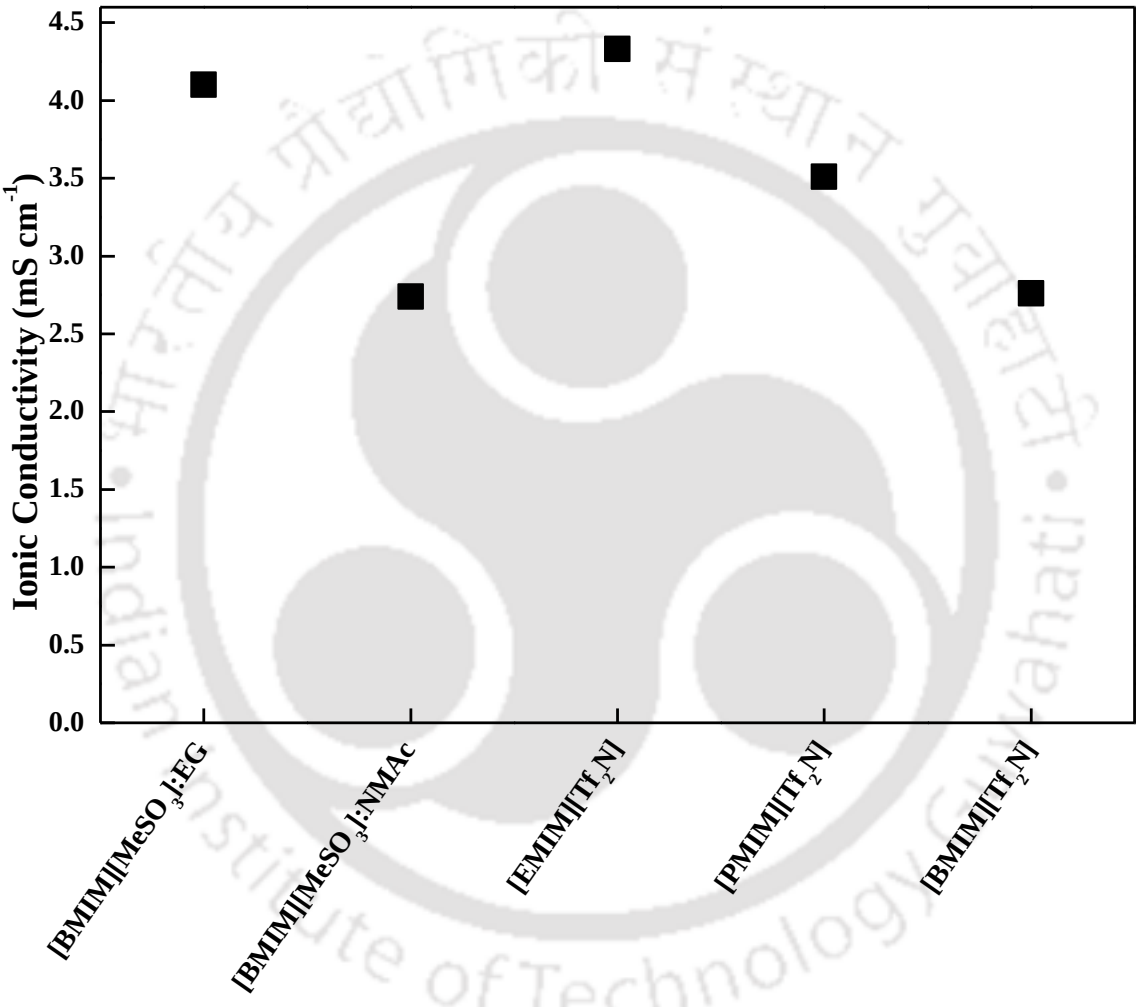

Figure 6.9: Ionic conductivity of DESs and IL electrolytes at 298.15 K

Furthermore, ionic conductivity of DESs were measured and compared with [AMIM][Tf_2N] ILs (Figure 6.9). [BMIM][$MeSO_3$]:EG possesses better ionic conductivity than [BMIM][$MeSO_3$]:NMAc. Here the weak hydrogen bonding interaction enhances the

diffusive nature of the ions resulting in greater ionic conductivity of [BMIM][$MeSO_3$]:EG by weakening the ionic interactions.

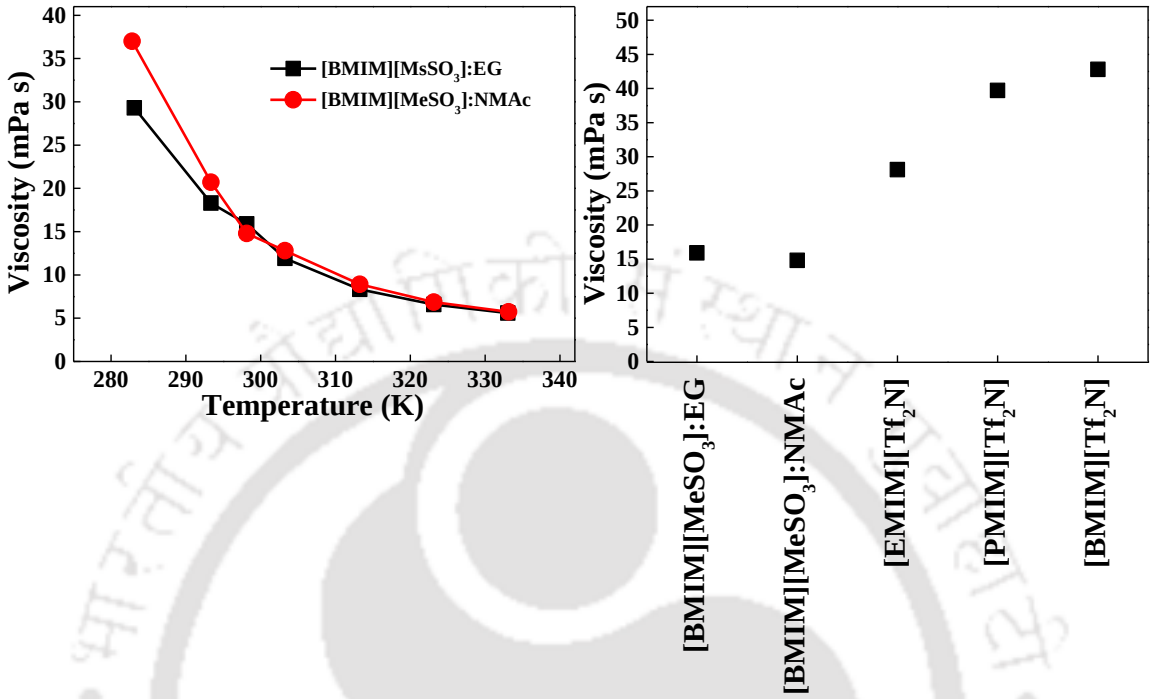

Figure 6.10: a) Viscosity variation with temperature and b) comparison of viscosity for studied DESs and conventional RTIL electrolytes at 298.15 K

The viscosity measurement was done at a shear rate of 1000 s^{-1} for the same temperature range as density by incorporating the arrangement of the Rheometer as per section 3.4.3 (Figure 6.10a). The generic liquid nature of exponential decrease in viscosity with increase in temperature is also valid for the studied DESs. Figure 6.10b compares the viscosity of the prepared DESs at 298.15 K with IL electrolytes namely [EMIM][Tf_2N], [PMIM][Tf_2N] and [BMIM][Tf_2N]. The dynamic viscosities of both the IL-based DESs are much lower than all the pure ILs used in this work (Table B1). Moreover, observed viscosity for the newly developed solvents is significantly lower than other BMIM cation based ILs as reported in literature [181]. Thus, the drawback of highly viscous RTILs can be overcome by proceeding towards ILs/RTILs based DESs with suitable HBDs.

6.6 Electrochemical Performance

LSV is an effective characterization method to determine the oxidation (anodic) and reduction (cathodic) limits of an electrolyte. Aiming at supercapacitor application, initially the ESPW was evaluated against glassy carbon electrode using LSV technique at a scan rate of 10 mV/s. Cathodic stability for both the electrolytes can be marked nearly at -2 V and the anodic limit is observed at 1.8 V resulting in ESPW equal to 3.8 V (Figure 6.11a). Electrolyte's purity greatly affects its electrochemical stability [119]. Since all the chemicals were used without any further purification except vacuum drying, wider ESPW can be expected with better purity of constituent chemicals. Further, RGO electrode was used to investigate operational parameters for EDLC. Initially, CV tests were performed by applying potential difference of 4 V to compare the ESPW obtained from LSV with glassy carbon electrode. However, CV results do not fulfil the expected nature of EDLC as clear indication of electrochemical decomposition can be observed near the potential limits*. Figure 6.11b represents the CV plots at 10 mV/s, which depicts the difference between ESPW and OPW for the electrolytes. The use of porous carbon electrode shrinks the cathodic and anodic stability of the electrolyte. Moreover, both the DESs result in different OPW unlike ESPW. Apart from the nature of the electrolyte the electrochemical stability also depends on the type of electrode material [119]. A similar observation was also made for RTILs [7].

*Please refer to APPENDIX D: Figure D1

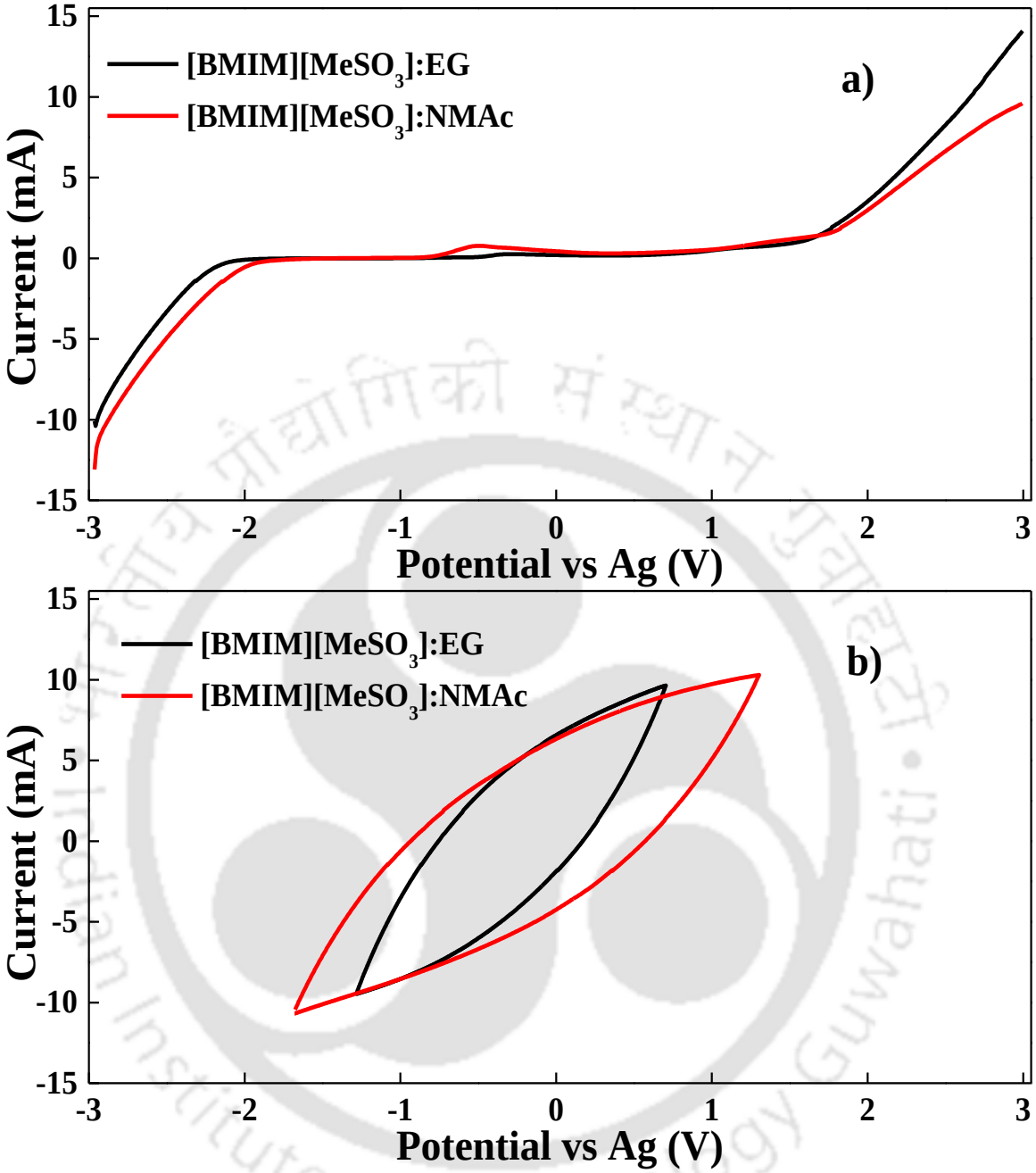

Figure 6.11: a) LSV at 10 mVs^{-1} with glassy carbon electrode and b) CV at 10 mVs^{-1} with RGO electrode

CV experiments were also performed at scan rates of 3 and 5 mVs^{-1} (Figure 6.12). Absence of any redox peaks ensures that charge storage mechanism is solely double layer in nature. The observed OPW for [BMIM][$MeSO_3$]:EG is limited to 2 V, while the same for [BMIM][$MeSO_3$]:NMAc is 3 V and comparable to IL electrolytes covered in this work.

This reveals the important role of water in determining the electrochemical stability of the DES. The higher water content of HBA:EG system leads to narrower OPW. Type of HBD may also be a possible factor in this regard while measuring OPW against carbon electrode.

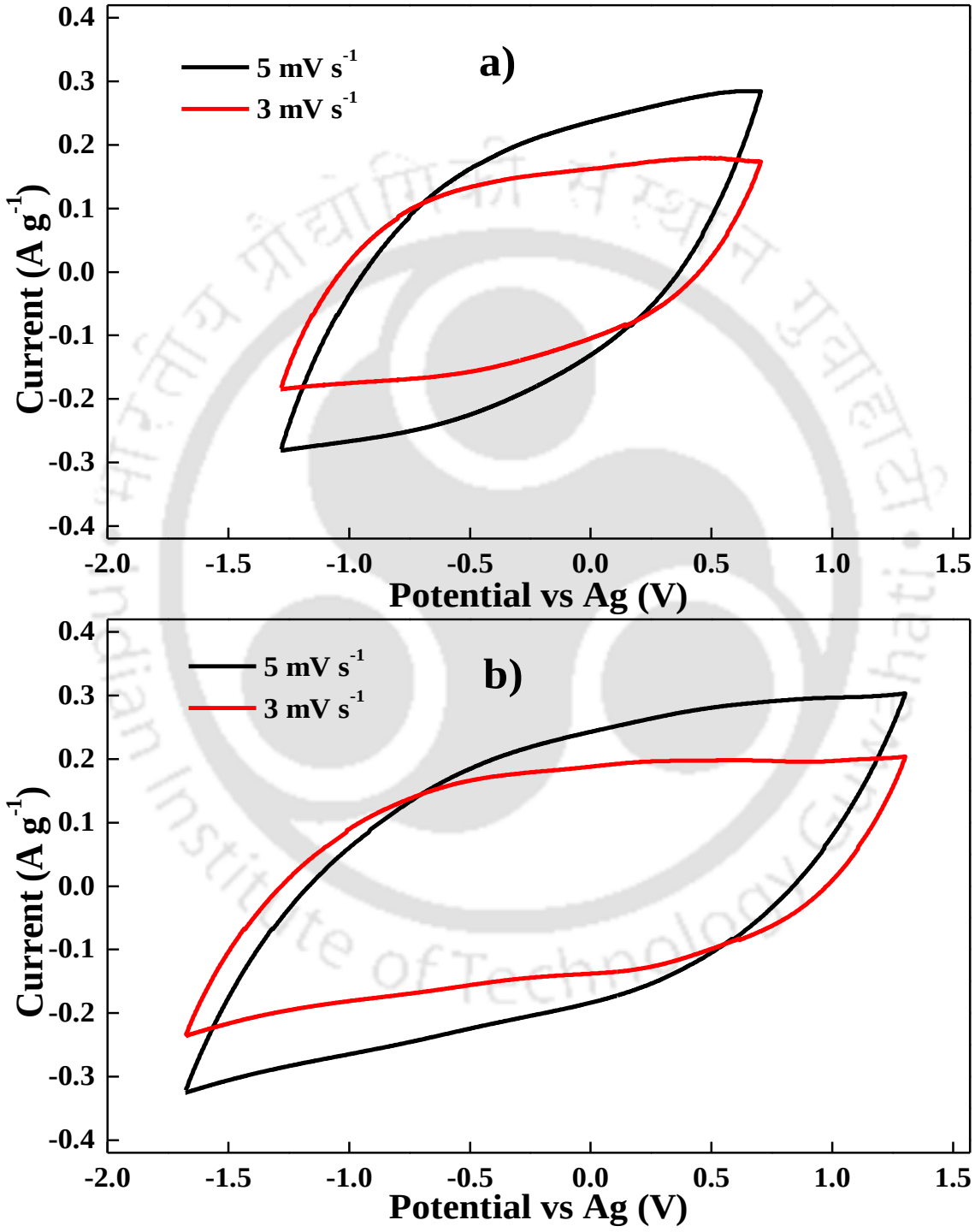

Figure 6.12: CV plots a) [BMIM][$MeSO_3$]:EG b) [BMIM][$MeSO_3$]:NMAc

Further specific capacitance measurement was carried out using CV data (Figure 6.13). The effect of scan rate due to lower rate performance of the electrode material is visible, which results in incomplete adsorption of charged species at electrode/electrolyte interface for higher scan rates involving shorter time. This effect is also observed for IL electrolytes as described earlier in Chapter 4. Literature also suggested similar trend for mesoporous carbon sphere based EDLC [47].

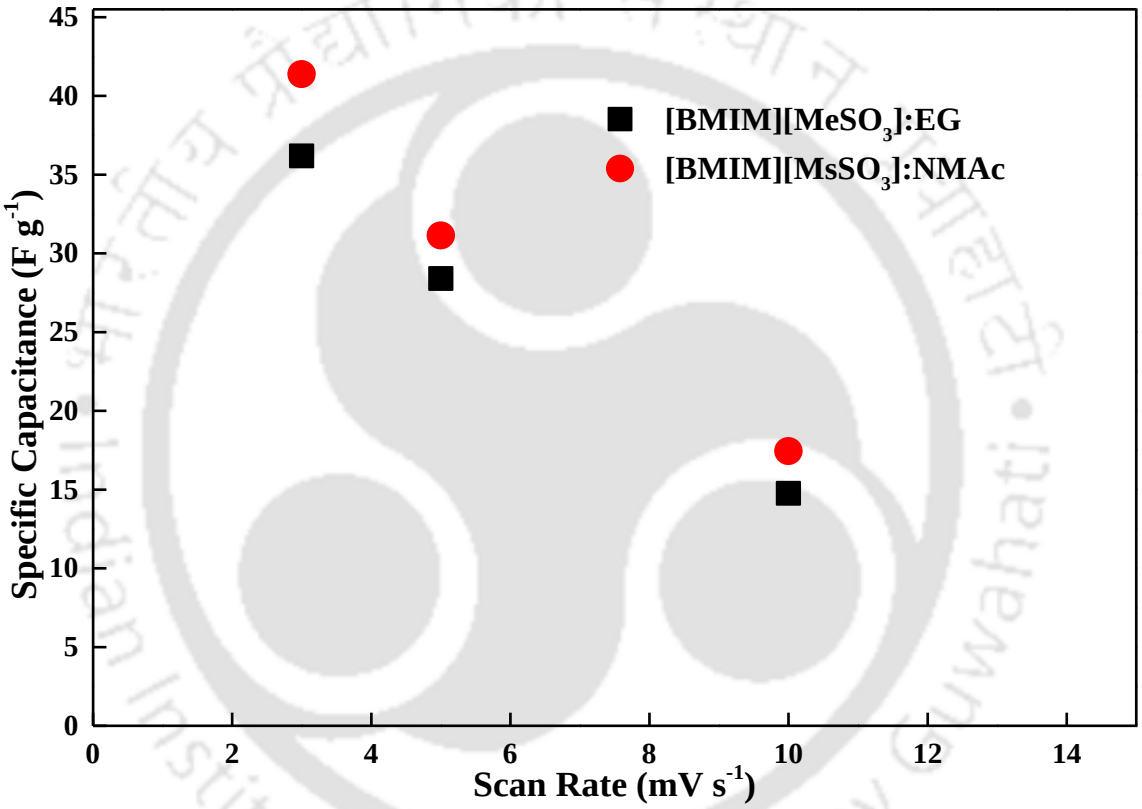

Figure 6.13: Specific capacitance evaluated from CV

OPW obtained from CV was confirmed from GCD performed at 0.1 and 0.3 Ag^{-1} (Figure 6.14). IR drop for 0.3 A g^{-1} is nearly thrice for that of 0.1 Ag^{-1} due to application of higher current. Further at 0.5 A g^{-1} the ohmic loss is extremely high. A comparison of OPW among DESs studied in this work and already reported in literature can be seen in Table 6.1 and the widest of 3 V can be found in our work. Even though 2.8 V was reported for $LiTf_2N$: NMAc [72], indication of peak towards anodic limit could be clearly observed at lower

scan rates, which might lead to gas evolution [75] inside the cell. Since OPW is a characteristic of both electrolyte and electrode, wider than 3 V can also be expected for [BMIM][$MeSO_3$]: NMAc using electrode materials having better electrochemical stability. Moreover, IL based DESs, prepared from ILs with ESPW equal to 5-6 V [45] should deliver wider OPW than other DESs based on metal salts and ChCl.

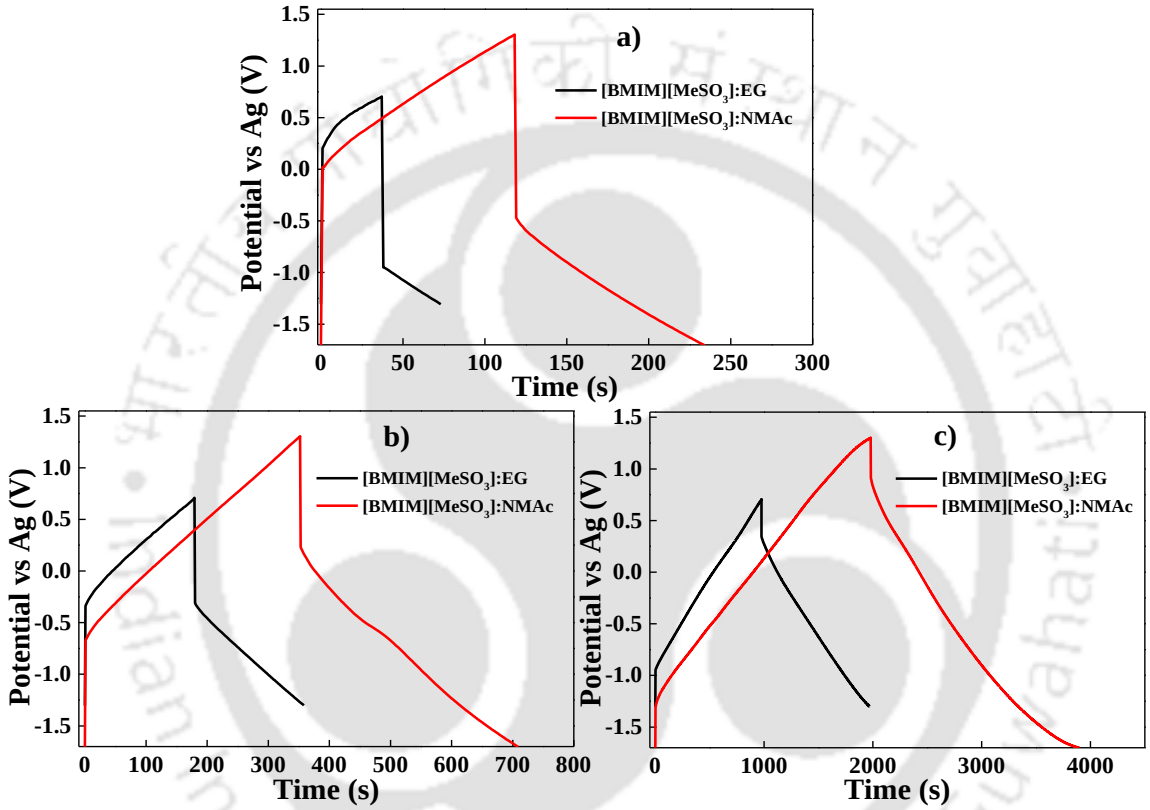

Figure 6.14: GCD plots at a) 0.5 A g^{-1}, 0.3 A g^{-1} and b) 0.1 A g^{-1}

Further CV measurements were conducted for [BMIM][$MeSO_3$]: NMAc to confirm the electrochemical stability in two-electrode configuration. Two symmetric carbon electrodes were used for the experiment. Figure D2 of APPENDIX D clearly depicts 3 V voltage window for the system. Hence, it is understood the DES can provide similar electrochemical stability in device level assembly.

Table 6.1: Comparison of OPW with reported DES electrolytes for supercapacitor

	OPW (V)	**Working electrode**
[BMIM][$MeSO_3$]:EG	2	RGO
[BMIM][$MeSO_3$]:NMAc	3	RGO
$LiTf_2N$: formamide [75]	1.2	Activated carbon
$LiPF_6$:NMAc [72]	2	Activated carbon
$LiNO_3$:NMAc [72]	1.8	Activated carbon
$LiTf_2N$:NMAc [72]	2.8	Activated carbon
ChCl: Glycerol [69]	2	RGO coated electrode
$NaNO_3$:NMAc [70]	2	Activated carbon

ESR computed from GCD data is still higher (Table 6.2) since viscosity of the electrolyte is more when compared with IL+ organic solvent electrolytes. The comparison of ESR at 0.3 A g^{-1} for DESs with pure ILs investigated in this work is provided in APPENDIX A (Table A1). Internal resistance or ESR arises from resistance associated with electrolyte, active layer i.e. electrode and contact between active layer and current collector [143]. Thus in addition to electrolyte viscosity, cell assembly can also play a major role in reduction of ESR by reducing the contact resistance [143]. The change in ESR can be expected for 2-electrode device level cell assembly with arrangements for reduction in contact resistance. Moreover, at higher temperature the enhanced mobility due to sufficient reduction in viscosity (Figure 6.10) of the DESs can definitely lower the ESR and thereby enhance charge storage. Following ESR, specific capacitance (Figure 6.15) was also estimated according to equation 3.4. Marginal variation in ESR and specific capacitance for the same system can be observed with specific current. The discharge capacitance for [BMIM][$MeSO_3$]:NMAc is somewhat higher in spite of its slightly greater ESR than

[BMIM][$MeSO_3$]:EG at 0.3 A g^{-1}. However, such little deviations cannot be excluded in experimental results. Overall, comparable values were obtained for both the DESs. The current generation (Figure 6.12) is also similar for both the DESs, which reflects in similar specific capacitance.

Table 6.2: Equivalent series resistance from GCD

	ESR (Ω)		
	0.5 A g^{-1}	0.3 A g^{-1}	0.1 A g^{-1}
[BMIM][$MeSO_3$]:EG	76.65	79.33	84.00
[BMIM][$MeSO_3$]:NMAc	82.40	83.41	88.74

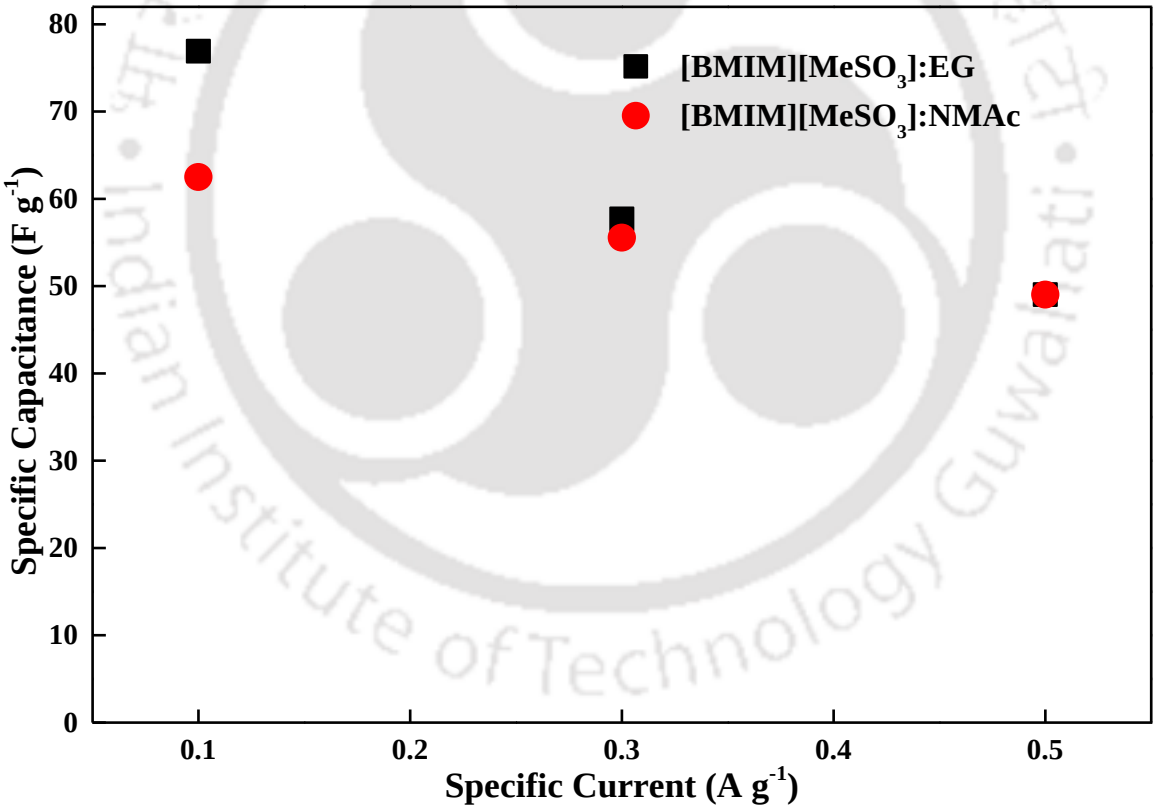

Figure 6.15: Specific capacitance evaluated from GCD

Eventually, performance of the DESs is rated by calculating the energy and power. The Ragone plot (Figure 6.16) estimates the performance of novel DESs and shows the

comparison with pure ILs. Due to the narrower potential window, [BMIM][$MeSO_3$]:EG delivers lower specific energy and power than [BMIM][$MeSO_3$]:NMAc and ILs. The energy density for BMIM][$MeSO_3$]:NMAc is the highest among all. It is also capable of delivering equivalent power to that of frequently reported IL i.e. [EMIM][Tf_2N]. Nonetheless power density is the supreme for [EMIM][BF_4], due to its lesser ESR (Figure 4. 22, Section 4.2).

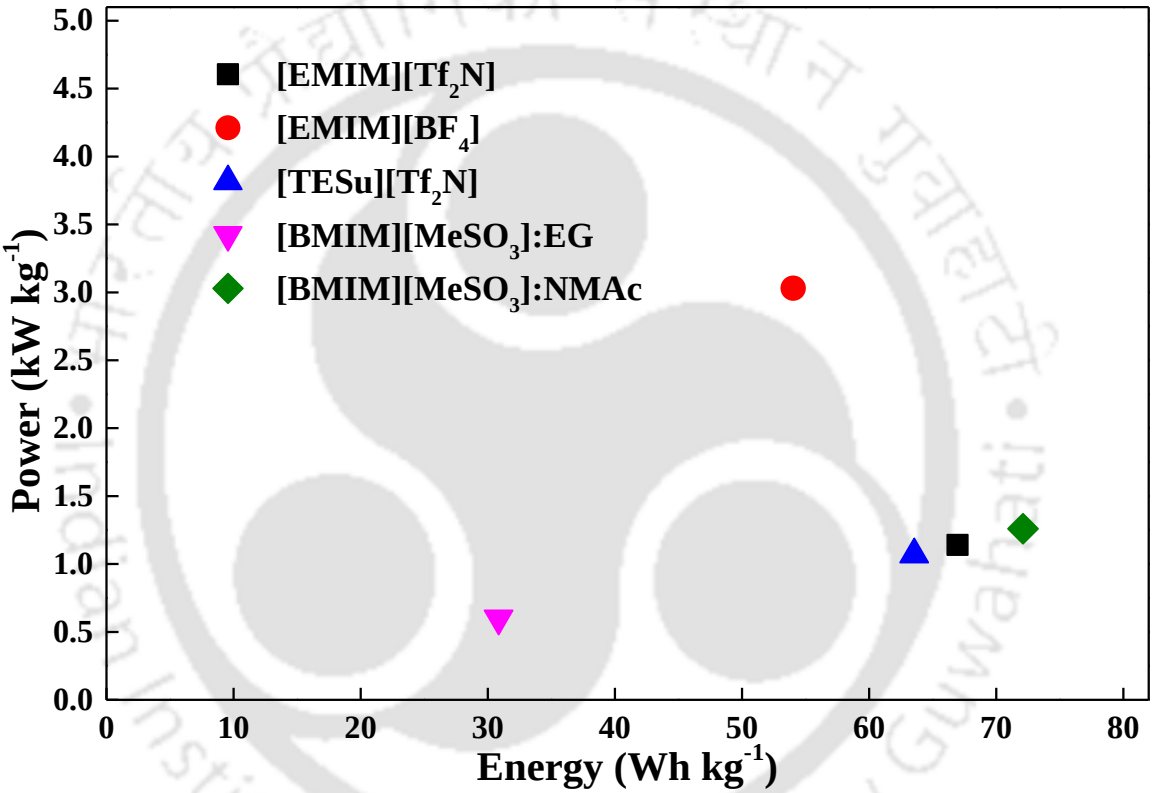

Figure 6.16: Ragone plot at 0.3 A g^{-1} for pure ILs and DESs

CHAPTER 7

Conclusions and Future Work

7.1 Conclusions

The thesis work investigated the performance of seven different RTILs and two novel DESs as electrolytes for EDLC. Several physicochemical and electrochemical characterization methods were employed for their performance evaluation. Electrochemical measurements with same WE established the relative and qualitative outcome. This chapter encapsulates the findings of the thesis and further addresses the future scope.

CV, GCD and EIS together provided the detailed insights how different cation-anion combination of IL contributed to the electrochemical behaviour of the EDLC. Solvation effects on electrochemical parameters of ILs revealed the advantages and disadvantages of IL+ organic solvent electrolytes. The OPW gradually constricted with increase in co-solvent concentration as confirmed by both CV and GCD. Pure IL offered the highest ESR even though it resulted in the widest OPW. AN provided improved charge storage and lesser ESR at room temperature as compared to BN and PC for [AMIM][Tf_2N]. Even though the priority was given to [EMIM][Tf_2N] by researchers, better performance by unfamiliar [PMIM][Tf_2N] was found in our work in solvated state. Alkyl imidazolium ILs with Tf_2N anion resulted in wider OPW than the same with BF_4. Addition of [BMIM][BF_4] to [EMIM][BF_4] intensified the electrochemical window. However, reduction in specific capacitance for mixed system is most likely a consequence of additional cation-cation interaction between EMIM and BMIM cations. Furthermore, Alkyl chain length showed noteworthy effects on electrochemical performance, particularly OPW and ESR, when EMIM and BMIM were compared. The study on [BMPy][BF_4] revealed that AN and PC could act differently on electrochemical performance of the IL, where IL+AN_I come up as the best electrolyte solution by delivering the highest specific capacitance, energy and power density. For imidazolium and sulfonium ILs, the best results were observed for

IL+co-solvent_II unlike [BMPy][BF_4]. Moreover, [BMPy][BF_4] resulted in narrower OPW than imidazolium ILs. Electrochemical performance of pure [TESul][Tf_2N] and [EMIM][Tf_2N] were observed to be equivalent irrespective of different cation. Overall, the ILs possessed double layer behaviour confirming absence of pseudocapacitance. The best performance, in terms of OPW, ESR, specific capacitance, energy and power, was obtained for [PMIM][Tf_2N]+AN_II solution.

Ionic conductivity passed through a maximum at IL+AN_II. Further it again decreased due to absence of sufficient ionic species. Viscosity of the electrolytes decreased with increase in solvent concentration. AN broke the large ion pair clusters by weakening the ionic interaction which helped in obtaining higher ionic conductivity and lower viscosity. The increasing MSD for IL+AN_II solution clearly indicated the enhancement of D and σ over pure ILs. Ionic conductivity values predicted from MD simulation showed a close match with experimental findings.

This objective of studying DESs as electrolytes facilitated the use of high melting salt (~ 74 °C) namely [BMIM][$MeSO_3$] at room temperature or even below. COSMO-SAC calculations predicted the eutectic points of the desired DESs, which confirmed the formation of DESs. ^{1}H NMR studies elucidated the absence of chemical interaction. NOESY NMR gave the insight of spatial arrangements of protons which was able to predict the sites of hydrogen bonding. The prepared DESs of this work offered impressive thermal stability for EDLC application at temperature as high as ~90 ºC. The ionic conductivity of the DESs were also comparable to neat RTILs. Additionally, viscosity of both the DESs were found to be significantly lower than conventional IL electrolytes indicating their potential towards supercapacitor application with ESPW of 3.8 V. The OPW corresponding to RGO electrode was wider for [BMIM][$MeSO_3$]:NMAc. Moderate value of specific

capacitance (55 – 67 Fg^{-1}) were obtained for the RGO-DES systems. Moreover, [BMIM][$MeSO_3$]:NMAc possessed nearly twice specific energy and power when compared to [BMIM][$MeSO_3$]:EG. Therefore, [BMIM][$MeSO_3$]:NMAc has emerged as more effective electrolyte for supercapacitor. The attempt with novel DESs brought impressive results regarding lower viscosity and equivalent electrochemical performance to ILs. However, higher internal resistance observed from 3-electrode configuration leaves the scope of further research on 2-electrode device level assembly with ESR reduction techniques.

7.2 Future Scope

The era of DES electrolytes has begun just a few years back. Hence the window is still open to design electrolyte of desirable properties. DESs possess the advantage of assembling HBAs and HBDs for a definite application. The absence of chemical interaction between HBA and HBD does not alter the resulting physicochemical properties of DES significantly. Based on the results and discussion obtained from this work, future extension can be summarized. A greater number of IL-based, metal or organic salt-based DESs can be explored with different HBDs in the future. Hence, effects of change in either HBA or HBD on OPW and specific capacitance can be determined. Moreover, DES with greater ionic conductivity and lower ESR than ILs needs to be studied so that the need of organic solvents can be minimized. In this regard, combination of RTIL with lower viscosity namely [EMIM][BF_4] and suitable HBDs can be explored. Further, investigation of temperature effects on electrochemical performance is also desirable. Gel electrolytes based on novel DESs may also emerge as potential GPEs. Moreover, there is the scope of studying the electrochemistry of DESs in depth to develop pathways for choosing EDLC's electrolytes.

References

[1] C. Zhong, Y. Deng, W. Hu, J. Qiao, L. Zhang, J. Zhang, A review of electrolyte materials and compositions for electrochemical supercapacitors, Chem. Soc. Rev. 44 (2015) 7484–7539. https://doi.org/10.1039/c5cs00303b.

[2] J. Máca, M. Sedla, Supercapacitors : Properties and applications, J. Energy Storage. 17 (2018) 224–227. https://doi.org/10.1016/j.est.2018.03.012.

[3] J. Zhang, H. Wu, J. Wang, J. Shi, Z. Shi, Pre-lithiation design and lithium ion intercalation plateaus utilization of mesocarbon microbeads anode for lithium-ion capacitors, Electrochim. Acta. 182 (2015) 156–164. https://doi.org/10.1016/j.electacta.2015.09.074.

[4] G. Wang, H. Wang, B. Zhong, L. Zhang, J. Zhang, Supercapacitors' Applications, Electrochem. Energy. (2015) 479–492. https://doi.org/10.1201/b19061-27.

[5] Supercapacitors in space, Agency, Eur. Sp. (2020). https://artes.esa.int/news/supercapacitors-space (accessed August 17, 2020).

[6] A. Brandt, S. Pohlmann, A. Varzi, A. Balducci, S. Passerini, Ionic liquids in supercapacitors, MRS Bull. 38 (2013) 554–559. https://doi.org/10.1557/mrs.2013.151.

[7] A. Eftekhari, Supercapacitors utilising ionic liquids, Energy Storage Mater. 9 (2017) 47–69. https://doi.org/10.1016/j.ensm.2017.06.009.

[8] A.P. Abbott, D. Boothby, G. Capper, D.L. Davies, R.K. Rasheed, Deep Eutectic Solvents formed between choline chloride and carboxylic acids: Versatile alternatives to ionic liquids, J. Am. Chem. Soc. 126 (2004) 9142–9147. https://doi.org/10.1021/ja048266j.

[9] B. Pal, S. Yang, S. Ramesh, V. Thangadurai, R. Jose, Electrolyte selection for

supercapacitive devices: A critical review, Nanoscale Adv. 1 (2019) 3807–3835. https://doi.org/10.1039/c9na00374f.

[10] H.Y. Lee, J.B. Goodenough, Supercapacitor Behavior with KCl Electrolyte, J. Solid State Chem. 144 (1999) 220–223. https://doi.org/10.1006/jssc.1998.8128.

[11] R. Chandrasekaran, M. Koh, A. Yamauchi, M. Ishikawa, Electrochemical Study on Aqueous Magnesium Nitrate Electrolyte System for EDLC Applications, Electrochemistry. 77 (2009) 51–55. https://doi.org/10.5796/electrochemistry.77.51.

[12] X. Zhang, X. Wang, L. Jiang, H. Wu, C. Wu, J. Su, Effect of aqueous electrolytes on the electrochemical behaviors of supercapacitors based on hierarchically porous carbons, J. Power Sources. 216 (2012) 290–296. https://doi.org/10.1016/j.jpowsour.2012.05.090.

[13] F. Barzegar, D.Y. Momodu, O.O. Fashedemi, A. Bello, J.K. Dangbegnon, N. Manyala, Investigation of different aqueous electrolytes on the electrochemical performance of activated carbon-based supercapacitors, RSC Adv. 5 (2015) 107482–107487. https://doi.org/10.1039/c5ra21962k.

[14] M. Kim, I. Oh, J. Kim, Effects of different electrolytes on the electrochemical and dynamic behavior of electric double layer capacitors based on a porous silicon carbide electrode, Phys. Chem. Chem. Phys. 17 (2015) 16367–16374. https://doi.org/10.1039/c5cp01728a.

[15] Z. Zhang, Z. Zhou, H. Peng, Y. Qin, G. Li, Nitrogen- and oxygen-containing hierarchical porous carbon frameworks for high-performance supercapacitors, Electrochim. Acta. 134 (2014) 471–477. https://doi.org/10.1016/j.electacta.2014.04.107.

[16] Z. Jin, X. Yan, Y. Yu, G. Zhao, Sustainable activated carbon fibers from liquefied

wood with controllable porosity for high-performance supercapacitors, J. Mater. Chem. A. 2 (2014) 11706–11715. https://doi.org/10.1039/c4ta01413h.

[17] Q. Chen, Y. Hu, C. Hu, H. Cheng, Z. Zhang, H. Shao, L. Qu, Graphene quantum dots-three-dimensional graphene composites for high-performance supercapacitors, Phys. Chem. Chem. Phys. 16 (2014) 19307–19313. https://doi.org/10.1039/c4cp02761b.

[18] X. Liu, P. Shang, Y. Zhang, X. Wang, Z. Fan, B. Wang, Y. Zheng, Three-dimensional and stable polyaniline-grafted graphene hybrid materials for supercapacitor electrodes, J. Mater. Chem. A. 2 (2014) 15273–15278. https://doi.org/10.1039/c4ta03077j.

[19] M. Jana, P. Khanra, N.C. Murmu, P. Samanta, J.H. Lee, T. Kuila, Covalent surface modification of chemically derived graphene and its application as supercapacitor electrode material, Phys. Chem. Chem. Phys. 16 (2014) 7618–7626. https://doi.org/10.1039/c3cp54510e.

[20] L.F. Chen, Z.H. Huang, H.W. Liang, H.L. Gao, S.H. Yu, Three-dimensional heteroatom-doped carbon nanofiber networks derived from bacterial cellulose for supercapacitors, Adv. Funct. Mater. 24 (2014) 5104–5111. https://doi.org/10.1002/adfm.201400590.

[21] Y. Mun, C. Jo, T. Hyeon, J. Lee, J. Lee, K.S. Ha, K.W. Jun, S.H. Lee, S.W. Hong, H.I. Lee, S. Yoon, Simple synthesis of hierarchically structured partially graphitized carbon by emulsion/block-copolymer co-template method for high power supercapacitors, Carbon N. Y. 64 (2013) 391–402. https://doi.org/10.1016/j.carbon.2013.07.092.

[22] Q. Wang, J. Yan, Y. Wang, T. Wei, M. Zhang, X. Jing, Z. Fan, Three-dimensional

flower-like and hierarchical porous carbon materials as high-rate performance electrodes for supercapacitors, Carbon N. Y. 67 (2014) 119–127. https://doi.org/10.1016/j.carbon.2013.09.070.

[23] J. Yin, L. Qi, H. Wang, Anti-freezing aqueous electrolytes for electric double-layer capacitors, Electrochim. Acta. 88 (2013) 208–216. https://doi.org/10.1016/j.electacta.2012.10.047.

[24] H. Tomiyasu, H. Shikata, K. Takao, N. Asanuma, S. Taruta, Y.Y. Park, An aqueous electrolyte of the widest potential window and its superior capability for capacitors, Sci. Rep. 7 (2017) 1–12. https://doi.org/10.1038/srep45048.

[25] M. Morita, M. Goto, Y. Matsuda, Ethylene carbonate-based organic electrolytes for electric double layer capacitors, J. Appl. Electrochem. 22 (1992) 901–908. https://doi.org/10.1007/BF01024137.

[26] Y. Lai, X. Chen, Z. Zhang, J. Li, Y. Liu, Tetraethylammonium difluoro(oxalato)borate as electrolyte salt for electrochemical double-layer capacitors, Electrochim. Acta. 56 (2011) 6426–6430. https://doi.org/10.1016/j.electacta.2011.04.136.

[27] A. Brandt, P. Isken, A. Lex-Balducci, A. Balducci, Adiponitrile-based electrochemical double layer capacitor, J. Power Sources. 204 (2012) 213–219. https://doi.org/10.1016/j.jpowsour.2011.12.025.

[28] S.H. Kwon, E. Lee, B.S. Kim, S.G. Kim, B.J. Lee, M.S. Kim, J.C. Jung, Activated carbon aerogel as electrode material for coin-type EDLC cell in organic electrolyte, Curr. Appl. Phys. 14 (2014) 603–607. https://doi.org/10.1016/j.cap.2014.02.010.

[29] I. Yang, S.G. Kim, S.H. Kwon, J.H. Lee, M.S. Kim, J.C. Jung, Pore size-controlled carbon aerogels for EDLC electrodes in organic electrolytes, Curr. Appl. Phys. 16

(2016) 665–672. https://doi.org/10.1016/j.cap.2016.03.019.

[30] D.E. Jiang, Z. Jin, D. Henderson, J. Wu, Solvent effect on the pore-size dependence of an organic electrolyte supercapacitor, J. Phys. Chem. Lett. 3 (2012) 1727–1731. https://doi.org/10.1021/jz3004624.

[31] E. Perricone, M. Chamas, L. Cointeaux, J.C. Leprêtre, P. Judeinstein, P. Azais, F. Béguin, F. Alloin, Investigation of methoxypropionitrile as co-solvent for ethylene carbonate based electrolyte in supercapacitors. A safe and wide temperature range electrolyte, Electrochim. Acta. 93 (2013) 1–7. https://doi.org/10.1016/j.electacta.2013.01.084.

[32] W. Qian, F. Sun, Y. Xu, L. Qiu, C. Liu, S. Wang, F. Yan, Human hair-derived carbon flakes for electrochemical supercapacitors, Energy Environ. Sci. 7 (2014) 379–386. https://doi.org/10.1039/c3ee43111h.

[33] X. Huang, B. Sun, S. Chen, G. Wang, Self-assembling synthesis of free-standing nanoporous graphene-transition- metal oxide flexible electrodes for high-performance lithium-ion batteries and supercapacitors, Chem. - An Asian J. 9 (2014) 206–211. https://doi.org/10.1002/asia.201301121.

[34] N. Jung, S. Kwon, D. Lee, D.M. Yoon, Y.M. Park, A. Benayad, J.Y. Choi, J.S. Park, Synthesis of chemically bonded graphene/carbon nanotube composites and their application in large volumetric capacitance supercapacitors, Adv. Mater. 25 (2013) 6854–6858. https://doi.org/10.1002/adma.201302788.

[35] H. Zhou, Y. Peng, H. Bin Wu, F. Sun, H. Yu, F. Liu, Q. Xu, Y. Lu, Fluorine-rich nanoporous carbon with enhanced surface affinity in organic electrolyte for high-performance supercapacitors, Nano Energy. 21 (2016) 80–89. https://doi.org/10.1016/j.nanoen.2015.12.016.

[36] H. Zhang, J. Wang, Y. Chen, Z. Wang, S. Wang, Long-term cycling stability of polyaniline on graphite electrodes used for supercapacitors, Electrochim. Acta. 105 (2013) 69–74. https://doi.org/10.1016/j.electacta.2013.04.114.

[37] D. Hanlon, C. Backes, T.M. Higgins, M. Hughes, A. O'Neill, P. King, N. McEvoy, G.S. Duesberg, B. Mendoza Sanchez, H. Pettersson, V. Nicolosi, J.N. Coleman, Production of molybdenum trioxide nanosheets by liquid exfoliation and their application in high-performance supercapacitors, Chem. Mater. 26 (2014) 1751–1763. https://doi.org/10.1021/cm500271u.

[38] R. Francke, D. Cericola, R. Kötz, D. Weingarth, S.R. Waldvogel, Novel electrolytes for electrochemical double layer capacitors based on 1,1,1,3,3,3-hexafluoropropan-2-ol, Electrochim. Acta. 62 (2012) 372–380. https://doi.org/10.1016/j.electacta.2011.12.050.

[39] M. Sevilla, A.B. Fuertes, Direct synthesis of highly porous interconnected carbon nanosheets and their application as high-performance supercapacitors, ACS Nano. 8 (2014) 5069–5078. https://doi.org/10.1021/nn501124h.

[40] S.H. Kwon, B.S. Kim, S.G. Kim, B.J. Lee, M.S. Kim, J.C. Jung, Preparation of nano-porous activated carbon aerogel using a single-step activation method for use as high-power EDLC electrode in organic electrolyte, J. Nanosci. Nanotechnol. 16 (2016) 4598–4604. https://doi.org/10.1166/jnn.2016.11009.

[41] R.R. Zhang, Y.M. Xu, D. Harrison, J. Fyson, F.L. Qiu, D. Southee, Flexible strip supercapacitors for future energy storage, Int. J. Autom. Comput. 12 (2015) 43–49. https://doi.org/10.1007/s11633-014-0866-6.

[42] W. Li, D. Chen, Z. Li, Y. Shi, Y. Wan, G. Wang, Z. Jiang, D. Zhao, Nitrogen-containing carbon spheres with very large uniform mesopores: The superior

electrode materials for EDLC in organic electrolyte, Carbon N. Y. 45 (2007) 1757–1763. https://doi.org/10.1016/j.carbon.2007.05.004.

[43] D.R. MacFarlane, M. Forsyth, P.C. Howlett, M. Kar, S. Passerini, J.M. Pringle, H. Ohno, M. Watanabe, F. Yan, W. Zheng, S. Zhang, J. Zhang, Ionic liquids and their solid-state analogues as materials for energy generation and storage, Nat. Rev. Mater. 1 (2016). https://doi.org/10.1038/natrevmats.2015.5.

[44] M. Watanabe, M.L. Thomas, S. Zhang, K. Ueno, T. Yasuda, K. Dokko, Application of Ionic Liquids to Energy Storage and Conversion Materials and Devices, Chem. Rev. 117 (2017) 7190–7239. https://doi.org/10.1021/acs.chemrev.6b00504.

[45] N. De Vos, C. Maton, C. V Stevens, Electrochemical Stability of Ionic Liquids : General Influences and Degradation Mechanisms, ChemElectroChem. 1 (2014) 1258–1270. https://doi.org/10.1002/celc.201402086.

[46] L. Wei, M. Sevilla, A.B. Fuertes, R. Mokaya, G. Yushin, Polypyrrole-derived activated carbons for high-performance electrical double-layer capacitors with ionic liquid electrolyte, Adv. Funct. Mater. 22 (2012) 827–834. https://doi.org/10.1002/adfm.201101866.

[47] G. Sun, K. Li, L. Xie, J. Wang, Y. Li, Preparation of mesoporous carbon spheres with a bimodal pore size distribution and its application for electrochemical double layer capacitors based on ionic liquid as the electrolyte, Microporous Mesoporous Mater. 151 (2012) 282–286. https://doi.org/10.1016/j.micromeso.2011.10.023.

[48] D. Zhou, H. Wang, N. Mao, Y. Chen, Y. Zhou, T. Yin, H. Xie, W. Liu, S. Chen, X. Wang, High energy supercapacitors based on interconnected porous carbon nanosheets with ionic liquid electrolyte, Microporous Mesoporous Mater. 241 (2017) 202–209. https://doi.org/10.1016/j.micromeso.2017.01.001.

[49] M.M. Hantel, A. Płatek, T. Kaspar, R. Nesper, A. Wokaun, R. Kötz, Investigation of diluted ionic liquid 1-ethyl-3-methyl-imidazolium tetrafluoroborate electrolytes for intercalation-like electrodes used in supercapacitors, Electrochim. Acta. 110 (2013) 234–239. https://doi.org/10.1016/j.electacta.2013.04.032.

[50] M. Shi, S. Kou, X. Yan, Engineering the Electrochemical Capacitive Properties of Graphene Sheets in Ionic-Liquid Electrolytes by Correct Selection of Anions, ChemSusChem. 7 (2014) 3053–3062. https://doi.org/10.1002/cssc.201402275.

[51] C. Tran, D. Lawrence, F.W. Richey, C. Dillard, Y.A. Elabd, V. Kalra, Binder-free three-dimensional high energy density electrodes for ionic-liquid supercapacitors, Chem. Commun. 51 (2015) 13760–13763. https://doi.org/10.1039/c5cc04359j.

[52] K.L. Van Aken, M. Beidaghi, Y. Gogotsi, Formulation of ionic-liquid electrolyte to expand the voltage window of supercapacitors, Angew. Chemie - Int. Ed. 54 (2015) 4806–4809. https://doi.org/10.1002/anie.201412257.

[53] N. Handa, T. Sugimoto, M. Yamagata, M. Kikuta, M. Kono, M. Ishikawa, A neat ionic liquid electrolyte based on FSI anion for electric double layer capacitor, J. Power Sources. 185 (2008) 1585–1588. https://doi.org/10.1016/j.jpowsour.2008.08.086.

[54] T. Kim, G. Jung, S. Yoo, K.S. Suh, R.S. Ruoff, Activated graphene-based carbons as supercapacitor electrodes with macro- and mesopores, ACS Nano. 7 (2013) 6899–6905. https://doi.org/10.1021/nn402077v.

[55] Y. Zhu, S. Murali, M.D. Stoller, K.J. Ganesh, W. Cai, P.J. Ferreira, A. Pirkle, R.M. Wallace, K.A. Cychosz, M. Thommes, D. Su, E.A. Stach, R.S. Ruoff, Carbon-Based Supercapacitors Produced by Activation of Graphene, Science (80-.). 332 (2011) 1537–1541. https://doi.org/10.1126/science.1200770.

[56] L. Qiao, A. Shougee, T. Albrecht, K. Fobelets, Oxide-coated silicon nanowire array capacitor electrodes in room temperature ionic liquid, Electrochim. Acta. 210 (2016) 32–37. https://doi.org/10.1016/j.electacta.2016.05.088.

[57] A. Balducci, U. Bardi, S. Caporali, M. Mastragostino, F. Soavi, Ionic liquids for hybrid supercapacitors, Electrochem. Commun. 6 (2004) 566–570. https://doi.org/10.1016/j.elecom.2004.04.005.

[58] V. Ruiz, T. Huynh, S.R. Sivakkumar, A.G. Pandolfo, RSC Advances Ionic liquid – solvent mixtures as supercapacitor electrolytes for extreme temperature operation {, RSC Adv. 2 (2012) 5591–5598. https://doi.org/10.1039/c2ra20177a.

[59] Z. Li, J. Liu, K. Jiang, T. Thundat, Nano Energy Carbonized nanocellulose sustainably boosts the performance of activated carbon in ionic liquid supercapacitors, Nano Energy. 25 (2016) 161–169. https://doi.org/10.1016/j.nanoen.2016.04.036.

[60] A. Orita, K. Kamijima, M. Yoshida, Allyl-functionalized ionic liquids as electrolytes for electric double-layer capacitors, J. Power Sources. 195 (2010) 7471–7479. https://doi.org/10.1016/j.jpowsour.2010.05.066.

[61] L. Timperman, P. Skowron, A. Boisset, H. Galiano, D. Lemordant, E. Frackowiak, F. Béguin, M. Anouti, Triethylammonium bis(tetrafluoromethylsulfonyl)amide protic ionic liquid as an electrolyte for electrical double-layer capacitors, Phys. Chem. Chem. Phys. 14 (2012) 8199–8207. https://doi.org/10.1039/c2cp40315c.

[62] L. Timperman, H. Galiano, D. Lemordant, M. Anouti, Phosphonium-based protic ionic liquid as electrolyte for carbon-based supercapacitors, Electrochem. Commun. 13 (2011) 1112–1115. https://doi.org/10.1016/j.elecom.2011.07.010.

[63] A.J.R. Rennie, V.L. Martins, R.M. Torresi, P.J. Hall, Ionic liquids containing

sulfonium cations as electrolytes for electrochemical double layer capacitors, J. Phys. Chem. C. 119 (2015) 23865–23874. https://doi.org/10.1021/acs.jpcc.5b08241.

[64] M.P.S. Mousavi, B.E. Wilson, S. Kashefolgheta, E.L. Anderson, S. He, P. Bu, A. Stein, Ionic Liquids as Electrolytes for Electrochemical Double-Layer Capacitors: Structures that Optimize Specific Energy, ACS Appl. Mater. Interfaces. 8 (2016) 3396–3406. https://doi.org/10.1021/acsami.5b11353.

[65] L. Mayrand-provencher, S. Lin, D. Lazzerini, D. Rochefort, Pyridinium-based protic ionic liquids as electrolytes for RuO 2 electrochemical capacitors, J. Power Sources. 195 (2010) 5114–5121. https://doi.org/10.1016/j.jpowsour.2010.02.073.

[66] S.P. Ong, O. Andreussi, Y. Wu, N. Marzari, G. Ceder, Electrochemical windows of room-temperature ionic liquids from molecular dynamics and density functional theory calculations, Chem. Mater. 23 (2011) 2979–2986. https://doi.org/10.1021/cm200679y.

[67] Q. Zhang, K. De Oliveira Vigier, S. Royer, F. Jérôme, Deep eutectic solvents: Syntheses, properties and applications, Chem. Soc. Rev. 41 (2012) 7108–7146. https://doi.org/10.1039/c2cs35178a.

[68] E.L. Smith, A.P. Abbott, K.S. Ryder, Deep Eutectic Solvents (DESs) and Their Applications, Chem. Rev. 114 (2014) 11060–11082. https://doi.org/10.1021/cr300162p.

[69] Y.J. Ju, C.H. Lien, K.H. Chang, C.C. Hu, D.S.H. Wong, Deep eutectic solvent-based ionic liquid electrolytes for electrical double-layer capacitors, J. Chinese Chem. Soc. 59 (2012) 1280–1287. https://doi.org/10.1002/jccs.201100698.

[70] W. Zaidi, L. Timperman, M. Anouti, Deep eutectic solvent based on sodium cations as an electrolyte for supercapacitor application, RSC Adv. 4 (2014) 45647–45652.

https://doi.org/10.1039/c4ra08178a.

[71] M. Figueiredo, C. Gomes, R. Costa, A. Martins, C.M. Pereira, F. Silva, Differential capacity of a deep eutectic solvent based on choline chloride and glycerol on solid electrodes, Electrochim. Acta. 54 (2009) 2630–2634. https://doi.org/10.1016/j.electacta.2008.10.074.

[72] W. Zaidi, A. Boisset, J. Jacquemin, L. Timperman, M. Anouti, Deep eutectic solvents based on N-methylacetamide and a lithium salt as electrolytes at elevated temperature for activated carbon-based supercapacitors, J. Phys. Chem. C. 118 (2014) 4033–4042. https://doi.org/10.1021/jp412552v.

[73] A. Boisset, J. Jacquemin, M. Anouti, Physical properties of a new Deep Eutectic Solvent based on lithium bis[(trifluoromethyl)sulfonyl]imide and N-methylacetamide as superionic suitable electrolyte for lithium ion batteries and electric double layer capacitors, Electrochim. Acta. 102 (2013) 120–126. https://doi.org/10.1016/j.electacta.2013.03.150.

[74] X. Baokou, M. Anouti, Physical properties of a new deep eutectic solvent based on a sulfonium ionic liquid as a suitable electrolyte for electric double-layer capacitors, J. Phys. Chem. C. 119 (2015) 970–979. https://doi.org/10.1021/jp5110455.

[75] S. Phadke, S. Amara, M. Anouti, Gas Evolution in Activated-Carbon-Based Supercapacitors with Protic Deep Eutectic Solvent as Electrolyte, ChemPhysChem. 18 (2017) 2364–2373. https://doi.org/10.1002/cphc.201700621.

[76] Y. Matsuda, K. Inoue, H. Takeuchi, Y. Okuhama, Gel polymer electrolytes for electric double layer capacitors, Solid State Ionics. 113–115 (1998) 103–107. https://doi.org/10.1016/s0167-2738(98)00281-1.

[77] G.P. Pandey, Y. Kumar, S.A. Hashmi, Ionic liquid incorporated PEO based polymer

electrolyte for electrical double layer capacitors: A comparative study with lithium and magnesium systems, Solid State Ionics. 190 (2011) 93–98. https://doi.org/10.1016/j.ssi.2011.03.018.

[78] P. Tamilarasan, S. Ramaprabhu, Stretchable supercapacitors based on highly stretchable ionic liquid incorporated polymer electrolyte, Mater. Chem. Phys. 148 (2014) 48–56. https://doi.org/10.1016/j.matchemphys.2014.07.010.

[79] Y.F. Huang, P.F. Wu, M.Q. Zhang, W.H. Ruan, E.P. Giannelis, Boron cross-linked graphene oxide/polyvinyl alcohol nanocomposite gel electrolyte for flexible solid-state electric double layer capacitor with high performance, Electrochim. Acta. 132 (2014) 103–111. https://doi.org/10.1016/j.electacta.2014.03.151.

[80] S.N. Syahidah, S.R. Majid, Ionic liquid-based polymer gel electrolytes for symmetrical solid-state electrical double layer capacitor operated at different operating voltages, Electrochim. Acta. 175 (2015) 184–192. https://doi.org/10.1016/j.electacta.2015.02.215.

[81] R. Na, G. Huo, S. Zhang, P. Huo, Y. Du, J. Luan, K. Zhu, G. Wang, A novel poly(ethylene glycol)-grafted poly(arylene ether ketone) blend micro-porous polymer electrolyte for solid-state electric double layer capacitors formed by incorporating a chitosan-based LiClO4 gel electrolyte, J. Mater. Chem. A. 4 (2016) 18116–18127. https://doi.org/10.1039/c6ta07846j.

[82] R. Na, C.W. Su, Y.H. Su, Y.C. Chen, Y.M. Chen, G. Wang, H. Teng, Solvent-free synthesis of an ionic liquid integrated ether-abundant polymer as a solid electrolyte for flexible electric double-layer capacitors, J. Mater. Chem. A. 5 (2017) 19703–19713. https://doi.org/10.1039/c7ta05358d.

[83] G.P. Pandey, T. Liu, C. Hancock, Y. Li, X.S. Sun, J. Li, Thermostable gel polymer

electrolyte based on succinonitrile and ionic liquid for high-performance solid-state supercapacitors, J. Power Sources. 328 (2016) 510–519. https://doi.org/10.1016/j.jpowsour.2016.08.032.

[84] M.Y. Chong, A. Numan, C.W. Liew, H.M. Ng, K. Ramesh, S. Ramesh, Enhancing the performance of green solid-state electric double-layer capacitor incorporated with fumed silica nanoparticles, J. Phys. Chem. Solids. 117 (2018) 194–203. https://doi.org/10.1016/j.jpcs.2018.02.030.

[85] J.A. Wang, Y.T. Lu, S.C. Lin, Y.S. Wang, C.C.M. Ma, C.C. Hu, Designing a Novel Polymer Electrolyte for Improving the Electrode/Electrolyte Interface in Flexible All-Solid-State Electrical Double-Layer Capacitors, ACS Appl. Mater. Interfaces. 10 (2018) 17871–17882. https://doi.org/10.1021/acsami.8b02046.

[86] N. Farah, H.M. Ng, A. Numan, C.W. Liew, N.A.A. Latip, K. Ramesh, S. Ramesh, Solid polymer electrolytes based on poly(vinyl alcohol) incorporated with sodium salt and ionic liquid for electrical double layer capacitor, Mater. Sci. Eng. B Solid-State Mater. Adv. Technol. 251 (2019) 114468. https://doi.org/10.1016/j.mseb.2019.114468.

[87] C. Yue, D. Fang, L. Liu, T.F. Yi, Synthesis and application of task-specific ionic liquids used as catalysts and/or solvents in organic unit reactions, J. Mol. Liq. 163 (2011) 99–121. https://doi.org/10.1016/j.molliq.2011.09.001.

[88] A. Safavi, F. Farjami, Electrodeposition of gold-platinum alloy nanoparticles on ionic liquid-chitosan composite film and its application in fabricating an amperometric cholesterol biosensor, Biosens. Bioelectron. 26 (2011) 2547–2552. https://doi.org/10.1016/j.bios.2010.11.002.

[89] J. Liu, F. Wang, L. Zhang, X. Fang, Z. Zhang, Thermodynamic properties and

thermal stability of ionic liquid-based nanofluids containing graphene as advanced heat transfer fluids for medium-to-high-temperature applications, Renew. Energy. 63 (2014) 519–523. https://doi.org/10.1016/j.renene.2013.10.002.

[90] E.J. González, N. Calvar, E. Gómez, Á. Domínguez, Application of [EMim][ESO4] ionic liquid as solvent in the extraction of toluene from cycloalkanes: Study of liquid-liquid equilibria at T=298.15K, Fluid Phase Equilib. 303 (2011) 174–179. https://doi.org/10.1016/j.fluid.2011.01.021.

[91] S.P.M. Ventura, F.A. E Silva, M. V. Quental, D. Mondal, M.G. Freire, J.A.P. Coutinho, Ionic-Liquid-Mediated Extraction and Separation Processes for Bioactive Compounds: Past, Present, and Future Trends, Chem. Rev. 117 (2017) 6984–7052. https://doi.org/10.1021/acs.chemrev.6b00550.

[92] T. Makino, M. Kanakubo, Absorption of n-butane in imidazolium and phosphonium ionic liquids and application to separation of hydrocarbon gases, Sep. Purif. Technol. 214 (2019) 139–147. https://doi.org/10.1016/j.seppur.2018.04.032.

[93] Y.S. Ng, N.S. Jayakumar, M.A. Hashim, Behavior of hydrophobic ionic liquids as liquid membranes on phenol removal: Experimental study and optimization, Desalination. 278 (2011) 250–258. https://doi.org/10.1016/j.desal.2011.05.047.

[94] K.M. Gupta, Y. Chen, J. Jiang, Ionic liquid membranes supported by hydrophobic and hydrophilic metal-organic frameworks for CO2 capture, J. Phys. Chem. C. 117 (2013) 5792–5799. https://doi.org/10.1021/jp312404k.

[95] A.A.C. Toledo Hijo, G.J. Maximo, M.C. Costa, E.A.C. Batista, A.J.A. Meirelles, Applications of Ionic Liquids in the Food and Bioproducts Industries, ACS Sustain. Chem. Eng. 4 (2016) 5347–5369. https://doi.org/10.1021/acssuschemeng.6b00560.

[96] R. Martínez-Palou, R. Luque, Applications of ionic liquids in the removal of

contaminants from refinery feedstocks: An industrial perspective, Energy Environ. Sci. 7 (2014) 2414–2447. https://doi.org/10.1039/c3ee43837f.

[97] M. Bin Dahbag, A. AlQuraishi, M. Benzagouta, Efficiency of ionic liquids for chemical enhanced oil recovery, J. Pet. Explor. Prod. Technol. 5 (2015) 353–361. https://doi.org/10.1007/s13202-014-0147-5.

[98] B. Banerjee, G. Pugazhenthi, T. Banerjee, Experimental Insights into the Thermal Dehydrogenation of Ethylene Diamine Bisborane Using Allyl-Based Ionic Liquids, Energy and Fuels. 31 (2017) 5428–5440. https://doi.org/10.1021/acs.energyfuels.6b02823.

[99] P. Dehury, U. Mahanta, T. Banerjee, Partitioning of butanol between a hydrophobic ionic liquid and aqueous phase: Insights from Liquid Liquid Equilibria measurements and Molecular Dynamics simulations, Fluid Phase Equilib. 425 (2016) 421–431. https://doi.org/10.1016/j.fluid.2016.06.007.

[100] M. Mohan, V. V. Goud, T. Banerjee, Solubility of glucose, xylose, fructose and galactose in ionic liquids: Experimental and theoretical studies using a continuum solvation model, Fluid Phase Equilib. 395 (2015) 33–43. https://doi.org/10.1016/j.fluid.2015.03.020.

[101] L. Bui-Le, C.J. Clarke, A. Bröhl, A.P.S. Brogan, J.A.J. Arpino, K.M. Polizzi, J.P. Hallett, Revealing the complexity of ionic liquid–protein interactions through a multi-technique investigation, Commun. Chem. 3 (2020) 1–9. https://doi.org/10.1038/s42004-020-0302-5.

[102] L.I.N. Tomé, V. Baião, W. da Silva, C.M.A. Brett, Deep eutectic solvents for the production and application of new materials, Appl. Mater. Today. 10 (2018) 30–50. https://doi.org/10.1016/j.apmt.2017.11.005.

[103] G. García, S. Aparicio, R. Ullah, M. Atilhan, Deep eutectic solvents: Physicochemical properties and gas separation applications, Energy and Fuels. 29 (2015) 2616–2644. https://doi.org/10.1021/ef5028873.

[104] J.C. Malaquias, M. Steichen, M. Thomassey, P.J. Dale, Electrodeposition of Cu-In alloys from a choline chloride based deep eutectic solvent for photovoltaic applications, Electrochim. Acta. 103 (2013) 15–22. https://doi.org/10.1016/j.electacta.2013.04.068.

[105] M.K. Hadj-Kali, K.E. Al-khidir, I. Wazeer, L. El-blidi, S. Mulyono, I.M. AlNashef, Application of deep eutectic solvents and their individual constituents as surfactants for enhanced oil recovery, Colloids Surfaces A Physicochem. Eng. Asp. 487 (2015) 221–231. https://doi.org/10.1016/j.colsurfa.2015.10.005.

[106] F.S. Ghareh Bagh, K. Shahbaz, F.S. Mjalli, M.A. Hashim, I.M. Alnashef, Zinc (II) chloride-based deep eutectic solvents for application as electrolytes: Preparation and characterization, J. Mol. Liq. 204 (2015) 76–83. https://doi.org/10.1016/j.molliq.2015.01.025.

[107] M.A. Farajzadeh, M.R. Afshar Mogaddam, B. Feriduni, Simultaneous synthesis of a deep eutectic solvent and its application in liquid-liquid microextraction of polycyclic aromatic hydrocarbons from aqueous samples, RSC Adv. 6 (2016) 47990–47996. https://doi.org/10.1039/c6ra04103e.

[108] S.T. Williamson, K. Shahbaz, F.S. Mjalli, I.M. AlNashef, M.M. Farid, Application of deep eutectic solvents as catalysts for the esterification of oleic acid with glycerol, Renew. Energy. 114 (2017) 480–488. https://doi.org/10.1016/j.renene.2017.07.046.

[109] S. Kumar-Krishnan, M. Guadalupe-Ferreira García, E. Prokhorov, M. Estevez-González, R. Pérez, R. Esparza, M. Meyyappan, Synthesis of gold nanoparticles

supported on functionalized nanosilica using deep eutectic solvent for an electrochemical enzymatic glucose biosensor, J. Mater. Chem. B. 5 (2017) 7072–7081. https://doi.org/10.1039/c7tb01346a.

[110] J.D. Mota-Morales, R.J. Sánchez-Leija, A. Carranza, J.A. Pojman, F. del Monte, G. Luna-Bárcenas, Free-radical polymerizations of and in deep eutectic solvents: Green synthesis of functional materials, Prog. Polym. Sci. 78 (2018) 139–153. https://doi.org/10.1016/j.progpolymsci.2017.09.005.

[111] D.A. Pethsangave, R. V. Khose, P.H. Wadekar, S. Some, Deep Eutectic Solvent Functionalized Graphene Composite as an Extremely High Potency Flame Retardant, ACS Appl. Mater. Interfaces. 9 (2017) 35319–35324. https://doi.org/10.1021/acsami.7b09587.

[112] P.K. Naik, P. Dehury, S. Paul, T. Banerjee, Evaluation of Deep Eutectic Solvent for the selective extraction of toluene and quinoline at T = 308.15 K and p = 1 bar, Fluid Phase Equilib. 423 (2016) 146–155. https://doi.org/10.1016/j.fluid.2016.04.018.

[113] P. Dehury, R.K. Chaudhary, T. Banerjee, A. Dalal, Evaluation of Thermophysical Properties of Menthol-Based Deep Eutectic Solvent as a Thermal Fluid: Forced Convection and Numerical Studies, Ind. Eng. Chem. Res. 58 (2019) 20125–20133. https://doi.org/10.1021/acs.iecr.9b01836.

[114] P. Dehury, J. Singh, T. Banerjee, Thermophysical and Forced Convection Studies on (Alumina + Menthol)-Based Deep Eutectic Solvents for Their Use as a Heat Transfer Fluid, ACS Omega. 3 (2018) 18016–18027. https://doi.org/10.1021/acsomega.8b02661.

[115] A.I. Akhmetshina, A.N. Petukhov, A. Mechergui, A. V. Vorotyntsev, A. V. Nyuchev, A.A. Moskvichev, I. V. Vorotyntsev, Evaluation of Methanesulfonate-

Based Deep Eutectic Solvent for Ammonia Sorption, J. Chem. Eng. Data. 63 (2018) 1896–1904. https://doi.org/10.1021/acs.jced.7b01004.

[116] A.P. Abbott, D. Boothby, G. Capper, D.L. Davies, R.K. Rasheed, Deep Eutectic Solvents formed between choline chloride and carboxylic acids: Versatile alternatives to ionic liquids, J. Am. Chem. Soc. 126 (2004) 9142–9147. https://doi.org/10.1021/ja048266j.

[117] R.K. Das, A.K. Golder, Co_3O_4 spinel nanoparticles decorated graphite electrode: Bio-mediated synthesis and electrochemical H_2O_2 sensing, Electrochim. Acta. 251 (2017) 415–426. https://doi.org/10.1016/j.electacta.2017.08.122.

[118] A. Saheb, J. Janata, M. Josowicz, Reference Electrode for Ionic Liquids, Electroanalysis. 18 (2006) 405–409. https://doi.org/10.1002/elan.200503435.

[119] Z. Xue, L. Qin, J. Jiang, T. Mu, G. Gao, Thermal, electrochemical and radiolytic stabilities of ionic liquids, Phys. Chem. Chem. Phys. 20 (2018) 8382–8402. https://doi.org/10.1039/c7cp07483b.

[120] S.T. Lin, S.I. Sandler, A priori phase equilibrium prediction from a segment contribution solvation model, Ind. Eng. Chem. Res. 41 (2002) 899–913. https://doi.org/10.1021/ie001047w.

[121] P.V.A. Pontes, E.A. Crespo, M.A.R. Martins, L.P. Silva, C.M.S.S. Neves, G.J. Maximo, M.D. Hubinger, E.A.C. Batista, S.P. Pinho, J.A.P. Coutinho, G. Sadowski, C. Held, Measurement and PC-SAFT modeling of solid-liquid equilibrium of deep eutectic solvents of quaternary ammonium chlorides and carboxylic acids, Fluid Phase Equilib. 448 (2017) 69–80. https://doi.org/10.1016/j.fluid.2017.04.007.

[122] E.A. Crespo, L.P. Silva, M.A.R. Martins, L. Fernandez, J. Ortega, O. Ferreira, G. Sadowski, C. Held, S.P. Pinho, J.A.P. Coutinho, Characterization and Modeling of

the Liquid Phase of Deep Eutectic Solvents Based on Fatty Acids/Alcohols and Choline Chloride, Ind. Eng. Chem. Res. 56 (2017) 12192–12202. https://doi.org/10.1021/acs.iecr.7b02382.

[123] M.A.R. Martins, E.A. Crespo, P.V.A. Pontes, L.P. Silva, M. Bülow, G.J. Maximo, E.A.C. Batista, C. Held, S.P. Pinho, J.A.P. Coutinho, Tunable Hydrophobic Eutectic Solvents Based on Terpenes and Monocarboxylic Acids, ACS Sustain. Chem. Eng. 6 (2018) 8836–8846. https://doi.org/10.1021/acssuschemeng.8b01203.

[124] C.H.J.T. Dietz, J.T. Creemers, M.A. Meuleman, C. Held, G. Sadowski, M. Van Sint Annaland, F. Gallucci, M.C. Kroon, Determination of the Total Vapor Pressure of Hydrophobic Deep Eutectic Solvents: Experiments and Perturbed-Chain Statistical Associating Fluid Theory Modeling, ACS Sustain. Chem. Eng. 7 (2019) 4047–4057. https://doi.org/10.1021/acssuschemeng.8b05449.

[125] R. Verma, T. Banerjee, Liquid-Liquid Extraction of Lower Alcohols Using Menthol-Based Hydrophobic Deep Eutectic Solvent: Experiments and COSMO-SAC Predictions, Ind. Eng. Chem. Res. 57 (2018) 3371–3381. https://doi.org/10.1021/acs.iecr.7b05270.

[126] T. Banerjee, M.K. Singh, A. Khanna, Prediction of binary VLE for imidazolium based ionic liquid systems using COSMO-RS, Ind. Eng. Chem. Res. 45 (2006) 3207–3219. https://doi.org/10.1021/ie051116c.

[127] T. Bharti, A., Kundu, D., Rabari, D., Banerjee, Phase Equilibria in Ionic Liquid Facilitated Liquid-Liquid Extractions., 1st Editio, CRC Press, Boca Raton, 2017. https://doi.org/https://doi.org/10.1201/9781315367163.

[128] M.D. Koretsky, Engineering and Chemical Thermodynamics, 2nd ed., John Wiley & Sons, Inc., Hoboken, New Jersery, 2012.

[129] N. Zdolšek, M. Bendová, F. Quirion, P. Vrbka, Z. Wagner, T. Trtić-Petrović, Phase behaviour of 1-butyl-3-methylimidazolium methanesulfonate as new thermal energy material, in: 2017. https://doi.org/10.13140/RG.2.2.20003.35364.

[130] G.S. Parks, K.K. Kelley, Thermal data on organic compunds.II.The heat capacities of five organic compunds. The entropies and free energies of some homologous series of aliphatic compunds, J. Am. Chem. Soc. 47 (1925) 2089–2097. https://doi.org/10.1021/ja01685a003.

[131] J. Ahlers, Binary Solid - Liquid Equilibria of Organic Systems Containing Different Amides and Sulfolane, J. Chem. Eng. Data. 44 (1999) 727–730. https://doi.org/10.1021/je9802975.

[132] T.K. and J.M. R. Dennington, GaussView, Semichem Inc., Shawnee Mission. KS. (2009).

[133] M.J. Frisch, G.W. Trucks, H.B. Schlegel, G.E. Scuseria, M.A. Robb, J.R. Cheeseman, G. Scalmani, V. Barone, G.A. Petersson, H. Nakatsuji, X. Li, M. Caricato, A. Marenich, J. Bloino, B.G. Janesko, R. Gomperts, B. Mennucci, H.P. Hratchian, J. V. Ort, D.J. Fox, Gaussian 09, Revision A.02, Gaussian, Inc., Wallingford CT. (2016).

[134] A.D. Becke, Density-functional thermochemistry. III. The role of exact exchange, J. Chem. Phys. 5648 (2006) 5648–5652.

[135] B. Diehl, Chapter 1 - Principles in NMR Spectroscopy, in: U. Holzgrabe, I. Wawer, B.B.T.-N.M.R.S. in P.A. Diehl (Eds.), NMR Spectrosc. Pharm. Anal., Elsevier, Amsterdam, 2008: pp. 1–41. https://doi.org/https://doi.org/10.1016/B978-0-444-53173-5.00001-9.

[136] I. Delso, C. Lafuente, J. Muñoz-embid, M. Artal, NMR study of choline chloride-

based deep eutectic solvents, J. Mol. Liq. 290 (2019) 111236. https://doi.org/10.1016/j.molliq.2019.111236.

[137] D. Banerjee, Experimental Techniques in Thermal Analysis Thermogravimetry (TG) Differential Scanning Calorimetry (DSC), IIT Kanpur. (2020). https://www.iitk.ac.in/che/pdf/resources/TGA-DSC-reading-material.pdf (accessed July 22, 2020).

[138] Gamry Instruments, Two, Three and Four Electrode Experiments, Gamry Instruments. (2019) 1–7. https://www.gamry.com/application-notes/electrodes-cells/two-three-and-four-electrode-experiments/ (accessed July 17, 2020).

[139] B.A. Mei, O. Munteshari, J. Lau, B. Dunn, L. Pilon, Physical Interpretations of Nyquist Plots for EDLC Electrodes and Devices, J. Phys. Chem. C. 122 (2018) 194–206. https://doi.org/10.1021/acs.jpcc.7b10582.

[140] Electrochemical Impedance Spectroscopy, Annu. Rev. Anal. Chem. 3 (2010) 207–229. https://doi.org/10.1146/annurev.anchem.012809.102211.

[141] B. Chang, S. Park, Electrochemical Impedance Spectroscopy, Annu. Rev. Anal. Chem. 3 (2010) 207–229. https://doi.org/10.1146/annurev.anchem.012809.102211.

[142] G.P. Pandey, S.A. Hashmi, Studies on electrical double layer capacitor with a low-viscosity ionic liquid 1-ethyl-3-methylimidazolium tetracyanoborate as electrolyte, Bull. Mater. Sci. 36 (2013) 729–733. https://doi.org/10.1007/s12034-013-0511-y.

[143] C. Lei, F. Markoulidis, Z. Ashitaka, C. Lekakou, Reduction of porous carbon/Al contact resistance for an electric double-layer capacitor (EDLC), Electrochim. Acta. 92 (2013) 183–187. https://doi.org/10.1016/j.electacta.2012.12.092.

[144] R. Kötz, M. Carlen, Principles and applications of electrochemical capacitors, Electrochim. Acta. 45 (2000) 2483–2498.

https://doi.org/https://doi.org/10.1016/S0013-4686(00)00354-6.

[145] Y. Zhang, A. Otani, E.J. Maginn, Reliable Viscosity Calculation from Equilibrium Molecular Dynamics Simulations : A Time Decomposition Method, J. Chem. Theory Comput. 11 (2015) 3537–3546. https://doi.org/10.1021/acs.jctc.5b00351.

[146] M. Chen, R. Pendrill, G. Widmalm, J.W. Brady, J. Wohlert, Molecular Dynamics Simulations of the Ionic Liquid 1 - n - Butyl-3- Methylimidazolium Chloride and Its Binary Mixtures with Ethanol, J. Chem. Theory Comput. 10 (2014) 4465–4479. https://doi.org/10.1021/ct500271z.

[147] L. Martínez, R. Andrade, E.G. Birgin, J.M. Martínez, Software News and Update Packmol : A Package for Building Initial Configurations, J. Comput. Chem. 30 (2009) 2157–2164. https://doi.org/10.1002/jcc.

[148] J. Wang, R.M. Wolf, J.W. Caldwell, P.A. Kollman, D.A. Case, Development and testing of a general amber force field, J. Comput. Chem. 25 (2004) 1157–1174. https://doi.org/10.1002/jcc.20035.

[149] J. Wang, W. Wang, P.A. Kollman, D.A. Case, Automatic atom type and bond type perception in molecular mechanical calculations, J. Mol. Graph. Model. 25 (2006) 247–260. https://doi.org/10.1016/j.jmgm.2005.12.005.

[150] K.. Case, D. A., Darden, T., Cheatham, T., Simmerling, C., Wang, J., Duke, R., Luo, R., Walker, R., Zhang, W., Merz, Amber 12 Reference Manual, 2012. https://ambermd.org/doc12/Amber12.pdf.

[151] I. Leontyev, A. Stuchebrukhov, Accounting for electronic polarization in non-polarizable force fields, Phys. Chem. Chem. Phys. 13 (2011) 2613–2626. https://doi.org/10.1039/c0cp01971b.

[152] J.C. Phillips, R. Braun, W. Wang, J. Gumbart, E. Tajkhorshid, E. Villa, C. Chipot,

R.D. Skeel, L. Kalé, K. Schulten, Scalable molecular dynamics with NAMD, J. Comput. Chem. 26 (2005) 1781–1802. https://doi.org/10.1002/jcc.20289.

[153] S. Nose, A unified formulation of the constant temperature molecular dynamics methods, J. Chem. Phys. 81 (1984) 511–519.

[154] W.G. Hoover, Canonical dynamics: Equilibrium phase-space distributions William, Phys. Rev. A. 31 (1985) 1695–1697.

[155] J. Chen, K.N. Houk, Molecular Modeling: Principles and Applications By Andrew R. Leach. Addison Wesley Longman Limited: Essex, England, 1996. 595 pp. ISBN 0-582-23933-8. $35, J. Chem. Inf. Comput. Sci. 38 (1998) 939. https://doi.org/10.1021/ci9804241.

[156] B.A. Luty, M.E. Davis, I.G. Tironi, W.F. Van Gunsteren, A Comparison of Particle-Particle, Particle-Mesh and Ewald Methods for Calculating Electrostatic Interactions in Periodic Molecular Systems, Mol. Simul. 14 (1994) 11–20. https://doi.org/10.1080/08927029408022004.

[157] S.S. Sarangi, W. Zhao, F. Müller-plathe, S. Balasubramanian, Correlation between Dynamic Heterogeneity and Local Structure in a Room-Temperature Ionic Liquid : A Molecular Dynamics Study of [bmim][PF 6], ChemPhysChem. 11 (2010) 2001–2010. https://doi.org/10.1002/cphc.201000111.

[158] R. Biswas, A. Malviya, T. Banerjee, P. Ghosh, S.M. Ali, Alkali Metal Ion Partitioning with Calix [4] arene-benzo-crown - 6 Ionophore in Acidic Medium : Insights from Experiments , Statistical Mechanical Framework , and Molecular Dynamics Simulations, J. Phys. Chem. B. 122 (2018) 2102–2112. https://doi.org/10.1021/acs.jpcb.7b10632.

[159] A. Scalia, A. Varzi, A. Moretti, P. Ruschhaupt, A. Lamberti, E. Tresso, S. Passerini,

Electrolytes based on N-Butyl-N-Methyl-Pyrrolidinium 4,5-Dicyano-2-(Trifluoromethyl) Imidazole for High Voltage Electrochemical Double Layer Capacitors, ChemElectroChem. 6 (2019) 552–557. https://doi.org/10.1002/celc.201801172.

[160] M. Yoke, A. Numan, C. Liew, H.M. Ng, K. Ramesh, S. Ramesh, Enhancing the performance of green solid-state electric double-layer capacitor incorporated with fumed silica nanoparticles, J. Phys. Chem. Solids. 117 (2018) 194–203. https://doi.org/10.1016/j.jpcs.2018.02.030.

[161] D.J. Bozym, B. Uralcan, D.T. Limmer, M.A. Pope, N.J. Szamreta, P.G. Debenedetti, I.A. Aksay, Anomalous Capacitance Maximum of the Glassy Carbon-Ionic Liquid Interface through Dilution with Organic Solvents, J. Phys. Chem. Lett. 6 (2015) 2644–2648. https://doi.org/10.1021/acs.jpclett.5b00899.

[162] X.H. Fan, Y.P. Chen, C.S. Su, Density and Viscosity Measurements for Binary Mixtures of 1-Ethyl-3-methylimidazolium Tetrafluoroborate ([Emim][BF4]) with Dimethylacetamide, Dimethylformamide, and Dimethyl Sulfoxide, J. Chem. Eng. Data. 61 (2016) 920–927. https://doi.org/10.1021/acs.jced.5b00753.

[163] O. Ciocirlan, O. Croitoru, O. Iulian, Densities and viscosities for binary mixtures of 1-butyl-3- methylimidazolium tetrafluoroborate ionic liquid with molecular solvents, J. Chem. Eng. Data. 56 (2011) 1526–1534. https://doi.org/10.1021/je101206u.

[164] A. Knorr, R. Ludwig, Cation-cation clusters in ionic liquids: Cooperative hydrogen bonding overcomes like-charge repulsion, Sci. Rep. 5 (2015) 1–7. https://doi.org/10.1038/srep17505.

[165] R. Newell, J. Faure-Vincent, B. Iliev, T. Schubert, D. Aradilla, A new high

performance ionic liquid mixture electrolyte for large temperature range supercapacitor applications (−70 °C to 80 °C) operating at 3.5V cell voltage, Electrochim. Acta. 267 (2018) 15–19. https://doi.org/10.1016/j.electacta.2018.02.067.

[166] M. Jayalakshmi, K. Balasubramanian, Simple Capacitors to Supercapacitors - An Overview, Int. J. Electrochem. Sci. 3 (2008) 1196–1217.

[167] M.P.S. Mousavi, B.E. Wilson, S. Kashefolgheta, E.L. Anderson, S. He, P. Bühlmann, A. Stein, Ionic Liquids as Electrolytes for Electrochemical Double-Layer Capacitors: Structures that Optimize Specific Energy, ACS Appl. Mater. Interfaces. 8 (2016) 3396–3406. https://doi.org/10.1021/acsami.5b11353.

[168] Z.-B. Zhou, H. Matsumoto, Tatsumi, Low-Melting, Low-Viscous, Hydrophobic Ionic Liquids: 1-Alkyl(Alkyl Ether)-3-methylimidazolium Perfluoroalkyltrifluoroborate, Chem. - A Eur. J. (2004) 6581–6591. https://doi.org/10.1002/chem.200400533.

[169] S.P. Ong, O. Andreussi, Y. Wu, N. Marzari, G. Ceder, Electrochemical windows of room-temperature ionic liquids from molecular dynamics and density functional theory calculations, Chem. Mater. 23 (2011) 2979–2986. https://doi.org/10.1021/cm200679y.

[170] C. Alberto, C. Ruiz, D. Be, D. Rochefort, Electrochemical and Spectroelectrochemical Evidence of Redox Transitions Involving Protons in Thin MnO 2 Electrodes in Protic Ionic Liquids, J. Phys. Chem. C. 117 (2013) 20397–20405. https://doi.org/10.1021/jp405047g.

[171] A. Bhattacharjee, A. Luís, J.H. Santos, J.A. Lopes-da-Silva, M.G. Freire, P.J. Carvalho, J.A.P. Coutinho, Thermophysical properties of sulfonium- and

ammonium-based ionic liquids, Fluid Phase Equilib. 381 (2014) 36–45. https://doi.org/10.1016/j.fluid.2014.08.005.

[172] Y. Cao, T. Mu, Comprehensive investigation on the thermal stability of 66 ionic liquids by thermogravimetric analysis, Ind. Eng. Chem. Res. 53 (2014) 8651–8664. https://doi.org/10.1021/ie5009597.

[173] C. Maton, N. De Vos, C. V. Stevens, Ionic liquid thermal stabilities: Decomposition mechanisms and analysis tools, Chem. Soc. Rev. 42 (2013) 5963–5977. https://doi.org/10.1039/c3cs60071h.

[174] A. Hofmann, M. Migeot, T. Hanemann, Investigation of Binary Mixtures Containing 1-Ethyl-3-methylimidazolium Bis(trifluoromethanesulfonyl)azanide and Ethylene Carbonate, J. Chem. Eng. Data. 61 (2016) 114–123. https://doi.org/10.1021/acs.jced.5b00338.

[175] E. Gómez, N. Calvar, E.A. MacEdo, Á. Domínguez, Effect of the temperature on the physical properties of pure 1-propyl 3-methylimidazolium bis(trifluoromethylsulfonyl)imide and characterization of its binary mixtures with alcohols, J. Chem. Thermodyn. 45 (2012) 9–15. https://doi.org/10.1016/j.jct.2011.08.028.

[176] M. Vranes, S. Dozic, V. Djeric, S. Gadzuric, Physicochemical characterization of 1-butyl-3-methylimidazolium and 1-butyl-1-methylpyrrolidinium bis(trifluoromethylsulfonyl)imide, J. Chem. Eng. Data. 57 (2012) 1072–1077. https://doi.org/10.1021/je2010837.

[177] S. Tsuzuki, W. Shinoda, H. Saito, M. Mikami, H. Tokuda, M. Watanabe, Molecular dynamics simulations of ionic liquids: Cation and anion dependence of self-diffusion coefficients of ions, J. Phys. Chem. B. 113 (2009) 10641–10649.

https://doi.org/10.1021/jp811128b.

[178] G.I. Egorov, D.M. Makarov, M. Kolker Arkadiy, Densities and Volumetric Properties of Ethylene Glycol + Dimethylsulfoxide Mixtures at Temperatures of (278.15 to 323.15) K and Pressures of (0.1 to 100) MPa, J. Chem. Eng. Data. 55 (2010) 3481–3488. https://doi.org/10.1021/acs.jced.7b00750.

[179] A.A. Dyshin, M.G. Kiselev, Density and Viscosity of Magnesium Chloride Solution in N-Methylacetamide over the Temperature Range from 308.15 to 328.15 K at Ambient Pressure, J. Chem. Eng. Data. 64 (2019) 2536–2541. https://doi.org/10.1021/acs.jced.9b00046.

[180] F.C. Auluck, D.S. Kothari, The Hole Theory of Liquids, Nature. 153 (1944) 777. https://doi.org/10.1038/153777b0.

[181] A. Yadav, A. Guha, A. Pandey, M. Pal, S. Trivedi, S. Pandey, Densities and dynamic viscosities of ionic liquids having 1-butyl-3-methylimidazolium cation with different anions and bis(trifluoromethylsulfonyl)imide anion with different cations in the temperature range (283.15 to 363.15) K, J. Chem. Thermodyn. 116 (2018) 67–75. https://doi.org/10.1016/j.jct.2017.08.032.

APPENDIX A

Performance Parameters of the Electrolytes

Equations 1.1 and 1.2 are used calculation of energy parameters as reported in Chapter 1. The unit of energy and power are Wh kg^{-1} and kW kg^{-1} respectively.

Table A1: Specific energy and power at different specific current of GCD measurements

IL	Electrolyte	1 A g^{-1}		0.5 A g^{-1}		0.3 A g^{-1}	
		Energy	Power	Energy	Power	Energy	Power
[EMIM][Tf_2N]	Pure IL	-	-	57.87	1.16	66.96	1.13
	IL+AN_I	55.29	2.04	58.65	2.16	63.53	2.03
	IL+AN_II	67.29	9.03	77.50	9.18	96.45	8.91
	IL+AN_III	36.552	2.07	42.09	1.87	49.02	1.62
[PMIM][Tf_2N]	IL+AN_I	93.98	6.15	115.74	6.02	-	-
	IL+AN_II	111.61	9.33	152.44	10.10	-	-
	IL+AN_III	61.56	4.59	80.38	4.81	-	-
	IL+BN_II	72.67	4.38	86.81	4.55	101.35	4.69
	IL+PC_II	68.68	3.21	74.4	3.21	81.52	3.21
[BMIM][Tf_2N]	IL+AN_I	89.29	4.31	100.81	4.08	-	-
	IL+AN_II	106.83	6.61	156.25	5.98	-	-
	IL+AN_III	63.45	4.97	76.15	4.83	-	-
	IL+BN_II	99.21	5.27	115.74	5.41	129.21	5.04
	IL+PC_II	67.20	2.96	71.84	3.06	78.13	3.12
[EMIM][BF_4]	Pure IL	29.31	2.07	32.93	2.05	54.04	3.03
	IL+AN_I	30.76	3.14	32.98	3.24	34.98	3.12
	IL+AN_II	30.61	3.74	32.61	3.57	35.533	3.44
	IL+AN_III	17.451	1.95	18.38	1.86	19.53	1.79
[BMIM][BF_4]	Pure IL	-	-	96.15	1.53	96.15	1.52
	IL+AN_I	81.00	3.37	90.4	3.25	89.34	2.93
	IL+AN_II	70.57	4.69	85.10	4.61	104.16	4.14
	IL+AN_III	19.781	1.42	22.32	1.33	24.67	1.25
[EMIM][BF_4] + [BMIM][BF_4]	IL+AN_I	46.50	2.06	52.48	2.08	58.00	2.04
	IL+AN_II	32.65	4.77	34.65	4.74	38.00	4.64

Table A1 continues

IL	Electrolyte	1 A g^{-1}		0.5 A g^{-1}		0.3 A g^{-1}	
		Energy	Power	Energy	Power	Energy	Power
[BMPy][BF_4]	IL+AN_I	44.52	4.28	46.68	4.31	49.19	4.13
	IL+AN_II	24.93	2.05	26.76	2.31	29.37	2.462
	IL+AN_III	19.58	2.19	21.13	2.19	22.72	2.08
	IL+PC_I	-	-	24.00	0.78	28.4	0.81
	IL+PC_II	29.48	1.89	32.32	1.95	33.61	1.98
	IL+PC_III	32.16	3.01	34.65	3.08	36.01	3.07
[TESu][Tf_2N]	Pure IL	-	-	59.52	1.26	63.54	1.07
	IL+PC_I	-	-	50.63	1.48	52.63	1.52
	IL+PC_II	-	-	51.03	2.91	58.23	2.46
	IL+PC_III	-	-	51.58	1.24	53.14	1.26
DES Electrolytes		0.5 A g^{-1}		0.3 A g^{-1}		0.1 A g^{-1}	
		Energy	Power	Energy	Power	Energy	Power
[BMIM][$MeSO_3$]: EG		27.23	0.61	30.86	0.59	34.72	0.56
[BMIM][$MeSO_3$]: NMAc		61.27	1.28	72.12	1.26	83.33	1.19

APPENDIX B

Viscosity of Ionic Liquid Electrolytes

Table B1: Viscosity for [AMIM][BF_4] and [BMPy][BF_4] electrolytes measured by Anton Paar Phsica MCR301 Rheometer at 298.15 K

Electrolyte	Viscosity (mPa.s)
[PMIM][Tf_2N]+BN_II	1.7
[PMIM][Tf_2N]+PC_II	6.7
[BMIM][Tf_2N]+BN_II	4.9
[BMIM][Tf_2N]+PC_II	4.7
[EMIM][BF_4]_Pure	26
[EMIM][BF_4]+AN_I	11.8
[EMIM][BF_4]+AN_II	8.2
[EMIM][BF_4]+AN_III	1.3
[BMIM][BF_4]_Pure	80.05
[BMIM][BF_4]+AN_I	6.6
[BMIM][BF_4]+AN_II	3.9
[BMIM][BF_4]+AN_III	0.78
[EMIM][BF_4]+[BMIM][BF_4]+AN_II	9.1
[EMIM][BF_4]+[BMIM][BF_4]+AN_II	1.7
[BMPy][BF_4]_Pure	134.6
[BMPy][BF_4]+AN_I	7.7
[BMPy][BF_4]+AN_II	1.3
[BMPy][BF_4]+AN_III	0.8
[BMPy][BF_4]+PC_I	20.5
[BMPy][BF_4]+PC_II	6.2
[BMPy][BF_4]+PC_III	3.8

Table B1 continues

Electrolyte	Viscosity (mPa.s)
[TESu][Tf_2N]_Pure	25.5
[TESu][Tf_2N]+PC_I	8.6
[TESu][Tf_2N]+PC_II	4.3
[TESu][Tf_2N]+PC_III	3.1

APPENDIX C

Partial Electrostatic Charges and NAMD Configuration File

Table C1: Partial charges fitted with restricted electrostatic potential module of AMBER12

Atom Name	Partial Charges
EMIM	
C1	-0.17602
C2	-0.25351
H1	0.256625
H2	0.273867
H3	0.275551
C3	0.049454
C4	-0.12312
H4	0.095383
H5	0.095383
H6	0.068128
H7	0.068128
H8	0.068128
C5	-0.26338
H9	0.161317
H10	0.161317
H11	0.161317
C6	-0.0581
N1	-0.02255
N2	0.162072

Table C1 continues

Atom Name	Partial Charges
PMIM	
C1	-0.49099
C2	-0.00391
H2	0.204933
N2	0.126407
C3	-0.21976
H3	0.149562
C4	0.473715
H4	-0.04713
H5	-0.04713
H6	-0.04713
H1	0.289356
N1	0.383116
C5	-0.35142
H7	0.209898
H8	0.209898
C6	-0.15759
H9	0.132004
H10	0.132004
C7	-0.17849
H11	0.077546
H12	0.077546
H13	0.077546

Table C1 continues

Atom Name	Partial Charges
BMIM	
C1	0.029762
C2	0.052265
C3	0.356584
H1	0.196313
H2	0.174871
H3	0.172148
N1	-0.20539
N2	-0.19576
C4	-0.2268
C5	0.063518
H4	0.111158
H5	0.111158
C6	0.224516
H6	0.023705
H7	0.023705
C7	-0.4032
H8	-0.01794
H9	-0.01794
H10	0.104104
H11	0.104104
H12	0.104104
C8	-0.26359
H13	0.159529
H14	0.159529
H15	0.159529

Table C1 continues

Atom Name	Partial Charges
Tf_2N	
S1	0.659611
O1	-0.50816
O2	-0.50816
C1	0.583837
S2	0.659611
O3	-0.50816
O4	-0.50816
C2	0.583837
F1	-0.1912
F2	-0.1912
F3	-0.1912
F4	-0.1912
F5	-0.1912
F6	-0.1912
N1	-0.30705
Atom Name	**Partial Charges**
AN	
C1	-0.40919
H1	0.164469
H2	0.164469
H3	0.164469
C2	0.408422
N1	-0.49264

C2: NAMD Configuration File

```
#############################################################
## JOB DESCRIPTION                                         ##
#############################################################

# Minimization of 69 molecules of IL and 931 Molecules of Acetonitrile

#############################################################
## ADJUSTABLE PARAMETERS                                   ##
#############################################################

ambercoor                ../common/Emim-TF2N100.inpcrd

set temperature    0
set outputname     EmimTF2N100_min
set restart        0

# Continuing a job from the restart files
if {$restart} {
set inputname      $outputname
Coordinates        ../$inputname.restart.coor
Velocities         ../$inputname.restart.vel  ;# remove the "temperature" entry if you use this!
extendedSystem             ../$inputname.xsc
}

firsttimestep      0
```

```
#####################################################################
## SIMULATION PARAMETERS                                           ##
#####################################################################
# Input
amber               on
parmfile            ../common/Emim-TF2N100.prmtop
if {$restart-1} {
temperature         $temperature
}

# Force-Field Parameters
dielectric          1.0                 # Value of the dielectric constant and Any value greater than 1.0
will be experimental
exclude             scaled1-4
nonbondedScaling    1.0
1-4scaling          1.0
cutoff              12.0        #Angstorm
switching           on
switchdist          10.0     #Angstorm
pairlistdist        14.0       #Angstorm

# Integrator Parameters
timestep            1.0      ;# 1fs/step
rigidBonds          all      ;# Apply SHAKE algorithm to all covalent bonds involving hydrogens
rigidTolerance      0.00001   ;# Desired accuracy in maintaining SHAKEed bond lengths
rigidIterations     100      ;# Maximum number of SHAKE iterations
nonbondedFreq       1
```

```
vdwGeometricSigma   yes

fullElectFrequency  2

stepspercycle       20

pairlistsperCycle   2


# Periodic Boundary Conditions

if {$restart-1} {

set X     40.00

set C     0.00

cellBasisVector1        $X      0.0     0.0     #Angstorm

cellBasisVector2        0.0     $X      0.0     #Angstorm

cellBasisVector3        0.0     0.0     $X      #Angstorm

cellOrigin              $C      $C      $C      #Angstorm


# PME (for full-system periodic electrostatics)

PME             yes

PMEGridSpacing      1.0

PMETolerance        0.000001    ;# The accuracy of computing the Ewald real space (direct) term


#manual grid definition

#PMEGridSizeX       45

#PMEGridSizeY       45

#PMEGridSizeZ       100

}

wrapAll             on


# Constant Temperature Control
```

```
if {0} {
langevin            on    ;# do langevin dynamics
langevinDamping     1     ;# damping coefficient (gamma) of 1/ps
langevinTemp        $temperature
langevinHydrogen    off    ;# don't couple langevin bath to hydrogens
}

# Constant Pressure Control (variable volume)
if {0} {
useGroupPressure      yes ;# needed for rigidBonds
useFlexibleCell       no
useConstantArea       no
langevinPiston        on
langevinPistonTarget  1.01325 ;#  in bar -> 1 atm
langevinPistonPeriod  100.0
langevinPistonDecay   50.0
langevinPistonTemp    $temperature
}

# Fixed Atoms Constraint (set PDB beta-column to 1)
if {0} {
fixedAtoms          on
fixedAtomsForces    on #Is it necessary?
fixedAtomsFile      myfixedatoms.pdb
fixedAtomsCol       B
}
```

```
# IMD Settings (can view sim in VMD)
if {0} {
IMDon           on
IMDport         3000    ;# port number (enter it in VMD)
IMDfreq         1       ;# send every 1 frame
IMDwait         no      ;# wait for VMD to connect before running?
}

# Output
outputName          $outputname
XSTfile             $outputname.xst

restartfreq         500     ;# 500steps = every 1ps
dcdfreq             2000
outputEnergies      100
outputPressure      100

binaryoutput            no
binaryrestart           no

#############################################################
## EXTRA PARAMETERS                                        ##
#############################################################


#############################################################
## EXECUTION SCRIPT                                        ##
```

```
#################################################################

# Minimization

minimization    on

seed            12345     ;# Random number seed used to generate initial Maxwell distribution of

velocities (d)

minimize        500000
```

APPENDIX D

CV Plots of Deep Eutectic Solvents

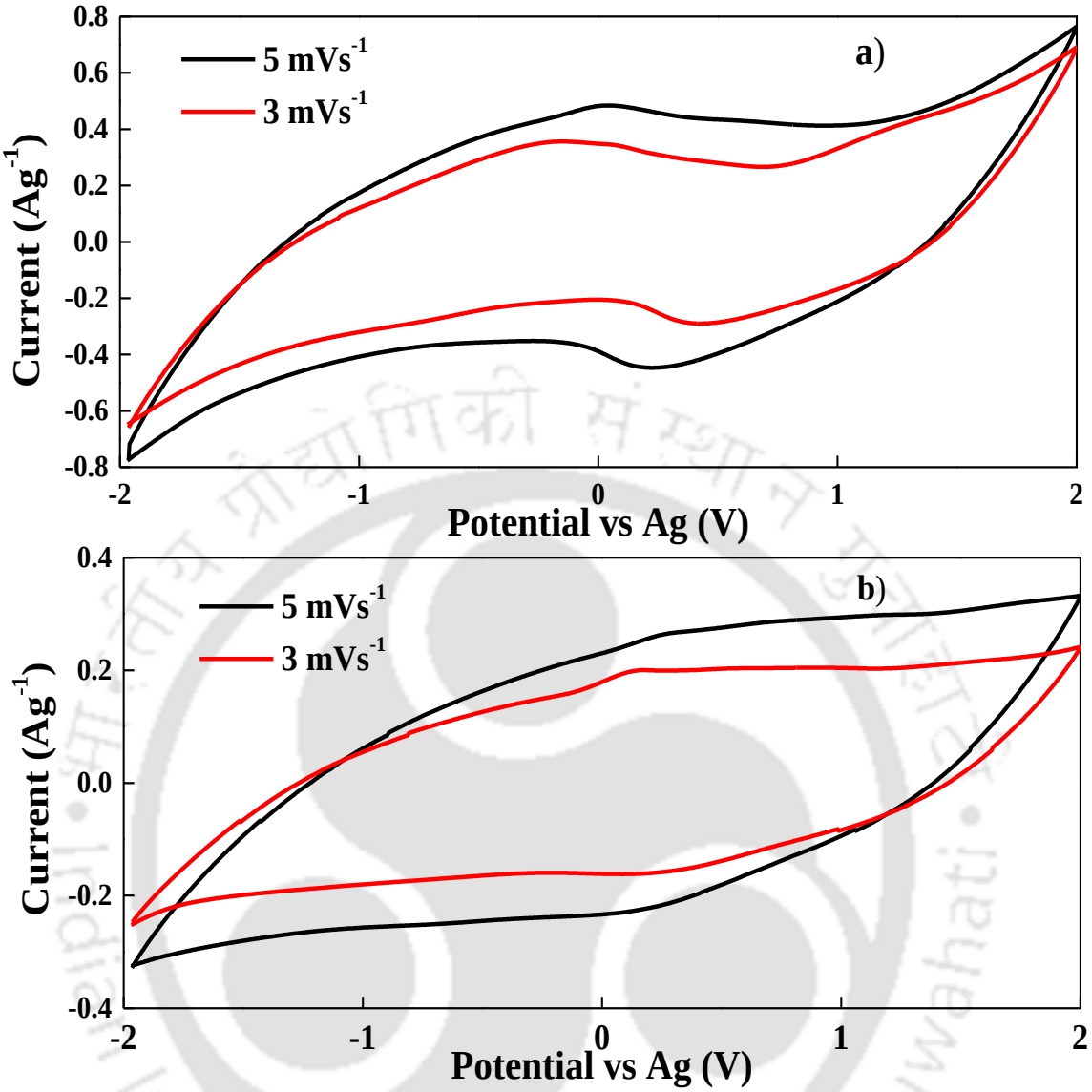

Figure D1: CV plots with RGO electrode a) [BMIM][$MeSO_3$]:EG and [BMIM][$MeSO_3$]:NMAc

[BMIM][$MeSO_3$]:EG shows sharper peaks than [BMIM][$MeSO_3$]:NMAc at higher potential confirming its poorer electrochemical stability with carbon electrode.

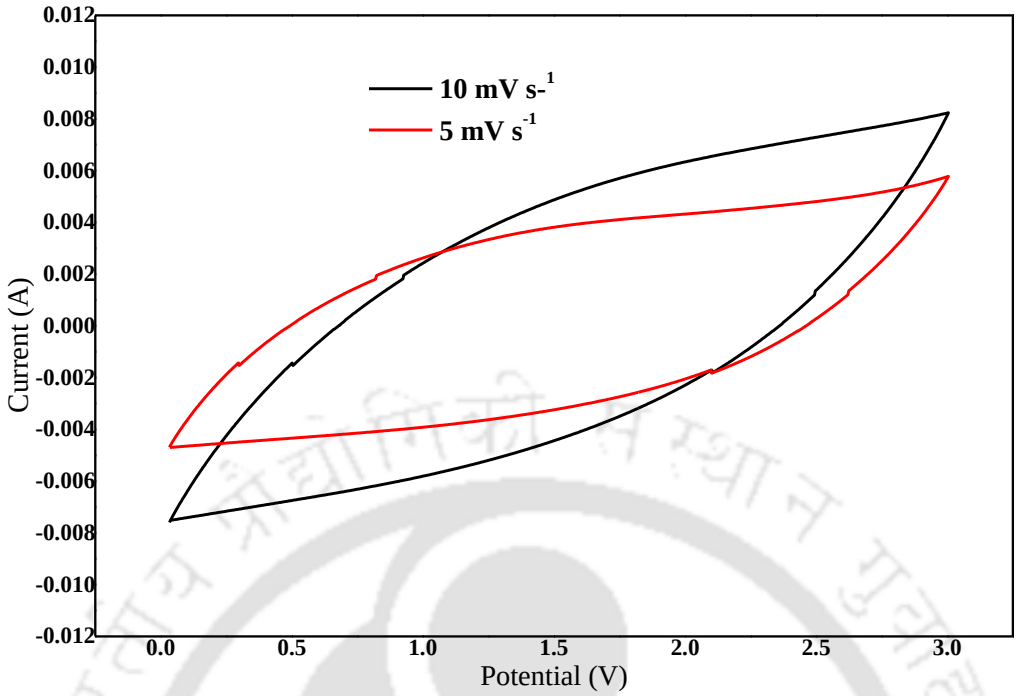

Figure D2: CV data with two symmetric RGO electrodes for [BMIM][$MeSO_3$]:NMAc

The two-electrode system was tried using a simple glass cell. Two symmetrical carbon electrodes are used for DES namely [BMIM][$MeSO_3$]: NMAc. The CV plot at 5 and 10 mV/s can be found in Figure D2. The results support the 3 V OPW obtained by three-electrode set up.

Research Outputs

Referred Journals:

1. **Upasana Mahanta**, R. Prasanna Venkatesh, S. Sujatha, S.A.Ilangovan and Tamal Banerjee. Imidazolium based Ionic Liquids as Electrolytes for Energy Efficient Electrical Double Layer Capacitor: Insights from Molecular Dynamics and Electrochemical Characterisation. **Journal of Solution Chemistry. 2019, 48 (7), 1119–1134.** https://doi.org/10.1007/s10953-019-00898-8
2. **Upasana Mahanta**, R. Prasanna Venkatesh, S. Sujatha, S.A.Ilangovan and Tamal Banerjee. Electrochemical performance and molecular structure of diluted 1-Alkyl-3 methylimidazolium tetrafluoroborate ionic liquids and their mixture as electrolytes for double layer capacitor: An integrated approach by electrochemical characterisation and molecular dynamics simulation. **Industrial Engineering and Chemistry Research.2019, 58 (51), 22741-22753.** https://pubs.acs.org/doi/10.1021/acs.iecr.9b04350
3. **Upasana Mahanta**, Sambita Choudhury, R. Prasanna Venkatesh, S. Sujatha, S.A.Ilangovan and Tamal Banerjee.Ionic Liquid-Based Deep Eutectic Solvents as Novel Electrolytes for Supercapacitors: COSMO-SAC predictions, Synthesis and Characterization. **ACS Sustainable Chemistry & Engineering. 2020, 8 (1), 372−381.** https://pubs.acs.org/doi/10.1021/acssuschemeng.9b05596
4. **Upasana Mahanta**, Ashray Karodiya, R. Prasanna Venkatesh, S. Sujatha, S.A.Ilangovan and Tamal Banerjee. Electrochemical Performance of 1-Butyl-4-methylpyridinium tetrafluoroborate Ionic Liquid Electrolyte for Graphene-based Double Layer Capacitor. **Bulletin of Materials Science. 2021, 44 (75), 1-8.** https://doi.org/10.1007/s12034-020-02337-7

Conference Presentations:

1. **Upasana Mahanta**, R. Prasanna Venkatesh, Tamal Banerjee and S. A. Illangovan. Ionic Liquids as Electrolytes for electrical double layer capacitor: Insights from molecular dynamics simulation and electrochemical characterization., **International Symposium on Solubility Phenomena and Related Equilibrium Processes (ISSP) 2018 (Poster Presentation), July 15-20th 2018, Tours, France.**
2. **Upasana Mahanta**, R. Prasanna Venkatesh, Tamal Banerjee and S. A. Illangovan. Investigation of Ionic Conductance of Ionic Liquids for Electrical Double Layer Capacitor using Molecular Dynamics Simulation., **International Symposium on Solubility Phenomena and Related Equilibrium Processes (ISSP) 2018 (Oral Presentation), July 15-20th 2018, Tours, France**
3. Ashray Koradiya, **Upasana Mahanta,** R Prasanna Venkatesh and Tamal Banerjee. Characterization of ionic liquid based electrical double layer supercapacitor (EDLC)., **Research Conclave, IIT Guwahati 2019 (Poster Presentation), March 15-17th 2019, Indian Institute of Technology, Guwahati, India.**

Journal of Solution Chemistry (2019) 48:1119–1134
https://doi.org/10.1007/s10953-019-00898-8

Imidazolium Based Ionic Liquids as Electrolytes for Energy Efficient Electrical Double Layer Capacitor: Insights from Molecular Dynamics and Electrochemical Characterization

Upasana Mahanta, et al. ***[full author details at the end of the article]***

Received: 19 December 2018 / Accepted: 24 April 2019 / Published online: 24 July 2019

Abstract

Ionic liquids (ILs) have attracted considerable interest as electrolytes for electrical double layer capacitors (EDLC) bringing in enhancement of energy efficiency. This work studied three imidazolium based ILs mixed with a co-solvent as the electrolytes for EDLC. A combined study involving molecular dynamics (MD) and electrochemical experiments was carried out to interpret the potential of the electrolyte solution. Initially, MD simulation was employed to compute ionic conductivity and viscosity of pure ILs, 1-ethyl-3-methylimidazolium bis(trifluoromethylsulfonyl)imide ([EMIM][Tf_2N]), 1-propyl-3-methylimidazolium bis(trifluoromethylsulfonyl)imide ([PMIM][Tf_2N]) and 1-butyl-3-methylimidazolium bis(trifluoromethylsulfonyl)imide ([BMIM][Tf_2N]) and the study was further extended to 1 mol·dm^{-3} solutions of these three ILs in acetonitrile (ACN). The MD results were sequentially validated by experiments. Based on the ionic conductivity and viscosity values obtained from MD and experiments, 0.5, 1.0 and 2.0 mol·dm^{-3} solutions of the ILs in ACN were further investigated as electrolytes for carbon based EDLC. Cyclic voltammetry, electrochemical impedance spectroscopy and galvanostatic charge discharge techniques were employed. From cyclic voltammetry, the observed highest value of the operating potential window was 3 V. The nearly rectangular and symmetric shape of cyclic voltammograms and vertical line of Nyquist plot at lower frequencies indicated good capacitive behavior of the system. The highest specific capacitance of 122 F·g^{-1} was achieved for the 1 mol·dm^{-3} solution of [PMIM][Tf_2N] at 0.5 A·g^{-1}. The highest energy density values were found to be 152 and 149 W·h·kg^{-1} for 1 mol·dm^{-3} solutions of [PMIM][Tf_2N] and [BMIM][Tf_2N], respectively. Overall, 1 mol·dm^{-3} solutions of the less explored [PMIM][Tf_2N] and [BMIM][Tf_2N] provided better electrochemical stability, energy and power density.

Keywords Ionic liquids · Ionic conductivity · Electrical double layer capacitor · Operating potential window · Specific capacitance

Electronic supplementary material The online version of this article (https://doi.org/10.1007/s10953-019-00898-8) contains supplementary material, which is available to authorized users.

I&EC research
Industrial & Engineering Chemistry Research

Article

Cite This: Ind. Eng. Chem. Res. 2019, 58, 22741−22753

pubs.acs.org/IECR

Electrochemical Performance and Molecular Structure of Diluted 1-Alkyl-3-methylimidazolium Tetrafluoroborate Ionic Liquids and Their Mixture as Electrolytes for Double-Layer Capacitors: An Integrated Approach by Electrochemical Characterization and Molecular Dynamics Simulation

Upasana Mahanta,[†] Debashis Kundu,[†] R. Prasanna Venkatesh,[†] S. Sujatha,[‡] S. A. Ilangovan,[§] and Tamal Banerjee*[,†]

[†]Department of Chemical Engineering, Indian Institute of Technology Guwahati, Guwahati 781039, India

[‡]Advanced Power Systems and [§]Chemical Systems Division, Vikram Sarabhai Space Centre (ISRO), Thiruvananthapuram 695022, India

Supporting Information

ABSTRACT: This paper reports the electrochemical studies of two room-temperature ionic liquids (RTILs), namely, 1-ethyl-3-methylimidazolium tetrafluoroborate ([EMIM][BF_4]) and 1-butyl-3-methylimidazolium tetrafluoroborate ([BMIM][BF_4]), and their mixture in 1:1 molar ratio as electrolytes of electrochemical double-layer capacitors (EDLCs). Neat RTILs resulted in better electrochemical stability and lower charge storage. An organic solvent, acetonitrile (ACN), was further added to improve the capacitive performance of the EDLC, reducing the resistance to diffusion of ions, which ensured enhanced specific capacitance but narrowed the electrochemical window. The mixture of RTILs possessed electrochemical stability that resided in between their individual stability limits and lower specific capacitance than either of its constituents. The widest operating potential window (OPW) of 2.7 V was achieved for a 3.5 mol dm^{-3} solution of [BMIM][BF_4]. Nearly equal specific capacitance (~70 F g^{-1}) was delivered by both the RTILs in 2 and 3.5 mol dm^{-3} electrolyte solutions. The longer alkyl chain length of [BMIM][BF_4] imparted better electrochemical stability and specific energy (60−70 W h kg^{-1}) to it. A 2 mol dm^{-3} solution of the RTIL mixture in ACN delivered the highest power of 5.7 kW kg^{-1}. Each system investigated in this study retained the Coulombic efficiency approaching 100%. Furthermore, a molecular dynamics simulation was performed on the RTIL + cosolvent systems to analyze the liquid structure at the microscopic level with the help of the radial pair distribution function and coordination number. Moreover, a study of diffusivity of ionic species facilitated the understanding of cosolvent effects in terms of mobility of ions.

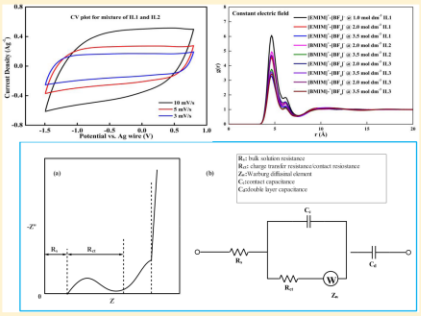

1. INTRODUCTION

The rapid increase in energy demand worldwide and the harmful environmental effects from combustion of fossil fuels have led the scientists and technologists to move toward alternative clean and sustainable energy development techniques. A significant amount of research work has been carried out to develop and scale up clean and sustainable energy storage systems. However, time and weather dependence of most of the renewable energy resources directs the research toward batteries, electrochemical capacitors (ECs), and fuel cells. These three electrochemical energy storage devices are highly recognized in the field of efficient energy harvesting. An electrochemical supercapacitor (ES), being the device delivering the highest power among these three devices, has attracted notable attention from researchers. In ECs (also called supercapacitors), energy may not be delivered through redox reactions like batteries and fuel cells. Based on the energy storage mechanism, ECs can be classified in two distinct categories: (1) pseudocapacitors involving pseudoredox reactions and (2) electrochemical double-layer capacitors (EDLCs) that involve adsorption of electrolyte ions onto the porous and electrically conductive electrodes. Most of the currently available ECs comprises EDLCs due to their more technical development.[1]

Room-temperature ionic liquids (RTILs) appear while potential electrolytes for electrochemical double-layer capacitors (EDLCs) are looked for, as their favorable properties, such as low volatility, high thermal and chemical stability, and a wide electrochemical window, result in energy-efficient and

Received: August 10, 2019
Revised: October 23, 2019
Accepted: November 22, 2019
Published: November 22, 2019

DOI: 10.1021/acs.iecr.9b04350
Ind. Eng. Chem. Res. 2019, 58, 22741−22753

ACS Sustainable Chemistry & Engineering

Research Article

Cite This: ACS Sustainable Chem. Eng. 2020, 8, 372−381

pubs.acs.org/journal/ascecg

Ionic-Liquid-Based Deep Eutectic Solvents as Novel Electrolytes for Supercapacitors: COSMO-SAC Predictions, Synthesis, and Characterization

Upasana Mahanta,[†] Sambita Choudhury,[†] R. Prasanna Venkatesh,[†] Sujatha SarojiniAmma,[‡] S. A. Ilangovan,[§] and Tamal Banerjee*[,†]

[†]Department of Chemical Engineering, Indian Institute of Technology Guwahati, Guwahati 781039, India

[‡]Advanced Power Systems and [§]Chemical Systems Division, Vikram Sarabhai Space Centre, Thiruvananthapuram 695022, India

Supporting Information

ABSTRACT: The current work investigated two ionic-liquid (IL)-based deep eutectic solvents (DESs) composed of ethylene glycol (EG) and *N*-methylacetamide (NMAc) as hydrogen bond donors (HBD) and high-melting IL, namely, 1-butyl-3-methylimidazolium methanesulfonate ([BMIM][$MeSO_3$]), as the hydrogen bond acceptor (HBA). Initially, the COSMO-SAC model was employed for prediction of the eutectic points of the DESs. The computed melting points of the formulated DESs were found to be 70−100 °C lower than that of HBA. The viscosity of the newly developed DESs (~15 cp) was significantly lower than that of neat room temperature IL electrolytes, and their ionic conductivity was found to be comparable to that of ILs. TGA study revealed no mass loss up to 90 °C, favoring the high temperature application of supercapacitors. To assess electrolytic performance in supercapacitors, electrochemical characterization was done using linear scan voltammetry (LSV), cyclic voltammetry (CV), and galvanostatic charge−discharge (GCD) techniques. LSV provided electrochemical stability up to 3.8 V against a glassy carbon electrode. [BMIM][$MeSO_3$] + EG and [BMIM][$MeSO_3$] + NMAc resulted in operating potential windows (OPWs) of 2 and 3 V, respectively, with a carbon electrode. Moderate values of specific capacitance (55−67 F g^{-1}) and power (0.56−1.3 kW kg^{-1}) were observed due to higher internal resistance. However, [BMIM][$MeSO_3$] + NMAc resulted in noteworthy specific energy (~84 Wh kg^{-1}) due to its wider OPW.

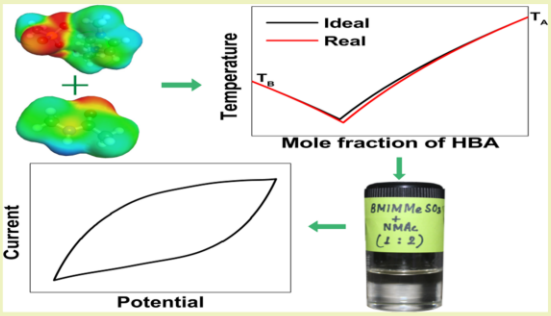

KEYWORDS: *deep eutectic solvents, supercapacitors, COSMO-SAC, viscosity, electrochemical stable potential window*

INTRODUCTION

Electrochemical supercapacitors, also known as ultracapacitors or simply supercapacitors, have gained considerable attention in recent research owing to their higher power densities (1000−1500 W kg^{-1}) and longer life cycles (>100 000) as compared to batteries and fuel cells.[1] Supercapacitors are broadly classified into electrochemical double-layer capacitors (EDLCs), pseudocapacitors, and hybrid capacitors. Of these three kinds, EDLCs are most widely researched. They mainly find application in the field of electric and hybrid vehicles[2,3] and are being commercially manufactured.[4] In an EDLC, the capacitance is produced by the electrostatic charge separation at the interface between the conductive and highly porous electrode and the electrolyte.[5] The typical capacitance of an EDLC is about 100 F g^{-1}, whereas that of a dielectric capacitor is in the order of μF g^{-1}.[6] However, the major drawback of EDLCs is the insufficient energy density (typically as low as 10 Wh kg^{-1}), which cannot fully meet the requirements of some high energy applications.[5] This challenge can be overcome by increasing the capacitance (C) and the cell voltage (V) of the EDLC, both of which are directly proportional to the energy density (E) as given by the following equation[5]

$$E = \frac{1}{2}CV^2 \quad (1)$$

While the capacitance generated is predominantly dependent on the electrode, the operating cell voltage of an EDLC is largely governed by the electrochemical stable potential window (ESPW) of the electrolyte used.[5] Hence, this work focuses on the development of novel electrolytes for energy-efficient EDLCs.

Despite having higher ionic conductivity, aqueous electrolytes have a relatively narrow ESPW, restricted by the decomposition of water. Aqueous solutions of KOH, H_2SO_4, Na_2SO_4, $(NH_4)_2SO_4$, and LiCl have been reported to have an operating potential window (OPW) in the range of 0.8−1.2

Received: September 19, 2019
Revised: November 21, 2019
Published: December 2, 2019

DOI: 10.1021/acssuschemeng.9b05596
ACS Sustainable Chem. Eng. 2020, 8, 372−381

Bull. Mater. Sci. (2021)44:75
https://doi.org/10.1007/s12034-020-02337-7

Electrochemical performance of 1-butyl-4-methylpyridinium tetrafluoroborate ionic liquid electrolyte for graphene-based double layer capacitor

UPASANA MAHANTA[1], ASHRAY KORADIYA[2], R PRASANNA VENKATESH[1], S SUJATHA[3], S A ILANGOVAN[4] and TAMAL BANERJEE[1,*]

[1]Indian Institute of Technology Guwahati, Guwahati 781039, India
[2]School of Engineering and Applied Science, Ahmedabad University, Ahmedabad 380009, India
[3]Advanced Power Systems, VSSC, Thiruvananthapuram 695022, India
[4]Chemical Systems Division, SSC, Thiruvananthapuram 695022, India
*Author for correspondence (tamalb@iitg.ac.in)

MS received 10 May 2020; accepted 30 September 2020

Abstract. Ionic liquids (ILs) have been emerged as the most promising class of electrolytes to achieve high energy density in electrochemical double layer capacitors (EDLCs) due to their unique properties. In this study, 1-butyl-4-methylpyridinium tetrafluoroborate ([BMPy][BF_4]) was explored as the electrolyte for graphene based EDLC in presence of co-solvent. Highly viscous [BMPy][BF_4] was diluted with two different organic solvents, namely acetonitrile (AN) and propylene carbonate (PC). Different weight ratios of [BMPy][BF_4]: organic solvents were investigated and corresponding variation of EDLC's performance was observed. Dynamic viscosity of these IL+solvent mixtures was also measured. Three electrochemical techniques, namely cyclic voltammetry, galvanometric charge discharge, electrochemical impedance spectroscopy were employed to analyse the effectiveness of these electrolyte–electrode systems. Maximum operating voltage 2.2 V was achieved for the four out of six studied systems. For PC based electrolytes, no effect of concentration of PC on operating potential window was observed. However with AN, electrochemical stability decreased with increase in solvent weight percentage. The highest specific energy (49 Wh kg^{-1}) and power (4.13 kW kg^{-1}) were obtained for 3:1 weight ratio of IL to AN. Reverse effect on specific capacitance and internal resistance was noticed for AN and PC based electrolytes.

Keywords. Supercapacitors; operating potential window; electrolyte; capacitance; specific power.

1. Introduction

The ever increasing demand of energy coupled with clean energy has prompted research on energy storage systems. Among the various energy storage devices so far, electrochemical double layer capacitors (EDLCs) have shown their technical maturity as potential energy storage device [1]. In EDLC, energy is stored through ion adsorption with no chemical reaction forming the double layer of the ions at working electrode/electrolyte interface. EDLCs are confined to a branch of supercapacitors and known for higher cyclic durability and high power density as compared to other energy storage devices, such as batteries and fuel cell. The stored energy density possesses dependency on capacitance of the electrode and operating potential window (OPW) of the electrolyte. Lower electrochemical stability (0.8–1.2 V) of aqueous electrolyte and inflammable and noxious nature of organic electrolyte restricts their application in EDLC [2–5]. Ionic liquids (ILs) with their promising physicochemical properties, e.g., lower flammability, less heat sensitivity, weakness for chemical changes, wider OPW overcome the drawbacks of aqueous and organic electrolytes [2,6]. A major limitation of IL based electrolytes is relatively high viscosity, which imparts diffusional limitations to ions resulting in an increase in internal resistance (IR) and subsequent decrease in power density. In this regard, dilution of ILs with organic solvents emerges as an alternative approach [3,7]. The most common organic solvent for EDLC is acetonitrile (AN), which is able to enhance ionic conductivity of ILs to a greater extent than propylene carbonate (PC) [8]. However, PC is known for its wider liquid range than AN. In this study, both AN and PC are employed to evaluate the effect of co-solvent on capacitance and OPW.

It is found in literature that the common choice of cations for ILs includes imidazolium and pyrrolidinium with different anions [2,6,9]. The ion pair combination affects both viscosity and electrochemical stability of electrolyte [10]. Literature for ILs, based on pyridinium, sulfonium and ammonium cations, is hard to find regarding EDLC

Published online: 30 March 2021

Other Publications

1. Pyarimohan Dehury, **Upasana Mahanta** and Tamal Banerjee. Partitioning of butanol between a hydrophobic ionic liquid and aqueous phase: Insights from Liquid Liquid Equilibria measurements and Molecular Dynamics simulations. Fluid Phase Equilibria, 425 (2016), 421-431. http://dx.doi.org/10.1016/j.fluid.2016.06.007
2. Pyarimohan Dehury, **Upasana Mahanta** and Tamal Banerjee. A Comprehensive Assessment on the use of Boron Nitride based Nanofluids Comprising Eutectic mixtures of Diphenyl Ether and Menthol for Enhanced Thermal Media. ACS Sustainable Chemistry & Engineering (2020). https://doi.org/10.1021/acssuschemeng.0c05648